The impact of dopamine on multisensory information processing in the associative striatum

Doctoral Thesis presented by

María Sáez García

- 2020 -

Thesis Director:

Ramón Reig García

PhD Program in Neuroscience

Universidad Miguel Hernández de Elche

Instituto de Neurociencias UMH-CSIC

INSTITUTO DE NEUROCIENCIAS

1999 - 2019 INSTITUTO DE NEUROCIENCIAS

EXCELENCIA SEVERO OCHOA

Sant Joan d'Alacant, de 2020

CONVENTIONAL DOCTORAL THESIS

To whom it may concern,

The doctoral thesis entitled "*The impact of dopamine on multisensory information processing in the associative striatum*" has been developed by myself, María Sáez García. This thesis is presented in a conventional format. It is based on experimental studies undertaken at the Instituto de Neurociencias UMH-CSIC during the PhD program in Neuroscience of the Miguel Hernández University. This work has been partially supported by: Formación del Personal Investigador (FPI) grant with reference BES-2015-072187 and Proyecto I+D+I para Jóvenes Investigadores (JIN) with the reference BFU2014-60809-JIN awarded by the Ministerio de Economía y Competitividad de España, as well as a CSIC-Severo Ochoa grant of the Instituto de Neurociencias UMH-CSIC with reference SEV-2013-0317-05.

Yours sincerely,

MARIA|SAEZ|GARCIA

Firmado digitalmente por MARIA|SAEZ|GARCIA
Fecha: 2020.11.30 14:20:05 +01'00'

María Sáez García

Sant Joan d'Alacant, de 2020

To whom it may concern,

The doctoral thesis entitled "*The impact of dopamine on multisensory information processing in the associative striatum*" has been developed by myself, María Sáez García. This thesis includes the following publication, of which I am the first author. I declare that the publication has not been used and will not be used in any other thesis in agreement with my thesis director Ramón Reig García.

A New Micro-holder Device for Local Drug Delivery during *In Vivo* Whole-cell Recordings.

María Sáez, Maya Ketzef, Javier Alegre-Cortés, Ramón Reig, Gilad Silberberg.

Neuroscience, 2018 Jun 15;381:115-123. doi: 10.1016/j.neuroscience.2018.04.011.

Yours sincerely,

MARIA|SAEZ|GARCIA

Firmado digitalmente por MARIA|SAEZ|GARCIA
Fecha: 2020.11.30 14:20:28 +01'00'

María Sáez García

Sant Joan d'Alacant, de 2020

D. Ramón Reig García, Investigador distinguido CSIC e Investigador principal en el Instituto de Neurociencias UMH-CSIC,

AUTORIZO la presentación de la Tesis Doctoral titulada "*The impact of dopamine on multisensory information processing in the associative striatum*" y realizada por Dª María Sáez García bajo mi inmediata dirección y supervisión como director de su Tesis Doctoral en el Instituto de Neurociencias (UMH-CSIC) y que presenta para la obtención del grado de Doctor por la Universidad Miguel Hernández.

Y para que conste, a los efectos oportunos, firmo el presente certificado.

Dr. Ramón Reig García

RAMON|
REIG|
GARCIA

Firmado digitalmente por RAMON|REIG|GARCIA
Fecha: 2020.11.30 20:24:52 +01'00'

Sant Joan d'Alacant, de 2020

D. Miguel Valdeolmillos López, Catedrático y Coordinador del programa de doctorado en Neurociencias del Instituto de Neurociencias de Alicante, centro mixto de la Universidad Miguel Hernández (UMH) y de la Agencia Estatal Consejo Superior de Investigaciones Científicas (CSIC),

CERTIFICO:

Que la Tesis Doctoral titulada "*The impact of dopamine on multisensory information processing in the associative striatum*" ha sido realizada por Dª. María Sáez García, bajo la dirección de D. Ramón Reig García como director, y doy mi conformidad para que sea presentada a la Comisión de Doctorado de la Universidad Miguel Hernández.

Y para que conste, a los efectos oportunos, firmo el presente certificado.

MIGUEL ANGEL|VALDEOLMILLOS|LOPEZ

Firmado digitalmente por MIGUEL ANGEL|VALDEOLMILLOS|LOPEZ
Fecha: 2020.12.01 09:02:34 +01'00'

Dr. Miguel Valdeolmillos López

E-mail :
miguel.valdeolmillos@umh.es
www.in.umh.es

Tel: +34 965 919540
Fax: +34 965 919549

Av Ramón y Cajal s/n
CAMPUS DE SANT JOAN
03550 SANT JOAN D'ALACANT– ESPAÑA

AGRADECIMIENTOS

La primera vez que entré en el laboratorio 139 estaba prácticamente vacío, no tenía los set ups en pie todavía y la mayoría de cosas estaban en sus cajas. Unos meses después, los set ups estaban en funcionamiento y sin apenas ruido. Fue así como me introduje en el mundo de la electrofisiología y más concretamente, en el sufrido mundo del patch-clamp *in vivo*, hace ahora más de cuatro años. Un doce de abril de 2016, y bajo la atenta mirada de Ramón, registré mi primera neurona en el estriado de un animal anestesiado. Tardé tiempo en asimilar que eso podía ocurrir y todavía recuerdo la emoción al hacer mi primer sello y cómo aguantaba la respiración mientras tenía que romper la membrana para poder registrar la actividad de la célula.

Después de tanto tiempo sigo aguantando la respiración al tener que abrir el sello, aunque añadiré que hago los registros con más soltura (o al menos, eso dicen). Durante todo este tiempo he registrado algunas neuronas más aquí y allá, aprendido algo de Matlab, frustrado con diferentes técnicas y tenido días malos y días buenos. Lo que es innegable es que si no me hubiera rodeado de gente excepcional, todo esto no hubiera podido salir adelante. Ramón, quien me dio la oportunidad de embarcarme en esta experiencia y confió en mí para ser su primera estudiante de doctorado. No puedo sino darte las gracias por muchas cosas: por haberme dejado aprender de ti tantas veces, por los consejos, por haber sido un guía en este camino y haberme acompañado. También por tantos días de registro frustrantes en los que a las siete de la tarde me has dado ánimos y apoyo para seguir. Pero sobre todo, gracias por la paciencia. Espero haber cumplido tus expectativas y que te sientas al menos, un poco orgulloso de mí.

Unos meses más tarde de empezar en el laboratorio llegaron mis primeros compañeros, Javier y Roberto. Con vosotros en el laboratorio me he sentido como en casa, y siempre me sentiré afortunada de haber formado parte del HubLab. Roberto, las horas que hemos pasado intentando hacer funcionar el puller y filosofando tras un día de experimento fallido harán que siempre nos recordemos el uno al otro. Javier, gracias por dejarme aprender de ti todos los días y por la paciencia. Trabajar contigo ha sido fácil aunque yo lo pusiera difícil, y creo que formamos un buen equipo. Alicia, la última en llegar aunque ya has conseguido enseñarme muchas cosas, espero que hayas podido aprender un poco de mí. Roberto, a veces estar entre dos mundos es duro, pero siempre que he necesitado, no has dudado en ayudarme o aconsejarme desde el frío norte. También me gustaría remarcar a los integrantes del Social lab, en especial a Diana. Sabes que desde aquel viaje a Granada hablo portugués perfectamente pero me gustaría dedicarte unas palabras en español. Nuestras “pequeñas” charlas y gossips me han ayudado a sobrellevar gran parte de esta travesía, y cuando he tenido cualquier problema sé que he podido contar contigo. No quiero olvidarme de Adam: a pesar de sus constantes bromas siempre me acordaré de Sikirevci. A ti, Cristina, no tendría espacio suficiente para poder agradecerte las veces que has estado ahí tanto profesional como personalmente. Gracias porque siempre has dado el máximo por ayudarme, por dar tu tiempo por el mío, por nuestras charlas, y en definitiva, por dejarme aprender de ti. Para mí eres un ejemplo a seguir.

Si algo saco en claro después de estos años, es que todo es importante, y tener gente que te ayuda desinteresadamente es lo mejor que te puede ocurrir. Desde la unidad de genotipado (en especial, Trini), que lo dan todo para que los genotipos salgan perfectos; pasando por Luís y Álvaro, que aguantaban estoicamente mis quejas sobre la fMRI y veían mapas donde yo no los veía; pasando por Víctor y su taller electrónico en el que siempre podíamos darle solución a cualquier cosa, y llegando hasta el laboratorio de Canals (Chema, Begoña, Raquel,...) donde siempre hay buenos consejos e igual te dejan una fibra óptica que un anticuerpo. En especial, Elena, compañera fotométrica de fatigas que siempre es capaz de sacarte una sonrisa. Nunca olvidaré la época en la que formaste parte del HubLab y aquel bizcocho de tu madre. No me quiero olvidar de Trini, aunque te haya dado poco trabajo estos años, lavar y autoclavar el material también es importante. También agradecer a todo el personal de administración su ayuda, en especial a Virtu (todavía estaría pensando qué hacer si no fuera por ti). En definitiva, este rincón es para cualquier persona que me haya ayudado durante todos estos años. Gracias.

Quan vaig començar aquesta aventura vaig deixar la casa dels meus pares per a anar-me'n a Alacant. Estar a 200 kilòmetres de casa ha sigut de vegades una benedicció i altres una càrrega de promeses incomplides. Papà, mamà: gràcies per donar-ho tot per mi sempre, sense condicions. Vos he sentit sempre amb mi, acompanyant-me pas a pas encara que no estiguereu ací físicament. Amb els meus èxits i sacrificis espere tornar-vos una milionèsima part de tot el que m'haveu donat. Em senc orgullosa de ser la vostra filla, espere que vosaltres estigau igual d'orgullosos de ser els meus pares.

No només vaig deixar als meus pares, sino que també vaig deixar a la família. Gràcies per enrecordar-vos i tindre'm sempre present. Pels que ja no estàn i els que segueixen estant. També vaig deixar amics enrere. En especial, Paola i Ainhoa, les quals m'han mantés lligada compartint algunes penes i moltes alegries durant aquestos anys i sempre m'han animat a continuar amb aquest projecte. Gràcies per ser i estar.

Era impossible que no fera menció a Zero ací. Gràcies per la teua companyia tots aquestos anys. Aquest últim any sense tu t'he trobat a faltar més del que pensava que podria.

Per últim, però no menys important, m'agradaria agrair-te, Javi, tantíssimes coses que no sabria per on començar. Per la paciència, per escoltar-me, per intentar entendre la meua feina, per vindre a arreplegar-me al laboratori quan acabava tardíssim de fer experiment; pels sacrificis que a vegades hem hagut de fer, per celebrar qualsevol detall, i en definitiva, gràcies per creure en mi fins quan jo no ho faig. Sempre t'ho dic, però em senc afortunada de tindre't com a company de viatge.

INDEX

LIST OF ABBREVIATIONS

6-OHDA	6-hydroxydopamine

A

AC	Adenyl cyclase
ACh	Acetylcholine
ADHD	Attention deficit and hiperactivity disorder
AMPARs	α-amino-3-hydroxy-5-methyl-4-isoxazolepropionic acid receptor
Au1	Auditory primary cortex

B

BDA	Biotin dextran amine
BG	Basal ganglia
BMI	Bicuculline methiodide

C

cAMP	Cyclic adenosine monophosphate
CB1	Cannabinoid receptor 1
CB2	Cannabinoid receptor 2
Cd	*Caudate* nucleus
ChIs	Cholinergic interneurons
CM/Pf	Centre median/parafascicular nuclei complex
CPG	Central pattern generator

D

D1DRs	D1 dopamine receptor
D2DRs	D2 dopamine receptor
DA	Dopamine
DAG	Diacylglycerol
DAT	Dopamine transporter
DLS	Dorsolateral striatum
DLS-ChIs	Cholinergic interneurons from the dorsolateral striatum

DLS-MSNs	Medium spiny neurons from the dorsolateral striatum
DMS	Dorsomedial striatum
DMS-ChIs	Cholinergic interneurons from the dorsomedial striatum
DMS-MSNs	Medium spiny neurons from the dorsomedial striatum
dMSNs	Medium spiny neurons from the direct pathway
DOPA	Dihydroxyphenylalanine
DS	Dorsal striatum
dStr	Dorsal striatum

E

eCB	Endocannabinoid
EPSPs	Excitatory post-synaptic potentials

F

FAI	Fast-Adapting Interneurons
FS	Fast spiking interneurons

G

GABA	Gamma-Aminobutyric acid
GAD	Glutamate decarboxylase
GPe	External segment of the *Globus pallidus*
GPi	Internal segment of the *Globus pallidus*

H

Hz	Hertz

I

iMSNs	Medium spiny neurons from the indirect pathway
IPSCs	Inhibitory post-synaptic currents
IPSPs	Inhibitory post-synaptic potentials
IT	Intratelencephalic tract neurons

K

KARs	Kainic acid receptors or kainate receptors

L

L-DOPA	Levodopa or l-3,4-dihydroxyphenylalanine
LFP	Local Field Potential
LTS	Low threshold spiking interneurons

M

µV	Microvolts
m/s	Meters per second
M1	Motor primary area
MPTP	1-methyl-4-phenyl-1,2,3,6-tetrahydropyridine
ms	Milliseconds
MSN	Medium Spiny Neuron
mV	Millivolts
mW	Milliwatts
MΩ	Mega Ohms

N

NAc	*Nucleus accumbens*
NMDARs	N-methyl-D-aspartate receptor
NOS	Nitric oxide synthase
NPY+	Neuropeptide Y interneurons

O

OCD	Obsessive compulsive disorder
OFC	Orbitofrontal cortex
OT	Olfactory tubercle

P

PD	Parkinson disease
PKA	Protein kinase A
PKC	Protein kinase C
POm	Medial posterior thalamic nuclei
PPN	Peduncupolontine nucleus

PT	Pyramidal tract neurons
Pu	Putamen
PV	Parvalbumine

R

RR	Retrorubral area

S

S1	Somatosensory primary area
SABIs	Spontaneously Active Bursty Interneurons
SN	*Substantia nigra*
SNc	*Substantia nigra pars compacta*
SNr	*Substantia nigra pars reticulata*
STN	Subthalamic nucleus
Str	Striatum
SWO	Slow wave oscillation

T

TH	Tyrosine hydroxylase
TS	Tourette syndrome
TTX	Tetrodoxin

V

V1	Visual primary cortex
Vm	Voltage membrane
VMAT	Vesicular monoamine transporter
vmPFC	Ventromedial prefrontal cortex
VS	Ventral striatum
VTA	Ventral tegmental area

LIST OF FIGURES AND TABLES

FIGURES

TABLES

ABSTRACT

The ability to process and integrate information from the environment and produce an adequate behavioural response is one of the basic mechanisms of animal survival. An important process underlying it is the multisensory integration of a variety of stimuli, which has an important impact on perception and a great variety of processes. Deficits in this integration have been documented in patients suffering from schizophrenia and attention deficit and hyperactivity disorder, as well as from Parkinson's disease.

The basal ganglia are a highly interconnected group of subcortical nuclei which are involved in motor and cognitive processes. Importantly, they are also related to the integration of sensorimotor information. The striatum is the input layer of the basal ganglia and receives cortical projections from motor, associative and sensory areas. In mice, the dorsal striatum has been divided into two different functional regions: the dorsolateral (DLS) or sensory-motor striatum and the dorsomedial region (DMS), also known as the associative striatum. Medium Spiny Neurons from the direct (dMSNs) and indirect (iMSNs) pathways receive sensory information in the whole dorsal striatum. Whereas MSNs in the DLS respond to tactile inputs, single MSNs in the DMS can be activated by tactile as well as by visual inputs. Nevertheless, the different latencies when processing visual and tactile information results in a delay which causes the independent integration of these inputs. In addition, the dorsal striatum is densely innervated by dopaminergic axons from the Substantia nigra *pars compacta* (SNc). Dopamine is known to modulate and induce changes in neuronal transmission and plasticity, and behaviourally it has been linked to a great variety of functions such as reinforcement and reward-dependent learning.

In this study we aim to explore the impact of dopamine on the modulation of visual, tactile and bimodal sensory responses in MSNs located in the DMS. In order to do so, we performed *in vivo* optopatch-clamp recordings on identified striatal MSNs with simultaneous local field potential recordings in primary visual and somatosensory cortices in anesthetized mice. Dopamine is released from the SNc terminals in the DMS by optogenetic stimulation while presenting visual, tactile and bimodal contralateral stimuli.

Our main finding describes a new mechanism in which dopamine enhances dMSNs efficiency to integrate multimodal information by synchronizing visual and tactile inputs. Dopamine modulates differently these sensory inputs due to the existence of a specific cortical projection towards the DMS. In addition, dopamine affects the spontaneous activity of MSNs, modulating the slow and fast oscillatory frequencies. The results obtained in this study represent a step forward towards understanding the role of DA in the striatal microcircuits. The described mechanism will help to decipher the unknown phenomenon by which the brain is able to integrate multisensory information. Moreover, it will be relevant to understand diseases such as attention deficit and hyperactivity disorder, schizophrenia or Parkinson's disease, all of them related with malfunctions in the associative striatum.

RESUMEN

Uno de los requisitos básicos para la supervivencia es la capacidad de procesar la información de nuestro entorno y producir un comportamiento adecuado. En este sentido, la integración multisensorial contribuye a una percepción correcta, rápida y eficaz. Déficits en este tipo de integración se han documentado en pacientes con diferentes enfermedades, entre ellas la enfermedad de Parkinson.

Los ganglios basales son un grupo de núcleos interconectados que participan en una gran cantidad de funciones motoras y cognitivas. Es importante destacar que también están involucrados en los procesos de integración de información sensorio-motora. El estriado es la entrada sináptica a los ganglios basales y recibe proyecciones desde diferentes áreas corticales motoras, asociativas y sensoriales. En el ratón, el estriado dorsal se ha dividido en dos regiones funcionalmente diferentes: la región dorsolateral (*DLS*) o estriado sensorio-motor; y la región dorsomedial (*DMS*), también llamada estriado asociativo. En el estriado dorsal, las neuronas de proyección GABAérgicas (*MSNs*) de la vía directa e indirecta reciben información sensorial. Mientras que las *MSNs* del *DLS* integran estímulos táctiles, las *MSNs* del *DMS* pueden integrar información de diferentes modalidades sensoriales, entre ellas táctil y visual. Sin embargo, las diferencias temporales en el procesamiento sensorial de estos estímulos evocan respuestas independientes en las *MSNs*. Por otra parte, el estriado dorsal recibe una gran densidad de axones dopaminérgicos de la parte compacta de la sustancia negra (SNc). Es sabido que la dopamina modula e induce cambios en la transmisión neuronal y la plasticidad sináptica en el estriado; y en cuanto al comportamiento, se la ha relacionado con una amplia variedad de funciones, como el refuerzo y el aprendizaje dependiente de recompensa.

El objetivo principal de esta tesis es explorar el impacto de la dopamina en el procesamiento sensorial de estímulos visuales, táctiles y bimodales en las *MSNs* del *DMS*. Para ello, realizamos registros intracelulares *optopatch-clamp* junto con registros simultáneos de la actividad extracelular de las cortezas visual y somatosensorial primarias en ratones anestesiados. Para estudiar el efecto de la dopamina, estimulamos optogenéticamente las terminales dopaminérgicas de la SNc en el *DMS* mientras presentamos estímulos contralaterales visuales, táctiles y bimodales.

El resultado principal de esta tesis doctoral es la descripción de un nuevo mecanismo de sincronización multisensorial mediado por el incremento de los niveles de dopamina. La dopamina mejora la eficiencia de las *MSNs* de la vía directa para integrar información, sincronizando las respuestas táctiles y visuales. Este proceso se explica por la existencia de una proyección cortical específica al *DMS*. Además, la dopamina también afecta a la actividad espontánea de las *MSNs*, modulando las frecuencias de oscilación lentas y rápidas. Los resultados obtenidos suponen un avance para entender el papel de la dopamina en los microcircuitos del estriado. Por otro lado, el mecanismo descrito contribuye a descifrar cómo el cerebro integra información multisensorial. También será relevante para comprender enfermedades como el déficit de atención e hiperactividad, la

esquizofrenia o la enfermedad de Parkinson, cuyos pacientes presentan deficiencias sensoriales que involucran al estriado asociativo.

Introduction

1. INTRODUCTION

One of the most impressive features of the nervous system is its ability to process information from a variety of stimuli originated by diverse sources. These stimuli such as light, sound, pressure or odours arrive to our sensory organs with very different delays. For instance, light travels at $3x10^8$ m/s, while the speed of sound is 340 m/s. Additionally to this disparity of delays, once the inputs arrive to our body, each sensory system requires particular time intervals to process the information before targeting primary sensory areas. However, the brain is able to arrange them in an integrated and comprehensible representation of the external world that is understandable to therefore produce an adequate behaviour. Nevertheless, the biological mechanism of multisensory integration explaining this phenomenon remains unknown.

1.1. A BASAL GANGLIA OVERVIEW

The world around us is continuously changing and stimulating our senses. One of the main functions of the nervous system consists on perceiving the diverse stimuli present in the outside world and subsequently process and integrate them to therefore produce adaptive signals and adequate behaviours. In order to do so, the central nervous system possesses specialized circuits in which sensorimotor information is coordinated at multiple levels of processing. For instance, the central pattern generator (CPG) distributed in different regions of the spinal cord, the cerebellum, the *superior colliculus* or the brain cortex, among others. A pivotal circuit which integrates sensorimotor information and coordinates and executes planned actions is the one composed by the basal ganglia (BG).

The BG, which is a group of highly interconnected subcortical nuclei, is connected with the cortex, thalamus and brainstem, and was first anatomically described in 1664 by Thomas Willis[1,2] (Fig.1). Most cortical areas send inputs to the BG, which then provides outputs to different brain systems. Traditionally, the BG is best known for its role in movement[3], being involved in the selection and inhibition of action commands[4], such as motor learning and action selection[5–11]. Importantly, the BG is characterized for its role in connecting the cortex with different neural systems and therefore creating a network to coordinate and execute planned and motivated behaviours through motor, cognitive and limbic circuits. Broadening this classical view, an increasing number of studies are showing that besides of being involved in motor tasks, BG is also involved in integrative and cognitive processes such as emotions, motivation, habit formation[11], mental imagery[12,13], planning[14], attention[15,16], language[17–19] and sensory processing[17,20].

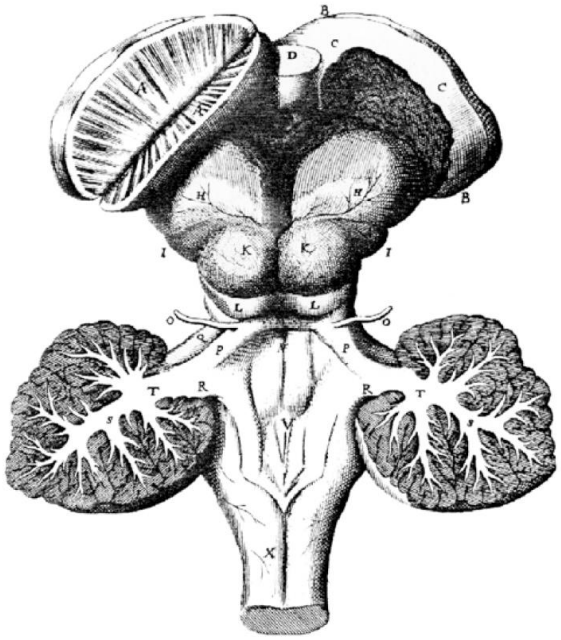

Figure 1. The basal ganglia seen by Thomas Willis. Reproduction of a plate showing a dorsal view of the brainstem and basal ganglia of a sheep. Hemispheres were removed to better illustrate the BG. The corpus striatum was cut in half to show its characteristic striations. From Parent, 2012[21].

BG malfunctions can lead to several motor-related diseases like Parkinson's Disease (PD) or Huntington's disease, but also to cognitive-like diseases, such as Tourette's Syndrome, Obsessive Compulsive Disorder (OCD) or the Attention Deficit and Hyperactivity Disorder (ADHD) among others[22]. Moreover, in motor-related diseases, such as PD, patients can suffer other symptoms, including: depression, insomnia and emotional problems[23].

1.1.1. Basal ganglia anatomy and circuitry

The components of the BG include the striatum –composed of the *caudate* nucleus, *putamen* and *Nucleus accumbens* (NAc)–, the external and internal segment of the *Globus pallidus* (GPe and GPi respectively), the subthalamic nucleus (STN), the *Substantia nigra pars compacta* (SNc) and the *Substantia nigra pars reticulata* (SNr)[2,24] (Fig. 2). The striatum receives glutamatergic inputs from layer 5, as well as from layer 2/3 of the cortex and the thalamus. The GPi and the SNr function as the output nuclei of the BG[2].

The main input layer of the BG is the striatum, which is mainly composed by GABAergic[25] projection neurons called Medium Spiny Neurons (MSNs)[26–29]. These populations of neurons receive excitatory inputs from different cortical areas and the thalamus[30,31] and are divided into two subpopulations: the "direct" and "indirect" MSNs (dMSNs and iMSNs respectively), which in turn give rise to the two output circuits of the BG: the direct and the indirect pathway (Fig. 2). This distinction relies on which family of dopamine receptors MSNs possess and its projection towards the BG output nuclei. Direct MSNs are so-named because they provide direct inputs to the output neurons of the BG in the GPi and SNr. On the other hand, indirect MSNs provide inputs to the GPe, which, together with the STN, comprises the main components of the

indirect basal ganglia pathway. Both arkypallidad and prototypic GPe GABAergic neurons project to the striatum[32]. In addition, prototypic neurons also project to the output nuclei of the BG (GPi and SNr) and to the STN[32–34].

In the classical BG model, glutamatergic projections from the cortex towards the striatum activate MSNs from the direct and the indirect pathway. On one hand, the direct pathway functions on the principle of the positive feedback. Once MSNs from the direct pathway are activated, they send inhibitory GABAergic projections towards the BG output: the GPi and the SNr, which in turn send inhibitory inputs to the thalamus and other brain structures. When the GPi and SNr are inhibited by direct MSNs, the thalamus gets disinhibited. This causes an increased synaptic transmission from the thalamus towards the cortex, promoting movement[2,35,36]. On the other hand, the indirect pathway functions by negative feedback. Once the MSNs from the indirect pathway are activated, they send inhibitory projections towards the GPe. The GPe, which normally sends inhibitory projections towards the STN, will then be inhibited by indirect MSNs causing a disinhibition of the STN. The STN will therefore send excitatory inputs towards the GPi, which in turn inhibits the thalamus, causing a decreased synaptic transmission towards the cortex, resulting in the prevention of movements[2,35,36]. Thus, the activation of the direct pathway results in an inhibition of the tonic inhibitory output of the BG, promoting movement; whereas the activation of the indirect pathway inhibits the GABAergic GPe output, which results in the disinhibition of the output neurons of BG and the STN which in the end prevents the unnecessary movements. Once the BG output nuclei are targeted, they project to multiple brain structures. One of the regions they target are different thalamic nuclei, which in turn project to frontal cortical areas involved in the planning and execution of movements. They project to the intralaminar thalamic nucleus which gives input to the neocortex and the striatum. In addition, they project to the intermediate layers of the *superior colliculus* which are related to the generation of head and eye movements. Finally, their inputs also reach the pedunculopontine nucleus (PPN), which is directly implicated in locomotor control, contributing to the speed and gait of movements[2,37].

In summary, the cortex and thalamus provide excitatory inputs to the striatum, which sequentially provides inhibitory and excitatory regulation of the output nuclei of the BG through the direct and indirect pathways. In general terms, the activity of these two pathways has been considered as a counterbalanced regulation of the output nuclei of the BG.

The STN is another entry point of the BG which, as happens in the striatum, receives projections from several cortical areas such as motor, oculomotor, associative and limbic. The STN then provides output to the GPe and to the GPi/SNr. The cortical projections towards the STN and the subsequent projections from this nucleus to the GPi/SNr have been termed the “hyperdirect” pathway. This pathway constitutes a faster route for the cortical input to modulate the activity in the BG output nuclei[2]. Different studies suggest that this pathway could act as a parallel signal to inhibit certain motor

programs[38,39] and therefore benefit the selected ones. In addition, lesions in this nuclei have resulted in the appearance of involuntary body movements[38].

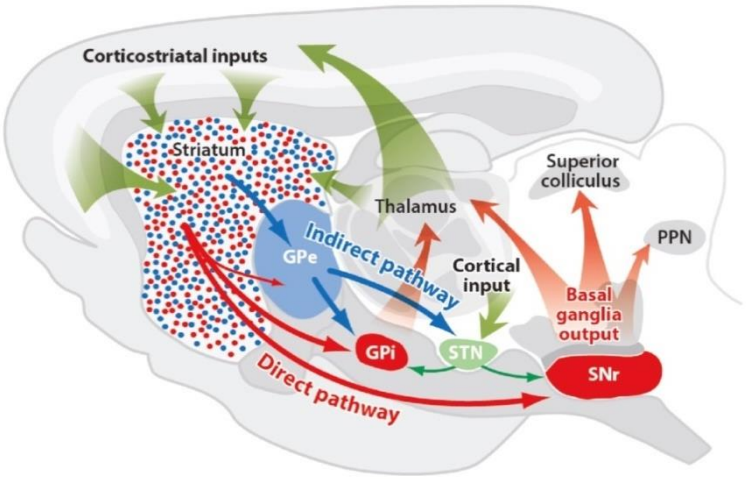

Figure 2. Diagram showing the basal ganglia circuitry. The striatum receives glutamatergic excitatory corticostriatal and thalamic inputs. The GPi and SNr function as the output nuclei of the BG, which are directed to the thalamus, *superior colliculus* and PPN. The direct pathway originates from MSNs expressing D1DRs and projects towards the GPi and the SNr output nuclei; whereas the indirect pathway originates from D2DRs expressing MSNs which project to the GPe. From Gerfen & Surmeier, 2011[24].

Besides the canonical BG circuits, there are several anatomical features that add complexity to this system. First of all, we have to take into account that the nigostriatal system provides a massive dopaminergic input to the striatum from the dopaminergic neurons of the ventral tegmental area (VTA) and SNc[40–42]. Secondly, the organization of the corticostriatal system, which provides high overlapped corticostriatal inputs to the striatum[31,43,44]. These features and others, such as the lack of physical boundaries in the striatum, the large quantity of different types of neurotransmitters and the different brain structures that target the BG output nuclei[2], add complexity to the BG circuitry, and the specific mechanism that regulates the output of the BG remains elusive.

1.2. THE STRIATUM

The striatum acts as a hub where multiple input streams converge. Glutamatergic afferents from the cortex are considered as the main driver of striatal activity, although glutamatergic inputs from the thalamus also target MSNs. In addition, the striatum receives GABAergic afferents from the midbrain[45] as well as from the GPe[33,45]. Moreover, it has been described an afferent cholinergic connection from the PPN and the laterodorsal tegmentum[46]. But one of the main features of the striatum is that it is the most innervated nuclei by dopaminergic terminals from the SNc and VTA in the entire brain[40,42] (Fig. 3).

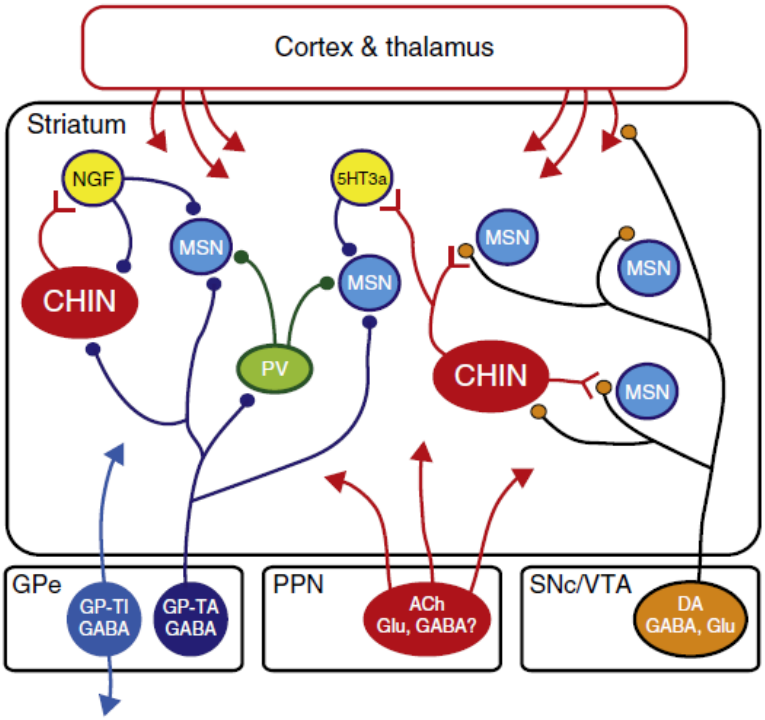

Figure 3. Afferent pathways in the striatum. Schematic representation of the afferent projections from the GPe, PPN and SNc/VTA towards the striatum and the intrastriatal connections within the striatum. From Silberberg & Bolam, 2015[45] .

1.2.1. Medium spiny neurons

MSNs comprise the 95% of neurons in the striatum, where they are homogeneously distributed. They display a cell diameter of around 12-20 µm from which several branched dendrites radiate, covering over 200 µm in diameter. They are termed “spiny” because their dendrites are densely laden with spines (Fig. 4, 20b).

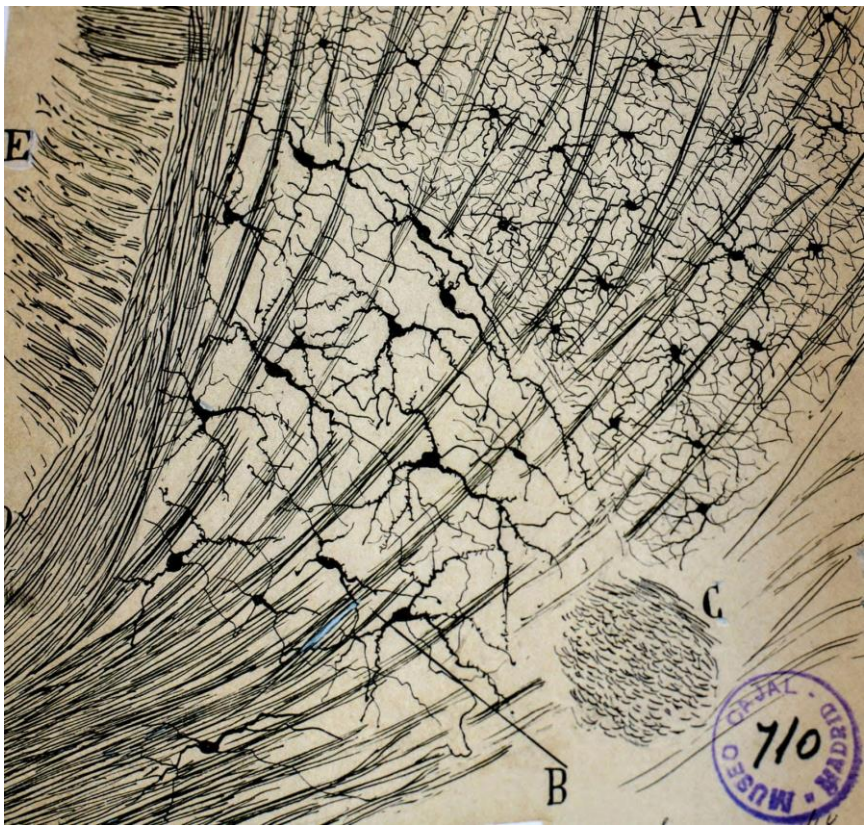

Figure 4. *Caudate* nucleus of a twenty-day old mouse seen by Santiago Ramón y Cajal. Reproduction of a slice illustrating MSNs (B) in the *caudate* nucleus along with several fiber tracts (C, E) which pass through the striatum. From Beautiful Brain: The Drawings of Santiago Ramon y Cajal[47].

1.2.1.1. Electrophysiological properties of MSNs

In conditions such as slow-wave sleep[48,49], anaesthesia or during behavioural rest[50], a Slow Wave Oscillation (SWO) originates in the cortex[51] and then propagates towards other brain regions[48,52] –including the striatum[53–56]–, modulating the resting state of MSNs[54,57] and interneurons[53]. This collective oscillatory activity of around 1 Hz of frequency is described as a bi-stable state in which the membrane potential of the neurons alternates from periods of activity and periods of silence[58] (Fig. 5). The "Up states" are characterized by periods of high synchronized synaptic activity and are defined by a depolarized membrane potential rich in synaptic activity[48,54,59,60]. On the other hand, the "Down states" are characterized by silence periods in which the neurons display hyperpolarized membrane potentials[58,61]. This pattern can be observed at the intracellular (Fig. 5b) as well as at the population level (Fig. 5a).

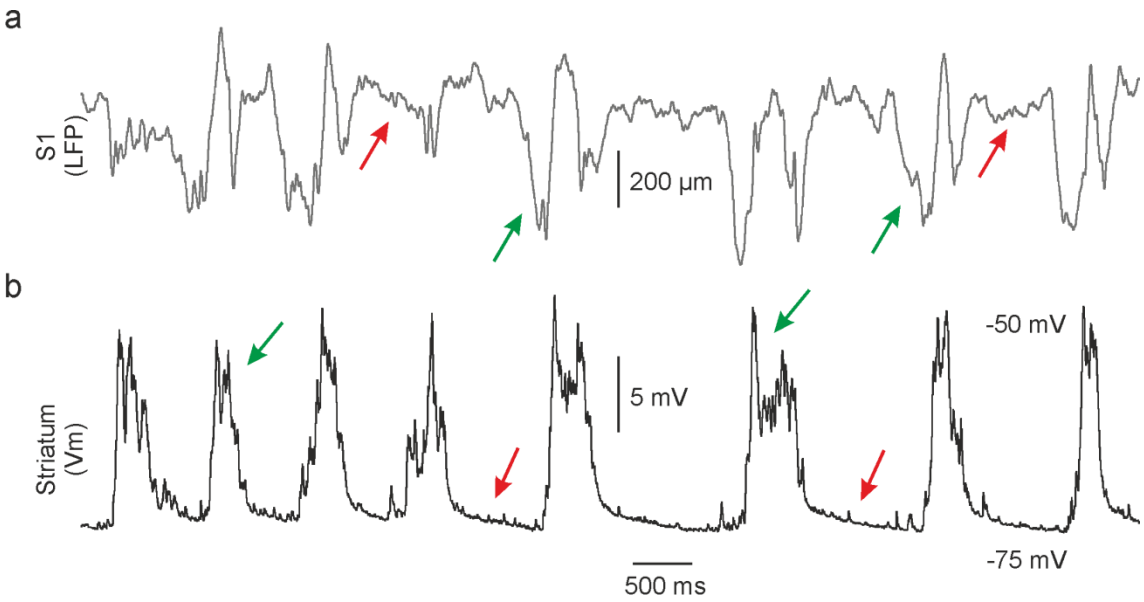

Figure 5. SWO activity during an anesthetized *in vivo* recording. Example of SWO activity at the population (a) and intracellular level (b) during an *in vivo* anesthetized recording displaying the characteristic Up and Down state pattern. Red arrows indicate Down state periods, whereas green arrows indicate Up state periods.

The Down state, which is near the reversal potential for K^+, is characterized by a very low level of synaptic input[54]. Because of this sparse input, a high input resistance would be expected when MSNs are hyperpolarized. Nevertheless, MSNs are dominated by inwardly rectifying K^+ channels (Kir2), which maintain an hyperpolarized potential *in vivo*[53,57,62,63] and *in vitro*[64,65] and decrease the input resistance of MSNs during the Down state[66]. As a consequence, the hyperpolarized resting membrane potential is quite far from the spiking threshold (approximately -40 mV)[67], and it is common for an MSN to be in the Up state for long periods without firing[66]. Nevertheless, MSNs can trigger action potentials, although irregularly and at a low frequency[53,62,63,66] displaying long-latency spike discharge at rheobase[65]. *In vitro*, it has been observed that MSNs show characteristic ramp responses and delayed firing to near-threshold current steps, mainly due to slow inactivating K^+ conductances[64,68]. Moreover, it has been shown that they display low time constants and input resistances[69,70]. Regarding direct and indirect MSNs, it has been reported that they display similar electrophysiological properties both *in vitro*[69,71] and *in vivo*[53,62] studies, although with indirect MSN displaying higher input resistances, which makes them more excitable than direct MSNs[62,69]. In addition, no differences in the membrane potential or the spiking threshold between these two subpopulations have been found[69].

During the low level of synaptic input at the Down state, when an excitatory glutamatergic synaptic input arrives but does not have any spatial or temporal convergence with other inputs, the Kir2 K^+ channels shunt this synaptic current, thus minimizing the cellular response. But if this input is highly convergent, the

glutamatergic inputs can overload Kir2 channels, promoting their closure[54]. The closure of these channels leads to an elevation of the input impedance of MSNs dendrites and a reduction in their electrotonic length[67,72]. These changes depolarize the cell membrane of MSNs and bring them nearer to the spiking threshold, leading to the Up states, which can last hundreds of milliseconds. In this moment is when MSNs can spike, although they fire scarcely[53,62,63]. The moment in which they switch from Down to Up states or viceversa are termed "state transitions". MSNs express a wide array of conductances whose properties can be modulated by the changes that accompany state transitions[73]. These conductances include voltage-sensitive Na^+ and K^+ channels, different classes of low- and high-threshold voltage-sensitive Ca^{+2} channels and ionotropic glutamate receptors[74]. Different neuronal processes in MSNs are regulated by Ca^{+2} influx, such as synaptic strength[75]. MSNs have different routes for Ca^{+2} entry, for instance, Ca^{+2}-permeable AMPA (AMPARs)[76,77], Kainate (KARs) and NMDA (NMDARs) receptors. Synaptic Ca^{+2} signals in the Down state are dominated by Ca^{+2}-permeable AMPARs and KARs[2,66]. Nevertheless, the membrane potential depolarization that occurs during the state transition switches the dominant source of Ca^{+2} to NMDARs[78]. In addition, it has been observed that NMDA receptors contribute to maintain the Up states[79–81]. In summary, the AMPA/Kainate receptors activation provides the necessary depolarization to allow the current flow through NMDA receptors[2,82,83].

1.2.1.2. The Direct and Indirect MSNs

MSNs project outside of the striatum towards the GPe and/or the GPi and the SNr[84]. Depending on their projection to these BG output nuclei and which family of dopamine receptor they express, MSNs have been divided into two subpopulations: the direct and the indirect pathway MSNs[84–86]. These two subpopulations seem equally distributed among the dorsal striatum[87]. All of them contain glutamic acid decarboxylase (GAD), which is used to syntethize GABA[88]. Nevertheless, only direct MSNs contain the substance P and dynorphin neuropeptides[86,89]; whereas only indirect MSNs contain enkephalin[90]. Additionally, direct MSNs are characterized by expressing D1 dopamine receptors (D1DRs). They are termed "direct" MSNs because they project directly to the SNr and to the GPi (Fig. 6). Due to this, direct MSNs are also termed striatonigral MSNs. On the other hand, indirect MSNs are characterized by expressing D2 dopamine receptors (D2DRs), which in turn co-localize with enkephalin. They are termed "indirect" because they project indirectly to the output nuclei of the BG, projecting first to the GPe and from there to the GPi and SNr[91,92] (Fig. 6). Based on their projections, they are also termed striatopallidal MSNs. The segregated expression of these two families of dopamine receptors in direct and indirect MSNs has been confirmed by several studies[93,94], and it has been described a very small proportion of neurons expressing both D1 and D2 dopaminergic receptors[95].

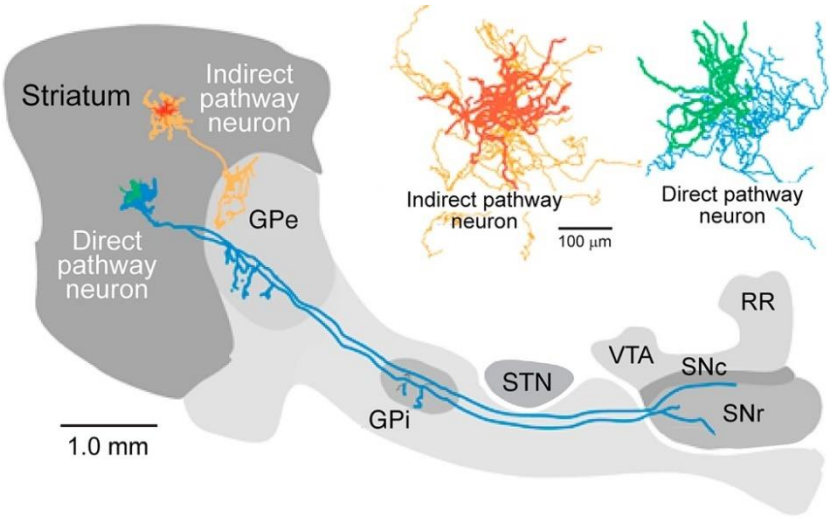

Figure 6. Schematic representation of direct and indirect pathway MSNs. Notice the direct projection of direct MSNs towards the GPi and SNr. From Handbook of Basal Ganglia Structure and Function[2].

Direct and indirect MSNs are quite similar when comparing their anatomy and their electrophysiological properties. Several studies have revealed differences between these two subpopulations, such as their somatodendritic anatomy[71,96]. In rodents, direct MSNs display a more complex dendritic arborisation[71], with no obvious difference in spine density. In addition, it has been reported that direct MSNs display bigger responses to tactile stimulation in the dorsolateral striatum[50,53,62] and it has been estimated that they receive stronger synaptic input than indirect MSNs[97]. In addition, *in vitro* studies revealed that direct MSNs display lower input resistances[62,69,71] and are less excitable than indirect MSNs[62,69]. In the striatum, MSNs contact with cholinergic interneurons, but not with fast-spiking GABAergic interneurons[98]. In addition, both MSNs types can target other MSNs, although this interconnectivity is sparse[64,99–101]. There is a highly prevalence of connections where indirect MSNs form synapses with direct MSNs, acting as the presynaptic cell; whereas a very few percentage of direct MSNs form connections onto indirect MSNs[100,101]. Furthermore, the synaptic connections formed by direct MSNs are weaker than those formed by indirect MSNs, probably due to a fewer number of $GABA_A$ receptors on the direct MSNs synapses[101].

Classically, in the case of motor function, the direct pathway is considered as the one that promotes actions, whereas the indirect pathway supresses not desired movements[102,103]. Nowadays there are several reports postulating that the co-activation of both pathways is important for action selection and action initiation[104], where direct pathway MSNs promote the wanted motor programs and indirect pathway MSNs inhibit competing motor programs[104,105]. In fact, the global activation of indirect MSNs population would inhibit most motor programs instead of only the unwanted ones, leading to disorders such as bradykinesia[103]. Similarly, ablating or depleting the indirect pathway MSNs population would abolish suppression of unwanted motor programs and induce hyperkinesia[106,107]. In addition, the simultaneous optogenetic activation of direct and indirect MSNs in 6-hydroxy-dopamine (6-OHDA) depleted animals induces involuntary movements similar to dyskinesias[108]. Nonetheless, both subpopulations

receive cortical innervation, which is mediated by pyramidal cortical neurons. However, the specific corticostriatal connectivity targeting the different types of neurons along the whole striatum is still not fully clear. These differences cause that direct and indirect MSNs also differ in their role in movement disorders such as PD[36,102].

1.2.2. Striatal interneurons

The remaining neuronal types that can be found in the striatum are interneurons[26,28]. Striatal interneurons do not project axons outside of the striatum, creating instead a micro-circuit of locally projecting axons within the nucleus. They make up approximately 5% of the striatal neuron population and they are morphologically and neurochemically quite defined. There are two major identified groups. One of them is the cholinergic interneuron[2,84,109,110] and the other is composed by an heterogeneous population of GABAergic aspiny interneurons, in which we can identify several classes.

1.2.2.1. Cholinergic interneurons

Cholinergic interneurons (ChIs) use acetylcholine as neurotransmitter and constitute one of the most important types of interneurons in the striatum. They are normally identified by their large soma size of about 40 μm of diameter[26,110,111] from which long aspiny dendrites split in several branches. Its fine and extensive axon can extend distances over 2 mm. Electrophysiologically, ChIs can also be distinguished by their depolarized resting membrane potential and high input resistance[112]. *In vivo*, they spontaneously tonically fire at a rate of 2-10 Hz due to their expression of Na^{+} currents and hyperpolarization-activated cation currents[113]. When they fire, there is a prominent afterhyperpolarization following each spike, due to Ca^{+2}-activated K^{+} channels[84,110,114] (Fig. 19b). They co-express D2 and D5 dopamine receptors[115]. Although they only comprise 1 or 2% of the striatal neurons, they exert a strong control on striatal circuits by disynaptic inhibition of MSNs[115,116]. In this case, the inhibition exerts its effect onto the MSNs through an intermediate connection which is still unknown[117,118]. ChIs receive excitatory innervation which comes primarily from the thalamus[119] and in a lesser extent, from the cortex[120]. They also receive inhibitory synapsis from MSNs[121].

Another characteristic feature of ChIs is their pause in tonic firing when responding to salient cues, such as reward prediction *in vivo*[122,123]. The origins of this pause are not established, but it is known that requires thalamic and dopaminergic innervation to occur[124]. Additionally, ChIs have been related to associative learning, reward processing and motor control[125]. In fact, it has been proposed that dopaminergic neurons could engage ChIs to control striatal circuits[114,115]. With all this information together, it is clear that ChIs create micro-circuits capable of modulating striatal output[126]. Moreover, ChIs display a functional gradient in the striatum, with higher activity in the medial regions[127,128], which suggests that they will exert a different control depending of the striatal region.

1.2.2.2. GABAergic interneurons

Several Golgi studies suggested that there are up to nine morphological different types of neurons in the striatum of rodents. The current point of view is that apart from the MSNs and the cholinergic interneurons, there are seven classes of GABAergic interneurons that present different electrophysiological and neurochemical properties[112,129–132]. Nevertheless, is probably that this view underestimates the diversity of GABAergic interneurons of the striatum.

1.2.2.2.1. Fast spiking interneurons

Fast spiking interneurons (FS) conform only a few percentage of striatal interneurons –around a 0.7%[133]–, express parvalbumin[134–136] and the D5 dopamine receptor[137]. This is why they can also be termed as PV+ interneurons. They can be physiologically identified because they present characteristic electrophysiological properties, such as an hyperpolarized resting membrane potential and a low input resistance similar to MSNs[53,70], as well as a high frequency firing rate[136]. These interneurons receive a large input from cortical neurons to then target MSNs by peri-somatic[138] feedforward inhibition[100,139,140]. This type of inhibition is suggested to contribute to action selection, supressing the activity of MSNs in unwanted actions[141]. Although both types of MSNs are targeted by this interneurons, it has been observed that FS have some kind of preference to target direct MSNs[140]. In addition, FS can target other FS but not low-threshold spiking interneurons or ChIs[130,142]. Different reports have demonstrated the presence of a dorsal to ventral and lateral to medial gradient of expression[143]. In fact, the dorsolateral striatum is relatively enriched in FS[132,139,141,144], suggesting that they may play an important role in sensorimotor integration. In addition, it has been observed the existence of diverse types of PV interneurons with different electrophysiological properties along the dorsal striatum[132,144], with dorsomedial PV interneurons having an increased excitability when compared to PV interneurons from the dorsolateral striatum[144].

1.2.2.2.2. Low Threshold Spiking interneurons

Low-Threshold Spiking Interneurons (LTS) express somatostatin, neuropeptide Y and nitric oxide synthase (NOS)[136,145,146]. Electrophysiologically, LTS interneurons are characterized by their plateau potentials and low-threshold spikes. In addition, they display higher input resistances and a relatively depolarized resting potential[112]. They receive monosynaptic excitatory inputs from the cortex which can evoke spikes and long lasting potentials[112,138,147]. It has been suggested that LTS interneurons and NPY+ interneurons –described in the section below–, represent the extremes of a single distribution[148], although the differences between these two classes were significant enough to classify them as a different type. Similarly to other GABAergic interneurons,

they also exert a strong inhibition towards MSNs, playing a significant role in mediating feedforward inhibition onto them by targeting the distal dendritic compartment of MSNs[116,126].

1.2.2.2.3. Somatostatin/NOS/Neuropeptide Y interneurons

A second type of GABAergic interneuron that expresses somatostatin, neuropeptide Y and NOS was first described in 1983[145,149]. These neurons are medium-sized, with a soma of 15-25 µm diameter, and are the second largest interneuron in the striatum after ChIs. They receive cholinergic and dopaminergic input[130], as well as synaptic input from the cortex[112,150]; and they express D5 dopamine receptors. The most characteristic electrophysiological attributes of this interneurons are the presence of a low threshold Ca^{+2} spike (LTS), a very high input resistance (> 600 MΩ) and a depolarized resting membrane potential (of around -50 mV)[70,130]. They seem to follow a gradient too, with a larger number present in ventral areas compared to dorsal areas[2].

MSNs are the major target of these interneurons. Axonal terminals of NPY+ interneurons form synapsis on the distal regions of the dendrites and on spines, largely avoiding the soma, inhibiting MSNs[151–154]. It has been reported that they also form synapses with ChIs[152,153,155], but synapses between other NPY+ interneurons have not been reported[130]. It has been observed that they inhibit MSNs, but evoking relatively weak GABAergic IPSCs, likely onto the distal dendrites of MSNs[142]. This has suggested that NPY+ interneurons could exert slow modulatory effects rather than fast synaptic effects[130] such as the potent inhibition on GABA release at MSN-MSN synapses[156]. No IPSC have been observed in other NPY+ interneurons, FSIs or ChIs[130].

1.2.2.2.4. Neurogliaform interneurons

About the 75% of the striatal NPY+ neurons are the ones already described on the previous sections. Nevertheless, the remaining 25% exhibited a different set of electrophysiological properties and a different morphology[157,158]. Additional reports revealed that this type of interneuron also expresses somatostatin and NOS; and that it displays a more complex dendritic arborisation when compared to other NPY+ interneurons[131]. Moreover, their soma is slightly smaller than the LTS interneurons[131]. These interneurons exhibit a very hyperpolarized resting membrane potential during *in vitro* recordings, and similar to MSNs, they are not spontaneously active[131]. As other interneurons, they synapse onto MSNs and their synaptic response is mediated by $GABA_A$ receptors[148,159]. Nevertheless, they elicit an IPSC/P with slow kinetics[157,158].

1.2.2.2.5. Calretinin interneurons

Calretinin interneurons are one of the three first identified GABAergic interneurons (together with FS and LTS interneurons) in the striatum of rodents, but very little is known about them. Recently, the first *in vivo* recording and juxtacellular labelling was performed[160] in this type of interneuron. Here, authors described three structural and

topographical distinct calretinin subpopulations. This distinction was previously observed based on their soma size and morphology[161].

1.2.2.2.6. Other types

Several studies suggest that we can find more subtypes of GABAergic interneurons in addition to the ones described above. One of them was first described in the striatum of adult monkeys by performing tyrosine hydroxylase (TH) immunocytochemistry techniques[162]. From that moment, these striatal TH-immunoreactive interneurons have been described in other species such as rat, mice and human[163,164]. Moreover, some studies suggest that there are at least two different populations of TH+ interneurons[165]. Studies regarding their somatic size are quite variable, describing them with a small diameter of 6-12 μm, or up to 20 μm[166]. It is difficult to describe them accurately, and some reports argue that these neurons only appear in lesioned animals, being absent in control ones such as rat[167] or monkey[168]; whereas other studies argue that they are totally absent in rat or mice but present in monkeys[162]. All these differences could be due to variations among species or even to technical artifacts when performing immunocytochemistry techniques.

Other studies which examined the Htr3a-cre mice –a BAC transgenic mouse line expressing cre under the control of the 5HT3a (Htr3a) promoter[169]–, revealed that a percentage of the labelled neurons did not express any of the markers listed above (somatostatin, NOS, tyrosine hydroxylase or calretinin)[131,170]. Based on the electrophysiological and morphological experiments, these neurons were divided into Fast-Adapting Interneurons (FAI)[170] and Spontaneously Active Bursty Interneurons (SABIs)[171].

1.2.3. Astrocytes

Striatal astrocytes are complex cells with multiple levels of branches that emanate from the cell body[172]. In the striatum, a spatial gradient of astrocyte distribution has been described with higher densities accumulated in ventral areas compared to more dorsal areas[173]. Astrocytes are important regulatory elements for different brain functions. They respond to neurotransmitters and release their own gliotransmitters[174] that can regulate synaptic transmission[175,176]. In the dorsal striatum, it has been observed that there is a selective regulation of specific synapses by astrocytes[177], suggesting that they are involved in the coordination of the striatal function and its dysfunction in brain disorders[177]. In the NAc (ventral striatum), astrocytes have been proposed to regulate neuronal excitability, addiction and drug-seeking behaviours[178,179]. A recent study showed that astrocytes are key regulatory elements in dopaminergic signalling in the NAc[180].

1.2.4. Corticostriatal afferents

The striatum is the main input entrance to the BG. The activity of the striatal neurons is mainly determined by excitatory inputs from cortex and thalamus. Therefore, the information that MSNs transmit to the BG output circuits is basically determined by corticostriatal and in a less extent thalamostriatal inputs, together with the striatal microcircuits interactions.

1.2.4.1. Corticostriatal neurons

Layer 5 and in some cases layer 2/3 cortical neurons from most cortical areas provide the majority of cortical input to the striatum. These are pyramidal neurons, and use glutamate as neurotransmitter[2]. Corticostriatal neurons are distinguished based on their projections to other brain areas and their laminar distribution within the cortex. There are two main subtypes of corticostriatal neurons based on the distribution of their axon collaterals when projecting subcortically: the corticostriatal pyramidal tract neurons (PT) and the corticostriatal intratelencephalic neurons (IT) (Fig. 7).

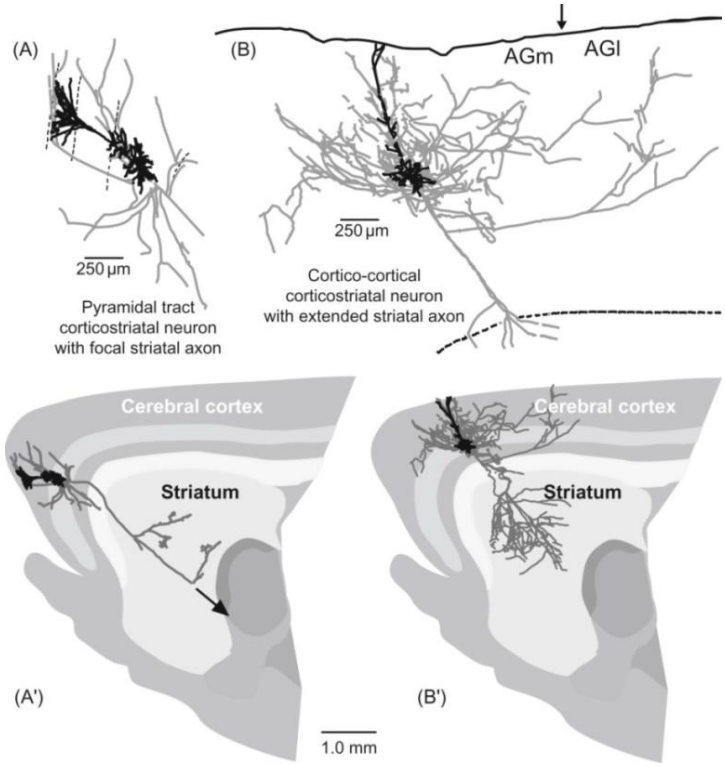

Figure 7. PT and IT cortical projections towards the striatum. Tracing of PT (left) and IT (right) dendrites (in black) and their respective cortical (A, B) and striatal (A', B') axons (in grey). From Handbook of Basal Ganglia Structure and Function[2].

IT corticostriatal neurons are very numerous when present in agranular cortical regions projecting exclusively to ipsi and contralateral striatum and cortex (Fig. 7), with no other subcortical targets[181]. They are mainly located in the superficial half of cortical layer 5 with some of them distributed in layers 2/3[182–184] and are characterized by having a simple apical dendritic tuft and a thin apical dendrite[184,185]. The second type or PT corticostriatal neurons send projections to the thalamus, subthalamic nucleus,

superior colliculus and brainsteam, leaving collaterals in the striatum, but do not project contralaterally to the cortex or the striatum[182,186] (Fig. 7). These neurons are normally placed in the deeper layers of cortical layer 5 and occasionally in layer 4, always deeper when compared to IT neurons. They are characterized by having a complex apical dendritic tuft and a thick apical dendrite[184] (Fig. 7). This corticostriatal projection provides the cortical motor signal that regulates movement. In a recent study, it was found that the proportion of IT neurons is slightly higher than PT neurons [187]. It has also been observed that the soma of PT neurons is larger than the soma of IT neurons[188]. They also differ in their arborisation: IT axons are more extensive than PT axons, which are distributed in a focally manner in the striatum[44].

These two types of neurons project and provide distinct patterns of innervation to the striatum[182], and also display specificity in their targets. Additionally, IT neurons connect with each other and project to PT neurons, but PT neurons do not connect to IT neurons[189]. Therefore, information being processed and transmitted from the cortex is conveying distinct messages[190]. Taking all this together, it has been suggested that PT and IT neurons likely function as distinct information channels[188].

1.2.4.2. Corticostriatal circuits

The cortical inputs that MSNs receive originate from the majority of cortical areas, including primary and higher sensory areas but also motor, premotor and prefontal as well as from limbic areas. The inputs from these areas are organized in a topographic manner where the spatial relationships between the cortical areas are moderately maintained when projecting to the striatum[29,191]. Nevertheless, there is also an important cortical overlapping when axons from the cortex project to the striatum[31]. This topographic organization embodied the idea of the striatal functional regions, where different regions in the striatum have different functional roles depending on the origin of the cortical inputs[4] (Fig. 8, 9). Therefore, dorsolateral regions in the striatum receive inputs from premotor and motor cortical areas, and are characterized as the "sensorimotor" regions of the striatum; the dorsomedial regions receive inputs from frontal cortical areas and are known as the "associative" regions; and the ventral regions receive cortical limbic inputs are characterized as the "limbic" regions of the striatum (Fig. 9). As a result of this, we can find three different areas in the striatum: the sensorimotor, associative and limbic area[192] (Fig. 8, 9). This functional subdivision is present in primates and suggested in rodents and suits perfectly the three areas which compose the striatum: the ventral striatum (VS) and the dorsomedial (DMS) and dorsolateral (DLS) striatum.

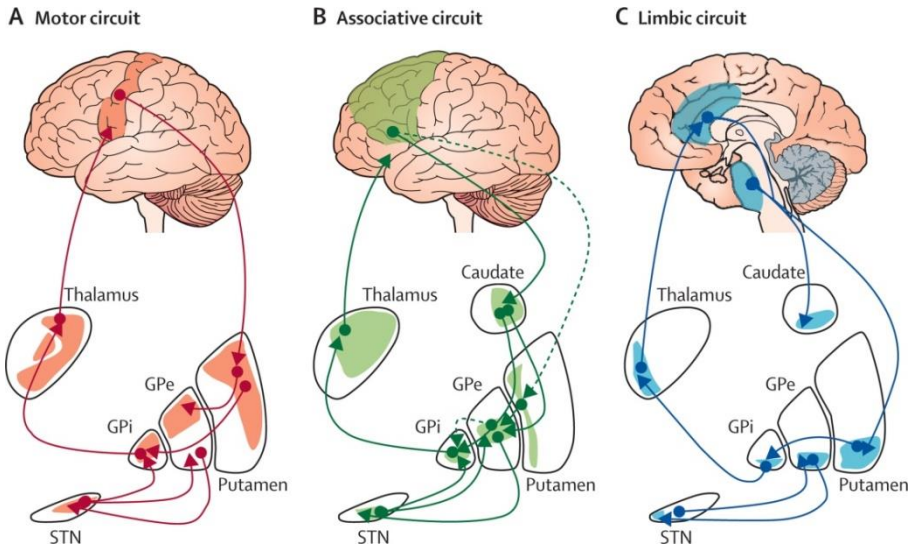

Figure 8. Schematic representation of the functional organisation of the basal ganglia. The basal ganglia is divided into motor (red, motor cortex), associative (green, prefrontal cortex) and limbic (blue, anterior cingulate cortex) regions which are moderately topographically segregated. From Rodriguez-Oroz et al., 2009[192].

Motor and premotor corticostriatal projections extend through the most lateral part of the DS and were the first to be identified[193]. This lateral region of the DS also receives overlapping projections from parietal areas that are associated with somatosensory function[194] (Fig. 8). Different studies support this association, demonstrating somatotopic maps and neuronal response to specific movement[195]. Therefore, this area mediates different aspects of motor behaviour such as planning, learning and execution[194]. Frontomedial corticostriatal axons extend their projections to the most medial part of the DS (Fig. 8). This medial part of DS has been linked to reward[196,197], motivation and higher cognition behaviours [194]. The amygdala, which is a limbic structure that plays a key role in emotion, also projects to the medial region of the DS[198]. Moreover, the basolateral nuclear group, which process higher-order sensory inputs, is the main amygdaloid input to the ventral striatum or NAc[199,200] (Fig. 9), although this area of the striatum also receives corticostriatal projections from frontal cortical areas, especially from the orbitofrontal cortex (OFC) and the ventromedial prefrontal cortex (vmPFC).

Although this topographic organization gives rise to three distinguishable areas in the striatum, the truth is that there is a great overlapping of corticostriatal projections that come from functionally related cortical areas. This will impact on how these areas functionally define the striatum.

1.2.5. Thalamostriatal connections

The structure of the thalamus comprises a large variety of diverse thalamic nuclei –as many as 50 have been identified[201]–, which are involved in several processes. It has been reported that some of them receive information from different sensory organs and then project to specific areas of the cortex, whereas other nuclei participate in motor

functions[201]. In addition, it has been generally believed that these different nuclei act as a relay station which transmits information between different subcortical areas and the cerebral cortex[2,202]. Besides being connected to the cerebral cortex, it also targets other subcortical nuclei such as the striatum[3]. Thalamostriatal signalling is primary excitatory using glutamate as neurotransmitter, although is regulated by inhibitory mechanisms. Nevertheless, the functional role of the thalamostriatal system[203] is still poorly understood.

The main source of thalamostriatal afferents in the striatum is the centre median/parafascicular nuclei complex (CM/Pf)[2,204–206], which in turn receives fibres from the cerebral cortex as well as other nuclei[207,208]. Although there are thalamic nuclei which receive visual, somatosensory or auditory information from the periphery and are considered as "sensory nuclei", this does not occur for this complex. Their functions are related to orientation and to the appropriate action selection for unexpected situations[209,210], and they have also been involved in the modulation of pain[211]. In addition, in rodents, the midline thalamic nuclei project mainly to the ventral striatum, although inputs to dorsal regions have also been reported[212–214]. In fact, it has been observed that the medial posterior thalamic nuclei (POm) sends projections towards the DLS[215]. However, POm neurons evoke weak responses when whisker deflection is performed under ketamine and urethane anaesthetics[216,217]. In addition, the blockage of S1 by TTX injections blocks the whisker responses in the DLS[218].

Based on the anatomical afferents between sections of the CM/Pf and the striatum, thalamostriatal axons project to the previously defined subregions of the striatum, namely: sensorimotor, associative and limbic. The rostral Pf is the main source of inputs to the limbic region of the striatum, the lateral part of the Pf is connected with the associative region, and the medial part of the CM is projecting towards the sensorimotor striatum[213,214]. When projecting, thalamostriatal CM/Pf neurons target the dendritic shafts of direct and indirect MSNs[219–221], as well as interneurons[119,213,221,222]. As mentioned, the thalamus has multiple functions. However, its role in the pallidal and nigral territories as well as in the BG system is recognized but still not fully understood. It has been observed that the deep brain stimulation of the CM/Pf complex ameliorates some of the motor symptoms of Tourette's syndrome as well as Parkinson's disease[2], generating interest in this system. In addition, it has been suggested that CM/Pf neurons could transmit information related to attentional values to the MSNs and play a role in regulating reward-related information processing of ChIs[205].

1.2.6. Striatum organization

The dorsal rodent striatum has always been considered a very homogeneous structure. This is mainly due to the lack of physical boundaries and its cytoarchitectural organization. Nevertheless, the striatum can still be organized in different regions with their own properties which are involved in different processes.

1.2.6.1. Dorsal and ventral striatum

The striatum is mainly comprised of the dorsal striatum (DS) and the ventral striatum (VS). The DS comprises the *caudate* nucleus and the *putamen*, which in primates and humans is separated by the internal capsule. Nevertheless, in rodents, the dorsolateral and dorsomedial striatal regions merge with the NAc. In humans, the NAc and the rostroventral caudate and putamen form the VS. Additionally, the olfactory tubercle and the rostrolateral portion of the anterior perforated space adjacent to the lateral olfactory tract are also included in the VS in primates[194]. The shell region, which is a subterritory of the VS, divides the VS in two parts: a medial/ventral shell region, and a core region[223]. Different studies in rodents have demonstrated the organization of shell and core and their relationship to different ventral striatal afferent and efferent projections[224,225].

The VS, the NAc in particular, is involved in mediating reward, cognition, reinforcement and motivational salience; whereas the DS is primarily involved in motor function, executive functions and stimulus-response learning[226–230]. There is a small degree of overlap, as the DS is also a component of the reward system, which together with the NAc core, mediates the encoding of new motor programs associated with future reward acquisitions, such as the motor response to a reward cue[226,228]. In addition, the VS has been linked to emotional coding of environmental stimuli and motivation[194].

1.2.6.2. Patch and matrix compartments

Under a light microscope, the striatum exhibits a uniform appearance due to the lack of any physical boundary. However, it has been noticed that there are neurochemical markers that label "patches" of the striatum, while other markers label the matrix surrounding these patches[231,232]. This patch/matrix organization is quite important during development[233]. Patch compartments represent approximately 10% of the total striatal volume and are identified by a dense μ-opioid receptor binding[234], substance P staining and a poor staining for cholinergic markers[231]. Due to the few cholinergic markers in the patches, cholinergic modulation is probably less present in these compartments. On the other hand, matrix compartments are identified by a rich acetylcholinesterase and choline acetyltransferase staining[145], as well as immunoreactivity for calbindin[135] and somatostatin. They seem to be strongly regulated by dopamine and acetylcholine.

Although different studies have demonstrated that the majority of cortical areas provide inputs to both compartments, it has been suggested that different cortical areas would project differently to the matrix or patch compartments[135,231,235–237]. In addition, it has been shown that neurons in different sublayers of layer 5 of the cortex project differently to matrix and patch compartments[238]. Normally, neurons that project to patch compartments are located in deep layer 5, whereas those projecting to matrix compartments are located in superficial layer 5.

1.2.6.3. Dorsomedial and dorsolateral striatum

In primates and other mammals, the DS is formed by two different nuclei: the *caudate* nucleus and the *putamen*, which are anatomically separated by the internal capsule (Fig. 9). Nevertheless, in rodents, the dorsal striatum does not have a proper cytoarchitectural organization as for example happens with the laminar organization of the cortex or the hippocampus. Due to this property, and together with multiple overlapping axonal connections from cortex[31,43,44], the rodent dorsal striatum has been considered an anatomically homogeneous structure. However, in the last few decades, more and more research has tried to divide the DS in two different regions defined by their behavioural roles[53,239]: the dorsomedial (DMS) and dorsolateral (DLS) striatum.

DMS and DLS striatal regions both participate in motor control, nevertheless, DMS regulates action-outcome associations, goal-directed actions, flexible shifting between behavioural strategies and in general, is related to higher cognitive behaviours; whereas DLS mediates habit, stimulus-response associations and navigation[239–241]. According to this, it has been stated that the DMS corresponds to the associative striatum, while DLS corresponds to the sensorimotor striatum[242] (Fig. 9). Therefore, the DMS has been compared to the *caudate* nucleus and the DLS to the *putamen*, based on their different roles in behaviour.

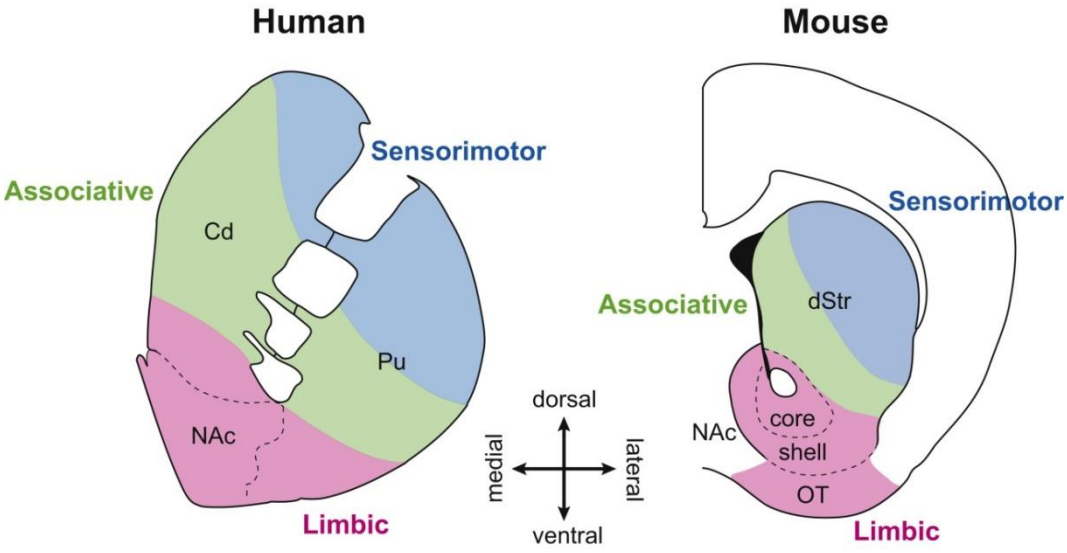

Figure 9. Schematic representation of the functional subdivision of the striatum in humans (left) and rodents (right). Notice the internal capsule separating the caudate from the putamen in human, not present in rodents. Cd: *caudate* nucleus; Pu: *putamen*; dStr: dorsal striatum; OT: olfactory tubercle; NAc: *Nucleus accumbens*. From Chuhma et al., 2017[243].

However, due to the absence of anatomical borders, the overlapping projections from different cortical areas, and the coincidence of some behavioural roles for both regions, a functional characterization of both striatal territories was needed. A recent study from our laboratory demonstrated that the rodent DS is organized into two non-overlapping

circuits with particular attributes and dynamics[63]. In this study, it was shown that DMS and DLS regions are two functional regions divided by a sharp functional boundary, differing in their coupling to multiple cortical regions, the integration of cortical activity and the properties of the direct and indirect MSNs. These results will have to be considered in next studies and give a new understanding to these two regions, which had only been tried to be divided based on their anatomy and behavioural roles, without a proper functional characterization.

Interestingly, cortical axons from sensory areas differ when sending projections to the DLS and DMS and transmit different sensory modalities like tactile, auditory or visual[244]. Several years ago, Reig & Silberberg observed that single neurons from the DMS are able to integrate information from different sensory modalities, specifically tactile and visual[53]. In addition, these striatal neurons were even able to integrate bimodal inputs (simultaneous tactile and visual stimulation). This occurs because primary somatosensory cortex (S1) sends projections to DLS, and with less density, to the DMS. On the other hand, axons from primary visual cortex (V1) only target the DMS[53]. In this study, authors described the temporal properties of visual and tactile integration in DMS-MSNs. The bimodal stimulation (simultaneous whisker and visual stimulation) did not generate a bigger response when compared to the independent single tactile and visual stimulation (Fig. 10). This is explained because the visual response is tens of milliseconds slower than the tactile one, providing a temporal delay between both responses. Only when the onset or peak delay of visual and tactile responses were forced to occur synchronously, –setting the time for the tactile stimulation–, the amplitude of the bimodal response increased[53] (Fig. 10), thus promoting the suitable time window for the synaptic integration between stimuli.

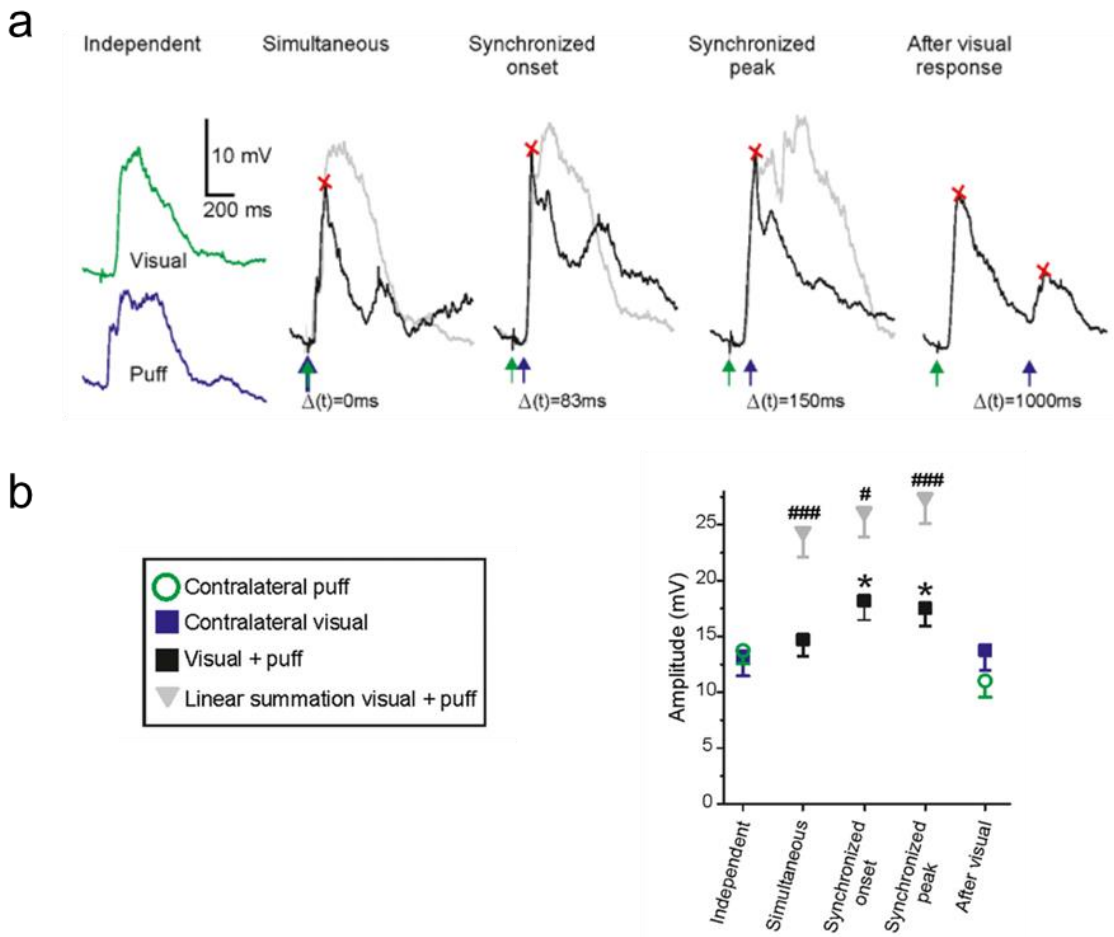

Figure 10. Tactile and visual response temporal integration. a, Waveform averages of (left to right): independent tactile and visual stimulation; simultaneous visual and tactile stimulation; synchronized visual and tactile onset stimulation; synchronized visual and tactile peak stimulation and tactile stimulation following the visual response. Red crosses indicate the maximum amplitude of the evoked response. Grey traces represent the simulated linear summation of the visual and tactile responses for the corresponding interstimuli intervals. **b,** Average of bimodal amplitude of visual and tactile stimulation presented as described in a. Grey triangles represent the amplitude of the respective linear summation for the different intervals. Adapted from Reig & Silberberg, 2014[53].

1.3. THE NIGROSTRIATAL PATHWAY

Dopaminergic and GABAergic neurons can be found in the ventral midbrain area. The dopaminergic neurons of this area, which are located in a) the ventral tegmental area (VTA), which is the most ventro-medial region of the midbrain; b) the *Substantia nigra* (SN) (*reticulata* (SNr) and *pars compacta* (SNc)); and c) the retrorubal area (RR), dorsal and caudal to the SN[245] (Fig. 11), give rise to the nigrostriatal system.

1.3.1. The *Substantia nigra*

The *Substantia nigra* is composed of dopaminergic and GABAergic neurons[246,247]. Dopaminergic neurons are mostly located on the dorsal part of the *Substantia nigra*, termed *pars compacta* (SNc)[245], but they are also located in the ventral part of it, termed *pars reticulata* (SNr). From the SNc, dopaminergic neurons provide massive inputs to the striatum, whereas dopaminergic neurons from the SNr send fewer inputs into other forebrain areas[2,135,245].

The *Substantia nigra* has a critical role in modulating motor movement and reward functions[248]. In fact, the nigrostriatal pathway –which is composed by the projections from the SNc to the striatum–, are critically involved in the motor deficits observed in PD. But the SN is also related to other brain functions such as eye movement[249], motor planning, reward-seeking[250,251], learning and addiction[250]. Many of the SN effects are mediated through the striatum. The SNc serves mainly as a neuromodulatory input to the BG circuitry, supplying the striatum with dopamine; whilst the SNr acts as an output, conveying the signals from the BG circuit to other brain structures[2].

1.3.2. Dopaminergic neurons from the *Substantia nigra*

Dopaminergic neurons are spontaneously active *in vivo* and *in vitro*[252–254]. When recorded *in vitro*, almost all the dopaminergic neurons exhibit a slow, very regular, tonic firing pattern[255]. This tonic firing persists in the absence of synaptic inputs, suggesting that this activity is generated intrinsically[253]. However, when the dopaminergic neurons are recorded *in vivo*, they exhibit a variety of different firing patterns[255–257]. These firing patterns can be classified as a) tonic; b) random and c) bursting modes[252,255]. The burst mode, which is characterized by clusters of two to eight spikes, is the most efficacious mode to increase the terminal dopamine levels, especially in the nigrostriatal pathway[255]. On the other hand, the tonic pattern is characterized by single spikes firing in a clock-like manner that are interrupted by infrequent bursts[252,258,259]. In awake animals it has been observed that the dopaminergic neurons burst at approximately 20 Hz of frequency during resting periods[258], whereas they increase their firing rate up to 30 Hz when performing a task[258,260]. Nevertheless, in the case of anaesthetised animals, values can range from 12-16 Hz[256,257,261], until 20 Hz[256]. Cells displaying these three modes can be found in both, the SNc and SNr[252].

1.3.3. Nigrostriatal pathway afferents and efferents

The main input arriving to SN is composed by GABAergic projections from the striatal direct MSNs and GPe neurons[255]. In addition, excitatory inputs from the STN also project towards the SN[255]. In turn, the specific nuclei to which the GABAergic neurons from the SNr send their nigral efferents differ across species due to the different cortical organization[2]. In rodents, the principal targets of the SNr are the ventromedial thalamic nuclei, which provides input to frontal cortical areas; and the paralaminar medial dorsal thalamus, which in turn projects to the cortical areas thought to be equivalent to the frontal eye fields in primates[2]. But the SNr GABAergic neurons are also characterized by projecting axon collaterals towards the neighbouring areas of the SNc and SNr, which will inhibit dopaminergic and GABAergic neurons[259,262].

The main nigrostriatal efferent from midbrain dopaminergic neurons innervates densely the striatum. These projections are distinguished and localized into two sets of dopaminergic neurons: the dorsal and the ventral tier (Fig. 11). This division has been suggested based on the neuronal localisation, morphology of neuronal dendrites, the expression of the calbindin protein and the innervation of patch or matrix compartments[245]. The dorsal tier includes the dopaminergic neurons that project to the striatum that are situated in the VTA, the dorsal part of the SNc and the RR (Fig. 11). These neurons extend their dendrites in the *pars compacta* and express calbindin as well as dopamine. Here, dorsal tier midbrain neurons situated more medially –such as the ones from the VTA–, project ventrally to the striatum (NAc); whereas the ones situated more lateral and caudal –such as the ones from the SNc– project to the dorsal striatum[2]. The ventral tier includes dopaminergic neurons situated in the ventral part of the *SNc* and groups of cells that are embedded in the SNr (Fig. 11). Different to dorsal tier neurons, ventral tier neurons extend their dendrites intro the *pars reticulata* and do not express calbindin. These neurons also display a topographic organization when projecting to the striatum[2].

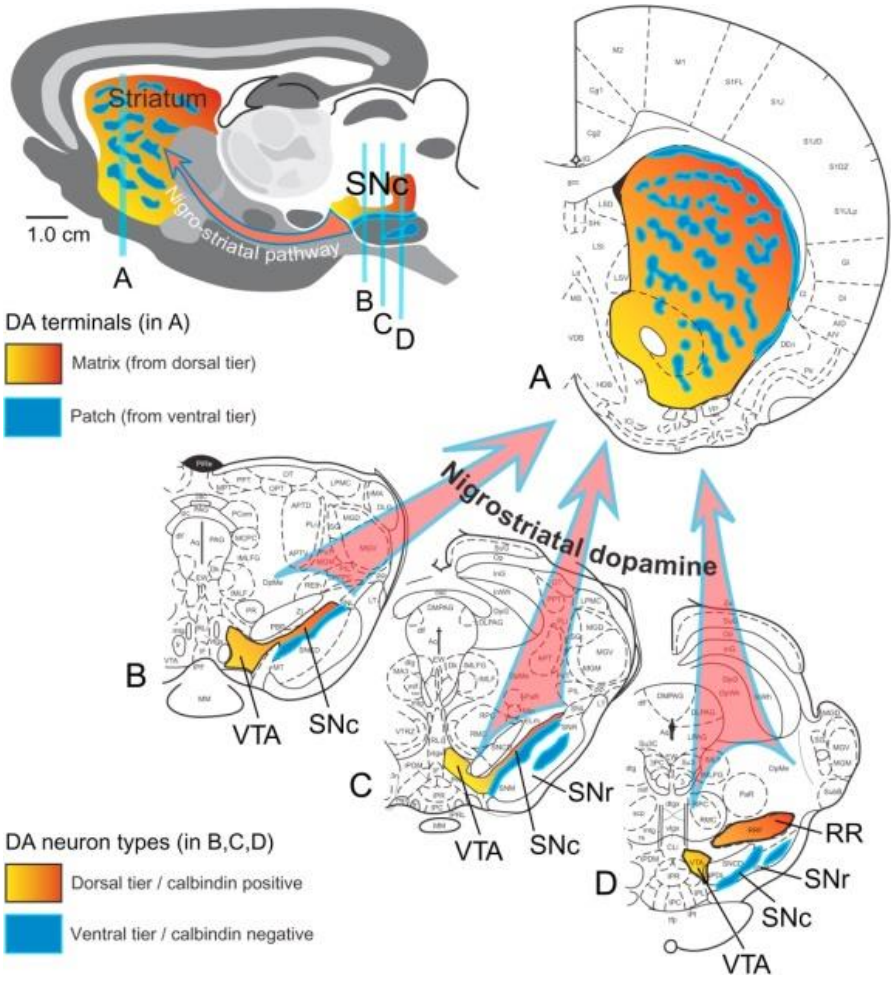

Figure 11. Nigrostriatal dopamine pathway innervation. Schematic representation of the organization of the dopaminergic projection from the midbrain areas towards the dorsal and ventral striatum (sagittal section, upper left). The coronal sections show the innervation of the dorsal and ventral striatum by different sets of midbrain dopaminergic neurons. From Handbook of Basal Ganglia Structure and Function[2].

1.4. DOPAMINE SIGNALLING AND MODULATION

1.4.1. Overview

Dopamine (DA, a contraction of 3,4-**d**ihydr**o**xy**p**henethyl**amine**), first identified in 1957[263], is one catecholamine neurotransmitter out of the five established biogenic amine neurotransmitters. DA works as a hormone and as a neurotransmitter largely studied through history, and its most important role involves the regulation of the activity of different functional networks in several brain structures[264]. It is produced by the action of dihydroxyphenylalanine (DOPA) decarboxylase on DOPA. Following its synthesis in the cytoplasm of presynaptic terminals, a vesicular monoamine transporter (VMAT) loads it into synaptic vesicles[3]. When DA is released, it works through G-protein coupled receptors. The majority of dopaminergic receptor subtypes either activate or inhibit adenyl cyclase (AC)[3]. The major effect that DA has into MSNs is mainly directed to the dendritic shafts and spine necks to modulate the excitatory input that is directed through the dendritic spines. Later, this effect is either terminated by the reuptake of DA into the nerve terminals or either by surrounding glial cells by a Na^+ dependent DA transporter (DAT)[265].

Over the years, DA has been linked to a large variety of functions and processes. It has been related to a great range of complex behaviours such as executive functions, motor control, arousal, reinforcement and reward[266]. For instance, DA has been reported to modulate the auditory midbrain processing of unexpected sensory inputs[267]. It is important to notice that there exist differences when it comes to DA release and its modulation depending on the striatal region[268]. For instance, it has been observed that DA modulates learning and goal-directed behaviours in the DMS, whereas it modulates habit formation in the DLS[241,269,270]. Changes in DA levels due to rewarding or adverse stimuli modulate MSNs activity in different manners by facilitating or depressing the activity of the direct and indirect pathways. Also, it has been described that DA depletion affects tactile responses in the DLS[62]. Moreover, it has been suggested by a computational model that an increased DA level boosts the network synchronization of direct MSNs activity, whereas the reverse was postulated for indirect MSNs[271].

Dysregulations of DA levels in the striatum have been implicated in several brain disorders such as obsessive compulsive disorder or attention deficit and hyperactivity disorder. Moreover, it has been linked to other mental problems like schizophrenia, psychosis or drug addiction[272,273]. Nevertheless, is specially implicated in Parkinson's disease.

1.4.2. Dopamine receptors

Dopamine receptors have attracted a lot of attention due to their use as targets for drugs in the treatment of schizophrenia and several BG disorders[274,275]. These receptors are G-protein coupled receptors that are divided into two subfamilies: D1-like receptors

(including D1 and D5), which stimulate AC; and D2-like receptors (including D2, D3 and D4) which inhibit AC[276]. Among these, D1 and D2 receptors are enriched in the striatum as well as in its projection areas. As mentioned before, D1 receptor is enriched in direct MSNs, whereas D2 receptor is enriched in indirect MSNs. Only around a 1% of MSNs in the striatum co-expresses both receptors[95]. D3 receptor is expressed in lower amounts in ventral striatum in direct and indirect MSNs. D4 receptor is mainly localized in the cerebral cortex as well as D5. This last receptor, additionally, is also enriched in striatal interneurons[277]. In the subthalamus there is also expression of a spectrum of dopamine receptors including D1, D2, D3 and D5[278,279]. In addition, it has been suggested the existence of D6 and D7 DA receptors, but such receptors have not been conclusively identified[280,281]. It has been reported that the affitiny of D2-like receptors for DA is generally 10 to 100-fold greater than that of D1-like receptors; where D3 and D4 display the highest sensitivity for DA, and D1 receptors the lowest[137,282].

1.4.2.1. D1 dopamine receptors

D1 dopamine receptors (D1DRs) are known to be involved in several important roles in learning and memory, locomotor activity and reward mechanisms. Moreover, they are involved in the symptoms of some neuropsychiatric disorders[6,283]. They are mainly expressed in the DS, NAc, SNr and the olfactory bulb[284,285]. They are also expressed, although at lower levels, in dorsolateral prefrontal cortex, cingulate cortex and the hippocampus[285,286]. In striatal MSNs, D1DRs are highly concentrated in dendritic spines including spine heads and the post-synaptic density of neurons[287] where they can modulate spine function[288]. The existence of pre-synaptic D1 autoreceptors which regulate DA release has been observed[289], whereas the presence of pre-synaptic D1 heteroreceptors is controversial[287,289,290]. The activation of post-synaptic D1DRs stimulates the heterotrimeric G-proteins $G_{\alpha s}$ and $G_{\alpha olf}$, which are positively coupled to AC, therefore increasing cAMP levels and leading to the activation of protein kinase A (PKA) and the phosphorylation of a variety of intracellular targets such as transcription factors, voltage-dependent channels or enzymes[291].

1.4.2.2. D2 dopamine receptors

The genes encoding for D2 dopamine receptors (D2DRs) contain several exons that are alternative spliced, giving rise to isoforms with different physiological properties[137]. These isoforms are the short and long variants of D2DRs. Both are present in the striatum, although the long isoform is the most abundant[292]. D2DRs activate $G_{\alpha i}$ and $G_{\alpha o}$ proteins, which will inhibit AC and limit the PKA activation[293,294].They are mainly expressed in the striatum, GPe, SNc, NAc, amygdala, cerebral cortex, hippocampus and pituitary[295,296]. They have been related to several complex processes such as locomotion, learning or memory[297]. Additionally, they have an important role in post-synaptic receptor-mediated extrapyramidal and behavioural activity[297]. In the striatum, D2DRs can function as pre- and post-synaptic receptors. It has been reported that the

short isoform of D2DRs regulates the synthesis and release of DA functioning pre-synaptically; whereas the long isoform of D2DRs mediate G-protein dependent and independent signalling post-synaptically[298].

1.4.3. Dopaminergic modulation

DA has been known as a critical modulator of striatal information processing from cortical and thalamic signals. How DA affects and modulates this processing is important for a wide range of psychomotor functions that take place in the BG such as habit learning or control of serial movement[102,299]. But the answer to how does DA modulate network processing is not trivial. Classically, it has been thought that DA was either excitatory or inhibitory based on synaptic transmission studies. Nevertheless, it is now known that DA does not modulate cellular function through ionotropic receptors which would depolarize or hyperpolarize the cell; but it activates G-protein coupled receptors that will modify how neurons respond to external signals. The signalling of G-protein coupled receptors is more than two orders of magnitude slower than that of ionotropic receptors[296]. This led to the assumption that DA is a volume transmitter which signals slowly and inaccurately. Nevertheless, recent studies have reported the existence of sparse secretory "hotspots" in the striatal dopaminergic axons[300]. Different reports propose that DA can be released rapidly and synchronously in these sites to generate an extracellular DA signal with rapid kinetics which relies on the Ca^{+2} sensor synaptotagmin-1[301]. It has been suggested that this mechanism may support already seen fast and precise DA coding functions in several processes such as locomotion[302] or spine plasticity[303].

In the case of the striatum, one of the main complexities is the existence of two different neuronal subpopulations which differ in their DA receptors expression[93,304], and cannot be identified based on their morphology or electrophysiological properties. In addition, these two types of dopaminergic receptors can function pre- and post-synaptically. Moreover, both subpopulations are embedded in their own microcircuit involving other MSNs and interneurons that are also modulated by DA. Due to this, it is very difficult to know exactly how DA is affecting directly and indirectly into the network. In the mid 1980's, when it was discovered that the direct pathway expressed high levels of substance P whereas the indirect pathway expressed enkephalin; it was observed that after DA-depleting lesions, striatal levels of enkephalin increased while substance P levels fell. In posterior studies it has been demonstrated the dichotomous expression and the differential dopaminergic modulation of neurons expressing D1- and D2DRs, even in the lamprey, which belongs to the oldest group of living vertebrates[305]. This supports the idea that DA is differentially modulating direct and indirect MSNs[306].

Three decades ago appeared what today is known as the "classical" model of how DA shapes and affects striatal activity[102]. In this model, by effect of DA, D1DRs would excite MSNs from the direct pathway, whilst D2DRs would inhibit MSNs from the indirect pathway. These effects were envisioned as acute and easy to reverse. Later studies have been quite consistent with the classical model, showing that the

dopaminergic activation of G-protein coupled receptors excites or inhibits MSNs by modulating the trafficking of voltage-dependent and ionotropic ion channels, therefore altering the excitability of cells, and finally, their output. But DA does not only modulate MSNs activity, it also modulates ChIs, which co-expresses D2 and D5 DA receptors[287,307,308].

1.4.3.1. D1 dopamine receptor modulation

Direct MSNs express D1DRs at high levels[309]. These receptors are positively coupled to AC[310], which increases cytosolic cAMP levels, leads to the activation of protein kinase A (PKA) and to the phosphorylation of a variety of intracellular targets[291], that in the end alters the cellular function. D1DRs stimulation has been reported to increase Cav1 L-type Ca^{+2} channel currents and decrease somatic K^+ A_s-currents[311–313], which potentiates Up state transitions, excitatory synaptic potentials and action potential discharge[80,137,311]. A number of studies have reported that D1/PKA cascade has direct effects on AMPA and NMDA receptor trafficking and function. For instance, D1DRs activation of PKA increases the expression of AMPA and NMDA receptors in the cell surface[24,314]. The mechanisms underlying this trafficking are still being studied, but several reports have suggested that the effect of D1DRs on NMDA currents is indirect and mediated by voltage-dependent channels[24,315]. In addition, across these years, voltage-dependent Na^+ channels were one of the first well-characterized targets of D1DR pathway in MSNs. Studies using the voltage-clamp technique have shown that D1DRs signalling led to a reduction in Na^+ channel availability with no alteration of voltage-dependence of fast activation or inactivation[316].

When the membrane potential of the cell is held for several hundred of milliseconds near the Up state potential (around -50 mV)[73], D1DRs stimulation produces quite a different effect compared to when it is held at the Down state potential (around -80 mV). When in the Up state membrane potential, the ion channels configuration governing the activity is re-configured. In this state, D1DRs stimulation increases the response to intrasomatic current injection[313]. This enhanced response is partly due to an increased opening of L-type Ca^{+2} channels after PKA phosphorylation[312,317]. The increased opening of these channels and NMDA receptors[79,318–320], makes the D1DRs stimulation able to promote synaptically driven plateau potentials of MSNs (similar to *in vivo* Up states) in slices[80].

In the case of sensory processing, there are two studies suggesting that DA affects sensory responses of direct MSNs located in the DLS. In 6-OHDA depleted rodents, a model used to study Parkinson's Disease, it has been observed an impairment of tactile sensory responses recovered by administration of L-DOPA[62]. On the other hand, in healthy rodents it has been observed an amplitude increase of the tactile response when preceded by a reward[50]. A "reward" is a concept used to describe the positive value that a human or animal assigns to an object, physical state or behaviour[321]. Several studies support that dopaminergic neurons construct and distribute information about rewarding

events[250,321,322], implicating midbrain dopaminergic activity in the reward dependent learning[321].

Taking this information together, these results suggest that the activation of D1DRs and the subsequent signalling through PKA increases the responsiveness of direct pathway MSNs to sustained or synchronous synaptic release of glutamate, but reduces the response to transient or uncoordinated glutamate release which is not able to depolarize the membrane for more than few tens of milliseconds[24].

1.4.3.2. D2 dopamine receptor modulation

Contrary to D1DRs, D2DRs are highly expressed in indirect MSNs. In the case of D2DRs, they are negatively coupled to AC[323].The activation of D2DRs signalling reduces inward, depolarizing channels through Cav1 (L-type) Ca^{+2} channels and Nav1 Na^{+} channels, while increasing outward, hyperpolarizing K^{+} channel currents[24,316]. In addition, their activation is capable to stimulate phospholipase Cb isoforms that in the end generate diacylglycerol (DAG) and protein kinase C (PKC) activation, as well as the mobilization of intracellular Ca^{+2} stores[324,325]. They are also capable of transactivating tyrosine kinases[326]. Moreover, it has been reported that dopaminergic D2 agonists elicit endocannabinoid (eCB) release in the striatum *in vivo*[327,328] by stimulating anandamide release[329], which is a highly potent endogenous agonist of CB1 and CB2 cannabinoid receptors. CB1 receptor expression levels are highest in the DLS and decrease along a ventromedial gradient[330]. In addition, the activation of CB1 receptors by cannabinoid agonists affects the corticostriatal and corticosubthalamic transmission in the medial prefrontal BG circuits[331], which are related to functions such as decision making, goal-directed behaviour, emotions, motivation or cognition[332]. Finally, it has also been reported that these receptors regulate dopaminergic neuronal activity by increasing DA neurons firing in the SNc and VTA[333], and DA release in the NAc *in vivo*[334].

Similar to what happens with D1DRs signalling; there are several studies that show that D2DRs signalling alters glutamate receptor function in dorsal striatal MSNs. The activation of these receptors has reported to decrease AMPA receptor currents of MSNs in slices[79,335]. In fact, when using acutely isolated neurons and voltage-clamp techniques, it has been shown a direct action on dendritic AMPA receptors[335]. D2DRs signalling leads to the phosphorylation of the GluR1 subunit, which promotes trafficking of AMPA receptors outside the synaptic membrane[336]. Moreover, D2DRs stimulation diminishes presynaptic release of glutamate[337].

Different studies of voltage-dependent channels agree with the proposition that D2DRs reduce the excitability of indirect MSNs and their response to glutamatergic synaptic input. The mobilization of intracellular Ca^{+2} through D2DRs leads to the negative modulation of Cav1.3 Ca^{+2} channels[325,338]. The activation of D2DRs reduces the opening of voltage-dependent Na^{+} channels[316]; as well as promotes the opening of K^{+} channels[339]. This ion channels modulation provides a mechanism for the ability of

D2DRs to reduce the responsiveness of MSNs in slices at Up state membrane potentials[325].

Taking this information together, these results suggest that the activation of D2DRs and the subsequent negative coupling to AC, which in turn inhibits the phosphorylation of intracellular targets by PKA, reduces the action of excitatory transmission therefore decreasing the responsiveness and excitability of indirect pathway MSNs.

1.4.3.3. Cholinergic interneurons modulation

The majority, if not all of the different types of interneurons in the striatum express DA receptors[126]. Due to this, when thinking how DA influences MSNs activity, it cannot be ignored the contribution of striatal interneurons. In fact, the major contributors when influencing striatal circuitry are ChIs. Additionally, it is known that ChIs also respond to tactile inputs in the DLS[53] and can therefore modulate MSNs responses.

Although ChIs comprise only 1-2% of striatal neurons, they control striatal circuits with their large axonal fields[115,116]. Also, the most prominent direct dopaminergic synaptic connection is observed in ChIs[340]. In primates, ChIs are involved in associative and motor learning functions[6], presumably mediated by alterations in the strength of MSNs glutamatergic synapsis. ChIs express both D2 and D5 DA receptors. D5DRs activation depolarizes ChIs through a cAMP dependent mechanism[341]. However, D2DRs activation inhibits voltage-sensitive Na^+ channels that reduce their excitability[342]. Therefore, these receptors exert opposite effects on ChIs excitability[343]. Besides expressing D2 and D5 DA receptors, ChIs also possess M2 and M4 acetylcholine (ACh) receptors[307,344]. The interplay between DA and ACh is also important for BG function, as it has been assumed that they counterbalance each other[345], where the increase in DA is associated with a decrease in the acetylcholine levels in the striatum. In addition, the balance of DA and Ach has been related to several processes, such as addiction[346] and reward-dependent learning[123,347–349].

As mentioned before, dopaminergic neurons from the SNc send massive inputs to the dorsal striatum. It has been previously shown that dopaminergic neurons have different functions depending on the striatal region they target (regarding DS and NAc)[251,340]. In addition, dopaminergic neurons make monosynaptic connections with ChIs[155] with striking region heterogeneity[243]. In the case of the dorsal striatum, it has been shown that dopaminergic bursts pause ChIs tonic firing[125,350], supporting the idea that DA release directly inhibits ChIs. In addition, DA release also exhibits changes in the dorsal striatal region they target (namely, DLS and DMS), causing variations in the strength of the signal[350]. Furthermore, there is a gradient of ChIs across dorsal striatal regions, in which a different impact occurs after the action potentials burst from dopaminergic neurons. DA release inhibits ChIs firing during approximately 1 second in the DMS (Fig. 12), whereas shorter inhibition followed by a rebound of spikes was described for the DLS-ChIs[350] (Fig. 12). This inhibition is mediated by D2DRs, as previously shown by others[115,340]. Classically, DA has been thought to function as a modulatory

transmitter. In conditioning tasks, ChIs –which normally are tonically active–, show a pause in their activity when DA is released during reward learning[123,347,348]. During this pause, an increase in DA levels and cessation of ACh release occurs simultaneously[349]. After conditioning, these pauses are highly coordinated with the learnt behaviour[6]. Therefore, ChIs pauses have been related with reward-learning and it has been proposed that dopaminergic bursts would be the ones mediating these type of plastic processes[6].

The regional heterogeneity displayed by ChIs in the dorsal striatum proposes that dopaminergic neurons do not display homogenous actions as previously thought, and suggests that ChIs pauses could convey discrete temporal information[340].

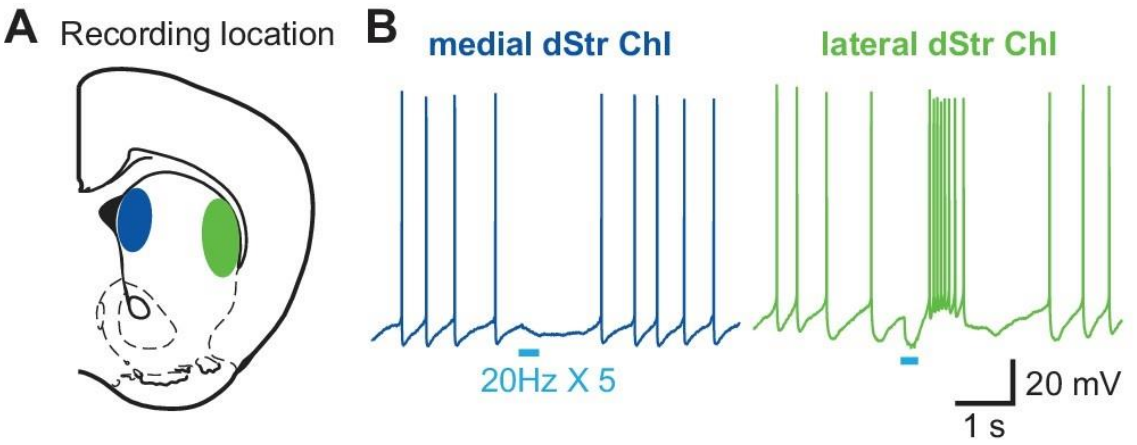

Figure 12. Differential ChIs response to DA release *in vitro* depending of the dorsal striatal region. **A,** Dopaminergic neuron terminals are activated optogenetically while recording ChIs in the DMS (blue) or the DLS (green). **B,** Optogenetic stimulation (light blue bars) pauses ChIs firing in the DMS, while pauses and increases ChIs firing in the DLS. Adapted from Chuhma et al., 2018[350].

1.5. BASAL GANGLIA DYSFUNCTION

The different nuclei which in the end conform the BG are components of a family of a parallel closed cortical-subcortical circuit, where the information sent from a cortical area to the BG is then processed and finally returned to the respective frontal cortical area by a feedback signal via the thalamus[351,352]. The traditional view sees BG nuclei as processing modules with shared anatomical functions whose specific purposes are determined by the cortical regions they receive the information from. Depending on the involved cortical region, the circuits are classified as motor, associative or limbic[353]. But each one of these divisions comprises numerous subcircuits. Abnormal activities of these circuits may produce symptoms that differ depending on the circuit involved. Diseases of the BG result in a spectrum of movement disorders, ranging from Parkinson's Disease (PD) to chorea and dystonia[354], although cognitive-like diseases can also occur, such as Tourette Syndrome or obsessive compulsive disorder (OCD).

One of the most known disorders that is related to the BG is the PD. PD is a progressive neurodegenerative disorder caused by a decreased dopaminergic transmission in the striatum[355], due to a loss of innervation from dopaminergic neurons in the SNc. In addition, eosinophilic protein deposits –known as Lewy bodies–, can be found in the cytoplasm of the cells[355,356]. Over the years, the scientific community has focused in studying the motor symptoms and their related changes in BG circuits thanks to animal models in which DA depletion can be achieved. In these models, dopaminergic toxins such as 1-methyl-4 phenil-1,2,3,6-tetrahydropyrine (MPTP) or 6-OHDA are used to produce a selective and permanent loss of dopaminergic transmission. Although motor symptoms of this disease can be quite variable, the main ones are mainly "motor", such as akinesia, tremor at rest and muscular rigidity[356–358]. Nevertheless, although PD has always been thought to be a pure "motor" disease, other non-motor symptoms such as depression, several sleep disorders and even cognitive impairment are in fact common complications[356]. Nevertheless, very little is known about the pathophysiology of the cognitive-like symptoms. Similar to what happens with the motor symptoms, cognitive-like symptoms can be quite variable and can also include some forms of dementia. PD can affect different cognition areas, such as attention and executive functions, memory, visuospatial skills and language[23]. Visuospatial skills complications have an added interest, as in PD patients, these complications include problems when processing the visual information[23,359,360]. Importantly, previous studies have shown that the use of sensory cues ameliorates and facilitates the motor problems of PD, even showing that PD patients walk better in the presence of rhythmic auditory cues[361]. Visual stimulation has also been used in order to improve the walking and has proved to ameliorate the stride of PD patients[362,363]. These studies suggest that sensory stimuli must have an important role regarding the striatal function. In addition, cortical axons carrying visual and auditory information project to the DMS.

Another signature of PD are exaggerated beta-band (10-20 Hz) synchronized oscillations of the STN and GPe populations[345,364–367] and some areas of the cortex such

as M2[368]. Therefore, the appearance of these exaggerated beta oscillations are usually taken as a sign of DA depletion. Normally, this aberrant oscillatory activity is reduced by L-DOPA treatment[364,365,367] which comes along with an improvement of motor symptoms[369,370], although L-DOPA induced dyskinesias are still a common complication[108,371]. Different animal models of PD have shown an increase in synchronized oscillatory beta range in the BG[372–378]. In a recent paper from our laboratory which uses a new way to decompose and analyse oscillatory activity, we described beta oscillations in healthy mice and show that they are different when comparing DMS and DLS-MSNs[63].

Besides PD, there are other cognitive-like disorders that can appear in the BG, such as the attention deficit and hyperactivity disorder (ADHD), the Tourette's syndrome (TS) or the obsessive compulsive disorder (OCD); where the dorsal striatum is involved. TS and OCD are characterized by the appearance of motor and vocal tics, and compulsive behaviours and performance of rituals, respectively. ADHD is a developmental cognitive-like disease characterized by a difficulty in paying attention and excessive activity[379]. Some patients also display difficulties in regulating emotions[380,381]. The neuropsychological deficits of ADHD include "top-down" cognitive control over behaviour processes such as sustained attention, working memory and inhibition control. The brain regions involved in these processes are the dorsal striatum, as well as prefrontal cortical areas. In addition, ADHD patients have a significant reduction of the *caudate* nucleus volume[382,383]. Moreover, lesions in the DMS result in an impairment in goal-directed behaviour, especially when tasks require a delayed reward[11].

1.6. MULTISENSORY INTEGRATION

The brain is constantly processing information conveyed by several sensory modalities to create accurate representations of the world so appropriate behaviours can be generated[384–386]. The ability of processing information from a variety of stimuli has an important impact on perception and relies on the binding together of appropriate multisensory signals or stimuli[387]. For a long time it was strongly believed that multisensory integration occurred in high-level brain areas or the cortex[388,389]. Nevertheless, in the past years, "new" subcortical multimodal structures have also been identified such as the striatum[53] or the amygdala[390].

However, the mechanism regarding how the brain combines multisensory signals to produce timed actions accurately is unknown. It is important to notice that there are quite a number of neural and non-neural factors which impact in how long it takes for sensory signals which come from a common source to reach multisensory neurons in the brain. For instance, light will arrive faster to the observer when compared to auditory or tactile inputs as light travels at $3x10^8$ m/s. However, the processing of visual stimulus will be longer when compared to the auditory or tactile ones because the sound transduction by the hair cells is many times faster than the phototransduction in the retina[391] (Fig. 13). A similar thing happens with tactile stimuli. This disparity of delays gives rise to a difference in the response latency of auditory, tactile and visual neurons of around 40-50 milliseconds, longer increased by the neural transmission times of the visual system (Fig. 13). This kind of temporal disparities were also demonstrated to occur in the striatum, where visual responses are tens of milliseconds slower than the tactile responses when being processed in the MSNs[53].

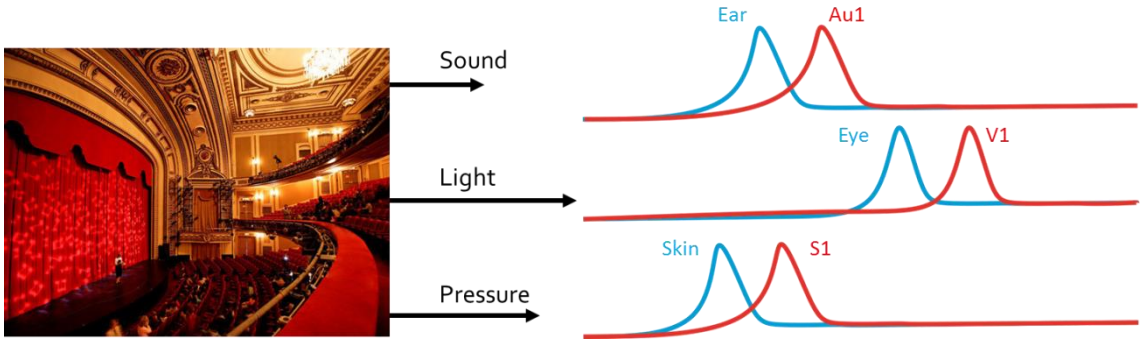

Figure 13. Timing and processing of sensory events in the brain. Due to the relatively fast speed of light, auditory and tactile stimuli reach the observer slightly later than visual stimuli. Nevertheless, auditory and tactile transduction is faster than visual transduction. In addition, the neural transmission time from the sensory organs to the cerebral cortex is longer in the visual system due to the long distances involved. Adapted from King, 2015[387].

In addition, due to the slow velocity of some sensory inputs such as the sound, the time it takes to arrive to the ears scales with distance; whereas light reaches the eye photoreceptors effectively instantaneously at all distances[387]. Therefore, the delay needed to cancel the difference in neural processing time is provided by a relatively

small range, limiting our ability to use temporal synchrony to bind multisensory signals. Importantly, it has been previously reported that the probability to integrate two signals depends on a temporal integration window. If the temporal discrepancy of two signals is within this window, signals will be integrated[392,393]. Previous reports describe that the combination of stimuli from the same sensory source often produces a response depression; whereas the combination of multimodal stimuli produces a response enhancement[394]. In addition, it has been observed that the nervous system is more likely to accept a tactile-visual pair of signals that differ in onset time than an audio-tactile pair of signals when originating from a common source[395]. Taken together, this information confirms the flexibility of neurons to register the relative timing of multisensory signals and highlights the adaptive capabilities of the brain[396,397].

Multisensory integration has been reported in several experimental tasks such as emotional processing[398,399], language[400,401], sensory awareness[402] and time perception[403] among others[404]. Deficits in multisensory integration have been documented in patients suffering from schizophrenia and disorders of the autism spectrum among others[405]. As mentioned in the previous section, PD patients can also display an impaired visual-spatial processing[359,360]. In addition, some patients display a broad spectrum of visual and auditory illusions[360] and hallucinations[406]. Some of them can also exhibit deficits in the detection and discrimination of sensory cues[407]. In addition, the temporal processing of sensory data can also be abnormal[408] and they can display an impaired detection of paired visual, tactile and auditory stimuli[409]. Interestingly, the administration of dopaminergic drugs improves visual and temporal deficits[409,410], involving DA with sensory gain modulation deficits[411].

Taking all these evidences together, sensory information must have an important role regarding the striatal function in health and disease. Direct and indirect MSNs from the DMS –region which has been related to reward-dependent processes[412–414] and receives a great dopaminergic innervation from the SNc–, are able to integrate visual and tactile inputs[53]. On the other hand, DA has been linked to a great variety of processes such as reinforcement, reward-dependent learning[266] and sensory gain modulation deficits[411]. Moreover, the increment in DA levels due to the expectation of rewarding stimuli modulates MSNs activity differently[412]. Finally, it has been already documented that DA depletion impairs the processing of tactile inputs in direct MSNs from the DLS[62] in anesthetized mice. Therefore, our hypothesis is that DA will impact on the sensory processing of DMS-MSNs. Will DA modify visual and tactile inputs integration? Will this effect be different for direct and indirect MSNs? Will MSNs select one sensory modality at the expense of the other? And, if that happens, will it be mediated by DA? The main objective of the present study is to understand how DA modulates the sensory processing of visual and tactile inputs in MSNs of the DMS.

Objectives

2. OBJECTIVES

The main aim of this thesis is to unravel how dopamine modulates the sensory processing and spontaneous activity of medium spiny neurons located in the dorsomedial striatum.

The specific objectives are:

- Unravel the dopaminergic modulation of tactile, visual and bimodal sensory responses of medium spiny neurons.
- Study the impact of dopamine in the direct and indirect pathways.
- Study the corticostriatal connectivity from primary somatosensory and visual cortices to the dorsal striatum.
- Explore the impact of striatal cholinergic interneurons when modulating the sensory responses.
- Investigate the impact of the Up and Down states on the sensory responses of medium spiny neurons.
- Study the dopaminergic modulation of the spontaneous activity of medium spiny neurons.
- Develop a new device to allow local drug application during *in vivo* patch-clamp recordings.

Material and Methods

3. MATERIAL AND METHODS

3.1. Animals

Ethical approval. All the experimental procedures were conformed to the directive 2010/63/EU of the European Parliament and of the Council, and the RD 53/2013 Spanish regulation on the protection of animals use for scientific purposes, approved by the government of the Autonomus Community of Valencia, under the supervision of the *Consejo Superior de Investigaciones Científicas* and the Miguel Hernandez University Committee for Animal use in Laboratory.

Animal models. The total amount of animals used in this study was 65. In the mice line D2-cre x ChR2 x DAT-cre, the expression of ChR2 in indirect MSNs was used to perform optogenetic differentiation of direct and indirect MSNs as previously described[62] (Fig. 14a), whereas the expression of cre in DAT neurons was used to selectively infect dopaminergic neurons of SNc with a cre dependent virus containing ChrimsonR[415] to release dopamine (n=15 animals) (Fig. 20d). To obtain this mice line, D2-Cre (ER44 line, GENSAT) mouse line was crossed with the Channelrhodopsin (ChR2)-YFP reporter mouse line (Ai32, the Jackson laboratory) to induce the expression of ChR2 in indirect MSNs. The resulting mouse line was then crossed with the mouse line DAT-cre (the Jackson laboratory). Additional animals from the DAT-cre mouse line were used to perform fiber photometry experiments (n=13 animals (7 + 6 control, Fig. 23e)). C57BL/6J mice (n= 8 animals) were used for BDA injections (Fig. 27a). OE25-cre (Tg(Chrna2-cre)OE25Gsat/Mmucd) (MMRC) (n=8 animals) and Tlx3-cre (Tg(Tlx3-cre)PL58Gsat/Mmucd) (MMRC) (n=8 animals) mice lines were used to perform PT and IT selective axonal tracing respectively from S1 and V1 cortices to the dorsal striatum (Fig. 28a). For the micro-holder experiments (Fig. 14b), whose methods are broader developed in the annex paper[57], C57BL/6J mice (n=13 animals) were used.

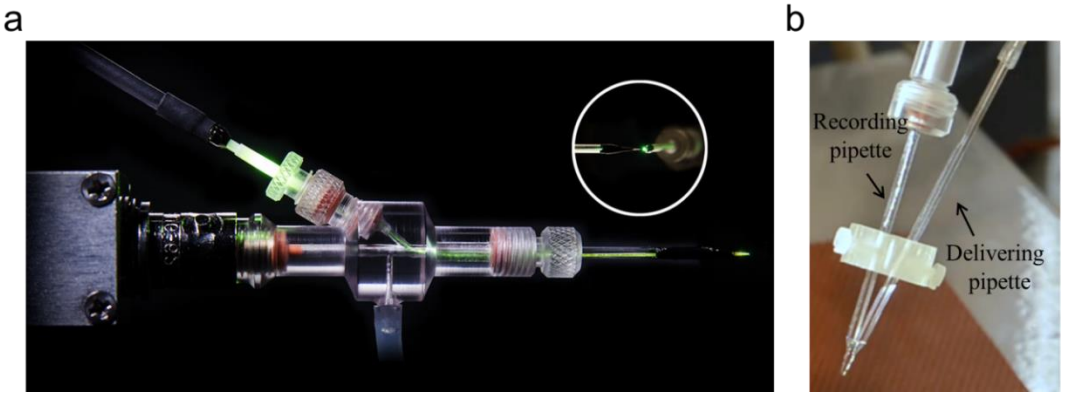

Figure 14. The optopatcher and the micro-holder. a, The optopatcher[416] is an electrode holder for simultaneous intracellular *in vivo* patch-clamp recordings and optical manipulation**.** Image taken from AM-Systems. **b,** The micro-holder[57] is a box-shaped construct in which a recording and a delivery pipette are mounted to perform a local drug delivery during *in vivo* patch-clamp recordings even in deep brain regions, such as the striatum.

3.2. Viral injection

Viral injection in SNc. In order to induce dopamine (DA) release by optogenetic stimulation, we infected the dopaminergic neurons in the SNc. Isofluorane anesthetized D2-cre x ChR2 x DAT-cre mice were immobilized in a Stereotaxic Alignment System (Kopf Instruments). AAV5-hSyn-FLEX-ChrimsonR-tdTomato (n=12 animals) or AAV5-CAG-FLEX-tdTomato (n=3 animals) (both from UNC Vector Core), were intracerebrally injected uni-laterally (500 nL) with an injector (Nanoliter, WPI) into the SNc using the following coordinates from Bregma: AP -3 mm, LM 1.5 mm, DV -3.5 mm, following Paxinos and Franklin[417]. Experiments were performed at least 8 weeks after the viral injection.

Viral injection in the DMS. In order to measure DA release in the DMS with the fiber photometry technique, DAT-cre mice (n=7 animals + 6 control animals) were first intracerebrally injected in the SNc, as described above. Then, 6 weeks later, a second injection was performed in the DMS unilaterally, using the following coordinates from bregma[417]: AP 0 mm, LM 2 mm and 3 depths below the surface (DV -1.6 mm, -1.9 mm, and -2.2 mm; 100 nl at each depth, total 300 nl), with AAV5-hSyn-dLight1.2-EGFP, obtained from Dr. Lin Tian laboratory (University of California Davis, USA) and Addgene. Experiments were performed at least 2 weeks after the viral injection.

Biotin Dextran Amine injection in S1 and V1. In order to trace the projections from S1 and V1 towards the striatum, C57BL/6J mice (n=8) were anesthetized and immobilized as described above. Biotin Dextran Amine (BDA) (Sigma Aldrich) was intracerebrally injected unilaterally in S1 (following coordinates from bregma: AP -1.5 mm, LM 3.25 and 3.75 mm, DV -0.8 mm), and V1 (following coordinates from bregma: AP -3.75 mm, LM 2.5 and 2.75 mm, DV -0.8 mm) following Paxinos and Franklin[417], injecting 150 nl in each lateromedial coordinate (300 nl in total) to cover the largest area as possible. For the anatomical study, mice were sacrificed 10 days after the injection by receiving an overdose of sodium pentobarbital (200 mg/kg I.P.).

Viral injection in S1 and V1. In order to selectively target PT and IT cortical neurons projecting towards the striatum, Tlx3-cre (n=8) and OE25-cre (n=8) mice were anesthetized and immobilized as described above and 300 nl of AAV2.EF1a.DIO.tdTomato.WPRE virus (UNC Vector Core) were intracerebrally injected unilaterally in S1 and V1 following the same coordinates as described above for BDA tracing to cover the largest area as possible. Sacrifice was performed 31 days post injection by receiving an overdose of sodium pentobarbital (200 mg/kg I.P.).

3.3. Electrophysiological recordings

Electrophysiological recordings. For experiments involving dopamine, D2-cre x ChR2 x DAT-cre mice of both sexes (n=15, n=9 males and 6 females), between 14 and 40 weeks of age were used to perform the experiments (Table 1). For micro-holder

experiments, C57BL/6J mice of both sexes (n=13, n=8 males and 5 females) between 8 and 24 weeks of age were used. Anaesthesia was induced by intraperitoneal injection of ketamine (75 mg/kg) and medetomidine (1 mg/kg) diluted in 0.9 % NaCl. A maintaining dose of ketamine (30 mg/kg i.m.) was administrated every 2 hours or after changes in the EEG or reflex responds to paw pinches. Tracheotomy was performed to increase mechanical stability during recordings by decreasing breathing related movements. Mice were placed in a stereotaxic device (customized Stoelting stereotaxic base) and air enriched with oxygen was delivered through a thin tube placed 1 cm from the tracheal cannula. Temperature was maintained at 36.5 ± 0.5°C using a feedback-controlled heating pad (FHC Inc.). Craniotomies were drilled (S210, Camo) at several sites from bregma. DA experiments: AP 0 mm, LM 2.5 mm (DMS); AP −1.5 mm, LM 3.25 mm (S1); AP −3.5 mm, LM 2.5 mm (V1); following Paxinos and Franklin[417]. Micro-holder experiments: three craniotomies were drilled for striatal-TTX experiments, or two craniotomies for S1-BMI experiments: AP −1.5 mm, LM 3.25 mm (S1); AP 2 mm, LM 2 mm (M1); AP 0 mm, LM 3.5/4 mm (DS). Animals were sacrificed after the experimental session by receiving an overdose of sodium pentobarbital (200 mg/kg I.P.).

Animals	15
Males	9
Females	6
Weight (gr)	33.33 ± 10.42
Male weight (gr)	38.66 ± 9.82
Female weight (gr)	25.33 ± 4.67
Age (weeks)	22.4 ± 8.55
Male age (weeks)	24.66 ± 10.09
Female age (weeks)	19 ± 4.33
Cells/animal	3.73 ± 1.09
Cells/male	3.44 ± 1.13
Cells/female	4.16± 0.98

Table 1. Description of the animals used for the whole-cell recordings in the DA study. The first three rows are total values, the rest show mean ± standard deviation.

Whole-cell recordings. For experiments involving DA, whole-cell recordings were obtained from the DMS between 2050 and 2567 µm deep in a perpendicular penetration angle of ~30°. For micro-holder experiments whole-cell recordings were obtained from cortical infragranular layers between 791 and 1303 µm deep or from the dorsal striatum between 2143 and 2610 µm deep in a perpendicular penetration angle of ~30°. The exposed brain was continuously covered by 0.9% NaCl to prevent drying. Signals were amplified using a MultiClamp 700B amplifier (Molecular Devices) and digitized at 20 KHz with a CED acquisition board and Spike 2 software (Cambridge Electronic Design). Borosilicate patch pipettes (1B150F-4, WPI), were pulled with a Flaming/Brown micropipette puller P-1000 (Sutter Instruments) and had an initial resistance of 6-12 MΩ, with longer tips than the standard ones to minimize cortical damage. Pipettes were back-filled with intracellular solution containing: 125 mM K-gluconate, 10 mM KCl, 10 mM Na-Phosphocreatine, 10 mM HEPES, 4 mM ATP-Mg and 0.3 mM GTP-Na. pH and osmolarity were adjusted to ~7.4 and ~280 mOsm/L, respectively. Biocitin (0.2-0.4%, Sigma Aldrich) was then added to the intracellular solution to reconstruct the recorded cell after every experiment (Fig. 20b). To implement the analysis of the spontaneous activity, 100 s of spontaneous activity (no current injection, no stimulation) were used from the recording. To analyse the dopaminergic modulation of spontaneous activity, 100 s of the recording without stimulation were compared to 100 s of the same recording in which DA was optogenetically released every 5 s to avoid brain state entrainment. 420 s of the recording with optogenetic and sensory stimulation were used to analyse the DA modulation on sensory responses, ensuring for each recording a minimum of 14 events for each condition/cell. For all the neurons, input resistance (Table 3) was measured as the slope of a linear fit between the injected current steps and membrane potential of 2 s duration. In order to quantify the described inward membrane rectification of MSNs[418,419], mean resistance during Up or Down states was analysed in response to negative and positive current steps (Table 3). Neurons with resistances < 100 MΩ were excluded from the analysis. The time constant (tau) was calculated as the time required for the membrane voltage change to reach the 63% of its maximum value. Capacitance was obtained by dividing the time constant between the voltage membrane resistance. Neurons with a resting membrane potential above -50 mV and/or having a deviation by more than 10 mV from their initial resting membrane potential were excluded from the analysis. The action potential threshold for our cells was determined to be -40 mV, therefore, the firing rate was calculated by using a threshold in the membrane potential of the cell (-20 mV) and counting the number of action potentials presented in a given time at that membrane potential. The SWO frequency was calculated as the number of Up states in a given recorded time. In the DA study, from the 61 recorded neurons, 56 were identified as MSNs by their electrophysiological properties and morphology (Fig. 20b, c). From the remaining 5, 2 were identified as FS and 3 as ChIs by their electrophysiological properties (Fig. 19, Table 3). The average recording time for all MSNs was 46.8 ± 12.81 min (minimum = 20 min, maximum = 72 min; n = 56). As the average recording time was quite variable, not in all neurons was possible to accomplish all the experimental protocols. Therefore, we followed this method: First, the

optogenetic identification of the recorded neuron, classified as a putative direct or indirect MSN by the means of the optopatcher[416] (Fig. 14a) [see Material and Methods section 3.5]; second, the study of its electrophysiological properties by injecting positive and negative intracellular current steps; third, 2 min of spontaneous activity were recorded to analyse the properties of its SWO; fourth, the study of the dopaminergic modulation of the spontaneous activity by releasing DA optogenetically every 5 s; fifth, optogenetic and sensory stimulation was performed to study the impact of DA on visual and tactile responses. Hence, from the 56 neurons identified as MSNs, all of them (34 direct MSNs and 22 indirect MSNs) were used to study their electrophysiological properties; 38 (24 direct MSNs and 14 indirect MSNs) to analyse the dopaminergic modulation of their spontaneous activity; and 29 (14 direct MSNs and 15 indirect MSNs) were included to study the effect of DA in sensory processing (Table 2).
For the micro-holder experiments, 11 neurons were recorded: 4 of them were cortical neurons and 7 of them were identified as MSNs by their electrophysiological properties.

	Total MSNs	Direct MSNs	Indirect MSNs
Total Recorded	56	34	22
Opto- & electrophysiological identification	56	34	22
DA on spontaneous activity	38	24	14
DA on sensory processing	29	14	15

Table 2. Data set description for the DA study. Table showing the number of direct and indirect MSNs used in this work for each experimental condition.

Extracellular recordings. Extracellular recordings were obtained using unipolar tungsten electrodes with impedances of 1-2 MΩ. The electrodes were placed in infragranular layers (1000 µm depth from the pia) of S1 and V1 with an angle between 15° and 25°. In the case of the micro-holder experiments, the extracellular recordings were placed in S1 and M1 as described previously. Recordings were amplified using a Differential AC Amplifier model 1700 (A-M Systems) and digitized at 10 KHz with CED and Spike-2 simultaneously with the whole-cell recording.

3.4. Stimulation protocols

In all the cases, the different stimuli were randomized, with an interstimulus interval of 5 s (0.2 Hz). For each cell, tactile, visual and bimodal stimuli were launched during a recording with a minimum duration of 420 s, ensuring at least 14 events for each stimulation/cell. Sensory stimulations were sometimes randomly preceded (30 ms) by

an optogenetic activation of DMS dopaminergic terminals. Therefore, 6 conditions were analysed: tactile, visual and bimodal stimulation with or without DA release.

Tactile stimulation. The displacement of the main whiskers was obtained by brief air puffs (15 ms of duration, 20 p.s.i.) by means of a Picospritzer unit (Picospritzer III, Parker Hannifin, NJ), via 1 mm diameter plastic tubes, placed at ~50 mm in front of the contralateral side of the snout. The latency between the computer command and the whisker movement was measured using an extracellular tungsten electrode placed in one of the central whiskers (Fig. 15), and was determined to occur 20.05 ± 0.1 ms (n = 5 animals) following the trigger command. Therefore, the reference onset time was determined as 20 ms following the computer trigger command. Tactile responses were confirmed by monitoring the activation of the ipsilateral S1 using LFP recordings.

Visual stimulation. A brief visual stimulation (15 ms of duration) was delivered by a white light LED positioned ~50 mm from the contralateral eye. The eye was covered with artificial eye drops (Viscotears, Bausch+Lomb, Germany) in order to prevent drying, as previously described[420]. Visual responses were confirmed by monitoring the activation of the ipsilateral V1 using LFP recordings.

Bimodal stimulation. Tactile and visual stimuli were delivered simultaneously using the same protocols as described above.

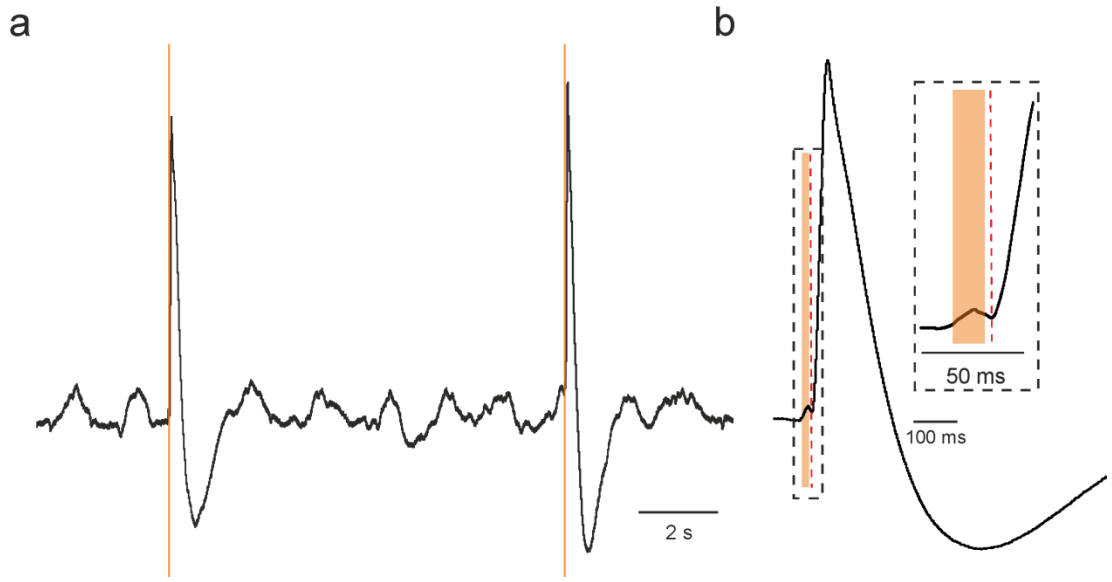

Figure 15. Reference time of whisker displacement. a, Raw example trace of an extracellular tungsten electrode placed in one of the central whiskers while performing tactile stimuli to determine de delay between the computer command and the whisker movement. **b,** Waveform average of the evoked response in a. Dashed black rectangle displays a zoom-in of the onset of the whisker displacement. Notice that the movement of the whiskers occurs 20 ms following the computer trigger command. Orange bars indicate the time of the tactile stimulation (15 ms). Red dashed line indicates the onset time of the whisker displacement.

3.5. Optogenetics

Optogenetic identification of *in vivo* recorded neurons. In order to identify "on line" the specific type of MSNs belonging to the direct and indirect pathways, the optopatcher was used[62,421,422] (Fig. 14a) (A-M systems, WA USA). Pulses (SLA-1000-2, Two-channel universal LED driver, Mightex systems) of blue light (Fiber-coupled LED light source FCS-0470-000, 470 nm, Mightex systems) controlled through Spike 2 software were delivered using an optic fiber (200 µm diameter, handmade) inserted into the patch-pipette, while recording their spontaneous activity (Fig. 20e). One or two serial pulses with 5 light steps of 500 ms each were delivered every 2 s with increasing intensity from 20 to 100 % of full LED power (minimal light intensity 0.166 mW; maximal intensity 0.83 mW at the tip of the fiber). Power light was measured with an energy meter console (PM100D, Thorlabs). Positive cells responded to light pulses by depolarizing their membrane potential. Positive cells (Fig. 20e, green trace) responded within 2.73 ± 1.29 ms of latency (ranging from 0.8 to 5 ms) to light pulses, by a step-like depolarization of 10.22 ± 8.33 mV (ranging from 2.9 to 19.6 mV) at maximal stimulation intensity. Negative cells did not show any depolarization to light pulses (Fig. 20e, black trace).

Optogenetic activation of dopaminergic terminals in the DMS. Optogenetic activation was done placing an optic fiber of 200 µm in the vicinity of the recording region with a 90º angle connected to a light source (high power LED Prizmatix) (Fig. 20a). Light intensity was 2.4 mW at the tip of the fiber. Based on previous descriptions[256,258,261], we designed an optogenetic train with 4 light pulses of 15 ms at 15 Hz (interpause of 66 ms) that mimicked the burst frequencies of action potentials discharge of dopaminergic neurons[256,257,261] (Fig. 23b). This optogenetic stimulation was randomly launched 30 ms before tactile, visual or bimodal stimulation and also without sensory stimuli, with a minimum interval of 5 s between stimulations.

Dopamine release measurement with fiber photometry. Experiments were carried out in 7 DAT-cre animals in which the SNc was injected with AAV5-hSyn-FLEX-ChrimsonR-tdTomato and in 6 DAT-cre control animals injected with AAV5-CAG-FLEX-tdTomato. Additionally, all animals were injected with AAV5-hSyn-dLight1.2-EGFP in the DMS as previously described [see Material and Methods section 3.2]. Fiber photometry experiments were then performed similarly as in previous reports[423]. For colour imaging, the 1-site 2-colour Fiber Photometry system was used (Doric Lenses): The 465 nm wavelength was used to capture the fluorescence changes related to the dLight1 sensor, whereas the 405 nm wavelength was used as isosbestic reference point to detect artefactual changes not related with the sensor[423]. The fluorescence captured from the 405 nm signal remained constant during our optogenetic stimulations (Fig. 23c, black traces), ensuring that the fluorescence increase observed in the 465 nm signal was not an artefact (Fig. 23c, blue traces). Acquired photometry data from the 405 and 465 nm channels were processed with custom codes written in Matlab. Raw data from each channel was down-sampled and low-pass filtered at 25 Hz using a 2nd

order Butterworth filter. To calculate the changes in fluorescence to yield the ΔF/F PSTHs, a linear fit was applied to both signals and afterwards we aligned them. Then, the fitted 405 nm signal was subtracted from the 465 nm signal. The resultant signal was then divided by the fitted 405 nm signal to yield the ΔF/F values. Afterwards, the ΔF/F values were smoothed and aligned to the stimulation trigger to compute the PSTHs. Changes in fluorescence showed by the PSTHs were compared with or without DA (Fig. 23d).

3.6. Histology

Morphological reconstruction. At the end of each experiment the mouse was sacrificed with a lethal dose of sodium pentobarbital and perfused with a solution containing 4% paraformaldehyde in 0.1 M phosphate buffer (PB, pH 7.4). Brains were extracted and stored in PBS solution until the cutting. Before cutting, brains were transferred into PBS containing 30 % sucrose for 24/48 hours. Coronal or sagittal slices (20 µm thick) of both hemispheres containing the entire striatum from the recorded side (from AP 1.4 mm to AP -1.3 mm, following Paxinos and Franklin[417]) were obtained using an automatic digital criotome (Microm) and collected on gelatin coated slides (ThermoFisher). Sections were incubated over night with Cy3-conjugated streptavidin (Jackson Immuno Research Laboratories) diluted (1:1000) in 1 % BSA, 0.3 % Triton-X 100 in 0.1 molar PBS. Finally, the gelatin coated slides were covered with mowiol (Calbiochem) and mounted with coverslips (ThermoFisher). Recorded and filled neurons were then reconstructed using a fluorescence microscope (DM 6000B, Leica) and a camera (DC350 FX, Leica) (Fig. 20b).

BDA, PT and IT axonal tracing. At the end of each experiment, the mouse was sacrificed and perfused, and the brain was stored as mentioned above. Before cutting, brains were transferred into PBS containing 30% sucrose for 24/48 hours. Coronal slices (40 µm thick) of both hemispheres from the entire brain (BDA brains, n=8) (PT and IT brains, n=16), were obtained using an automatic digital criotome and collected on gelatin coated slides as described above. BDA slices were incubated over night with Cy3-conjugated streptavidin diluted (1:1000) in 1 % BSA, 0.3 % Triton-X 100 in 0.1 molar PBS. PT and IT slices were not incubated. Afterwards, all slices were incubated 20 min at RT with DAPI (Sigma). Finally, the glass slides were covered with mowiol (Calbiochem) and mounted with coverslips (ThermoFisher). To perform the anatomical study, we took images in half of the slices containing the DMS and DLS from the recorded side (from bregma: AP 1.4 mm to AP -1.3 mm, following Paxinos and Franklin)[417]. Images were obtained with a fluorescence microscope (DM 4000B, Leica) and a camera (Retiga 2000R, Qimaging). Each taken image covered an approximate area of 129600 μm^2 (approximately 360 µm per side) in the DMS or DLS (Fig. 27a, 28a). We also took images of the injection place in S1 and V1 in each of the brains to ensure that the number of infected cells and the fluorescence expression was similar between brains (Fig. 16). When analysing the images, as V1 sends quite a large density of projections towards the DMS and to avoid counting mistakes, we did not count each

axon separately. Instead, we transformed the taken images to binary images with custom codes written in Matlab by applying the same threshold (mean fluorescence intensity plus 6 standard deviations) to all the images. We then computed the total area of white pixels, which corresponded to the area covered by the labelled axons.

Micro-holder experiments. At the end of each experiment, the mouse was sacrificed, perfused and the brain was stored as mentioned above. Coronal slices (12-24 µm thick) were obtained using a criostate (SLEE medical) and collected on gelatin coated slides. Slices were then incubated with Cy2-conjugated streptavidin diluted (1:500) in 1% BSA, 0.1% sodium Deoxycholic acid and 0.3% triton in 0.01 PBS overnight at 4°C. Slides were washed in PBS and viewed on a fluorescent microscope (Olympus AB, and Leica DM 6000B). Photomicrographs of the slices were taken with Leica DFC 350 FX or an Olympus XM10 (Olympus AB) digital camera.

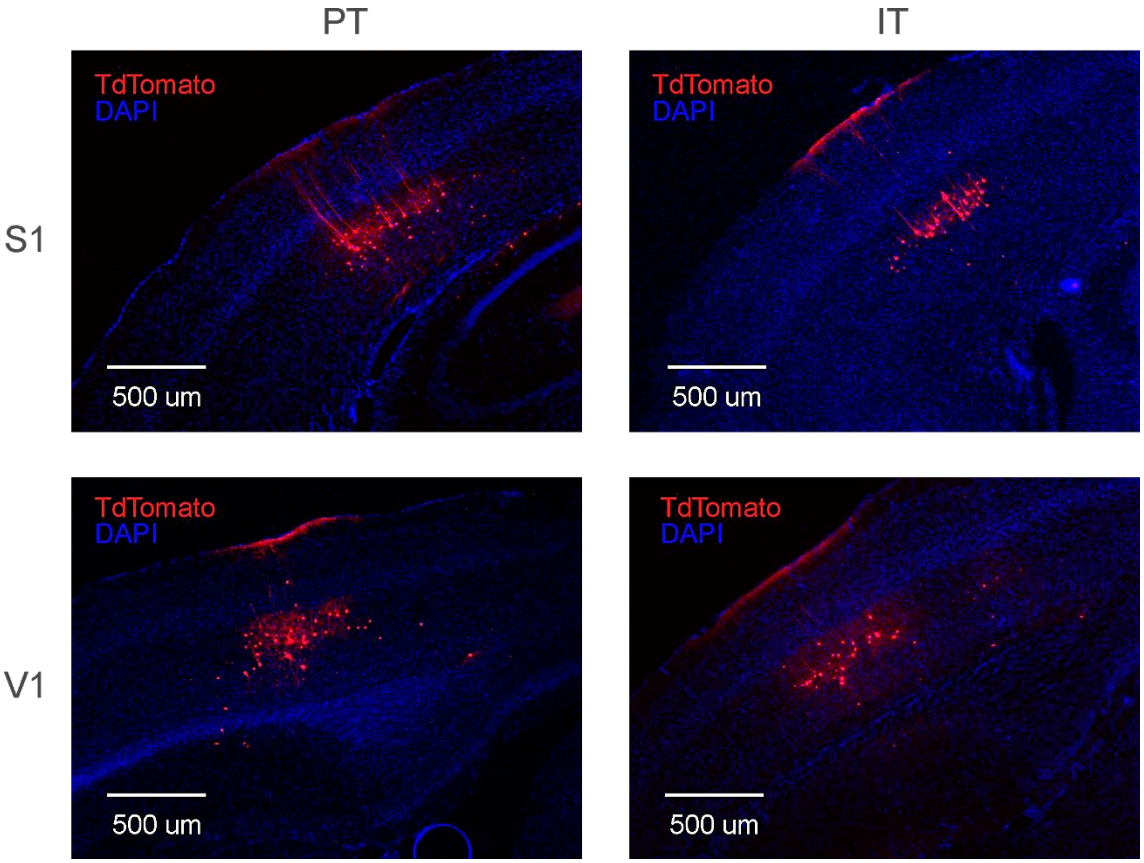

Figure 16. Selective targeting of PT and IT neurons in layer 5 of S1 and V1. OE25-cre (left) and Tlx3-cre (right) mice were injected in layer 5 of S1 (top) and V1 (bottom) cortices with the viral construct AAV2.EF1a.DIO.tdTomato.WPRE to target PT and IT neurons respectively.

3.7. Analysis.

3.7.1. Experiments to unravel the role of DA

SWO decomposition using NA-MEMD. Neural oscillations such as the ones recorded in this study are nonlinear [424–426]. Frequency and Time-Frequency analysis are the most common used methods to analyse the oscillatory properties of neural oscillations. Nevertheless, traditional decomposition approaches present limitations to analyse this type of data. For instance, when applying Fast Fourier Transform (FFT)[427,428] to neural signals, the result is a low temporal and frequency resolution signal[424]. The use of alternatives, such as the wavelet analysis[429,430], greatly improves the temporal and frequency resolution but it relies on fixed wave templates resulting in a loss of information[424]. Therefore, techniques which do not depend on fixed wave templates need to be implemented. In this study, we used the Noise-assisted Multivariate Empirical Mode Decomposition (NA-MEMD) algorithm[431] together with Hilbert transform[432] for the analysis of the oscillations of MSNs membrane potential. The original EMD[432] is a data driven algorithm suitable for nonlinear and non-stationary signals that does not rely on any predetermined template. It decomposes a given signal into a subset of oscillatory modes called Intrinsic Mode Functions (IMFs) (Fig. 17). Each IMF contains the oscillations of the original data in a certain frequency range, from the fastest to the slowest. Then, Hilbert transform is applied onto each IMF in order to compute its instantaneous frequency and amplitude to retain the original temporal resolution of the signal. The MEMD[431] is a multivariate extension of the original EMD to n-dimensional signals. The MEMD is computed simultaneously in all dimensions of the signal to ensure the same number of IMFs as output. In addition, new dimensions can be added to the data containing White Gaussian Noise (WGN) to increase its performance, as it has been described that WGN addition reduces mode mixing produced by signal intermittence[433], acting as a quasidyadic filter that enhances time frequency resolution[431,434]. The application of MEMD to the desired signal together with extra White Gaussian Noise dimensions is known as NA-MEMD analysis[431]. In this study, we applied NA-MEMD algorithm to a multivariate signal composed by the intracellular recording, both LFPs and one extra WGN channel as previously described[63]. The main advantage of this technique is the capacity to deal with the nonlinear and nonstationary properties of neural oscillations[424] obtaining an enriched decomposition of the oscillatory activity that cannot be achieved by traditional techniques. In order to apply NA-MEMD analysis to our data, we adapted the MEMD Matlab package (http://www.commsp.ee.ic.ac.uk/mandic/research/emd.htm). Standard stopping criterion was described previously[435]. At last, we extracted the IMF carrying the SWO as the one with maximum correlation with the membrane voltage and visually confirmed it in all the recorded cells. Once we isolated the SWO of each recording using NA-MEMD, they were stored for further analysis.

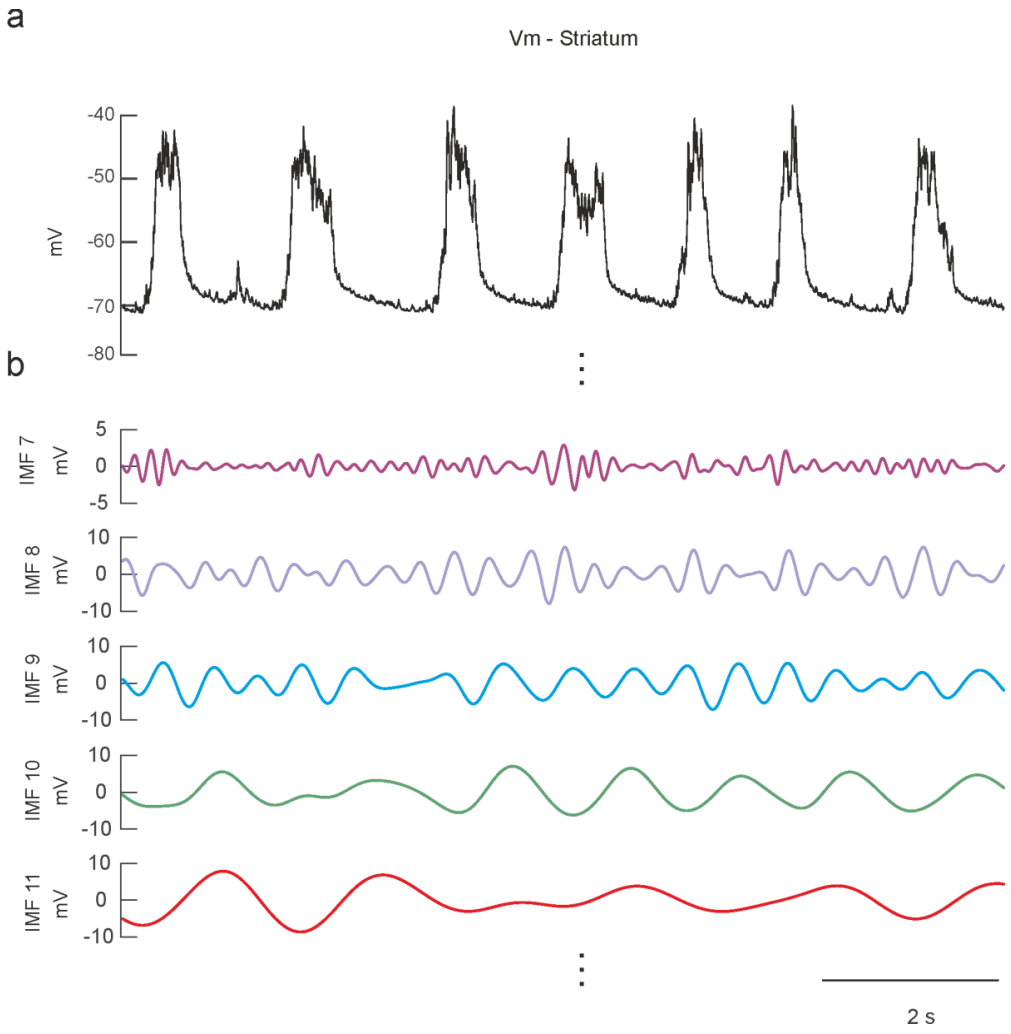

Figure 17. Example of the decomposition of a whole-cell recording by the NA-MEMD algorithm. a, Example trace of a whole-cell recording in the DMS. **b,** Consecutive IMFs obtained by applying NA-MEMD algorithm to the signal in a, starting from the 7th IMF. The IMF classifies the oscillatory activity from the fastest to the slowest. Frequency range for each IMF: 7=4.39 Hz; 8=2.35 Hz; 9=1.32 Hz; 10=0.70 Hz; 11=0.38 Hz. The 10th IMF corresponds to the SWO.

Hilbert transform. We computed the frequency of the SWO and theta (6-10 Hz), beta (10-20 Hz) and gamma-bands (20-80 Hz) as the instantaneous frequency using the Hilbert transform[432]. For a given time series x(t), its Hilbert transform H(x)(t) is defined as:

$$d(x)(t) = \frac{1}{\pi} C \left\{ \int_{-\infty}^{\infty} \frac{x(t')}{t-t'} dt' \right.$$

where C indicates the Cauchy principal value. Hilbert transform results in a complex sequence with a real part which is the original data and an imaginary part which is a version of the original data with a 90◦ phase shift; this analytic signal is useful to calculate instantaneous amplitude and frequency; instantaneous amplitude is the amplitude of H(x)(t), instantaneous frequency is the time rate of change of the instantaneous phase angle.

Extraction of features during the Up states. In order to describe the properties of the SWO of the recorded MSNs, we computed several parameters from the Up state (Fig. 25b). First, we subtracted the IMFs carrying oscillations faster than 50 Hz from the MSNs membrane voltage recordings to eliminate the spikes. Then, in order to isolate Up and Down states from the membrane voltage we started by smoothing the trace using a 200 ms window. Then, we extracted the Up states using a threshold consisting of the mean value of the membrane potential plus 0.5 standard deviations. Then, we merged the parts of fragmented Up states, detected as an interval shorter than 250 ms between the transition of a prospective Up state to a prospective Down state to the transition from a prospective Down state to a prospective Up state. Finally, detected Up states shorter than 200 ms where discarded. Then, we calculated the mean, standard deviation and minimum and maximum values of the Up state membrane potential. Additionally, we computed the peak to peak distance, which is the difference between the maximum and minimum values of the Up state membrane potential, the maximum and minimum value of the Up state derivative and the number of peaks in the Up state. To do so, we used the *findpeaks* Matlab function on the smoothed (200 ms smooth) Up state with a minimum peak height of 0.3 standard deviations and a minimum distance between peaks of 160 ms. We also computed the length, amplitude and the speed of the transition from the Down to the Up state and from the Up to the Down state as well as the Slope transition ratio, which consisted of the magnitude of the Down to Up transition relative to the Up to Down transition. In order to measure the slopes, we first located the transition between states with a time window starting 100 ms before and lasting Up to 200 ms after the crossing point of the voltage threshold that was used to detect the Down and Up state (See above). Then, we smoothed (100 ms smooth) the selected region and computed its derivative. We delimited the transition between states computing the region over a threshold calculated as the mean plus 0.3 standard deviations of the derivative. Once we had delimited the transition, we fitted a lineal function to that region of the recording to compute the slope speed.

Parameters obtained from the evoked sensory responses. In order to quantify the sensory responses (Fig. 26c-e), we first subtracted the IMFs carrying oscillations faster than 50 Hz from the MSNs membrane voltage recordings to eliminate action potentials. In order to extract Up and Down states, we performed a cross-correlation to look for the decomposed IMF that was most similar as possible to the original trace. This IMF contained the SWO. Then, we applied a threshold (the value of the membrane potential plus 0.5 standard deviations) to separate Up from Down states. We developed an interface with custom code written in Matlab to extract the parameters and help us visualize the evoked responses aligned with the trigger. We calculated separately the PSTHs from the evoked visual, tactile or bimodal responses with or without DA during Down and Up states and extracted the mean onset and peak delay, slope, and amplitude for each condition and cell. The **onset delay** was calculated as the average time between the stimulus trigger and the onset of the evoked potential. The first time derivative of the membrane potential was used to determine the onset of the sensory response within a 250 ms time-window after sensory stimulation. The **peak delay** was calculated as the

average time between the stimulus trigger and the time in which the response reached its maximum peak inside a 250 ms window from the stimulus. The **slope** was obtained as the first derivative (*dv/dt*) between the onset and peak delay time interval, and the response **amplitude** was defined as the voltage difference between the peak delay and the onset time (Fig. 18). The amplitudes of the responses during the Up states were very small or absent, with a rate of failures of 73.95% ± 9.79% excluding their reliable measure. Hence, all evoked responses showed in this study are extracted from the Down states, in which at least 14 stimuli were averaged for each condition.

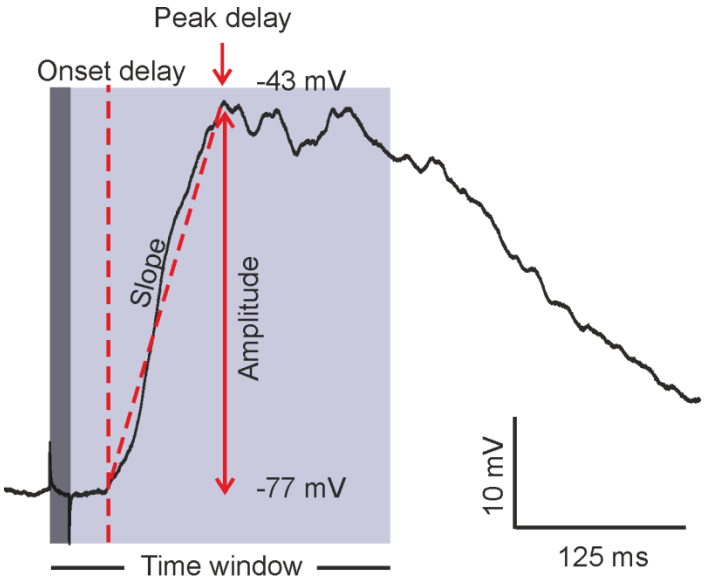

Figure 18. Parameters of the sensory responses. Example of an evoked sensory PSTH to illustrate how responses are measured. Dark grey line indicates the time in which the sensory stimulation is occurring (15 ms). Light grey square indicates the 250 ms time window in which the onset, peak delay, amplitude and slopes are calculated.

Statistical analysis. Wilcoxon Signed rank test was used for comparison of different conditions in matched samples. Wilcoxon Rank-sum test was used for comparison of different conditions in independent samples. The error bars presented in the bar graphs represent the standard error unless stated otherwise. Regarding the boxplots, the red line indicates the median, whereas the bars indicate the lowest and upper 25% of the data values. In the cases in which a linear regression was performed, the values and significance are displayed in the figure legend. Values exhibited in the tables represent the mean ± standard deviation. Confidence level was set to p=0.05. All statistical analyses were done in Matlab (Mathworks).

3.7.2. Experiments involving the micro-holder

Up and Down states from the SWO were detected in the intracellular recording trace. The transition points were defined by computing the local mean and standard deviation on a sliding window of 30 s. A dynamic threshold consisting of the mean plus 1.5 standard deviations was used to separate the Up from Down states in each window. Then, we used the times of the detected Up states to search for the Up states in the LFP

recordings. To prevent the loss of information due to the temporal delays between the striatal and cortical Up states, we extended the detected Up state regions 200 ms in both directions. Once Up and Down states were detected, their durations in the intracellular and LFP recordings were calculated. Transition slope magnitudes were extracted by computing the first derivative at the Down to Up state transition. To do this, we thresholded the obtained derivative using its mean plus 1 standard deviation in the case of the membrane voltage or minus 1 standard deviation of the LFPs. The detected slope was then adjusted with a first-order linear fitting in order to compute its magnitude. In order to analyse the changes in the SWO induced by BMI, we extracted the mean transition slope magnitude by averaging Down to Up state transitions during 40 s before and after BMI application in the intracellular and LFP recordings (Fig. 33D). The time in which the BMI diffused from the delivery pipette to the recorded neuron differed among recordings, due to the different distances between recording and delivery pipettes. For this reason, the 40 s window used to average the slopes during BMI application was centered with respect to the maximum slope value detected after application. The amplitude of the Up states was calculated by subtracting the mean value of the membrane potential in the Up states from the mean value of the membrane potential in the Down states. The firing rate was calculated by using a threshold in the membrane potential of the cell (-20 mV) and counting the number of action potentials presented in a given time at that membrane potential. Oscillation frequency was calculated as the number of Up states in a given recording time.

For statistical analysis, Mann–Whitney's U test was used. Data are presented as means with standard error of the mean (SEM).

Results

4. RESULTS

4.1. *In vivo* whole-cell recordings in the DMS

The main objective of this thesis was to understand the impact of dopamine in MSNs from the DMS when processing visual and tactile information. To that end, we obtained *in vivo* whole-cell patch-clamp recordings from 61 neurons located between 2050 and 2567 µm ventrally in the DMS of D2-cre x ChR2 x DAT-cre mice. All the recorded neurons displayed a rhythmic slow wave oscillation (SWO) with prominent Up and Down states (Fig. 19a, 20c, 24, 25a, 26a, 29a). 56 neurons were classified as MSNs, 2 as fast spiking interneurons (FS) and 3 as cholinergic interneurons (ChIs). MSNs were identified from other striatal types by their electrophysiological properties (Fig. 20c) as well as by their morphology, as they present prominent spines on their dendrites (Fig. 20b). FS and ChIs were clearly distinguishable by their electrophysiological properties. ChIs displayed their characteristic voltage sag response to current step injections (7.78 ± 2.20 mV) (Fig. 19b), depolarized membrane potential (-51 ± 6.55 mV), and spontaneous discharge activity (1.35 ± 0.41 Hz) (Fig. 19a, Table 3).

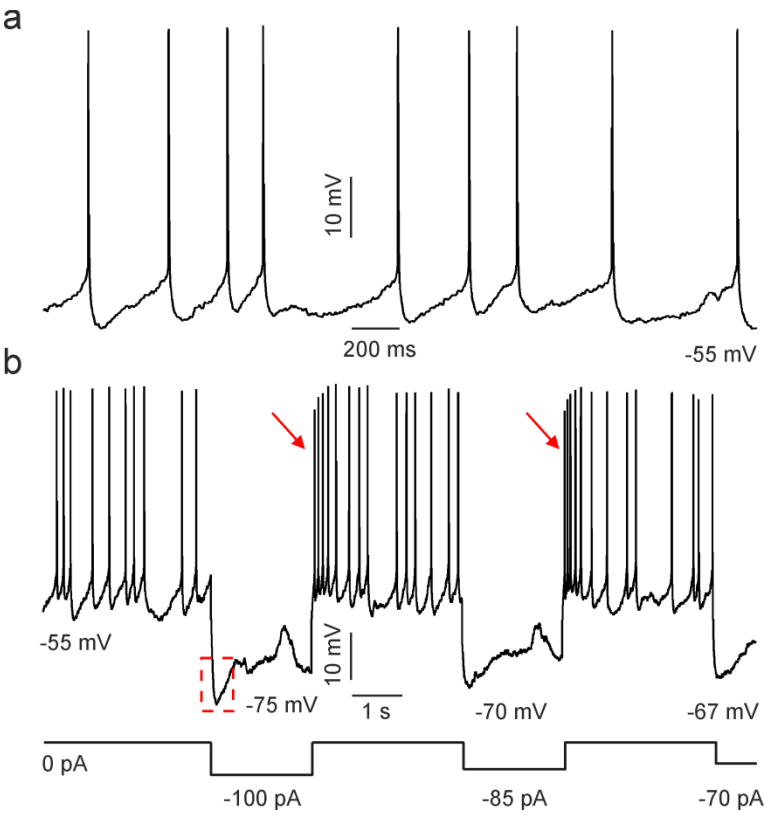

Figure 19. Cholinergic interneuron recorded *in vivo*. a, Example of the spontaneous activity of a cholinergic interneuron recorded *in vivo*. Notice its spontaneous tonic activity. **b,** Response of the same cholinergic interneuron to step current injections. Notice the voltage sag response (red dashed trace) and the rebound spikes characteristic in cholinergic interneurons (red arrows).

In addition to the electrophysiological characterization, all MSNs were identified belonging to the direct (striatonigral) or indirect (striatopallidal) pathways, by means of the optopatcher[421]. To that end, we delivered one or two trains of 5 pulses of blue light

(470 nm wavelength) every two seconds, each of them with 500 ms of duration and different intensities, from 20% (0.166 mW, minimal light intensity), to 100% of full LED power (0.83 mW, maximal light intensity) (Fig. 20e) [see methods]. Positive cells expressing Channelrhodopsin 2 (ChR2) were depolarized an average of 10.22 ± 8.33 mV after light stimulation for the maximal intensity light (ranging from 2.9 mV to 19.6 mV), generating action potentials in 12 neurons; whereas negative cells were not activated (Fig. 20e). Therefore, by few light pulses, MSNs were easily identified by their depolarization as indirect MSNs, while non-depolarized MSNs were classified as putative direct MSNs. The average recording time for all MSNs was 46.8 ± 12.81 min (minimum = 20 min, maximum = 72 min; n = 56). Simultaneously, double local field potential (LFP) recordings were obtained from S1 and V1 (Fig. 20a, c), to ensure that visual and tactile stimulations were eliciting a response in their respective primary cortical areas.

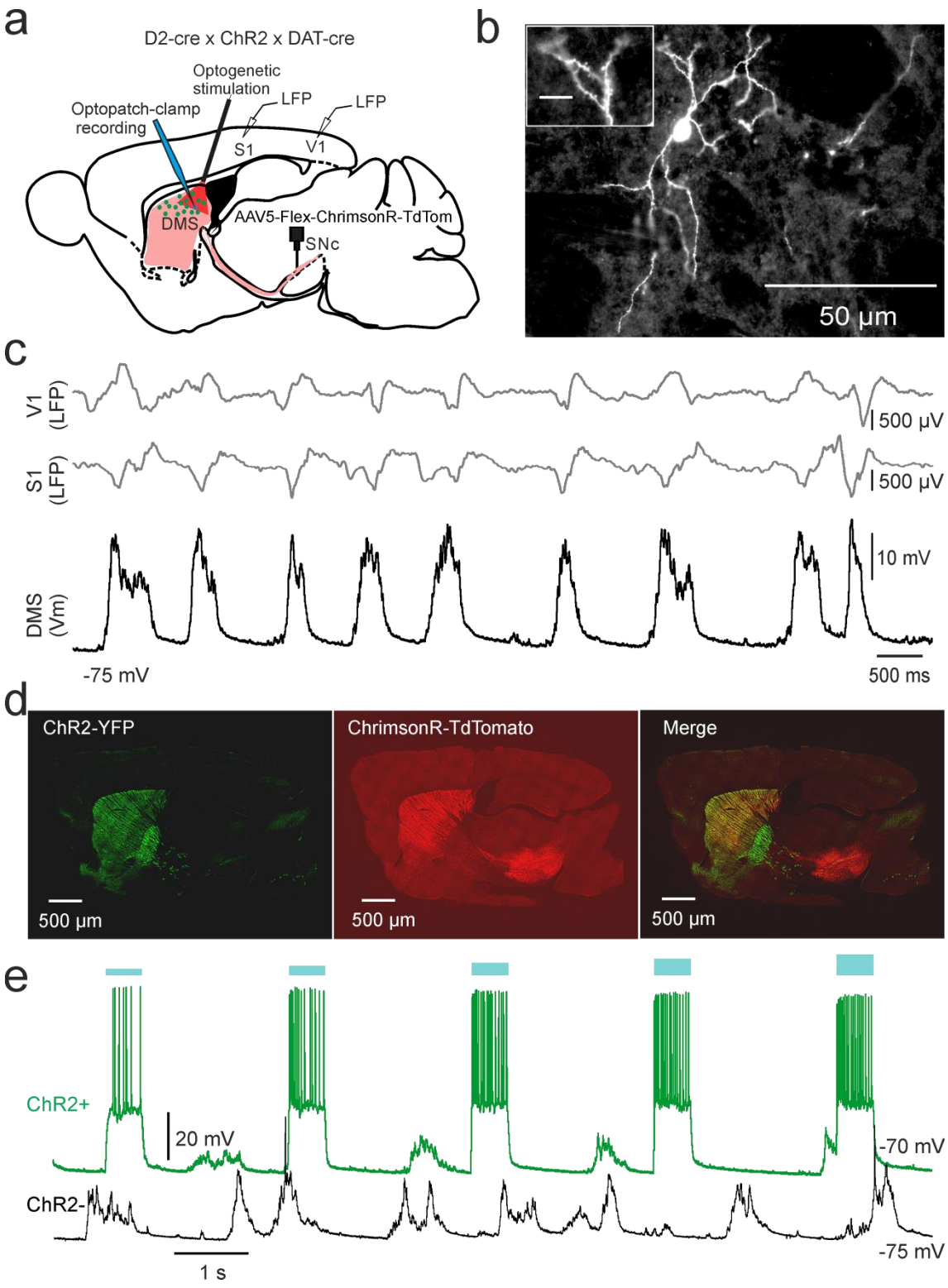

Figure 20. Experimental approach. a, Schematic representation of the experimental set up, *in vivo* whole-cell optopatch-clamp recordings with simultaneous LFP in S1 and V1. **b,** Morphological reconstruction of a dorsomedial MSN. Different scales show neuron magnitude and its dendritic spines, confirming that the recorded neuron is a MSN. Inset bar scale corresponds to 20 µm. **c,** Example of a recorded MSN in the DMS (black trace) with simultaneous LFP in S1 and V1 (grey traces). **d,** Sagittal images of a D2-cre x ChR2 x DAT-cre mice injected with the virus expressing the opsin ChrimsonR-TdTomato in the SNc. Left: Expression of ChR2-YFP in the indirect MSNs. Middle: Dopaminergic terminals of the SNc expressing the opsin ChrimsonR-TdTomato in the SNc after at least 8 weeks post

injection. Right: Merge of both images. Notice that the yellow colour indicates the merge between the dopaminergic terminals and the indirect MSNs expression only in the striatum. **e,** Example showing an *in vivo* identification of a MSN using the optopatcher. Indirect MSNs in the D2-cre x ChR2 x DAT-cre mice (top trace, ChR2+, green) responded to light pulses, inducing a depolarization in the MSN. Negative cells (bottom trace, ChR2-, black) did not respond to light pulses. Blue bars indicate the intensity of the light pulse stimulation, from 20 to 100 %.

4.2. Electrophysiological properties of MSNs from the DMS

We characterized several electrophysiological properties of the MSNs, such as the voltage membrane potential, input resistance, time constant (tau) and capacitance (34 direct MSNs and 22 indirect MSNs, Table 3, Fig. 21). Input resistance was measured in response to negative and positive current injection steps. In addition, to better understand how the states of the SWO could affect the electrophysiological properties, we calculated it separately for Down and Up states. During Down states, the resistance significantly increased in response to positive pulses from 223 ± 93.37 MΩ to 245 ± 81.16 MΩ (p=0.0014). In the case of the Up states, we did not find differences between negative and positive current injections, probably due to the voltage variability induced by the spontaneous activity. In addition, the resistance in response to the negative current steps in Down states was significantly lower when compared to the Up states. In summary, in agreement with previous results[53,62], our data shows that depolarization increases the input resistance of MSNs, either induced by current injection or by the spontaneous depolarization that occurs during the Up states. When calculating the average of tau (4.38 ± 1.35 ms) and the capacitance (19.10 ± 6.78 pF), we found similar values to the ones described previously[63].

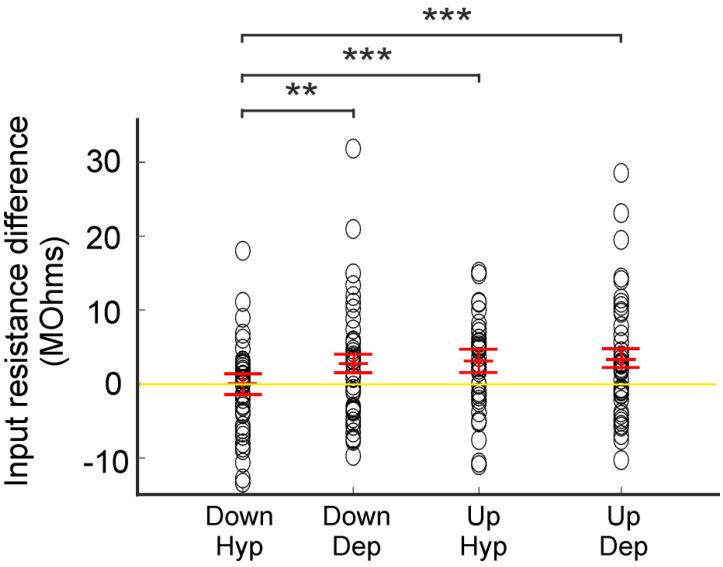

Figure 21. MSNs input resistance. Differences in the input resistance of MSNs during Up and Down states calculated during negative and positive current steps. All values are subtracted with respect to the Down Hyp condition. Yellow line indicates the value 0. **p<0.01; *** p<0.001

Electrophysiological properties were also compared between direct and indirect MSNs. Our result does not show significant differences in their resistance, capacitance, tau,

membrane potential or oscillation frequency values (Table 3). Therefore, we conclude that both types of MSNs have similar electrophysiological properties in the DMS, in contrast with the previous description of the direct and indirect pathways MSNs in the DLS[53,62]. The differences between dorsal striatal regions strongly suggest particular functional properties between pathways in the DLS and DMS.

	All MSNs	direct MSNs	indirect MSNs	ChIs	FS
Input Resistance (MΩ)	242 ± 77.5	247 ± 87.93	235 ± 50.49	203 ± 37.87	250 ± 21.92
Resistance Down state hyp. (MΩ)	223 ± 93.37	229 ± 105.57	214 ± 73.33	205 ± 44.37	239 ± 20.50
Resistance Down state dep. (MΩ)	245 ± 81.16	251 ± 93.81	236 ± 58.74	186 ± 55.56	263 ± 25.45
Resistance Up state hyp. (MΩ)	249 ± 97.96	253 ± 109.34	242 ± 80.40	208 ± 45.61	257 ± 22.62
Resistance Up state dep. (MΩ)	253 ± 81.82	252 ± 88.21	255 ± 73.64	185 ± 48.41	224 ± 11.31
Capacitance (pF)	19.10 ± 6.78	20.38 ± 7.73	17.19 ± 4.62	32.38 ± 24.1	16 ± 7.1
Tau (ms)	4.38 ± 1.35	4.65 ± 1.32	3.98 ± 1.34	6.09 ± 3.38	3.52 ± 0.76
Sag (mV)	0 ± 0	0 ± 0	0 ± 0	7.78 ± 2.20	0 ± 0
Membrane potential (mV)	-69.72 ± 5.48	-70.13 ± 5.51	-68.85 ± 3.97	-51 ± 6.55	-65 ± 7.07
Firing rate (Hz)	0.193 ± 0.29	0.191 ± 0.29	0.196 ± 0.30	1.35 ± 0.41	2.69 ± 0.95
Oscillation frequency (Hz)	0.68 ± 0.10	0.66 ± 0.10	0.70 ± 0.10	0.79 ± 0.08	0.72 ± 0.01

Table 3. Intrinsic properties of dorsomedial direct and indirect MSNs, ChIs and FS. All values are means ± standard deviation. MSNs: n=56 (34 direct MSNs; 22 indirect MSNs). ChIs: n=3. FS: n=2.

We also analysed the spontaneous firing rate of MSNs, which only occurs during the Up states and at a very low frequency[53,62,63]. In agreement with previous reports, our average rate of spontaneous action potentials was 0.193 ± 0.29 Hz (Table 3), with no differences between the direct and indirect MSNs (direct MSNs = 0.191 ± 0.29 Hz, indirect MSNs = 0.196 ± 0.30 Hz (p=1). On the contrary, ChIs and FS interneurons displayed a very high frequency of spontaneous action potentials as already reported[113,136] (Table 3).

4.3. Modulation of the sensory responses during the SWO cycle

The membrane potential of MSNs during the SWO exhibits a bimodal distribution switching from Up to Down states[54] (Fig. 20c). To understand how sensory responses

are modulated during the SWO cycle, responses were separated to those occurring during the Up or Down states. Sensory stimulations were randomly launched every 5 s, therefore, they occurred during any of these states. Because all of the stimuli are randomized and due to the longer duration of the Down states (1100 ± 217 ms) with respect to the Up states (391 ± 44 ms) (p=0.003), the 79.52 ± 4.94% of the stimulus occurred during the Down states, whereas only the 20.47 ± 4.94% did so during the Up states. In addition, it has been reported that sensory responses of MSNs are robustly reliable during the Down states, whereas during the Up states they are characterized by low amplitudes and a high probability of failure[53,436,437]. In agreement, our data shows that the amplitude of visual, whisker or bimodal responses was very small or zero when occurring during the Up states (Fig. 22a). Moreover, we observed a significant negative lineal voltage-dependent relationship between the amplitude of the tactile, visual and bimodal responses and the membrane potential of the MSNs. The more hyperpolarized the membrane potential was (corresponding to the Down state), the largest amplitudes were exhibited (Fig. 22b).

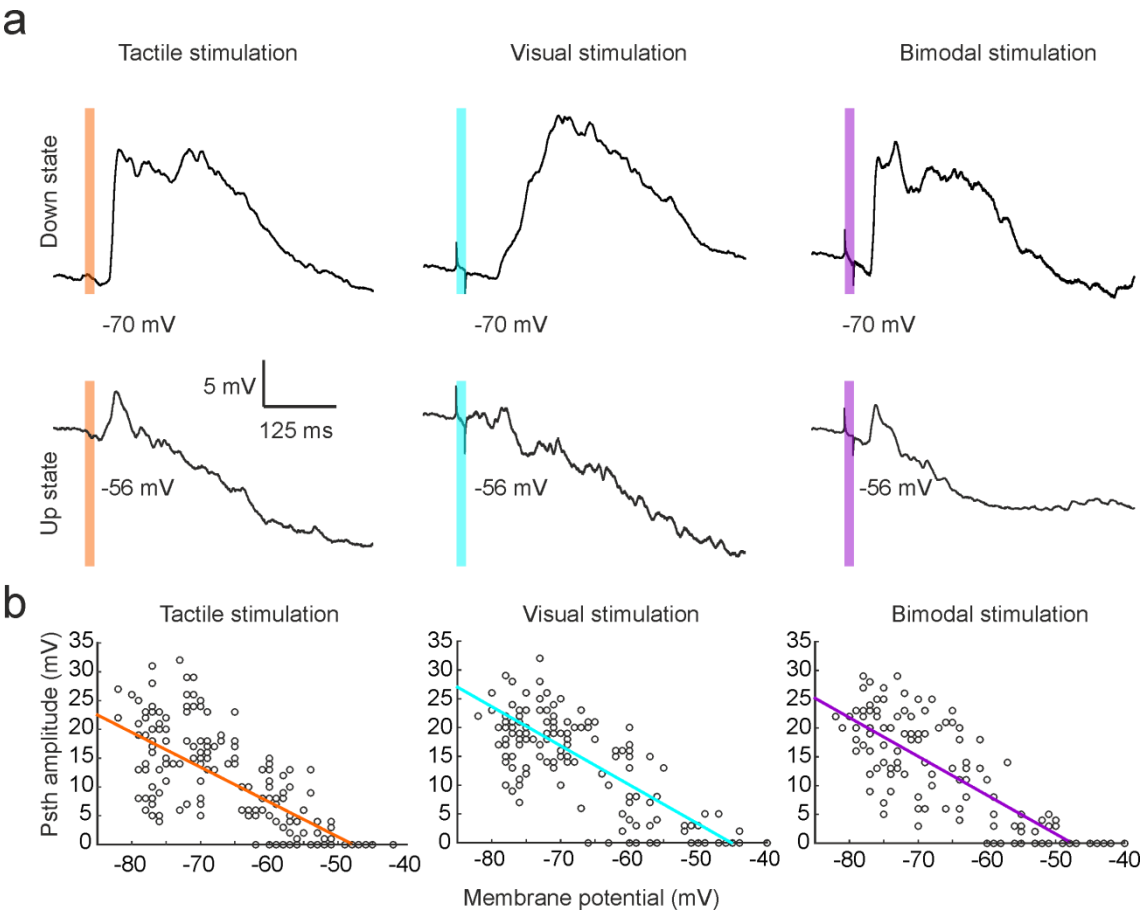

Figure 22. Voltage-dependence of sensory evoked responses. a, Waveform averages of an example MSN responding to tactile (left), visual (middle) and bimodal (right) stimulation during Down (upper traces) or Up states (bottom traces). Total trials in Down state/cell n=51. Total trials in Up state/cell n=11. The coloured line represents the sensory stimulation**. b,** Variation of amplitudes at different membrane potentials corresponding to Up and Down states for tactile (left), visual (middle) and bimodal (right) stimulation. Each point represents a sensory response in all the recorded neurons. A linear regression

between -85 and -40 mV values (Tactile: R^2 0.61; $p<0.0001$; Visual: R^2 0.68; $p<0.0001$; Bimodal: R^2 0.67; $p<0.0001$) illustrates the voltage dependence of the sensory responses.

Taking into account the poor reliability and absence of the MSN responses during the Up states, we focused on the study of the responses evoked during the Down states.

4.4. Optogenetic control of dopamine release in the DMS

The SNc is mainly compounded by dopaminergic neurons projecting to the striatum[2,262]. Nevertheless, the SNr, a very close structure which contains GABAergic as well as dopaminergic neurons, sends projections towards several brain regions[2] with higher density to the thalamus and forebrain areas[194,246,438]. For these reasons, direct electrical stimulation of the SNc is an unspecific method as it would activate all types of neurons projecting towards the striatum besides other brain structures that could affect the outcome. In order to understand the specific impact of DA on MSNs, we activated optogenetically the dopaminergic terminals directly in the DMS. To that end, we injected the cre dependent virus AAV5-hSyn-FLEX-ChrimsonR-tdTomato, which expresses the opsin ChrimsonR[415], in the SNc of D2-cre x ChR2 x DAT-cre mice, to infect the dopaminergic neurons (Fig. 20a, d) [see methods]. This mice line expresses ChR2 in the indirect MSNs and cre recombinase in the dopamine transporter (DAT) expressing cells, allowing the stimulation with two different opsins: ChrimsonR (peak excitation wavelength of ~660 nm) to activate the dopaminergic terminals; and ChR2 (peak excitation wavelength of ~470 nm) (Fig. 20d) to identify MSNs belonging to the direct and indirect pathways with the optopatcher (Fig. 20e).

But before carrying out the described experimental approach, we checked the efficiency and reliability of the optogenetic stimulation to release DA from the axon terminals in the DMS (Fig. 23a, b). To that end, we used a recently developed[423] intensity-based genetically encoded DA sensor called dLight1. This sensor enables the optical recording of DA dynamics allowing the detection of extracellular DA with sub-second resolution and insignificant sensitivity to other monoamines, GABA, and glutamate[423,439,440]. To measure the efficiency of DA release elicited by our optogenetic stimulation, we did a set of fiber photometry experiments using a virus encoding dLight1. To that end, we first injected the virus expressing the opsin ChrimsonR in the SNc, as described before. Then, six weeks later, the AAV5-hSyn-dLight1.2-EGFP[423] virus was injected in the DMS to induce the expression of the dLight1 sensor (n= 7 DAT-cre mice, Fig. 23a, e). Two weeks later, we stimulated optogenetically with a 660 nm LED light while performing fiber photometry experiments. During wakefulness and also under anaesthesia, dopaminergic neurons burst approximately at a range of 12-20 Hz[256,257,261], so we designed an optogenetic train with 4 light pulses of 15 ms each at 15 Hz (with an interpause of 66 ms) (Fig. 23b) that mimics their discharge.

We first measured the changes on fluorescence related to DA release in response to the stimulation directly in the SNc: the levels of fluorescence increased to 2.29 ± 0.10%, a similar value to the ones reported previously[423]. Then, we repeated the experiment but stimulating in the dopaminergic terminals of the DMS. In this case, the fluorescence

increased to 0.56 ± 0.25% (Fig. 23c, d), approximately a quarter of the one obtained when stimulating the SNc (p=0.002). In both cases, the onset and peak delays of the responses were similar between stimulations (Onset delay: SNc = 62.4 ± 12.03 ms, striatal terminals = 55.57 ± 10.01 ms (p=0.67); Peak delay: SNc = 399.5 ± 56.99 ms, striatal terminals = 430.14 ± 27.67 ms (p=0.42)).

Anatomical studies were performed after every experiment, to confirm that the DA increase was always accompanied of a correct expression of both viruses (Fig. 23e). Finally, we performed a set of control experiments, in which we injected AAV5-CAG-FLEX-tdTomato in the SNc, a cre dependent virus that was not expressing the ChrimsonR opsin (n= 6 DAT-cre mice) [see methods]. In this case, changes in fluorescence related to DA release were undetectable (0% of fluorescence increase) (Fig. 23c-d).

In summary, these set of experiments demonstrate that our experimental approach is a very controlled and reliable method to release DA from the striatal terminals, even though the stimulation of the SNc induced a larger release.

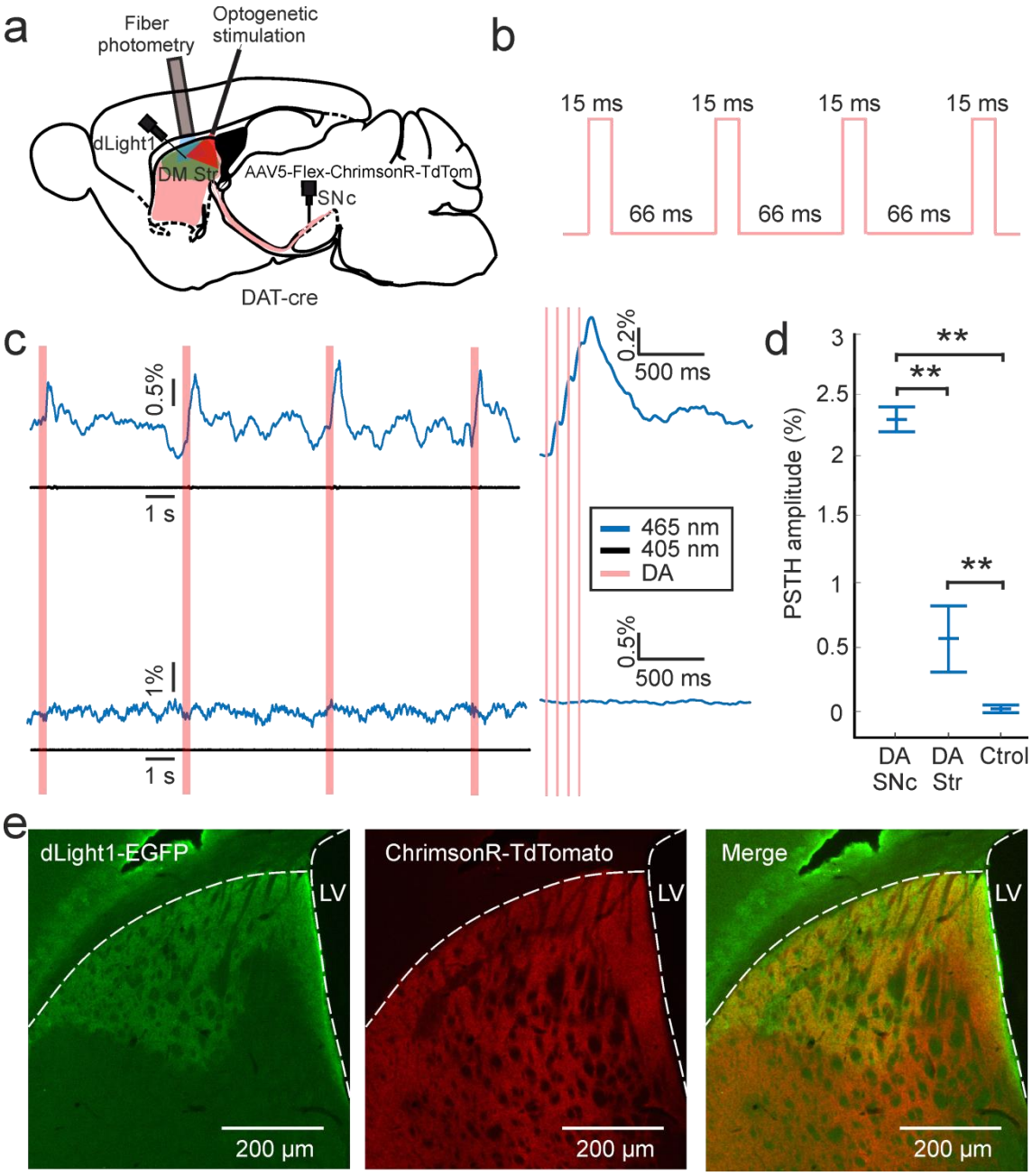

Figure 23. Optogenetic dopamine release in the DMS. a, Schematic representation of the fiber photometry experimental set up. **b,** Optogenetic stimulation train used in this study. **c,** Left: Trace example of the fluorescence measurements along time from one of the recording sessions. Right: Waveform average of the elicited DA release in the DMS when stimulating optogenetically the dopaminergic terminals in the DMS with the virus expressing the opsin ChrimsonR (top) or with the control virus (bottom). Blue traces correspond to the 465 nm signal. Black traces correspond to the isosbestic 405 nm signal (used as a reference point) [see methods]. Red bars represent the time of the optogenetic stimulation trains. **d,** Quantification of the changes in fluorescence when stimulating directly the SNc (DA SNc), the dopaminergic terminals in the DMS (DA Str) or during control conditions (Ctrol). ** $p<0.01$. **e,** Coronal images of a DAT-cre mice injected with the viruses expressing the sensor dLight1-EGFP and the opsin ChrimsonR-TdTomato in the DMS and SNc respectively**.** Left: Image showing the expression of the dLight1 sensor injected in the dorsal striatum. Middle: Image showing the expression of the ChrimsonR opsin in the dopaminergic terminals. Right: Merge of both images.

4.5. Dopamine impact on spontaneous activity

4.5.1. Neurotransmitter co-release in the DMS

Once we checked the reliability of the optogenetic stimulation, we then studied whether DA could affect the spontaneous activity of MSNs. To that end, we analysed 18 direct and 10 indirect MSNs identified as previously described (Fig. 20e) from 12 D2-cre x ChR2 x DAT-cre injected mice, comparing 100 s of spontaneous activity with or without DA (Fig. 25a). Previous *in vitro* studies have described glutamate and GABA co-release in the striatum[243,441–444]. In order to explore this possibility in the DMS *in vivo*, DA terminals were optogenetically stimulated while spontaneous activity was recorded. Our results did not show any fast depolarization (EPSPs) aligned with the stimulation (Fig. 24). In addition, in order to study the inhibitory components (IPSPs) that could be induced by DA, some MSNs were depolarized (n= 6) by injecting positive current, moving their membrane potential close to the excitatory reversal potential. Nevertheless, we could neither detect any IPSPs aligned with the optogenetic stimulation (Fig. 24).

In summary, there were not fast responses induced by DA, either excitatory or inhibitory, hence glutamate or GABA co-release was not detected. This result strongly suggests that only DA acts as neuromodulator on DMS-MSNs.

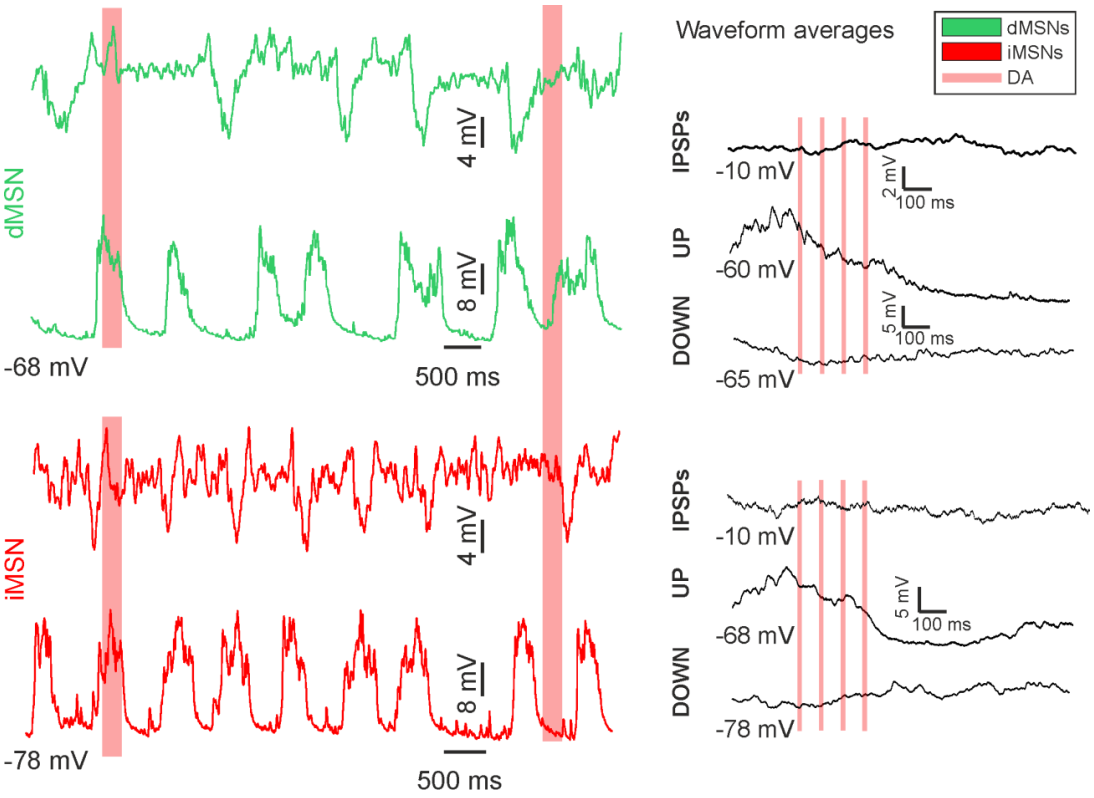

Figure 24. DA release during the spontaneous activity of MSNs. Left: Example trace of an *in vivo* whole-cell recording of a direct (top) and indirect (bottom) dorsomedial MSN while stimulating optogenetically every 5 seconds. Right: Waveform averages of the same example MSNs at different membrane potentials. Coloured lines represent the optogenetic stimulation.

4.5.2. Slow Wave Oscillations

It has been reported a reduction of the oscillatory frequency of the SWO in MSNs of DA depleted mice in the DLS[62]. Hence, we wondered whether MSNs SWO activity would be affected when DA is released in the DMS. To that end, we analysed how DA impacted on the SWO frequency and resting membrane potential during the Down states. In addition, we characterized the SWO in presence and absence of DA in the identified direct and indirect MSNs by measuring 13 features of the Up states (Table 4) [see methods for a detailed description of features]:

1. **Average voltage of the Up state, calculated as the mean voltage value displayed.**
2. Standard deviation of the Up state, calculated as the standard deviation of the mean voltage.
3. **Minimum voltage of the Up state, calculated as the lowest voltage value.**
4. **Maximum voltage of the Up state, calculated as the highest voltage value exhibited.**
5. Peak to peak distance in the Up state, calculated as the difference between the minimum and maximum voltage displayed.
6. Maximum value of the derivative of the Up state, calculated as the highest value of the derivative.
7. Minimum value of the derivative of the Up state, calculated as the lowest value of the derivative
8. Number of peaks in the Up state.
9. **Length of the Up state, calculated as the time from the onset until the end of the Up state.**
10. **Amplitude of the Up state, calculated as the difference between the mean voltages exhibited by the cell during the Down and Up states.**
11. Slope of the transition from the Down to the Up state, calculated as the speed of the transition of the Down to the Up state.
12. Slope of the transition from the Up to the Down state, calculated as the speed of the transition of the Up to the Down state.
13. Transition ratio of the slopes, calculated as the division between the slope of the transition from the Down to the Up state and the slope of the transition from the Up to the Down.

The SWO frequency was not affected by DA (control = 0.68 ± 0.10 Hz, DA= 0.68 ± 0.13 Hz, p=0.91), for both direct and indirect MSNs (control: direct MSNs = 0.66 ± 0.10 Hz, indirect MSNs = 0.70 ± 0.10 Hz, p=0.22; DA: direct MSNs = 0.66 ± 0.11 Hz, indirect MSNs = 0.72 ± 0.16 Hz, p=0.24).

Nevertheless, we found some modulatory effects of DA during the SWO. The average voltage of the Up state (Feature **nº1**) changed in direct (control = -54.53 ± 8.07 mV, DA = -59.70 ± 8.81 mV, p=0.003) and indirect MSNs (control = -56.00 ± 3.32 mV, DA = -

59.75 ± 5.91 mV, p=0.01); as well as the maximum voltage in the Up state (Feature **nº4**) (dMSNs: control = -44.84 ± 8.18 mV, DA = -52.15 ± 9.80 mV, p=0.0002; iMSNs: control = -45.19 ± 3.72 mV, DA = -51.10 ± 5.24, p=0.002) (Fig. 25b, Table 4). In addition, the minimum voltage in the Up state (Feature **nº3**) changed for direct MSNs (control = -59.96 ± 8.22 mV, DA = -64.20 ± 8.28 mV, p=0.01) (Fig. 25b, Table 4). Interestingly, the membrane potential of the Down states did not show any change in both types of MSNs (dMSNs: control = -70.13 ± 5.51 mV, DA = -70.86 ± 5.70 mV, p=0.7; iMSNs: control = -68.85 ± 3.97 mV, DA = -68.95 ± 3.45 mV, p=0.8). These modulatory changes in the voltage values had a discrete impact in the amplitude of the Up states (Feature **nº10**) which showed a tendency to decrease (dMSNs: control = 16.84 ± 4.66 mV, DA = 15.43 ± 5.38 mV, p=0.07; iMSNs: control = 16.27 ± 3.45 mV, DA = 15.51 ± 2.97 mV, p=0.08). Finally, the Up state length (feature **nº9**) was increased from 405 ± 47 ms to 418 ± 51 ms (p=0.02) only in the case of the direct pathway MSNs (Fig. 25c, Table 4), showing a slightly elongation when DA is released.

4.5.3. High frequency oscillations

High frequency oscillations have been related with different processes in health and disease[365,445]. For instance, they have been linked to cognitive operations such as selective attention[446,447] or working memory[448,449]. They normally occur during wakefulness and during the Up states[49,450] of the SWO as well. Importantly, exaggerated beta-band oscillations have been established as one of the signatures of PD[365–367,451], and its appearance is usually taken as a sign of DA depletion. It has been widely reported that this exaggerated beta-band oscillatory activity is reduced by L-DOPA treatment in the STN and GPi of PD patients[364,365,367,451,452].

To analyse the spontaneous SWO (<1Hz) and the high frequency oscillations over Up states we applied the Noise-Assisted Multivariate Empirical Mode Decomposition algorithm (NA-MEMD)[453], followed by the application of the Hilbert transform [see methods]. The main advantage of this technique when compared to traditional decomposition techniques such as Fast Fourier transform or wavelet analysis is the capacity to deal with the nonlinear and non-stationary properties of neural oscillations[63,424]. We computed the energy of the theta- (6-10 Hz), beta- (10-20 Hz) and gamma-bands (20-80 Hz) to explore whether the release of DA could affect the high frequency components of the oscillatory activity. Our results show that DA decreases the energy of all of them: theta- (control= 2.20 ± 0.63 mV, DA= 1.79 ± 0.45 mV^2, p=0.000003), beta- (control= 3.11 ± 0.55 mV^2, DA= 2.72 ± 0.41 mV^2, p=0.00009) and gamma-band (control= 0.60 ± 0.33 mV, DA= 0.36 ± 0.21 mV^2, p=0.000004) in both MSNs subpopulations (Fig. 25d, green and red traces).

This decrease was always paired with the correct expression of ChrimsonR in the DMS (Fig. 20d). To ensure that this energy decrease was related to DA release, we performed a set of control experiments. As described previously, 3 D2-cre x ChR2 x DAT-cre mice were injected the SNc with the cre dependent virus AAV5-CAG-FLEX-tdTomato which does not express ChrimsonR (as control virus). In this case, the optogenetic

stimulation did not change the energy in any of the explored frequency bands (theta, beta and gamma) (Fig. 25d, black and grey traces), confirming that the energy decrease is induced by DA. When comparing between direct and indirect MSNs, differences were not detected (Fig. 25d).

In summary, our data shows that DA decreases theta-, beta- and gamma-bands over Up states in DMS-MSNs. These results suggest that the changes affecting the amplitude of the Up states, showed in the previous section (Fig. 25b), reflect the decline of the high frequency oscillations (Fig. 25d).

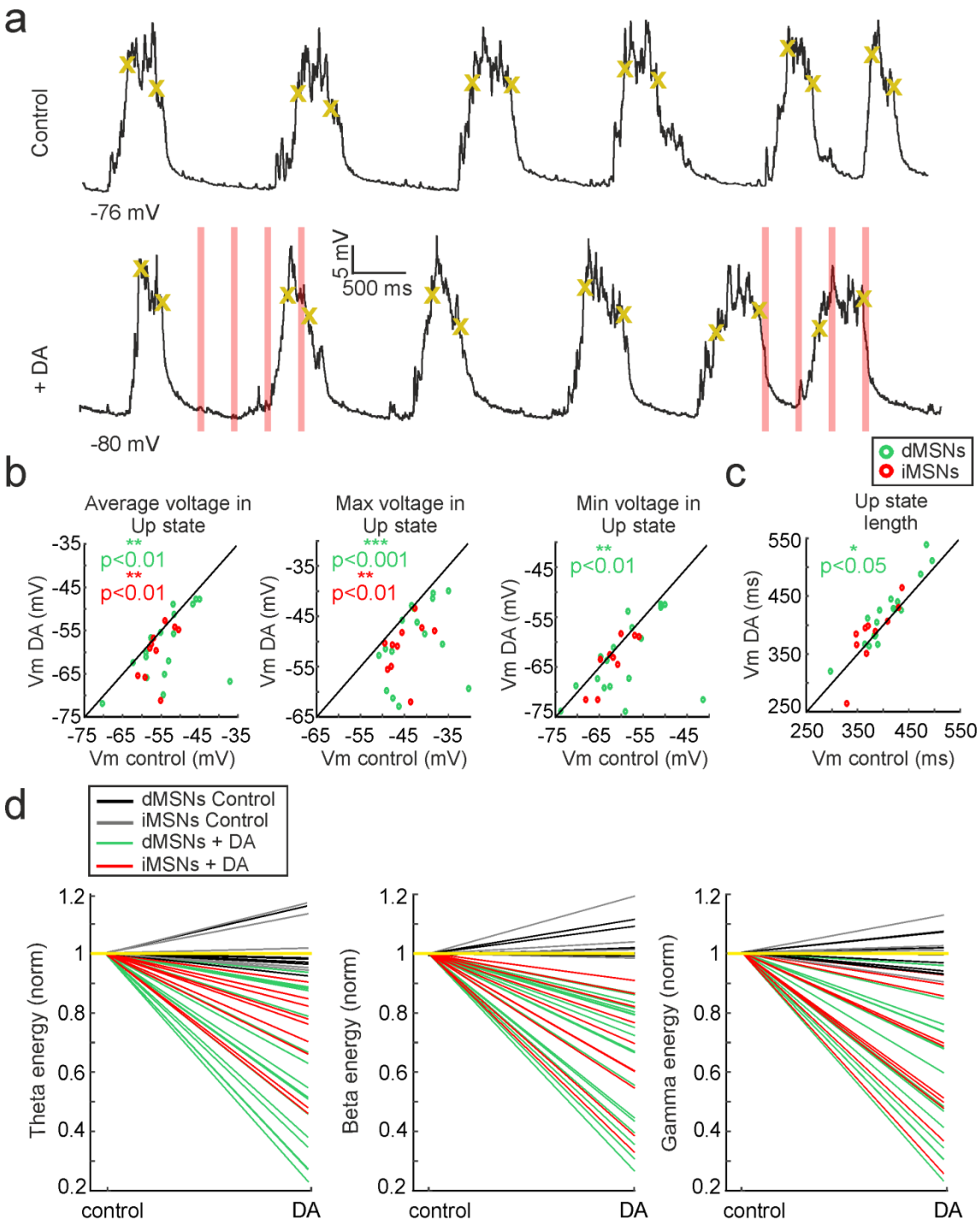

Figure 25. DA impact on the spontaneous activity of dorsomedial MSNs. a, Example traces of the SWO in MSNs in control (upper trace) and during DA release (bottom trace). Coloured red lines indicate the optogenetic stimulation. Ochre crosses indicate the onset and end of the detected Up states. **b, c,** Direct and indirect MSNs SWO changes in the Up state voltage (b) and length (c) in the Up states when releasing DA. Green p values represent change for direct MSNs. Red p values represent change for indirect MSNs. Black line is added to illustrate the changes mediated by DA. **d,** Theta- (left), beta- (middle) and gamma-band (right) normalized energy of direct and indirect MSNs. Yellow line indicates the normalized value 1. The normalization was done with respect to the average value presented in control conditions in each frequency band for each neuron.

Feature	All MSNs	direct MSNs	indirect MSNs
1) Average voltage in Up state (mV)	**-55.06 ± 6.72*** **	**-54.53 ± 8.07** **	**-56.00 ± 3.32** **
1) Average voltage in Up state (mV) + DA	**-59.72 ± 7.78*** **	**-59.70 ± 8.81** **	**-59.75 ± 5.91** **
2) Up state standard deviation (mV)	5.67 ± 1.38	5.46 ± 1.57	6.05 ± 0.88
2) Up state standard deviation (mV) + DA	4.74 ± 1.32	4.57 ± 1.55	5.05 ± 0.71
3) Min voltage in the Up state (mV)	-60.62 ± 6.92	**-59.96 ± 8.22** **	-61.79 ± 3.70
3) Min voltage in the Up state (mV) + DA	-64.44 ± 7.51	**-64.20 ± 8.28** **	-64.87 ± 6.25
4) Max voltage in the Up state (mV)	**-44.96 ± 6.84*** **	**-44.84 ± 8.18*** **	**-45.19 ± 3.72** **
4) Max voltage in the Up state (mV) + DA	**-51.77 ± 8.36*** **	**-52.15 ± 9.80*** **	**-51.10 ± 5.24** **
5) Peak to peak in the Up state (mV)	-22.19 ± 4.91	-21.44 ± 5.66	-23.53 ± 2.96
5) Peak to peak in the Up state (mV) + DA	-18.35 ± 4.93	-17.73 ± 5.83	-19.46 ± 2.59
6) Max of Up state derivative (dmV/dt)	0.69 ± 0.17	0.66 ± 0.20	0.76 ±0.08
6) Max of Up state derivative (dmV/dt) + DA	0.56 ± 0.16	0.54 ± 0.18	0.60 ± 0.09
7) Min of Up state derivative (dmV/dt)	-0.56 ± 0.15	-0.54 ± 0.18	-0.59 ± 0.09
7) Min of Up state derivative (dmV/dt) + DA	-0.44 ± 0.12	-0.42 ± 0.14	-0.46 ± 0.10
8) Number of peaks in the Up state (units)	1.10 ± 0.08	1.10 ± 0.09	1.09 ± 0.08
8) Number of peaks in the Up state (units) + DA	1.10 ± 0.08	1.10 ± 0.08	1.09 ± 0.07
9) Up state length (ms)	395 ± 45.21	**405 ± 47.79***	378 ± 36.09
9) Up state length (ms) + DA	401 ± 52.85	**418 ± 51.19***	389 ± 53.03
10) Up state amplitude (mV)	16.47 ± 3.97	16.84 ± 4.66	16.27 ± 2.45
10) Up state amplitude (mV) + DA	15.25 ± 4.42	15.43 ± 5.38	15.51 ± 1.97
11) Down to Up transition slope (mV/ms)	0.718 ± 0.23	0.695 ± 0.25	0.762 ± 0.19
11) Down to Up transition slope (mV/ms) + DA	0.611 ± 0.25	0.588 ± 0.29	0.653 ± 0.14
12) Up to down transition slope (mV/s x 10^2)	0.474 ± 0.23	0.462 ± 0.28	0.495 ± 0.10
12) Up to down transition slope (mV/s x 10^2) + DA	0.370 ± 0.23	0.363 ± 0.29	0.382 ± 0.65
13) Slope transition ratio (arbitrary units)	1.51 ± 0.34	1.50 ± 0.37	1.53 ± 0.31
13) Slope transition ratio (arbitrary units) + DA	1.65 ± 0.34	1.61 ± 0.36	1.70 ± 0.34

Table 4. Characterization of the SWO in presence and absence of DA. All values display means ± standard deviation. Each feature was compared for significance with and without DA. * $p<0.05$, ** $p<0.01$, *** $p<0.001$.

4.6. Dopamine impact on sensory responses

The main objective of this study was to understand whether DA could modulate tactile and visual sensory responses in DMS-MSNs. Moreover, we wondered its impact on the direct and indirect pathways. To that end, we recorded *in vivo* a set of 29 neurons (14 direct and 15 indirect MSNs) from the D2-cre x ChR2 x DAT-cre mice injected as previously described (n= 12, Fig. 20d). To evoke sensory responses, we randomly launched contralateral tactile or visual stimuli (Fig. 26a) [see methods]. 30 ms prior to the sensory stimulation, DA was released by optogenetic stimulation in the axonal dopaminergic terminals of the DMS, as previously described. Simultaneously, we performed double LFP recordings in S1 and V1 to ensure and monitor the sensory responses evoked in their respective cortical areas (S1 and V1, Fig. 26a). Both tactile and visual responses occurred earlier in cortex than their respective striatal activation (Table 5-7), suggesting a sequential activation from cortex to striatum, in agreement with previous results[53,218]. In addition, evoked responses where similar in presence or absence of DA release (Table 5).

	Onset delay (ms)	Peak delay (ms)	Amplitude (μV)	Slope (μV/ms)
Tactile responses evoked in S1	12.75 ± 3.91	40.25 ± 5.12	521 ± 42.42	18.94 ± 5.52
Tactile responses evoked in S1 + DA	11.65 ± 3.73	43.19 ± 6.17	540 ± 40.69	17.13 ± 4.28
Visual responses evoked in V1	49.23 ± 10.87	95.26 ± 18.49	505 ± 45.41	11.67 ± 4.59
Visual responses evoked in V1 + DA	50.74 ± 11.97	97.65 ± 21.46	499 ± 50.23	10.21 ± 5.13

Table 5. Mean values of tactile and visual evoked responses in S1 and V1 LFP recordings with or without DA release. All values are mean ± standard deviation.

4.6.1. Dopamine release during tactile responses

In the DLS region which receives the highest density of axons from S1, whisker responses are sharper and bigger compared with the ones recorded in the DMS[53,62]. Nevertheless, whisker stimulation also induces strong and fast responses in the DMS-MSNs with the same onset delay than the dorsolateral ones[53]. Consistent with previous results, the average onset delay of our responses was 22.39 ± 3.72 ms (dMSNs = 23.05 ± 3.03 ms; iMSNs = 21.79 ± 2.29 ms) (Table 6). In addition, they displayed an average

peak delay of 95.96 ± 26.14 ms (dMSNs = 93.52 ± 26.62 ms; iMSNs = 98.22 ± 26.49 ms), amplitude of 10.20 ± 5.72 mV (dMSNs = 8.79 ± 6.21 mV; iMSNs = 11.51 ± 5.09 mV) and slope of 0.163 ± 0.126 mV/ms (dMSNs = 0.155 ± 0.149 mV/ms; iMSNs = 0.171 ± 0.106 mV/ms) (Table 6).

It has been reported that DA depletion in 6-OHDA mice impairs tactile responses in DLS direct MSNs, abolishing the differences between ipsi and contralateral whisker responses observed in healthy control animals[62]. Therefore, we wondered whether DA would modulate tactile responses in the DMS-MSNs. Nevertheless, when releasing DA prior to the tactile stimulation, neither direct nor indirect MSNs displayed any significant difference (Table 6, Fig. 26b, c). Therefore, we conclude that the release of DA has not impact on tactile responses of the DMS-MSNs.

	Onset delay (ms)	Peak delay (ms)	Amplitude (mV)	Slope (mV/ms)
Direct MSNs	23.05 ± 3.03	93.52 ± 26.62	8.79 ± 6.21	0.155 ± 0.149
Direct MSNs + DA	22.61 ± 4.25	94.58 ± 25.17	10.26 ± 7.35	0.182 ± 0.203
Indirect MSNs	21.79 ± 2.29	98.22 ± 26.49	11.51 ± 5.09	0.171 ± 0.106
Indirect MSNs + DA	21.32 ± 3.95	94. 53 ± 28.24	11.83 ± 5.41	0.188 ± 0.114

Table 6. Mean values of tactile responses for direct and indirect MSNs with or without DA release. All values are mean ± standard deviation. n=29 (14 direct MSNs; 15 indirect MSNs).

4.6.2. Dopaminergic modulation of visual responses

In contrast with the DLS-MSNs, which only respond to tactile sensory inputs, the DMS-MSNs integrate information from different modalities, where tactile responses precede visual ones by few tens of milliseconds[53]. In agreement with this, we observed that the average onset delay of the visual responses was 57.09 ± 12.47 ms (dMSNs = 59.47 ± 11.69 ms; iMSN s= 54.87 ± 13.16 ms), being much slower than the tactile ones (Table 6 and 7). Visual responses exhibited an average amplitude of 12.76 ± 6.12 mV (dMSNs = 13.05 ± 6.71 mV; iMSNs = 12.55 ± 5.46 mV); peak delay of 123.80 ± 24.82 ms (dMSNs = 130.61 ± 25.24 ms; iMSNs = 120.44 ± 23.47 ms) and slope of 0.167 ± 0.085 mV/ms (dMSN s= 0.189 ± 0.56 mV/ms; iMSNs= 0.143 ± 0.66 mV/ms). In addition, they displayed similar values between direct and indirect MSNs in control conditions (Table 7). However, when DA was released, the peak delay of the visual responses of the direct MSNs was reduced with respect to control conditions (control = 130.61 ± 25.24 ms, DA = 122.71 ± 24.41 ms, p=0.0046) (Table 7, Fig. 26d). This reduction was

accompanied by a fastened slope from the Down to the Up state (control = 0.189 ± 0.56 mV/ms, DA = 0.244 ± 0.16 mV/ms, p=0.04) (Table 7, Fig. 26d). The reduction in the peak delay together with the fastened slope strongly suggests that DA accelerates visual responses (Fig. 26b, d). Indirect MSNs did not show the same effect, their peak delays and slopes were similar before or after DA release (control peak delay = 120.44 ± 23.47 ms, DA peak delay = 118.79 ± 22.55 ms, p=0.35; control slope = 0.143 ± 0.66 mV/ms, DA slope = 0.155 ± 0.54, p=0.63 mV/ms). These results indicate that DA has a different modulatory effect on direct and indirect MSNs visual responses.

	Onset delay (ms)	Peak delay (ms)	Amplitude (mV)	Slope (mV/ms)
Direct MSNs	59.47 ± 11.69	**130.61 ± 25.24****	13.05 ± 6.71	**0.189 ± 0.56***
Direct MSNs + DA	60.61 ± 11.63	**122.71 ± 24.41****	12.97 ± 5.92	**0.244 ± 0.16***
Indirect MSNs	54.87 ± 13.16	120.44 ± 23.47	12.55 ± 5.46	0.143 ± 0.66
Indirect MSNs + DA	56.62 ± 14.12	118.79 ± 22.55	13.72 ± 5.06	0.155 ± 0.54

Table 7. Mean values of visual responses for direct and indirect MSNs with or without DA release. All values are mean ± standard deviation. n=29 (14 direct MSNs; 15 indirect MSNs). Asterisks indicate significant differences between direct and indirect MSNs + DA values. * p<0.05, ** p<0.01.

4.6.3. Dopaminergic modulation of bimodal responses

In control conditions, the simultaneous tactile and visual stimulation evokes a synaptic response in which two components are identified, with tactile inputs preceding visual ones by few tens of milliseconds[53] (Table 6 and 7). Nevertheless, because DA modified the temporal integration of visual responses (Fig. 26d), we wondered whether DA could modify the bimodal integration. To that end, the previous whisker and visual stimuli were launched simultaneously. The recorded bimodal responses displayed an average onset delay of 22.76 ± 5.58 ms (dMSNs = 23.35 ± 4.83 ms; iMSNs = 22.21 ± 6.31 ms), a very similar value to the one exhibited by single tactile responses (Table 6 and 8), reflecting that the first component of the bimodal responses is induced by the whisker input, which presents the fastest responses. The mean amplitude of the bimodal responses in control was 13.40 ± 6.53 mV (dMSNs = 12.87 ± 6.04 mV; iMSNs = 14.04 ± 7.02 mV), with no differences between de direct and indirect pathways (Table 8) and similar to the single visual responses as well (Table 7). However, the amplitude of the direct MSNs increased ~25%, from 12.87 ± 6.04 mV to 16.02 ± 5.16 mV (p=0.003) when DA was released, whereas indirect MSNs were not affected (Table 8, Fig. 26b, e). Thus, DA increases bimodal responses selectively in direct MSNs.

How can this amplitude increase be explained? Prior to this study, Reig and Silberberg showed the temporal properties of visual and tactile integration in DMS-MSNs[53]. Authors reported that only when the onset or peak delay of visual and tactile responses were forced to occur simultaneously, the bimodal response amplitude increased (Fig. 10), thus promoting the suitable time window for the synaptic integration between stimuli. Therefore, our results strongly suggest that the acceleration of the visual responses induced by DA (Fig. 26d) decreases the latency between visual and tactile responses. This must lengthen the time window that facilitates the synaptic summation between tactile and visual inputs, which is reflected by the amplitude increase of the bimodal responses.

	Onset delay (ms)	Peak delay (ms)	Amplitude (mV)	Slope (mV/ms)
Direct MSNs	23.35 ± 4.83	104.97 ± 22.40	**12.87 ± 6.04****	0.400 ± 0.192
Direct MSNs + DA	23.46 ± 4.51	106. 46 ± 24.19	**16.02 ± 5.16****	0.410 ± 0.272
Indirect MSNs	22.21 ± 6.31	97.55 ± 23.06	14.04 ± 7.02	0.343 ± 0.239
Indirect MSNs + DA	21.80 ± 5.97	97.95 ± 22.91	14.13 ± 5.57	0.313 ± 0.166

Table 8. Mean values of bimodal responses for direct and indirect MSNs with or without DA release. All values are mean ± standard deviation. n=29 (14 direct MSNs; 15 indirect MSNs). Asterisks indicate significant differences between direct and indirect MSNs + DA values. ** $p<0.01$.

In summary, our results demonstrate that DA synchronizes the bimodal responses of the direct pathway MSNs in the DMS (Fig. 26b, e). This effect can be explained by the acceleration of the visual responses facilitated by DA, decreasing the delay difference between visual and tactile responses (Fig. 26b, d), which expands the feasible time window for synaptic integration. This optimization of synchronization is reflected by a clear increase of the bimodal sensory response amplitude (Fig. 26b, e). Overall, our results are revealing a new process in which the brain can integrate multisensory information through DA release in the striatal neurons.

The next step was understanding the mechanism underlying this process, but previously we needed to address: Why did DA affect only visual responses whereas the tactile ones were unaffected?

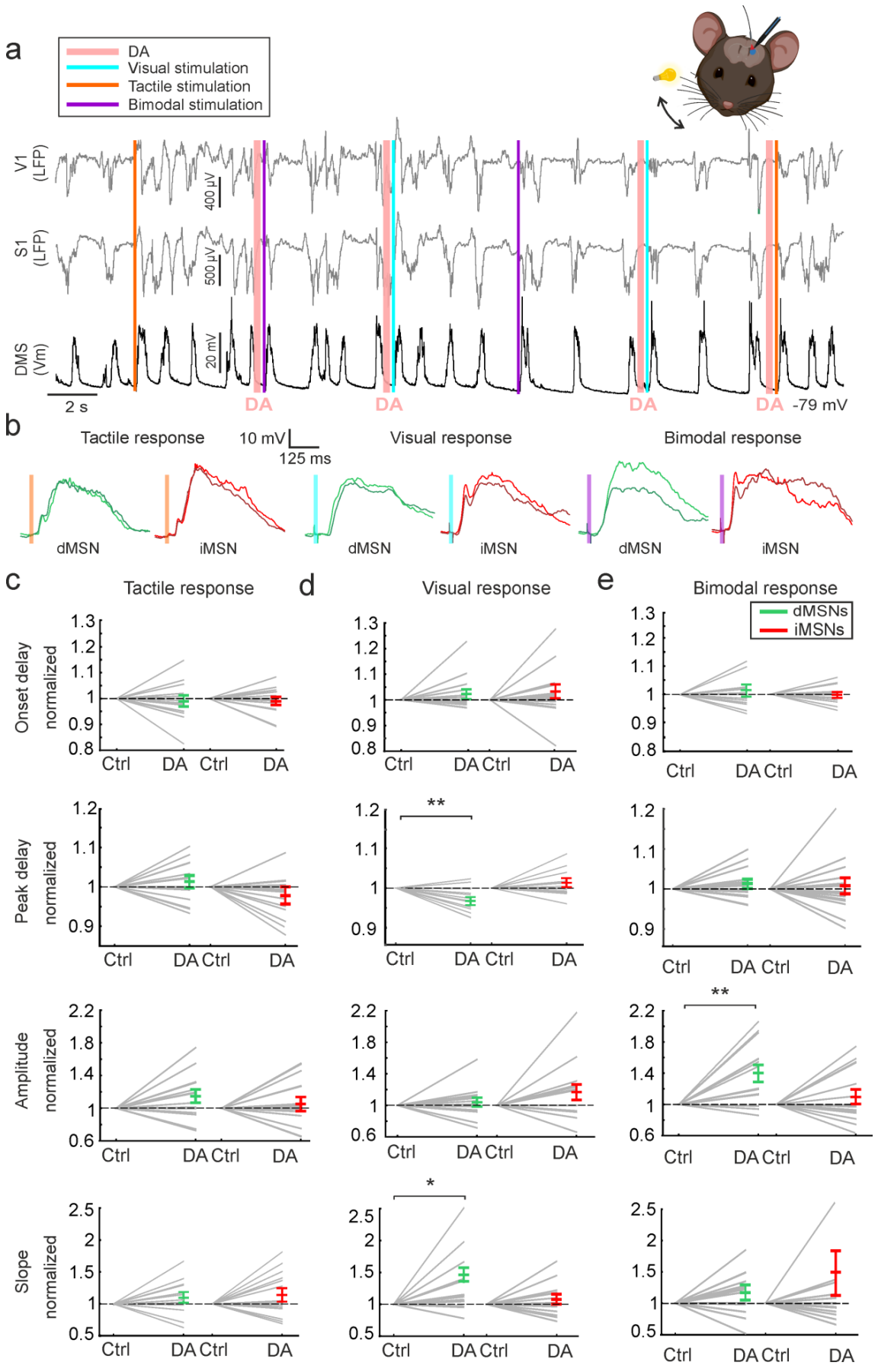
a
DA
Visual stimulation
Tactile stimulation
Bimodal stimulation
V1 (LFP)
400 µV
S1 (LFP)
500 µV
DMS (Vm)
20 mV
2 s
DA
DA
DA
DA
-79 mV
b
Tactile response
10 mV
125 ms
Visual response
Bimodal response
dMSN
iMSN
dMSN
iMSN
dMSN
iMSN
c
Tactile response
d
Visual response
e
Bimodal response
dMSNs
iMSNs
Onset delay normalized
Peak delay normalized
Amplitude normalized
Slope normalized
Ctrl
DA
Ctrl
DA
**
*

Figure 26. Dopaminergic modulation of sensory responses in DMS. a, Example of an *in vivo* whole-cell patch-clamp recording (black trace) with simultaneous LFPs in V1 and S1 (grey traces), while performing optogenetic, visual, tactile and bimodal stimulation randomly. **b,** Waveform averages of direct (green) and indirect (red) MSNs for the different sensory stimulations in presence (light colours) or absence of DA (dark colours). Vertical coloured line indicates the time of the sensory stimulation. **c, d, e,** Normalized averages of direct and indirect MSNs responses after DA release, for tactile (c), visual (d) and bimodal (e) stimulation. The normalization was done with respect to the average value presented in control conditions during the Down states for each neuron. * $p<0.05$, ** $p<0.01$.

4.7. Type-specific cortical projection to the DMS

Previous studies described that the DLS is densely innervated by axons from S1[31,454], while the DMS receives projections from both V1 and S1, although with less density from the last one[53].To confirm the S1 and V1 projections to the dorsal striatum, we injected 8 C57BL/6J animals in S1 and V1 with BDA [see methods]. We observed clear differences in the axonal tracing of S1 and V1 towards the DMS and DLS (Fig. 27) when measuring the covered area by the cortical axonal projections [see methods]. DLS was densely innervated by axons from S1 (99 ± 4%), whereas was basically empty of projections from V1 (0.5 ± 0.3%) ($p=0.026$) (Fig. 27a-b). On the other hand, DMS received axons from both, S1 (56 ± 11%) and V1 (97 ± 11%) although with considerably less density of axons from S1 ($p=0.028$) (Fig. 27a, b).

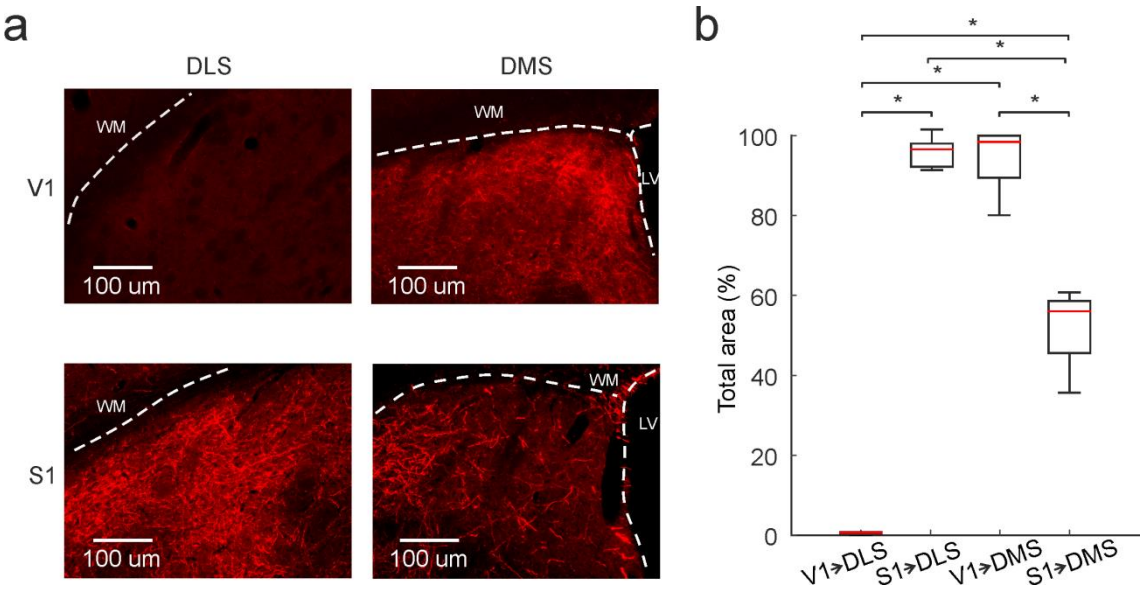

Figure 27. V1 and S1 projections towards the DLS and DMS. a, Representative image of the labelled projections from V1 (top) and S1 (bottom) towards the DLS (left) and the DMS (right). **b,** Quantification of the covered area by the labelled axons from V1 and S1 towards the DLS and DMS.

Cortical pyramidal neurons projecting to the striatum are divided into two subtypes depending on the distribution of their axon collaterals when projecting subcortically: the corticostriatal pyramidal tract neurons (or PT neurons) and the corticostriatal intratelencephalic neurons (or IT neurons)[182]. IT neurons only project to ipsi and contralateral striatum and cortex[181]; whereas PT neurons project exclusively ipsilateral axons towards the brainsteam, leaving collaterals in the striatum[182,186]. Because we

observed that the DMS receives around half of the innervation from S1 axons when compared to the DLS (Fig. 27b), we then wondered whether both types of pyramidal neurons from V1 and S1 project to the DLS and DMS differently. To explore this hypothesis, we selectively infected PT and IT neurons in S1 and V1 injecting the cre dependent virus AAV2.EF1a.DIO.tdTomato.WPRE, in 8 Tlx3-cre and 8 OE25-cre mice [see methods] (Fig. 16). We used OE25-cre and Tlx3-cre mice lines, which express cre recombinase in PT and IT neurons, respectively, to ensure that only PT or IT neurons were targeted. Half of the mice of each line were injected in S1, while the rest were injected in V1 (n= 16).

Our result shows that both IT and PT neurons sent axons to the DMS from V1 (Fig. 28a, left). However, whereas IT S1 neurons projected towards the DMS, PT projections from S1 were barely detectable (IT S1= 51.7 ± 21.7%, PT S1= 4.8 ± 2%; p=0.026) (Fig. 28a, right). Moreover, the covered area by PT S1 axons was always significantly and clearly lower when compared to the covered area by PT V1 axons (PT S1= 4.8 ± 2%, PT V1= 34.8 ± 12.5%; p=0.028) (Fig. 28a, b). In addition, we observed that IT V1 axons covered a larger area when compared to PT V1 axons (IT V1 axons = 78.5 ± 4%, PT V1= 34.8 ± 12.5% p=0.028) (Fig. 28a, b). The near absence of PT S1 projections suggests that there is a type-specific corticostriatal projection from S1 to the DMS. We wondered whether this type-specific projection could be important when explaining why only visual responses are the ones affected by DA release. In this direction, a recent study indicates that only PT neurons make synapses with ChIs[455], avoiding IT axons. Therefore, following these anatomical results, we hypothesize that visual but not tactile stimulation will activate ChIs.

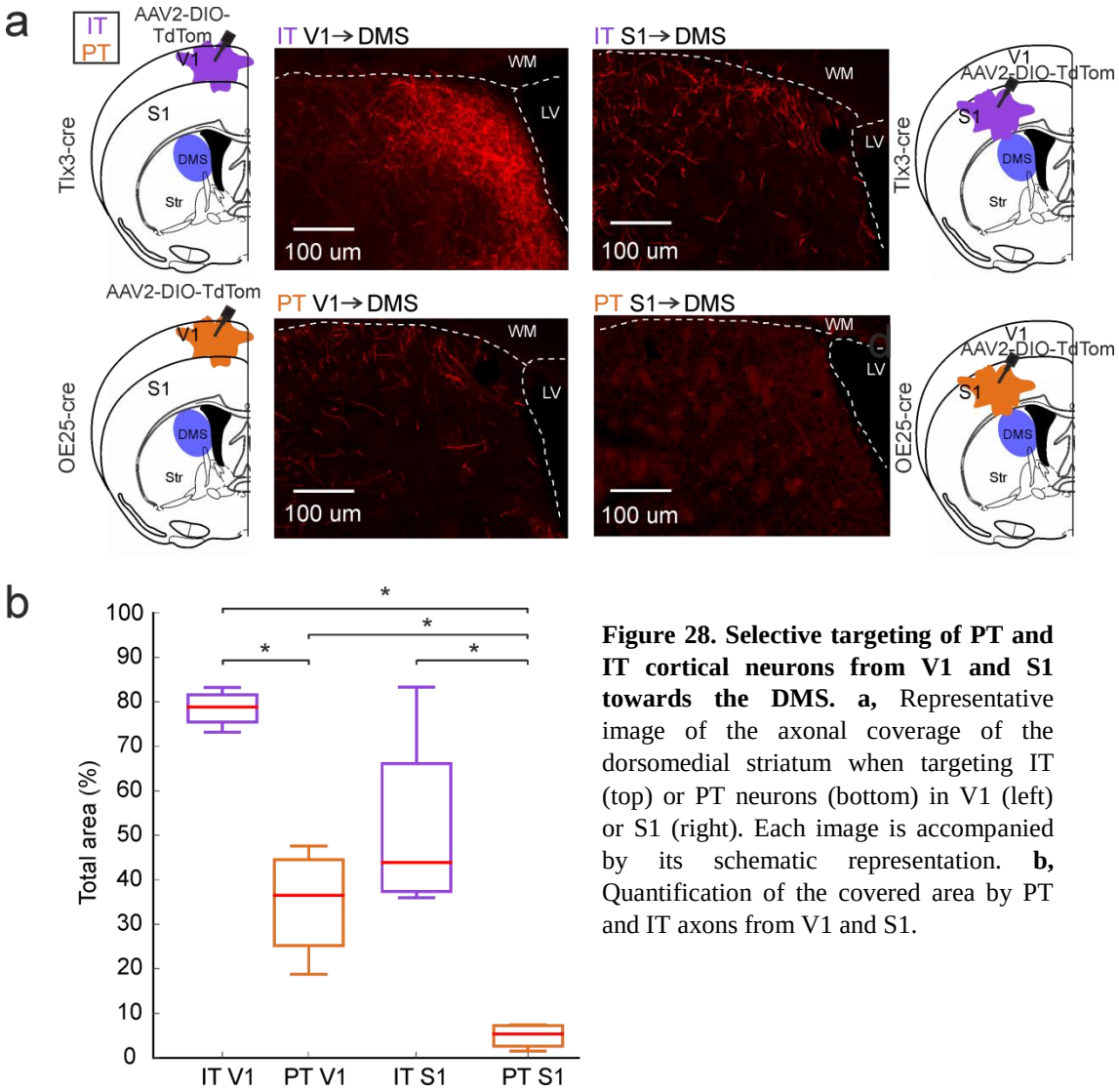

Figure 28. Selective targeting of PT and IT cortical neurons from V1 and S1 towards the DMS. a, Representative image of the axonal coverage of the dorsomedial striatum when targeting IT (top) or PT neurons (bottom) in V1 (left) or S1 (right). Each image is accompanied by its schematic representation. **b,** Quantification of the covered area by PT and IT axons from V1 and S1.

4.8. Cholinergic modulation of sensory responses

ChIs are critical regulators of the striatal microcircuits activity due to their large axonal fields[115,116] and tonic discharge[113]. These interneurons inhibit the activity of MSNs by disynaptic inhibition[115,116], activating different populations of interneurons[127] as a result of a large volume of acetylcholine release. ChIs receive a massive dopaminergic innervation, inhibiting their activity in the dorsal striatum[125,350]. Nonetheless, its effect changes depending on their location: in the DLS, DA induces a brief temporal blockage (~200-500 ms) followed by a rebound of excitation; whereas in the DMS, DA blocks ChIs activity up to 1 s without any detected rebound of activity[350] (Fig. 12). In addition, ChIs respond to tactile stimulation in the DLS[53]. Therefore, we were wondering whether they could modulate the sensory processing of MSNs in the DMS.

Because ChIs comprise only 1-2% of the total striatal neurons, the probability of recording them during blind *in vivo* patch-clamp recordings in a deep brain region is very low. In any case, we recorded 3 ChIs in the DMS that could be clearly

distinguishable by their electrophysiological properties (Fig. 19), and we launched the visual and tactile stimulation while recording them (Fig. 29a). In these few cases, we observed that the visual stimulation increased their firing rate (Fig. 29c). Nevertheless, this was not happening in the case of tactile stimulation, where the firing rate of ChIs did not change (Fig. 29b).

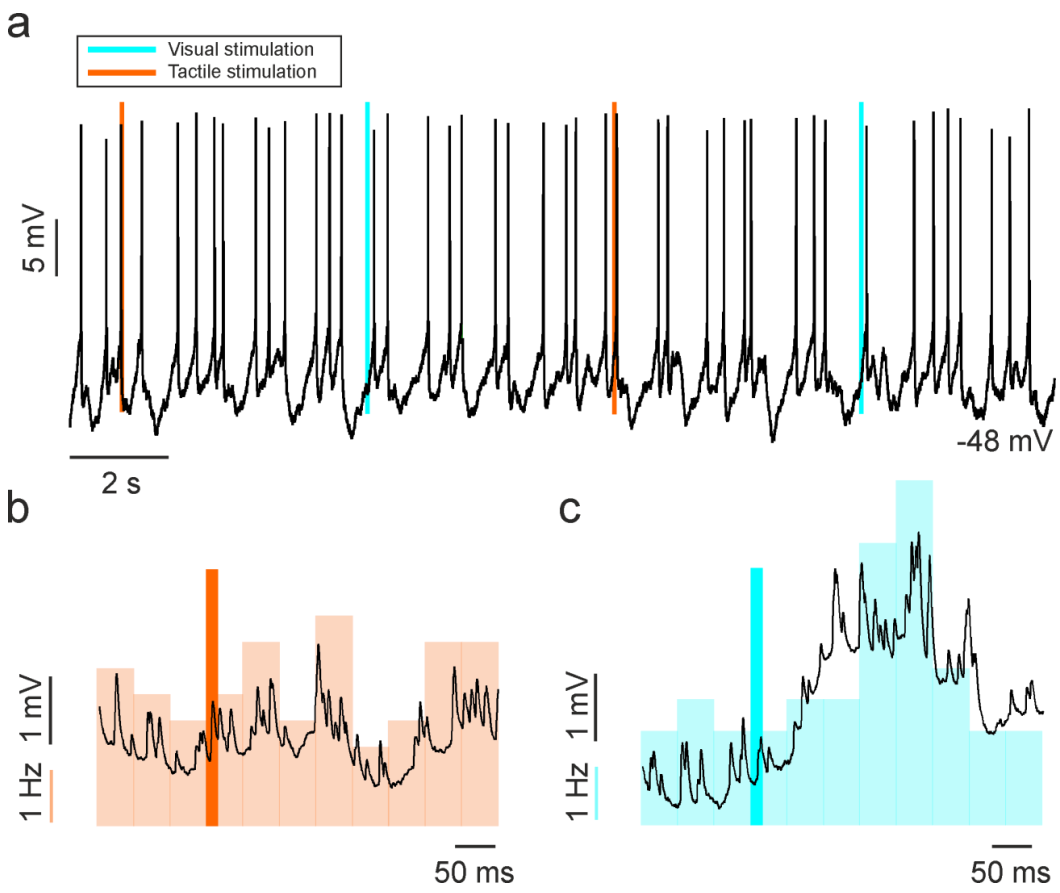

Figure 29. DMS-ChIs respond to visual stimulation. a, Example of a recorded *in vivo* cholinergic interneuron while performing visual and tactile stimuli. **b-c,** In coloured bars, PSTH of the firing rate after tactile (orange) and visual (blue) stimulation (Bin size = 35 ms). The dark coloured line represents the sensory stimulation (15 ms). Black line over the PSTH represents the waveform average of the same neuron.

4.9. Visual input is synchronized by the PT-ChIs interaction

Our results confirm that PT S1 axons barely project towards the DMS (Fig. 28). In addition, we know by previous reports that ChIs make synapses with cortical PT axons, whereas they avoid IT neurons axons[455]. This is consistent with our description, where we observe a firing rate increase in ChIs when responding to visual stimulation, but not to the tactile one (Fig. 29b, c). Taking all this information together, we propose a model to explain why visual inputs are specifically modulated by DA release (Fig. 30). In control conditions, PT V1 axons activate ChIs, whereas the absence of PT S1 projections makes impossible for the tactile inputs to activate ChIs in the DMS. ChIs,

which are tonically active[113], will then inhibit direct and indirect MSNs by disynaptic inhibition[115,116] (Fig. 30a). When DA is released it will inhibit ChIs, mediated by their D2DRs activation[115,125,342,350], resulting in the disinhibition of MSNs (Fig. 30b). Due to this disinhibition, visual responses are "unbraked", accelerating their responses by increasing their slopes and decreasing their peak delays (Fig. 26). Therefore, during bimodal stimulation, the delay difference between visual and tactile responses decreases, facilitating the synaptic summation of tactile and visual inputs, which increases the synchronization between inputs from different modalities (Fig. 26).

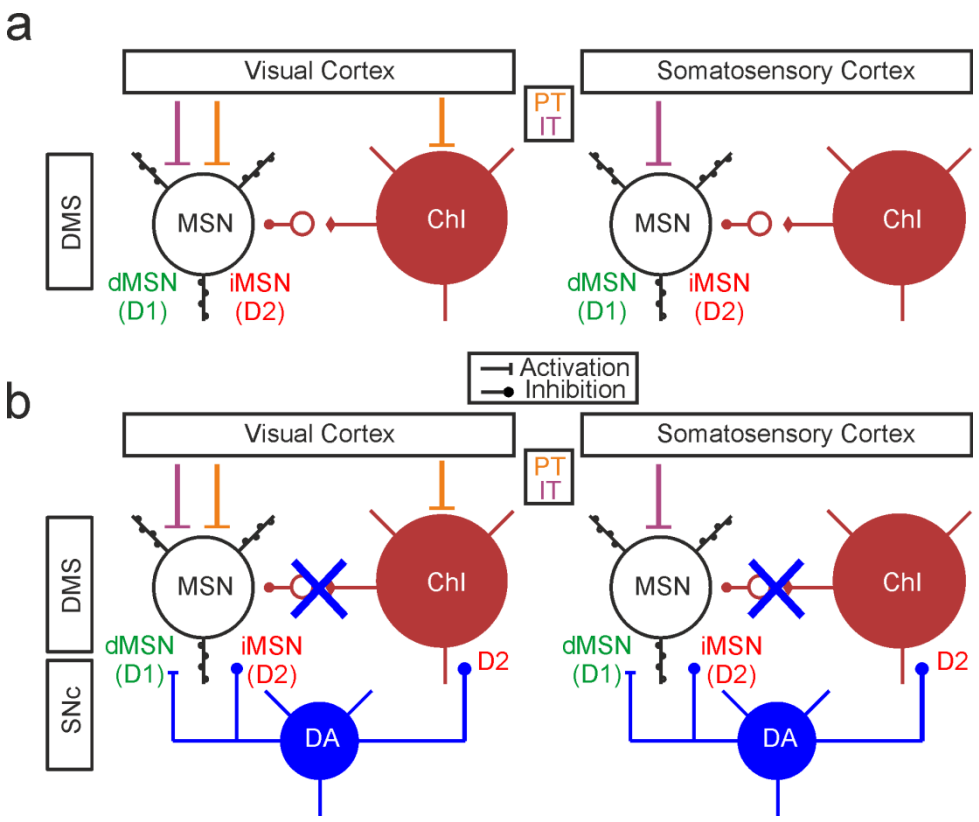

Figure 30. Visual input is synchronized by the PT-ChIs interaction. a-b, Schematic representation of the corticostriatal interactions in control conditions (a) and when DA is released (b) in the DMS. Note that the disynaptic inhibition from ChIs towards direct and indirect MSNs is supressed when DA is released, thus promoting the visual input in the direct pathway MSNs.

In this model there is another essential point to address, as our results show an increase of synchronization facilitated by DA impacting only on direct pathway MSNs; whereas indirect MSNs remain unaffected. Previous studies have described the implication of the dichotomous expression of D1- and D2DRs in MSNs, establishing that DA modulates differently the intrinsic excitability and synaptic transmission on direct and indirect MSNs. It is known that the activation of D1DRs in direct MSNs increases the excitability of the cells, boosting the glutamatergic excitatory transmission[24]. In contrast, activating D2DRs in indirect MSNs results in a reduction of the cells excitability and responsiveness[456] [for more details see Introduction, section 1.4.3]. Considering this information, the release of DA would inhibit ChIs through the activation of their D2DRs, but also indirect MSNs. On the other hand, it would make

direct MSNs more predisposed to respond to sensory stimuli, increasing their excitability by the activation of D1DRs (Fig. 30b). In conclusion, the desinhibition of visual inputs together with the excitability increase mediated by the D1DRs activation can explain why DA synchronizes bimodal information in the direct pathway MSNs.

4.10. Local drug delivery during in vivo whole-cell recordings

During the completion of this thesis, I also contributed to the work entitled: "*A New Micro-holder Device for Local Drug Delivery during In Vivo Whole-cell Recordings*" [57], included in the annex section.

Along this study, we have explored how DA affects visual and tactile inputs. In order to release DA, we optogenetically stimulated the dopaminergic terminals directly in the DMS. This approach eliminates problems from other methods such as the unspecificity of the electrical stimulation. However, one of the main complexities of this work is the dichotomous expression of D1 and D2 dopaminergic receptors, which modulate differently direct and indirect MSNs, as we have observed. One possible solution to dissect the direct and indirect MSNs roles would be to specifically activate or block the different types of dopaminergic receptors. Moreover, other DA receptors are expressed in striatal interneurons, such as D5 in ChIs[2,115], which its function *in vivo* remains unknown. For years, *in vitro* experiments in brain slices have combined electrophysiological recordings with a controlled drug application, either globally via bath application or locally via methods such as aided puffing or uncaging of pharmacological agents[457–459]. Nevertheless, the combination of local drug delivery with *in vivo* patch-clamp recordings in deep brain structures such as the striatum has specific challenges. For instance, the possible drug leakage into neighbouring brain areas or the mechanical stability needed in this kind of recordings. In order to overcome these challenges, we developed the "micro-holder", a new tool which when mounted onto the recording pipette, enables the local and stable application of any pharmacological agent during *in vivo* whole-cell recordings in deep brain structures. With the development of the micro-holder, we will be able to perform pharmacological experiments to locally release agonists or antagonists of the different dopaminergic receptors while MSNs are identified and recorded using optopatch-clamp recordings.

The micro-holder is a 12.85 x 5.95 x 4.12 mm box-shaped construct made of polypropylene with 2 screws to secure the recording and delivery pipettes at a convenient position (Fig. 31A-C). This construct is perforated in two sites: the recording pipette hole, perpendicular to the body holder; and the delivery pipette hole, with a 12 degrees angle (Fig. 31C, D). Both holes have a 1.7 mm diameter and they are separated by 4.62 mm and 3.35 mm in the top and bottom holder, respectively. To demonstrate the reliability of the micro-holder to deliver a drug locally to the recording site, we performed two experimental approaches.

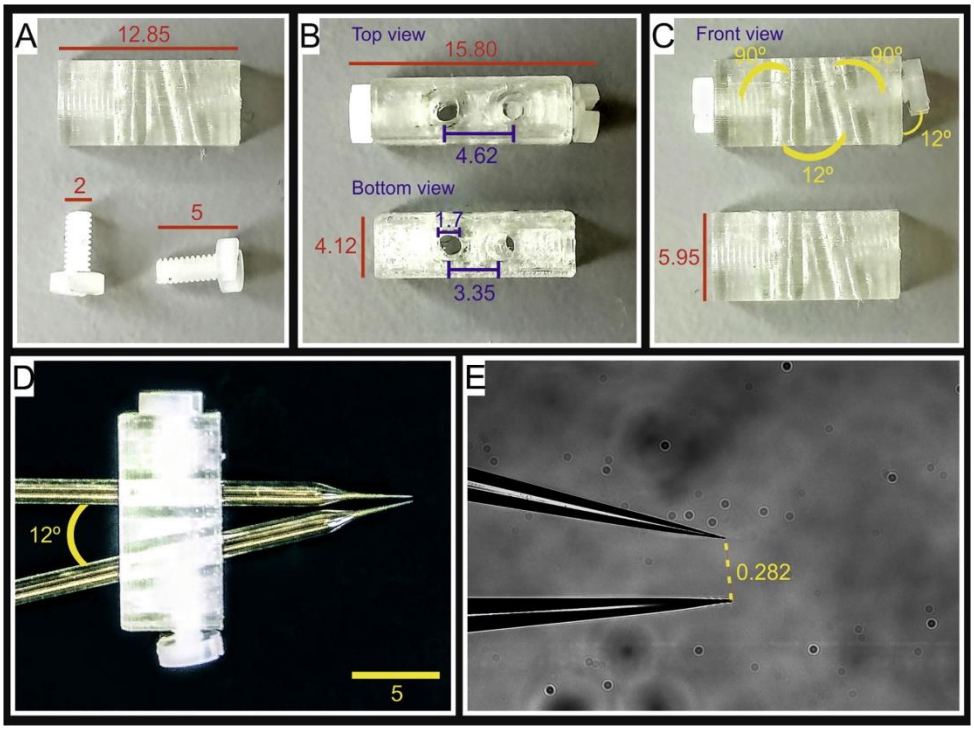

Figure 31. Micro-holder characteristics. (A) Length of the main piece of the construct and screws**. (B)** Total length of the micro-holder when mounted and pipette holes distance from the top of the holder (top). Width of the main piece of the construct with no screws and pipette holes diameter and distance from the bottom of the holder (bottom). **(C)** Angles between pipette holes and the screws and both insertion pipette holes (top). Height of the main piece of the construct with no screws (bottom). **(D)** Recording and delivery pipettes mounted onto the micro-holder. Notice the 12° angle between them. **(E)** Distance between the pipettes with higher magnification. All measures are in millimetres.

In order to test the use of the micro-holder in the striatum, we delivered TTX —a Na^+ channel blocker—, during *in vivo* patch-clamp recordings in the striatum with simultaneous LFP recordings in S1 and M1. When TTX was delivered, the action potentials were blocked and the Down to Up transitions were nearly abolished in the recorded MSNs (Fig. 32Ab, Bb). Importantly, no change in the LFP cortical activity was observed following TTX application (Fig. 32C-E). Afterwards, in 3 of the recorded MSNs, TTX was cleared from the tissue, as they recovered their action potentials and state transitions (Fig. 32Ac, Bc, E).

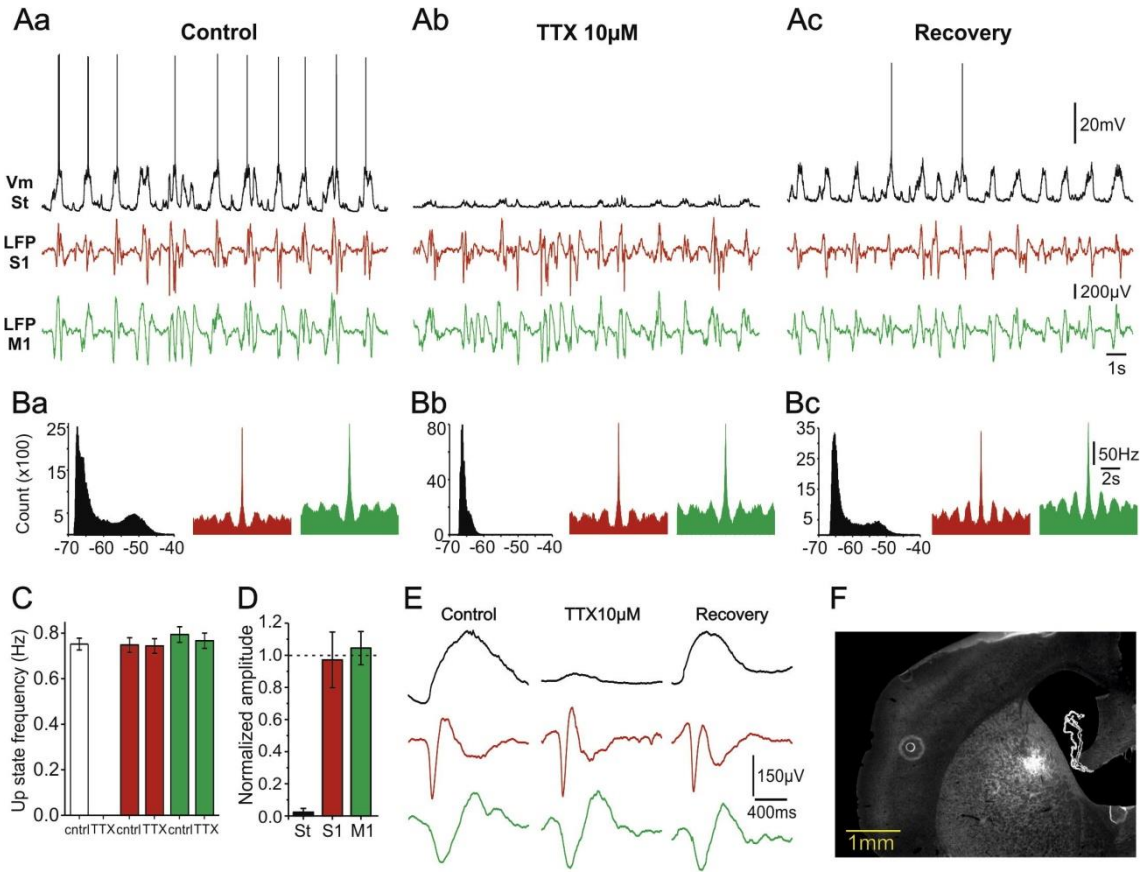

Figure 32. Focal delivery of 10 µM TTX in the striatum. (A) Example of an *in vivo* whole-cell patch-clamp recording from a striatal MSN (black trace) and simultaneous LFP recordings in S1 (red trace) and M1 (green trace) during SWO in control conditions (Aa, left), following the application of 10 µM TTX (Ab, middle) and after washout (Ac, right). **(B)** All-point-histogram of the MSN membrane potential (black) and cortical autocorrelograms (S1, red; M1, green) for the same conditions in A. **(C)** Frequency of the Down to Up state transitions under control conditions (ctrl) and in presence of TTX in a whole-cell recorded MSNs (black) and cortical LFP in S1 (red) and M1 (green). **(D)** Amplitude of the Down to Up state transition when TTX was delivered normalized to control conditions for MSN (black), S1 (red) and M1 (green). **(E)** Waveform averages of the Up states recorded in MSN (black trace), S1 (red trace) and M1 (red trace) under control conditions (left), after delivery of TTX (middle) and after washout (right). **(F)** Coronal section showing the local spread of BDA in the striatum with no cortex staining.

Moreover, we delivered BMI —a $GABA_A$ receptor antagonist—, to layer 5 of S1 while performing *in vivo* patch-clamp recordings with simultaneous LFP recordings in S1 and M1. In *in vitro* active slices it has been reported that the application of low concentrations of BMI increased the slope of the Down to Up states transitions of cortical neurons[460]. Consistent with this, the upward state transition slopes were accelerated when delivering BMI 200 µM with the micro-holder pipette (Fig. 33A-C). Importantly, the Down to Up transitions in the LFP recordings only showed a slight change when BMI was applied (Fig. 33C, D), most probably due to the high interconnectivity between cortical areas. In addition, the duration of the Down states increased significantly in the intracellular recording when BMI was applied, whereas the duration of the Up states decreased (Fig. 33G). Recorded neurons also increased their firing rate and Up state amplitude after BMI application (Fig. 33E, F). Importantly,

the application of BMI did not change any of these parameters in the LFP recordings (Fig. 33G).

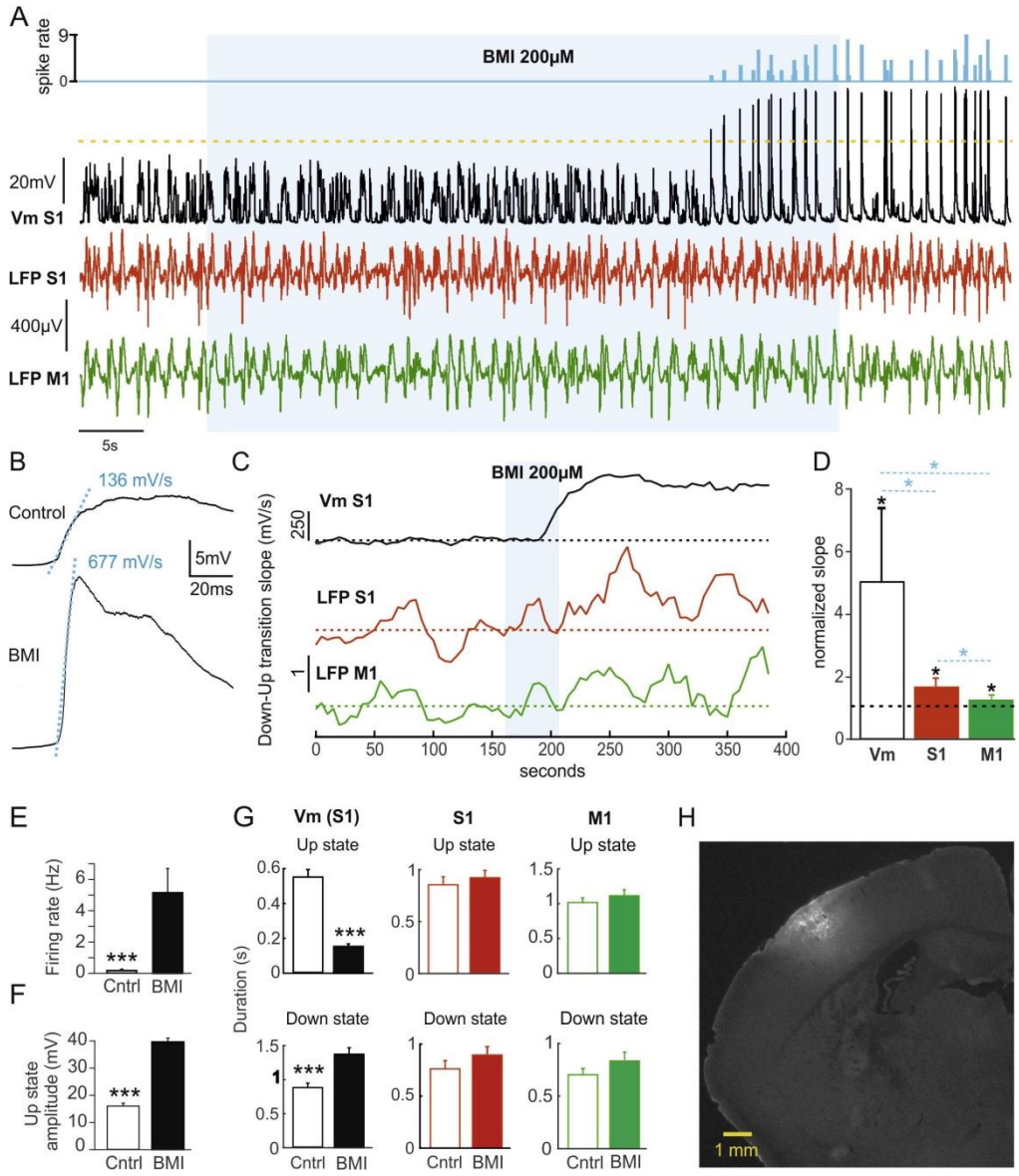

Figure 33. Focal delivery of 200 µM BMI in the somatosensory cortex. (A) Histogram of action potentials (blue) extracted from the *in vivo* whole-cell patch-clamp recording of the spontaneous activity of a cortical pyramidal neuron located in layer 5 (black trace), LFPs in S1 (red) and M1 (green) when delivering 200 µM of BMI (light blue shade). Notice the modulation in the whole-cell recorded spontaneous activity (black trace) and the lack of effect in the simultaneous S1 and M1 recorded LFPs. **(B)** Waveform averages of the membrane potential whole-cell recorded neuron in A before (top) and after (bottom) BMI application. Upward transition slopes (dashed blue line) were calculated by fitting a linear regression. **(C)** Upward transition slope values plotted over 400 s for the recordings in A. Light blue line indicated BMI application. **(D)** Average of the upward transition slopes normalized to control values. **(E, F)** Firing rate and Up state amplitude of whole-cell recordings respectively under control conditions and following BMI application. **(G)** Average of the Up state duration for the whole-cell and LFP recordings. **(H)** Coronal section showing the local spread of BMI in S1. Histogram bin size = 100 ms. * $p < 0.05$, *** $p < 0.001$, Mann–Whitney's U test.

In summary, these results show that the micro-holder enables the precise and local drug application during *in vivo* whole-cell patch-clamp recordings. In both approaches, the delivery was efficient and limited. Future studies with the micro-holder will be performed to dissect the specific roles of dopaminergic receptors in MSNs.

Discussion

5. DISCUSSION

How the brain creates an integrated and comprehensible representation of the external world to therefore produce adequate behaviours is one of the most impressive features of the nervous system. A pivotal process underlying it is the multimodal sensory integration of a variety of stimuli, such as the mechanism described in this work. Multisensory integration has an important impact on perception and has been related to several functions such as emotional processing[398,399], language[400,401], sensory awareness[402] and time perception[403] among others[404]. Nevertheless, the biological mechanism behind this process remains unknown. Deficits in multisensory integration have been documented in patients suffering from schizophrenia and disorders from the autism spectrum among others[405]. Importantly, in motor-related diseases such as Parkinson's disease (PD), sensory impairment induces deficits in the detection and discrimination of sensory cues[407] and impaired detection of paired visual, tactile and auditory stimuli among others[409]. Interestingly, the use of sensory cues ameliorates and facilitates the motor problems of PD[361–363], which suggests that sensory stimuli must have an important role regarding the striatal function. Moreover, it has been reported that the administration of dopaminergic drugs improves sensory problems in PD patients[409,410], which links DA with sensory gain modulation deficits[411]. The unraveling of a new mechanism explaining how the brain synchronizes sensory information will help to understand perception and diseases such as PD, schizophrenia or ADHD, all of them related with malfunctions of the DMS.

In this work we used *in vivo* whole-cell patch-clamp recordings to study the impact of DA on the sensory processing and spontaneous activity of MSNs from the DMS. We have observed that DA affects the spontaneous activity of direct and indirect MSNs, changing both the slow and fast oscillatory activity. We have noticed a modulation of the Up states of the SWO and a robust decrease of the theta-, beta-, and gamma-band energy in the presence of DA. When processing visual and tactile information, DA modulates these inputs differently, accelerating visual responses whereas not affecting tactile ones in direct pathway MSNs. Our main result demonstrates that DA synchronizes the sensory information of direct pathway MSNs, boosting the synchronization between inputs from different modalities. In summary, our results reveal a new mechanism for the integration of multimodal sensory information in the brain.

5.1. Dopamine facilitates sensory synchronization in direct MSNs of the DMS

In control conditions, tactile inputs precede the visual ones by tens of milliseconds (Table 6, 7). The longer latencies of visual responses are mainly attributed to retinal processing[391]. This causes that the simultaneous trigger of visual and tactile inputs does not generate a bigger response when compared to the independent tactile and visual stimulation (Table 6-8). Several years ago, Reig and Silberberg studied the temporal properties of these inputs, and determined that only when the onset or peak delay of

visual and tactile responses were artificially forced to occur simultaneously, the bimodal response amplitude increased (Fig. 10). In this study we have observed that this process occurs after DA release, which accelerates visual responses, decreasing the delay difference between visual and tactile inputs (Fig. 26d), resulting in the lengthening of the window that enables the synaptic integration between sensory modalities. This was reflected by the increase of the amplitude of the bimodal responses. Therefore, we proposed that DA is facilitating the bimodal sensory synchronization in direct pathway MSNs.

But how is DA facilitating this synaptic summation? One of the critical regulators of the striatal microcircuits are cholinergic interneurons (ChIs). They inhibit MSNs activity by disynaptic inhibition[115,116], activating different types of interneurons[127]. In addition, they receive a large synaptic input from dopaminergic neurons which inhibit their activity through their D2DRs expression[115,125,342,350]. However, dopaminergic neurons have different functions depending on the striatal region they target[251,340] causing differences in the strength of the signal. In the DMS, DA release inhibits ChIs firing during approximately 1 second[350] (Fig. 12). This inhibition results in the disinhibition of MSNs, which are normally inhibited by the tonic activity of ChIs. Therefore, our hypothesis considers that visual inputs are "unbraked", accelerating their responses by decreasing their peak delays and increasing their slopes when DA is released, facilitating the synaptic summation of tactile and visual inputs.

There are two possible mechanisms that could explain this synchronization. The first one is through the pre-synaptic control of DA release and the second one is through post-synaptic mechanisms. As previously mentioned, D1- and D2DRs are located pre- and post-synaptically in the striatum. However, the existence of pre-synaptic D1- and D2DRs functioning as heteroreceptors in the striatum is controversial and not conclusive[287,289,290]. It has been indeed reported that both types can function pre-synaptically as autoreceptors in the striatum[289,298]. Nevertheless, when they function as autoreceptors, they modulate and regulate DA release, but they do not mediate G-protein dependent and independent signalling post-synaptically. In addition, there are several other evidences supporting a post-synaptic mechanism. It has been largely observed that both D1- and D2DRs function as post-synaptic receptors in the striatum[287,298]. It could be, however, that these receptors were expressed pre-synaptically in the pyramidal neurons of the cortex and exert their modulation when projecting towards the striatum. For both D1- and D2DRs it has been documented that they are not highly expressed on the cerebral cortex, reducing their presence to prefrontal, enthorinal and cingulate areas[285,295,296,461]. Importantly, no D1- or D2DRs expression has been observed in S1 or V1[296]. Finally, in the hypothetical case in which these receptors were expressed pre-synaptically in S1 and V1 axon terminals projecting towards the DMS, a similar modulation of tactile and visual inputs would be expected. Nevertheless, the dopaminergic modulation is occurring only for the visual inputs. Thus, all these evidences strongly suggest that the mechanism underlying the bimodal synchronization must be occurring trough post-synaptic machinery.

Beyond the activation of dopamine receptors, two essential questions emerge to explain our observed synchronization: 1) Why is DA affecting the visual but not the tactile responses? 2) Why is this increased synchronization occurring only in the direct pathway MSNs?

5.2. Type-specific S1 corticostriatal projection towards the DMS

Quite a number of cortical areas send inputs towards the striatum, causing a great overlapping of corticostriatal projections[31,43,44,454]. Nevertheless, cortical axons from some sensory areas differ when sending projections to the DLS and DMS[31,454] and transmit different sensory modalities like tactile, auditory or visual[244]. When studying the corticostriatal connectivity of S1 and V1, we confirmed that the DLS is densely innervated by projections from S1[31,53,454]; whereas the DMS is receiving projections from V1 as well as from S1, although the last one with a lower density of axons[53] (Fig. 27). These corticostriatal connections make DMS-MSNs able to process visual and tactile inputs.

Cortical neurons projecting to the striatum are divided into intratelencephalic (IT) or pyramidal (PT) tract neurons depending on their subcortical targets[182]. In this work we observed that the DMS received around half of the innervation of S1 axons when compared to the DLS (Fig. 27b). Therefore, we wondered whether both types of cortical neurons from V1 and S1 projected to the DLS and DMS differently. This matter was previously addressed by Hooks et al., 2018, who observed that corticostriatal PT and IT projections from S1 tended to target the same striatal region[44]. Nevertheless, this study only focused on the dorsal and ventral striatum, ignoring the possible differences between DLS and DMS. When studying the specific PT and IT corticostriatal connectivity of S1 and V1 towards the DMS, we observed the near absence of PT S1 projections; which suggests a type-specific corticostriatal projection from S1 towards the DMS (Fig. 28).

The reason why this type-specific corticostriatal projection exists can be explained based on how PT and IT cortical populations project towards their cortical and subcortical targets. As previously described, IT neurons project only to the contralateral cortex as well as to the ipsi- and contralateral striatum from some specific cortical areas such as the frontal ones[44,70,218]; whereas PT neurons project exclusively ipsilaterally towards the brainsteam and the thalamus[44,182] leaving collaterals in the striatum on their way. Therefore, a large number of IT neurons from S1 and V1 will project towards the contralateral hemisphere through the *corpus callosum*, leaving quite a number of projections in the DMS. Contrary to this, as PT S1 neurons only project ipsilaterally targeting the DLS, they will leave a very few number of axons in the DMS when projecting straight towards the brainsteam (Fig. 28).

In addition, during the anatomical tracing study we also observed that IT V1 corticostriatal axon projections covered a larger area compared to PT V1 neurons when

projecting towards the DMS (Fig. 28). As mentioned previously, there are studies which support the idea that there is a scarcer number of PT neurons[187,188]. In addition, PT cells are less extensive and elaborate than IT neurons[44] (Fig. 8), which in the end could make PT axons cover a lower striatal area due to their less complex arborisation. Moreover, as mentioned in the previous paragraph, the way PT and IT neurons project towards their subcortical targets will also determine the number of axons they leave in the striatum, leaving a higher number when IT V1 axons project towards the contralateral cortex through the *corpus callosum*.

5.3. Direct MSNs disinhibition accelerates visual responses in the DMS

It has been reported that ChIs in the DLS respond to tactile stimulation[53]. Nevertheless, in our study we have observed that DMS-ChIs do not increase their firing rate when receiving tactile inputs (Fig. 29b); whereas we have detected a firing rate increase caused by visual stimulation (Fig. 29c). We know by a recent study that PT neurons are the only ones making synaptic contacts with ChIs[455]. The absence of PT projections from S1 towards the DMS explains why DMS-ChIs increase their firing rate when receiving visual but not tactile inputs.

In our functional model, we hypothesize that in control conditions, PT V1 axons will activate DMS-MSNs and ChIs (Fig. 30a). This will make MSNs respond to the visual input, but they will be partially disynaptically inhibited by ChIs which are tonically active[113]. Importantly, the described type-specific corticostriatal projection will synchronize only the visual input through the PT-ChIs interaction. In addition, the implications of the dopaminergic modulation of neurons expressing D1- and D2DRs have been already addressed throughout this work. The activation of D1DRs in direct MSNs increases their excitability, boosting the excitatory synapsis[24]. On the other hand, the activation of D2DRs in indirect MSNs and ChIs results in a reduction of the cells excitability and responsiveness[456]. Therefore, when DA is released, it inhibits ChIs and indirect MSNs by their D2DRs activation[115,125,342,350]; whereas it increases the excitability of direct MSNs through their D1DRs activation[24], causing direct MSNs to be more predisposed to respond to sensory stimuli (Fig. 30b). As previously mentioned, MSNs disinhibition will last around 1 second[350], and together with their increased excitability, will unbrake visual inputs in direct MSNs, accelerating their responses by decreasing and accelerating their peak delays and slopes, respectively (Fig. 26d). This will decrease the delay difference between visual and tactile responses during the bimodal stimulation, facilitating the synaptic summation between visual and tactile inputs only in direct MSNs (Fig. 26e).

Although visual inputs are synchronized in both MSNs subpopulations due to the existence of a PT V1 corticostriatal projection towards the DMS, no dopaminergic modulation was observed on indirect MSNs (Fig. 26). The activation of D2DRs after DA release would result in a reduction of responsiveness of indirect MSNs. Therefore, a negative modulation would be expected. Nevertheless, we could not observe any modulation at all. In our functional model, once DA is released, ChIs and indirect

MSNs are inhibited. However, the resulting indirect MSNs disinhibition by ChIs could balance the dopaminergic inhibition, yielding very similar responses to control conditions, acting as a compensatory feedback. It has been reported that the co-activation of both MSNs pathways is important for several processes such as action selection and action initiation[104]. Therefore, this mechanism may need the normal responsiveness of indirect MSNs, for instance to inhibit competing motor programs. Future studies regarding this hypothesis will have to be addressed.

5.4. Sensory processing of tactile and visual stimuli during the SWO cycle

During sleep, anaesthesia and resting wakefulness, the brain is dominated by synchronous activity called slow wave oscillations (SWO)[48,49,436]. This SWO originates in the cortex[51] and propagates to other brain regions such as the striatum[53–56]. This bi-stable state is composed of intermingled periods of activity (Up states) and silence (Down states)[58]; and is able to modulate the synaptic transmission[436,462] and sensory processing[53,436,437,463,464] of neurons. Previous studies in the DLS have reported that whisker stimulation during the Down states triggers reliable and robust sensory responses with higher amplitudes than the ones triggered during the Up states[53,62]. Consistent with these results, the amplitude of our responses was very small or zero when occurring during the Up states (Fig. 22a). In addition, we observed a significant negative lineal voltage-dependent relationship between the amplitude of the sensory responses and the membrane potential of the MSNs. The more hyperpolarized the membrane potential was (corresponding to the Down state), the largest amplitudes were exhibited (Fig. 22b).

There are several opposite factors underlying this phenomenon. During Down states or at resting membrane potential, MSNs are dominated by inwardly rectifying K^+ channels (Kir2), which are closed at depolarized membrane potentials or during Up states. Changes in the Kir2 channels state modify the input resistance of MSNs, which increases during Up states[66] (Table 3) and enhances their excitability as a consequence[69]. Therefore, based on this property, it would be expected that Up states facilitate the integration of synaptic inputs. In addition, the striatum receives activity from cortical neurons that discharge during the Up states of the SWO. Then, why are the responses smaller during the Up states? Different mechanisms could explain it. When the membrane potential of the neuron depolarizes to reach the Up state, it is closer to the excitatory reversal potential, which causes a lower driving force for Ca^{+2} and Na^+ ions to enter the neuron. Besides, when this happens, there is a major increase of the K^+ currents which are dependent on Ca^{+2} and Na^+, which in case of the MSNs strongly control their activity when they are close to the action potential threshold[54,66]. Furthermore, the sensory evoked excitation of striatal neurons is accompanied by inhibition[465], which originates from striatal interneurons and MSNs collaterals[148,466]. In the DLS, it has been reported that the excitatory responses are followed a few milliseconds later by a proportional inhibition[53]. Therefore, the inhibitory synaptic

component of the sensory responses may be enhanced during the Up states, which are as well, triggered by synaptic excitation.

Several cortical studies have investigated how the SWO can affect cellular responsiveness and sensory transmission[436,467,468]. They described that the effect of the network state results in gain modulation of the arriving synaptic inputs, enhancing the small ones and attenuating very large ones[467]. In addition, they reported a relationship between the amplitude of the sensory responses during the Down states and their degree of enhancement during Up states, with responses with lesser amplitudes enhanced at a greater extent[436]. In our results, bimodal responses exhibited by direct MSNs are enhanced, increasing their amplitudes when DA is released (Fig. 26e, Table 8). When exploring our data, we observed the existence of direct MSNs presenting bimodal responses with very large amplitudes during the Down states. This made us wonder if the cells displaying these responses would be enhanced by DA similarly to the ones exhibiting smaller responses. We observed that direct MSNs which had smaller bimodal amplitudes presented a greater enhancement compared to the ones that showed larger amplitudes (Fig. 34). These results suggest that when bimodal responses exhibit large amplitudes during the Down states in control conditions, the enhancement that DA can exert over them is lower. This is probably due to diverse mechanisms already discussed in the previous paragraph, including a lower driving force for Ca^{+2} and Na^{+} ions, a major increase of the Ca^{+2}- and Na^{+}-activated K^{+} currents and an enhanced inhibitory synaptic recruitment during the Up states. This could attenuate the enhancement effect that DA exerts onto the smaller responses. Therefore, the amplitude increase produced by DA presented in this study, which corresponds to a ~25%, could be underestimated.

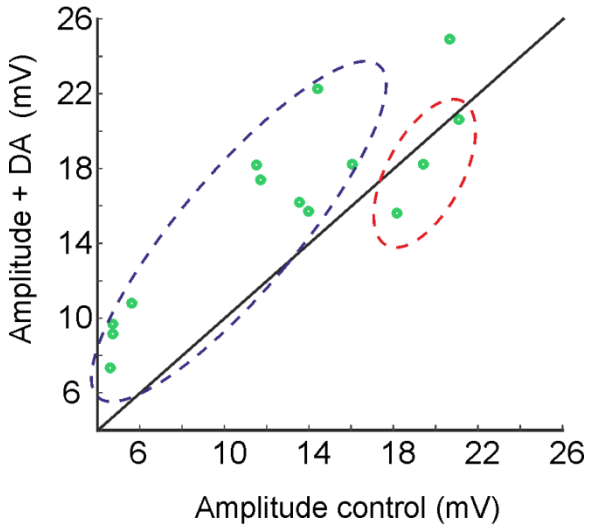

Figure 34. Dopamine enhancement of sensory bimodal responses. Raster plot showing the relationship between the amplitude of bimodal responses of direct MSNs during the Down states in control conditions and in presence of DA. Each dot represents the bimodal response amplitude of single direct MSNs. Notice that the amplitude of cellular responses increases when DA is released for the smaller responses (blue dashed line), whereas does not change for larger responses (red dashed line). Black line is added to illustrate the changes mediated by DA.

5.5. Dopaminergic modulation of MSNs spontaneous activity in the DMS

It has been reported that MSNs of the DLS recorded in DA depleted mice exhibit a reduction of the SWO frequency cycle related to a prolongation of the Down states[62]. Our results indicate that DA does not affect the frequency of the SWO cycle. Interestingly, we do observe a significant elongation of the Up states duration in presence of DA only in direct MSNs (Fig. 25c). As previously mentioned, MSNs express a variety of conductances such as voltage-sensitive Ca^{+2} channels, whose properties can be modulated during the state transitions from the Down towards the Up state and viceversa[73]. It is known that synaptic Ca^{+2} signals in the Down state are dominated by Ca^{+2}-permeable AMPARs and KARs[2,66]. Nonetheless, the membrane voltage depolarization that occurs during state transition switches the dominant source of Ca^{+2} to NMDA receptors[78]; who also contribute to maintain the Up states[79–81]. In addition, the dopaminergic activation of D1DRs decreases somatic K^+ currents[311–313], which potentiate Up state transitions. Therefore, when DA is released, D1DRs are activated in direct MSNs, which will lead to the activation of PKA and to the phosphorylation of a variety of intracellular targets[291], rapidly activating AMPARs and potentiating transitions towards the Up state. Once there, the increased activity of NMDARs[79–81] by the D1DRs activation can contribute to maintain the Up states. Therefore, we suggest that the observed Up state elongation may be mediated through Ca^{+2} voltage dependent channels.

Studies in PD patients have widely reported an exaggerated beta-band (10-20 Hz) synchronized oscillation of the STN and GPe populations[345,364–367], which is usually taken as a sign of DA depletion. This aberrant oscillatory activity is normally reduced by L-DOPA administration –a metabolic precursor of DA–, in the STN and GPe of PD patients[364,365,367,451,452]. Therefore, as the precursor of DA reduces the beta-band exaggerated oscillatory activity, it is expected that the power of the beta-band will also be reduced by DA release. But, surprisingly, we found that the decrease in the beta-band energy was also followed by the reduction of the theta- and gamma-bands energy in healthy mice (Fig. 25d). This was not occurring during the control experiments, where the stimulation was carried out using a viral construct not expressing any opsin, ensuring that this decrease was related to DA. Perhaps the beta-band energy decrease following L-DOPA administration is more obvious than theta- and gamma-bands energy diminution due to the exaggerated increase of this specific frequency band in PD patients. In this work we have demonstrated a general energy decrease of the high frequency oscillatory components mediated by DA release (Fig. 25d).

In addition, in this study we observed a modulation of the Up state voltage values when DA was released (Fig. 25b), which came accompanied by a slight reduction in the Up state amplitude. This is consistent with the energy reduction of theta-, beta- and gamma-bands. Therefore, the small changes observed over the Up states are reflecting the decline of the high frequency oscillatory components.

5.6. The optogenetic activation of dopaminergic terminals releases DA in the DMS

Different methods can be used to induce DA release onto the striatum, including the electric or optogenetic activation of SNc dopaminergic neurons. Electrical stimulation directly in the SNc is a reliable way of releasing DA[469], but in turn, is an unspecific method which activates all the neuronal types projecting to the striatum as well as other neighbouring areas such as the SNr which can affect the final outcome. On the other hand, the direct optogenetic activation of dopaminergic cells from the SNc has been proved to be more selective due to the use of viral constructs and transgenic animals[470]. Nevertheless, the optogenetic stimulation of cells directly in the SNc results in a release of DA not only in the DMS, but also in other striatal subregions such as the DLS or NAc. In addition, in mice, the SNc and SNr are two small nuclei localized very close to each other. The optogenetic activation of the SNc could therefore activate the dopaminergic cells located in the SNr projecting to frontal cortical areas[2,135,245], which could mask our results. In order to understand the specific impact of DA onto DMS-MSNs, we decided to activate the striatal dopaminergic terminals directly in the DMS. As previously reported, the activation of striatal dopaminergic terminals results in the release of DA[471]. Nevertheless, we first needed to check the reliability of our designed optogenetic stimulation paradigm.

To do so, we performed fiber photometry experiments using dLight1 (Fig. 23), a recently developed[423] intensity-based genetically encoded DA sensor which enables the optical recording of DA dynamics allowing the detection of extracellular DA. When optogenetically activating the DMS dopaminergic terminals, we observed a reliable release of DA in the DMS (Fig. 23c, d). This release was not occurring when carrying out the same experiment in control conditions, using a viral construct not expressing any opsin (Fig. 23c, d). This data confirmed that our optogenetic stimulation was indeed releasing DA. Interestingly, we detected a higher release of DA when activating the dopaminergic cells directly in the SNc (Fig. 23d). The higher expression of the viral construct containing the opsin in the cell soma would explain a larger neurotransmitter release when compared to the stimulation of the axonal terminals. The cell soma stimulation could also induce a faster release of DA; nevertheless, in both cases the onset and peak delay of DA release were similar between stimulations. This suggests that the direct activation of the cell soma produces a larger but not a faster neurotransmitter release.

5.7. Dopamine does not co-release GABA or glutamate in the DMS

Different studies have described that dopaminergic neurons can co-release various neurotransmitters, such as GABA[472] or glutamate[473]. Several years ago, an *in vitro* study reported that the activation of dopaminergic terminals rapidly inhibited the action potentials in both direct and indirect MSNs from the dorsal striatum[471]. This inhibition was occurring through the vesicular release of GABA requiring the vesicular

monoamine transporter VMAT2[471], which is the vesicular transporter for DA. Posterior reports have found that this GABA co-release displays a new synthesis pathway independent from the conventional GABA-synthesizing enzymes GAD65 and GAD67[443]. In more recent studies, different approaches have confirmed that midbrain DA neurons co-release glutamate and/or GABA in the striatum[243,441–444]. Nevertheless, in this work we did not induce any direct excitation (EPSPs) or inhibition (IPSPs) on MSNs when DA was released (Fig. 24). Therefore, we did not observe any neurotransmitter co-release, not even when dopaminergic neurons were directly activated in the SNc with electrical stimulation (Fig. 35).

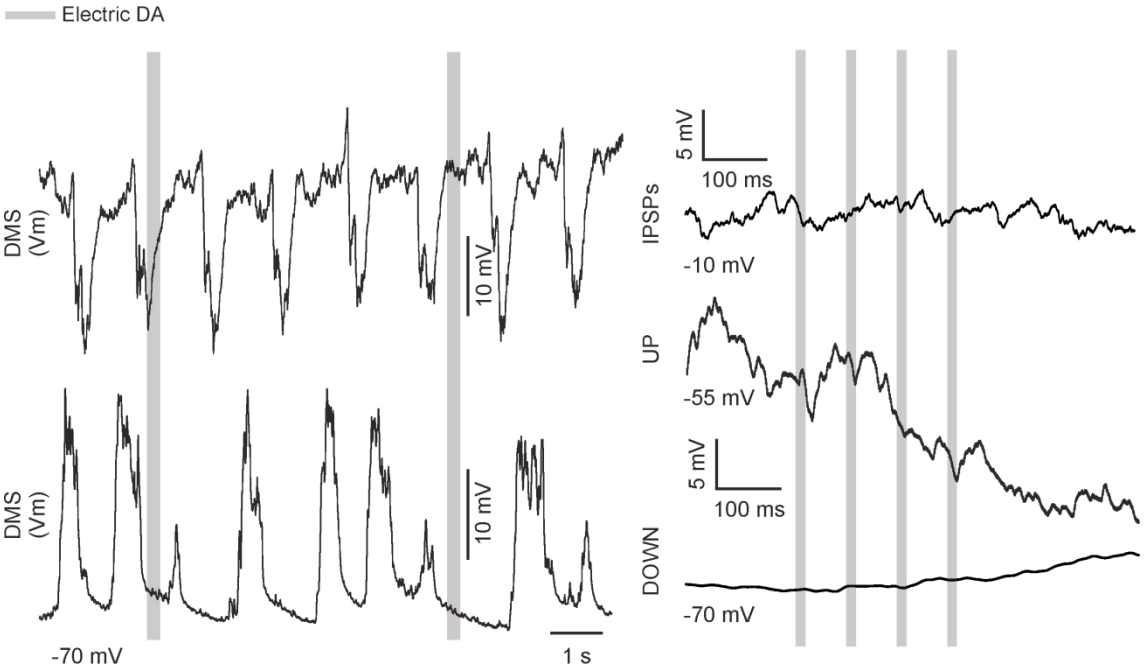

Figure 35. Electric stimulation of the SNc. Left: Example traces of *in vivo* whole-cell recordings of a dorsomedial MSN while activating dopaminergic neurons by electrical stimulation in the SNc at different membrane potentials. Right: Waveform averages of the same example MSNs at different membrane potentials. Grey lines represent the electrical stimulation.

Recently, it has been shown that glutamate co-release is dependent of the striatal location: it has been strongly reported in the NAc[474], less powerful in the DLS[243,443,444,471] and mainly absent in the DMS[471,474]; explaining its absence in our experiments. In addition, GABA co-release has always been studied disregarding the functional differences of the DLS and DMS subregions; approaching the dorsal striatum as a homogeneous region. Therefore, it is not clear if GABA co-release occurs similarly in both DLS and DMS. It seems that most dopaminergic neurons are capable of co-releasing GABA[443,475], although the studies which support this idea seem to have been performed in the more lateral regions of the dorsal striatum. In addition, the evoked GABA IPSPs amplitude decays rapidly when repeated stimulations are performed[476]. Lately, it has been documented that DA neurons engage distinct receptors in diverse postsynaptic neurons depending on the dorsal striatal subregion to convey striking different signals[350]. This results in DA release exhibiting changes depending on the dorsal striatal region, causing variations in the dopaminergic strength signal[350]. Taking

this information and our results together, it seems that GABA co-release could not be as strong as observed in both striatal regions, exerting a more powerful effect in the DLS. Thus, glutamate co-release towards the MSNs is extended from the NAc towards the DLS, but not to the DMS[243]. Future studies will have to focus on this matter and study GABA co-release independently in the DLS and DMS.

Furthermore, other factors could be playing an important role in how GABA is co-released. For instance, the different experimental conditions: namely, *in vitro* vs. *in vivo* recordings. Numerous valuable conclusions have been extracted from *in vitro* slices; nevertheless, in most cases, cutting the tissue results in a changed environment with a different neurotransmitter concentration as well as the lack of the whole input system that could be affecting the final outcome. As mentioned in the previous paragraph, co-released GABA IPSPs amplitude decays rapidly when repeated stimulations are performed. This could imply that the typical absence of spontaneous activity of *in vitro* preparations could maintain higher levels of GABA in the dopaminergic terminals, but once they are activated, they release GABA until there is no more left. On the other hand, *in vivo* experiments have shown that DA neurons discharge spontaneously during wakefulness, sleep or under anaesthesia[252–254], activating the synapse every few tenths of a second, that could prevent the accumulation of GABA in the axonal terminal. In addition, the extent and expression of the elected opsin to perform the stimulation is also something important to consider. The studies which have reported GABA co-release activate the striatal terminals with the ChR2 opsin[444,471], whereas in this study we used the ChrimsonR opsin. Distinct opsins can engage different patterns of excitation dynamics[477], with ChR2 inducing a faster and more powerful activation than ChrimsonR[415,477]. These differences could cause a major excitation of the terminals when stimulating with ChR2, releasing everything on the synaptic terminal. Finally, a study published early this year has shown that during *in vitro* whole-cell patch-clamp recordings in the DLS, GABA co-release is not observed at all, and happens only in minor cases during *in vitro* perforated patch-clamp recordings[444]. Anyhow, this study highlights that GABA co-release is not as reliable as it was thought.

5.8. Direct and indirect MSNs display similar electrophysiological properties in the DMS

Corticostriatal inputs innervate both the direct and indirect pathway MSNs[53,62,478,479]. Nevertheless, over time, several studies have described differences between these two subpopulations[53,62]. Besides their disparity when expressing dopaminergic receptors and the distinct output nuclei they target, other dissimilarities have been observed depending on their striatal location.

In the DLS, indirect MSNs display higher input resistances *in vivo*[53,62]. In addition, they have been reported to be more excitable than direct MSNs[62,69]. Moreover, several reports have shown that in this striatal region direct MSNs exhibit bigger responses to tactile stimulation when compared to the ones from indirect MSNs[50,53,62]. DMS-MSNs have been less characterized, but it has been observed that direct and indirect MSNs do

not show differences on their electrophysiological properties[63]. Furthermore, it is known that both subpopulations can respond to visual, tactile and bimodal inputs[53]; although their respective integration properties have not been deeply studied.

As mentioned, direct MSNs in the DLS display bigger responses to tactile stimulation[53,62]. However, our results indicate that both direct and indirect DMS-MSNs integrate visual and tactile inputs similarly (Table 6 and 7). DLS-MSNs exhibit differences in their electrophysiological properties[53,62,69]. Therefore, it is expected that changes in the membrane properties can affect the neuronal synaptic integration properties, hence the sensory integration. On the other hand, DMS-MSNs show similar electrophysiological properties as shown in this study and others[63] (Table 3), so following the same rationale, resembling sensory integration properties from both subpopulations should be expected. In addition, as bimodal inputs rely on how visual and tactile inputs are processed, no change in the bimodal integration would be expected. Consistent with this, direct and indirect MSNs displayed alike bimodal responses (Table 8). Recently this year, it was demonstrated that DLS and DMS subregions conform two non-overlapping circuits, which differ in their functional coupling to multiple cortical regions, the integration of cortical activity and the properties of the direct and indirect MSNs[63]. Our results show that direct and indirect DMS-MSNs exhibit resembling electrophysiological properties as well as a similar sensory processing, contrary to what happens with DLS-MSNs. This strongly suggests particular functional properties between pathways in the dorsal subregions of the striatum.

5.9. Functional significance

The ability to process and integrate information from the external world and produce an adequate behavioural performance is one of the basic mechanisms of animal survival. Due to the large quantity of information and stimuli generated by the environment, organisms have developed several mechanisms to better integrate the information to therefore produce an effective adaptation. Dopamine has been linked to a great variety of functions and processes. Several studies support that dopaminergic neurons construct and distribute information about rewarding events[250,266,321,322], which implicates midbrain dopaminergic activity in the reward-dependent learning[321] and motivated behaviours[480–482]. In fact, the increase in DA levels induced by the expectation of rewarding stimuli modulates MSNs activity[412]. In addition, the DMS has been involved in mediating reward-dependent learning[412–414]. Also, the performance of skilled movements can be modulated by the expectancy of a reward[483,484].

Several studies over the years have explored the possible benefit of a multimodal signal over a unimodal one. Authors argue that multimodal signals improve the performance of subjects[485,486] and that they can improve signal perception or processing[487]. In other words, multimodal signals may be beneficial due to the fact that they stimulate multiple sensory systems, causing intersensory facilitation (a faster reaction time) and increased separability (an enhanced ability to dissociate the components)[488]. In fact, previous

reports have observed that the combination of multimodal stimuli produces an enhancement of the neuronal response[394]. When considered from a behavioural perspective, when inputs from different modalities occur in close temporal and spatial proximity, they are likely to be originated from the same external event[394]. It has been proposed that as multimodal inputs reinforce one another, they increase the likelihood to detect and initiate an adequate response to the relevant event as seen in cats[489–491] and humans[492–494].

The striatum acts as a hub where multiple inputs converge, including a great range of sensory modalities. The DMS, which is also known as the associative striatum, receives a great dopaminergic innervation from the SNc and as previously mentioned, has been involved in mediating reward-dependent processes[412–414]. MSNs in this striatal subregion can integrate visual, tactile and bimodal inputs. Nevertheless, the different latencies when processing visual and tactile inputs results in a delay which causes the independent integration of these inputs. Our results show that DA enhances the direct MSNs efficiency in the DMS to integrate multimodal information, by synchronizing visual and tactile inputs. Taking all this information together, a motivational event with a rewarding component, which creates expectation, can increase the activity of the dopaminergic neurons located in the SNc. This will raise DA release in the DMS, which will boost the synchronization of visual and tactile inputs in the direct pathway DMS-MSNs as seen in this study. In turn, direct DMS-MSNs are regulated by positive feedback, where their activation results in an increment of the synaptic transmission from the thalamus towards other brain structures. In the context of the classical model of the basal ganglia, the activation of the direct pathway promotes movement as well as action selection[35,36,495]. DA would make direct DMS-MSNs more prepared and predisposed to integrate multimodal sensory inputs which can result in an improved subject performance when carrying out a task, for instance, displaying a faster reaction time or improving signal perception. This could help the nervous system to produce an effective and upgraded behavioural response. In addition, the revelation of a multisensory integration process could aid to comprehend the biological mechanism behind perception and other related processes.

5.10. The Micro-holder enables an stable and local drug delivery during *in vivo* whole-cell recordings

In this study we have developed the micro-holder, a tool to perform local drug applications in superficial and deep brain structures which do not compromise the stability of *in vivo* whole-cell recordings. With two different approaches, in the striatum and in the cortex, we have shown an efficient and stable drug delivery. No global changes in the frequency of any of the recorded activity were observed when delivering TTX or BMI[57]. We used the precision and stability of the micro-holder to perform *in vivo* whole-cell recordings. Nevertheless, this device can be used with other types of electrodes such as extracellular tungsten electrodes; together with an optic fiber during optogenetic experiments or even accompanying other tools such as the optopatcher.

Moreover, the diameter, length of the support screws or angle can be easily modified according to the experimental needs.

The micro-holder could be used to address open questions of this study. Here, we hypothesised that ChIs inhibition is the responsible for the boosting of visual inputs. The micro-holder could be used to assess the pivotal role of ChIs in the described synchronization mechanism. Furthermore, other related topics could be studied, for instance, the *in vivo* function of the D5 dopaminergic receptor in ChIs, which is still unknown, by releasing specific antagonists such as a dibenzazecine-based compound that has been described as the most potent and selective dopamine D5 receptor ligand showing low selectivity for the D1DRs[496].

Future perspectives

6. FUTURE PERSPECTIVES

In this study, we have unraveled a new brain mechanism, mediated by DA, in which the brain can integrate bimodal sensory information in direct MSNs from the DMS. We have hypothesized that the release of DA inhibits ChIs and indirect MSNs by their D2DRs activation[115,125,342,350], disinhibiting direct MSNs and causing an acceleration of their visual responses. We know that only cortical PT neurons make synapses with ChIs[455], and we have revealed that PT S1 neurons barely project towards the DMS. In order to functionally confirm this specific corticostriatal projection, we recorded the activity of some ChIs in the DMS. Nevertheless, due to the low density of ChIs and the type of blind recordings we performed, we recorded a total number of 3. In these cells, we observed that only the visual stimulation increased their firing rate. In order to endorse this trend, we plan to carry out multichannel recordings in the DMS. With this kind of electrophysiological recordings, the number of recorded ChIs can be increased. In addition, the same optogenetic and sensory stimulation as the one performed in this study can be done.

The micro-holder has proved to enable a stable and local drug application during *in vivo* whole-cell patch-clamp recordings, limiting the drug effect only to the recorded neuron and its vicinity. This device could be used to assess hypotheses of this work, for instance, the pivotal role of ChIs in the described synchronization mechanism. But other matters could be also investigated, such as the dichotomous expression of D1 and D2 dopaminergic receptors *in vivo* and the function of the D5 dopaminergic receptor in ChIs, which its function *in vivo* is still unknown.

Experimental approaches during this study have been performed in anesthetized mice. This experimental paradigm enables the activation of sensory pathways whilst avoiding interferences with any motor or other related inputs. Once we have revealed that DA is pivotal in the synchronization of multisensory information in the DMS, future studies involving awake, behaving animals can be performed. The DMS has been involved in mediating reward-dependent processes[412–414]. Furthermore, it has been supported that dopaminergic neurons construct and distribute information about rewarding events[250,266,321,322], and it has been observed that the performance of skilled movements can be modulated by the expectancy of a reward[483,484]. In addition, the increase in DA levels due to the expectation of rewarding stimuli modulates MSNs activity[412]. As showed in this study, DA modulation results in an improved efficiency of direct DMS-MSNs to synchronize multimodal information, which based on previous reports could cause an increased neuronal activity enhancement[394], leading to a better behavioural performance. In order to understand if DA could be acting in motivational events to improve the performance of the subjects, the use of reward-dependent tasks to train awake animals to receive a reward when a visual, tactile or bimodal stimulus is launched can be performed. When comparing rewarded and not-rewarded conditioned tasks, the rewarded ones should result in an increased performance, for instance displaying higher accuracy and velocity when completing a task. To confirm that at the

behavioural level DA is the molecule facilitating this upgraded performance, a not-rewarded task with the artificial optogenetic release of DA should result in an improved task execution similar to the one obtained when launching a rewarded stimuli. The fulfilment of this hypothesis would demonstrate the function of DA in motivational reward-dependent events.

Conclusions/Conclusiones

7. CONCLUSIONS

This doctoral thesis represents a step forward towards understanding how the brain integrates multimodal information. The main conclusion of this thesis is the description of a new synchronization mechanism mediated by DA. Specifically, it shows how DA enhances the efficiency of MSNs located in the DMS to integrate visual and tactile information, lengthening the feasible time window for the synaptic summation, which results in a more efficient integration of bimodal information. This synchronization is reflected by a clear increase of the bimodal response amplitude in the presence of dopamine. The results obtained in this doctoral thesis can help to comprehend how the nervous system produces an improved and effective behavioural response, which in turn is important for animal survival. Moreover, it will be relevant to understand diseases such as attention deficit and hyperactivity disorder, schizophrenia or Parkinson's disease, all of them related with abnormal sensory processing in the associative striatum.

Specific conclusions:

- Dopamine modulates the slow wave oscillation activity by modifying the Up state voltage in both MSNs subpopulations as well as by lengthening the Up state duration specifically in direct pathway MSNs.

- Dopamine decreases the theta, beta and gamma high frequency oscillations of the Up states.

- Dopamine modulates visual and tactile inputs differently, accelerating visual responses, whereas not affecting the tactile ones in MSNs from the direct pathway.

- Dopamine facilitates the synchronization of visual and tactile inputs selectively in MSNs of the direct pathway, which is reflected by an increase of the bimodal response amplitude.

- Cell type-specific corticostriatal projection from intratelencephalic tract neurons of the somatosensory cortex towards the dorsomedial striatum.

- The micro-holder enables local and stable drug applications during *in vivo* whole-cell patch-clamp recordings.

7. CONCLUSIONES

Esta tesis doctoral representa un avance para entender cómo el cerebro integra información multisensorial. La conclusión principal de este trabajo es la descripción de un nuevo mecanismo de sincronización de la información mediado por la dopamina. Concretamente, se muestra cómo este neurotransmisor aumenta la eficacia de las *MSNs* de la vía directa para integrar información táctil y visual en el *DMS*. El incremento en los niveles de dopamina desencadena una secuencia de cambios funcionales que amplían la ventana temporal de integración, mejorando la sumación sináptica de los estímulos bimodales. Esta sincronización se ve reflejada en el aumento de la amplitud de la respuesta bimodal en presencia de dopamina. Los resultados de esta tesis pueden ayudar a entender cómo el sistema nervioso produce un comportamiento más adecuado y efectivo, que a su vez es importante para la supervivencia. Así como a mejorar la comprensión de determinados síntomas presentes en enfermedades como el déficit de atención e hiperactividad, la esquizofrenia o la enfermedad de Parkinson, las cuales presentan deficiencias sensoriales que involucran al estriado asociativo.

Las conclusiones generales de esta tesis son:

- La dopamina modula la actividad oscilatoria lenta modificando el voltaje de los *Up states* en las dos poblaciones de las *MSNs*, así como también alargando la duración de los *Up states* específicamente en las neuronas de la vía directa.

- La dopamina disminuye las frecuencias de oscilación rápidas *theta*, *beta* y *gamma* de los *Up states*.

- El procesamiento sensorial táctil y visual de las *MSNs* de la vía directa es modulado de manera diferente por la dopamina: las respuestas visuales son aceleradas mientras que las respuestas táctiles no se ven afectadas.

- La dopamina facilita la sincronización de la información visual y táctil selectivamente en las *MSNs* de la vía directa, cuyo efecto se refleja en el aumento de la amplitud de las respuestas bimodales.

- Existe una proyección cortico-estriatal específica de neuronas del tracto intratelencefálico de la corteza somatosensorial primaria al estriado dorsomedial.

- El *micro-holder* permite una aplicación estable y local de fármacos durante registros *whole-cell patch-clamp in vivo* en núcleos subcorticales.

Bibliography

8. BIBLIOGRAPHY

1. Willis, T. *Cerebri Anatome Cui Accessit Nervorum Descriptio et Usus*. (Flesher, Martyn and Allestry, 1664).

2. *Handbook of Basal Ganglia Structure and Function*. (Academic Press, 2016). doi:10.1016/b978-0-12-802206-1.00052-0

3. Purves, D. *et al. Neuroscience 4th edition*. *4th edition* (2008).

4. Alexander, G. Parallel Organization of Functionally Segregated Circuits Linking Basal Ganglia and Cortex. *Annu. Rev. Neurosci.* **9**, (1986).

5. Cisek, P. & Kalaska, J. F. Neural Mechanisms for Interacting with a World Full of Action Choices. *Annu. Rev. Neurosci.* **33**, (2010).

6. Graybiel, A. M., Aosaki, T., Flaherty, A. W. & Kimura, M. The basal ganglia and adaptive motor control. *Science (80-.).* **265**, (1994).

7. Hikosaka, O., Takikawa, Y. & Kawagoe, R. Role of the basal ganglia in the control of purposive saccadic eye movements. *Physiological Reviews* **80**, (2000).

8. Mink, J. W. The basal ganglia: Focused selection and inhibition of competing motor programs. *Prog. Neurobiol.* **50**, (1996).

9. Redgrave, P., Prescott, T. J. & Gurney, K. The basal ganglia: A vertebrate solution to the selection problem? *Neuroscience* **89**, (1999).

10. Wichmann, T. & DeLong, M. R. Functional neuroanatomy of the basal ganglia in Parkinson's disease. *Advances in neurology* **91**, (2003).

11. Yin, H. H. & Knowlton, B. J. The role of the basal ganglia in habit formation. *Nature Reviews Neuroscience* **7**, (2006).

12. Lotze, M. *et al.* Activation of cortical and cerebellar motor areas during executed and imagined hand movements: An fMRI study. *J. Cogn. Neurosci.* **11**, (1999).

13. Munzert, J., Lorey, B. & Zentgraf, K. Cognitive motor processes: The role of motor imagery in the study of motor representations. *Brain Research Reviews* **60**, (2009).

14. Berns, G. S. & Sejnowski, T. J. How the Basal Ganglia Make Decisions. in (1996). doi:10.1007/978-3-642-79928-0_6

15. van Schouwenburg, M., Aarts, E. & Cools, R. Dopaminergic Modulation of Cognitive Control: Distinct Roles for the Prefrontal Cortex and the Basal Ganglia. *Curr. Pharm. Des.* **16**, (2010).

16. Provost, J. S., Petrides, M. & Monchi, O. Dissociating the role of the caudate nucleus and dorsolateral prefrontal cortex in the monitoring of events within human working memory. *Eur. J. Neurosci.* **32**, (2010).

17. Kotz, S. A., Schwartze, M. & Schmidt-Kassow, M. Non-motor basal ganglia functions: A review and proposal for a model of sensory predictability in

auditory language perception. *Cortex* **45**, (2009).

18. Friederici, A. D. & Kotz, S. A. The brain basis of syntactic processes: Functional imaging and lesion studies. in *NeuroImage* **20**, (2003).

19. Booth, J. R., Wood, L., Lu, D., Houk, J. C. & Bitan, T. The role of the basal ganglia and cerebellum in language processing. *Brain Res.* **1133**, (2007).

20. Mizumori, S. J. Y., Puryear, C. B. & Martig, A. K. Basal ganglia contributions to adaptive navigation. *Behavioural Brain Research* **199**, (2009).

21. Parent, A. The History of the Basal Ganglia: The Contribution of Karl Friedrich Burdach. *Neurosci. Med.* **03**, (2012).

22. Nieoullon, A. Dopamine and the regulation of cognition and attention. *Progress in Neurobiology* **67**, (2002).

23. Watson, G. S. & Leverenz, J. B. Profile of cognitive impairment in parkinson's disease. in *Brain Pathology* **20**, (2010).

24. Gerfen, C. R. & Surmeier, D. J. Modulation of Striatal Projection Systems by Dopamine. *Annu. Rev. Neurosci.* **34**, (2011).

25. Kita, H. GABAergic circuits of the striatum. *Prog. Brain Res.* **99**, (1993).

26. DiFiglia, M., Pasik, P. & Pasik, T. A Golgi study of neuronal types in the neostriatum of monkeys. *Brain Res.* **114**, (1976).

27. Wilson, C. J. & Groves, P. M. Fine structure and synaptic connections of the common spiny neuron of the rat neostriatum: A study employing intracellular injection of horseradish peroxidase. *J. Comp. Neurol.* **194**, (1980).

28. Bishop, G. A., Chang, H. T. & Kitai, S. T. Morphological and physiological properties of neostriatal neurons: An intracellular horseradish peroxidase study in the rat. *Neuroscience* **7**, (1982).

29. Kemp, J. M. & Powell, T. P. The structure of the caudate nucleus of the cat: light and electron microscopy. *Philos. Trans. R. Soc. Lond. B. Biol. Sci.* **262**, (1971).

30. Doig, N. M., Moss, J. & Bolam, J. P. Cortical and Thalamic Innervation of Direct and Indirect Pathway Medium-Sized Spiny Neurons in Mouse Striatum. *J. Neurosci.* **30**, 14610–14618 (2010).

31. Hintiryan, H. *et al.* The mouse cortico-striatal projectome. *Nat. Neurosci.* **19**, (2016).

32. Saunders, A., Huang, K. W. & Sabatini, B. L. Globus Pallidus Externus Neurons Expressing parvalbumin Interconnect the Subthalamic Nucleus and Striatal Interneurons. *PLoS One* **11**, (2016).

33. Mallet, N. *et al.* Dichotomous Organization of the External Globus Pallidus. *Neuron* **74**, (2012).

34. Abdi, A. *et al.* Prototypic and arkypallidal neurons in the dopamine-intact external globus pallidus. *J. Neurosci.* **35**, (2015).

35. Alexander, G. E. & Crutcher, M. D. Functional architecture of basal ganglia circuits: neural substrates of parallel processing. *Trends Neurosci.* **13**, 266–271 (1990).

36. DeLong, M. R. Primate models of movement disorders of basal ganglia origin. *Trends in Neurosciences* **13**, (1990).

37. Caggiano, V. *et al.* Midbrain circuits that set locomotor speed and gait selection. *Nature* (2018). doi:10.1038/nature25448

38. Nambu, A., Tokuno, H. & Takada, M. Functional significance of the cortico-subthalamo-pallidal 'hyperdirect' pathway. *Neurosci. Res.* **43**, (2002).

39. Nambu, A. Seven problems on the basal ganglia. *Current Opinion in Neurobiology* **18**, (2008).

40. Parent, A., Mackey, A. & De Bellefeuille, L. The subcortical afferents to caudate nucleus and putamen in primate: A fluorescence retrograde double labeling study. *Neuroscience* **10**, (1983).

41. Lynd-Balta, E. & Haber, S. N. Primate striatonigral projections: A comparison of the sensorimotor-related striatum and the ventral striatum. *J. Comp. Neurol.* **345**, (1994).

42. Haber, S. N. The place of dopamine in the cortico-basal ganglia circuit. *Neuroscience* **282**, (2014).

43. Kincaid, A. E., Zheng, T. & Wilson, C. J. Connectivity and convergence of single corticostriatal axons. *J. Neurosci.* **18**, (1998).

44. Hooks, B. M. *et al.* Topographic precision in sensory and motor corticostriatal projections varies across cell type and cortical area. *Nat. Commun.* **9**, (2018).

45. Silberberg, G. & Bolam, J. P. Local and afferent synaptic pathways in the striatal microcircuitry. *Curr Opin Neurobiol* **33**, 182–187 (2015).

46. Dautan, D. *et al.* A major external source of cholinergic innervation of the striatum and nucleus accumbens originates in the Brainstem. *J. Neurosci.* **34**, (2014).

47. Swanson, L. W., Newman, E., Araque, A. & Dubinsky, J. M. *Beautiful Brain: The Drawings of Santiago Ramon y Cajal.* (Harry N. Abrams, 2017).

48. Sanchez-Vives, M. V. & McCormick, D. A. Cellular and network mechanisms of rhytmic recurrent activity in neocortex. *Nat. Neurosci.* **3**, (2000).

49. Compte, A. *et al.* Spontaneous high-frequency (10-80 Hz) oscillations during up states in the cerebral cortex in vitro. *J. Neurosci.* **28**, (2008).

50. Sippy, T., Lapray, D., Crochet, S. & Petersen, C. C. H. Cell-Type-Specific Sensorimotor Processing in Striatal Projection Neurons during Goal-Directed Behavior. *Neuron* **88**, 298–305 (2015).

51. Steriade, M., Nunez, A. & Amzica, F. A novel slow (< 1 Hz) oscillation of neocortical neurons in vivo: depolarizing and hyperpolarizing components. *J*

Neurosci **13**, 3252–3265 (1993).

52. O'Donnell, P. & Grace, A. A. Synaptic interactions among excitatory afferents to nucleus accumbens neurons: Hippocampal gating of prefrontal cortical input. *J. Neurosci.* (1995). doi:10.1523/jneurosci.15-05-03622.1995

53. Reig, R. & Silberberg, G. Multisensory Integration in the Mouse Striatum. *Neuron* **83**, 1200–1212 (2014).

54. Wilson, C. J. & Kawaguchi, Y. The origins of two-state spontaneous membrane potential fluctuations of neostriatal spiny neurons. *J. Neurosci.* **16**, 2397–410 (1996).

55. Calabresi, P., Mercuri, N. B., Stefani, A. & Bernardi, G. Synaptic and intrinsic control of membrane excitability of neostriatal neurons. I. An in vivo analysis. *J. Neurophysiol.* (1990). doi:10.1152/jn.1990.63.4.651

56. Wilson, C. J. & Groves, P. M. Spontaneous firing patterns of identified spiny neurons in the rat neostriatum. *Brain Res.* **220**, 67–80 (1981).

57. Sáez, M., Ketzef, M., Alegre-Cortés, J., Reig, R. & Silberberg, G. A New Micro-holder Device for Local Drug Delivery during In Vivo Whole-cell Recordings. *Neuroscience* **381**, 115–123 (2018).

58. Sanchez-Vives, M. V. & Mattia, M. Slow wave activity as the default mode of the cerebral cortex. *Arch. Ital. Biol.* **152**, (2014).

59. Steriade, M., McCormick, D. A. & Sejnowski, T. J. Thalamocortical oscillations in the sleeping and aroused brain. *Science (80-.).* **262**, (1993).

60. Lampl, I., Reichova, I. & Ferster, D. Synchronous membrane potential fluctuations in neurons of the cat visual cortex. *Neuron* **22**, (1999).

61. Sanchez-Vives, M. V, Massimini, M. & Mattia, M. Shaping the Default Activity Pattern of the Cortical Network. *Neuron* **94**, 993–1001 (2017).

62. Ketzef, M. *et al.* Dopamine Depletion Impairs Bilateral Sensory Processing in the Striatum in a Pathway-Dependent Manner. *Neuron* **94**, 855-865.e5 (2017).

63. Alegre-Cortés, J., Sáez, M., Montanari, R. & Reig, R. Medium spiny neurons spontaneous activity reveal the discrete segregation of mouse dorsal striatum. *bioRxiv* 2020.02.21.959692 (2020). doi:10.1101/2020.02.21.959692

64. Silberberg, G. & Planert, H. Optogenetic dissection of the striatal microcircuitry. in *Neuromethods* **113**, (2016).

65. Morera-Herreras, T., Gioanni, Y., Perez, S., Vignoud, G. & Venance, L. Environmental enrichment shapes striatal spike-timing-dependent plasticity in vivo. *Sci. Rep.* **9**, (2019).

66. *The Basal Ganglia IX*. **58**, (Springer New York, 2009).

67. Wilson, C. J. The generation of natural firing patterns in neostriatal neurons. *Prog. Brain Res.* **99**, (1993).

68. Nisenbaum, E. S., Xu, Z. C. & Wilson, C. J. Contribution of a slowly inactivating potassium current to the transition to firing of neostriatal spiny projection neurons. *J. Neurophysiol.* (1994). doi:10.1152/jn.1994.71.3.1174

69. Planert, H., Berger, T. K. & Silberberg, G. Membrane Properties of Striatal Direct and Indirect Pathway Neurons in Mouse and Rat Slices and Their Modulation by Dopamine. *PLoS One* **8**, (2013).

70. Johansson, Y. & Silberberg, G. The Functional Organization of Cortical and Thalamic Inputs onto Five Types of Striatal Neurons Is Determined by Source and Target Cell Identities. *Cell Rep.* (2020). doi:10.1016/j.celrep.2019.12.095

71. Gertler, T. S., Chan, C. S. & Surmeier, D. J. Dichotomous anatomical properties of adult striatal medium spiny neurons. *J. Neurosci.* **28**, (2008).

72. Day, M., Wokosin, D., Plotkin, J. L., Tian, X. & Surmeier, D. J. Differential excitability and modulation of striatal medium spiny neuron dendrites. *J. Neurosci.* **28**, (2008).

73. Wickens, J. R. & Wilson, C. J. Regulation of action-potential firing in spiny neurons of the rat neostriatum in vivo. *J. Neurophysiol.* **79**, (1998).

74. Monaghan, D. T., Olverman, H. J., Nguyen, L., Watkins, J. C. & Cotman, C. W. Two classes of N-methyl-D-aspartate recognition sites: Differential distribution and differential regulation by glycine. *Proc. Natl. Acad. Sci. U. S. A.* **85**, (1988).

75. Calabresi, P., Maj, R., Mercuri, N. B. & Bernardi, G. Coactivation of D1 and D2 dopamine receptors is required for long-term synaptic depression in the striatum. *Neurosci. Lett.* **142**, (1992).

76. Chih-Hui Chen, A., McDonald, B., Moss, S. J. & Gurling, H. M. D. Gene expression studies of mRNAs encoding the NMDA receptor subunits NMDAR1, NMDAR2A, NMDAR2B, NMDAR2C, and NMDAR2D following long-term treatment with cis- and trans-flupenthixol as a model for understanding the mode of action of schizophrenia drug treatment. *Mol. Brain Res.* **54**, (1998).

77. Stefani, A. *et al.* Physiological and molecular properties of AMPA/kainate receptors expressed by striatal medium spiny neurons. *Dev. Neurosci.* **20**, (1998).

78. Carter, A. G. & Sabatini, B. L. State-dependent calcium signaling in dendritic spines of striatal medium spiny neurons. *Neuron* **44**, (2004).

79. Cepeda, C., Buchwald, N. A. & Levine, M. S. Neuromodulatory actions of dopamine in the neostriatum are dependent upon the excitatory amino acid receptor subtypes activated. *Proc. Natl. Acad. Sci. U. S. A.* **90**, (1993).

80. Vergara, R. *et al.* Spontaneous voltage oscillations in striatal projection neurons in a rat corticostriatal slice. *J. Physiol.* **553**, (2003).

81. Tseng, K. Y., Snyder-Keller, A. & O'Donnell, P. Dopaminergic modulation of striatal plateau depolarizations in corticostriatal organotypic cocultures. *Psychopharmacology (Berl).* **191**, (2007).

82. Sgambato, V., Maurice, N., Besson, M. J., Thierry, A. M. & Deniau, J. M. Effect

of a functional impairment of corticostriatal transmission on cortically evoked expression of c-fos and zif 268 in the rat basal ganglia. *Neuroscience* **93**, (1999).

83. Ferguson, S. M. & Robinson, T. E. Amphetamine-evoked gene expression in striatopallidal neurons: Regulation by corticostriatal afferents and the ERK/MAPK signaling cascade. *J. Neurochem.* **91**, (2004).

84. Kawaguchi, Y., Wilson, C. J. & Emson, P. C. Projection subtypes of rat neostriatal matrix cells revealed by intracellular injection of biocytin. *J. Neurosci.* **10**, (1990).

85. Loopuijt, L. D. & Van der Kooy, D. Organization of the striatum: Collateralization of its Efferent Axons. *Brain Res.* **348**, (1985).

86. Gerfen, C. R. & Scott Young, W. Distribution of striatonigral and striatopallidal peptidergic neurons in both patch and matrix compartments: an in situ hybridization histochemistry and fluorescent retrograde tracing study. *Brain Res.* **460**, (1988).

87. Gangarossa, G. *et al.* Distribution and compartmental organization of GABAergic medium-sized spiny neurons in the mouse Nucleus Accumbens. *Front. Neural Circuits* (2013). doi:10.3389/fncir.2013.00022

88. Kita, H. & Kitai, S. T. Glutamate decarboxylase immunoreactive neurons in rat neostriatum: their morphological types and populations. *Brain Res.* **447**, (1988).

89. Haber, S. N. & Watson, S. J. The comparison between enkephalin-like and dynorphin-like immunoreactivity in both monkey and human globus pallidus and substantia nigra. *Life Sci.* **33**, (1983).

90. Gerfen, C. R. *et al.* D1 and D2 dopamine receptor-regulated gene expression of striatonigral and striatopallidal neurons. *Science (80-.).* **250**, (1990).

91. Alexander_Crutcher_1990.pdf.

92. Smith, Y., Bevan, M. D., Shink, E. & Bolam, J. P. Microcircuitry of the direct and indirect pathways of the basal ganglia. *Neuroscience* **86**, 353–387 (1998).

93. Surmeier, D. J., Song, W. J. & Yan, Z. Coordinated expression of dopamine receptors in neostriatal medium spiny neurons. *J. Neurosci.* **16**, (1996).

94. Gong, S. *et al.* A gene expression atlas of the central nervous system based on bacterial artificial chromosomes. *Nature* **425**, (2003).

95. Ince, E., Ciliax, B. J. & Levey, A. I. Differential expression of D1 and D2 dopamine and m4 muscarinic acetylcholine receptor proteins in identified striatonigral neurons. *Synapse* **27**, (1997).

96. Fujiyama, F. *et al.* Exclusive and common targets of neostriatofugal projections of rat striosome neurons: A single neuron-tracing study using a viral vector. *Eur. J. Neurosci.* **33**, (2011).

97. Filipović, M. *et al.* Direct pathway neurons in mouse dorsolateral striatum in vivo receive stronger synaptic input than indirect pathway neurons. *J. Neurophysiol.*

122, 2294–2303 (2019).

98. Chuhma, N., Tanaka, K. F., Hen, R. & Rayport, S. Functional connectome of the striatal medium spiny neuron. *J. Neurosci.* (2011). doi:10.1523/JNEUROSCI.3833-10.2011

99. Czubayko, U. & Plenz, D. Fast synaptic transmission between striatal spiny projection neurons. *Proc. Natl. Acad. Sci. U. S. A.* (2002). doi:10.1073/pnas.242428599

100. Planert, H., Szydlowski, S. N., Hjorth, J. J. J., Grillner, S. & Silberberg, G. Dynamics of synaptic transmission between fast-spiking interneurons and striatal projection neurons of the direct and indirect pathways. *J. Neurosci.* **30**, (2010).

101. Taverna, S., Ilijic, E. & Surmeier, D. J. Recurrent collateral connections of striatal medium spiny neurons are disrupted in models of Parkinson's disease. *J. Neurosci.* (2008). doi:10.1523/JNEUROSCI.5493-07.2008

102. Albin, R. L., Young, A. B. & Penney, J. B. The functional anatomy of basal ganglia disorders. *Trends Neurosci.* **12**, (1989).

103. Kravitz, A. V. *et al.* Regulation of parkinsonian motor behaviours by optogenetic control of basal ganglia circuitry. *Nature* **466**, (2010).

104. Cui, G. *et al.* Concurrent activation of striatal direct and indirect pathways during action initiation. *Nature* **494**, 238 (2013).

105. Isomura, Y. *et al.* Reward-modulated motor information in identified striatum neurons. *J. Neurosci.* **33**, (2013).

106. Bateup, H. S. *et al.* Distinct subclasses of medium spiny neurons differentially regulate striatal motor behaviors. *Proc. Natl. Acad. Sci. U. S. A.* **107**, (2010).

107. Durieux, P. F. *et al.* D"2R striatopallidal neurons inhibit both locomotor and drug reward processes. *Nat. Neurosci.* **12**, (2009).

108. F. Hernández, L., Castela, I., Ruiz-DeDiego, I., Obeso, J. A. & Moratalla, R. Striatal activation by optogenetics induces dyskinesias in the 6-hydroxydopamine rat model of Parkinson disease. *Mov. Disord.* (2017). doi:10.1002/mds.26947

109. Bolam, J. P. Synapses of identified neurons in the neostriatum. *Ciba Foundation symposium* **107**, (1984).

110. Kawaguchi, Y. Large aspiny cells in the matrix of the rat neostriatum in vitro: Physiological identification, relation to the compartments and excitatory postsynaptic currents. *J. Neurophysiol.* **67**, (1992).

111. Chang, H. T., Wilson, C. J. & Kitai, S. T. A Golgi study of rat neostriatal neurons: Light microscopic analysis. *J. Comp. Neurol.* **208**, (1982).

112. Kawaguchi, Y. Physiological, morphological, and histochemical characterization of three classes of interneurons in rat neostriatum. *J. Neurosci.* **13**, (1993).

113. Bennett, B. D., Callaway, J. C. & Wilson, C. J. Intrinsic membrane properties underlying spontaneous tonic firing in neostriatal cholinergic interneurons. *J.*

Neurosci. **20**, (2000).

114. Wilson, C. J. & Goldberg, J. A. Origin of the slow afterhyperpolarization and slow rhythmic bursting in striatal cholinergic interneurons. *J. Neurophysiol.* **95**, (2006).

115. Kreitzer, A. C. Physiology and Pharmacology of Striatal Neurons. *Annu. Rev. Neurosci.* **32**, (2009).

116. Kawaguchi, Y., Wilson, C. J., Augood, S. J. & Emson, P. C. Striatal interneurones: chemical, physiological and morphological characterization. *Trends in Neurosciences* **18**, (1995).

117. Faust, T. W., Assous, M., Tepper, J. M. & Koós, T. Neostriatal GABAergic interneurons mediate cholinergic inhibition of spiny projection neurons. *J. Neurosci.* **36**, (2016).

118. Sullivan, M. A., Chen, H. & Morikawa, H. Recurrent inhibitory network among striatal cholinergic interneurons. *J. Neurosci.* **28**, (2008).

119. Lapper, S. R. & Bolam, J. P. Input from the frontal cortex and the parafascicular nucleus to cholinergic interneurons in the dorsal striatum of the rat. *Neuroscience* **51**, (1992).

120. Thomas, T. M., Smith, Y., Levey, A. I. & Hersch, S. M. Cortical inputs to m2-immunoreactive striatal interneurons in rat and monkey. *Synapse* **37**, (2000).

121. Bolam, J. P. *et al.* Substance P-Containing terminals in synaptic contact with cholinergic neurons in the neostriatum and basal forebrain: a double immunocytochemical study in the rat. *Brain Res.* **397**, (1986).

122. Graybiel, A. M., Hirsch, E. C. & Agid, Y. The nigrostriatal system in Parkinson's disease. *Advances in neurology* **53**, (1990).

123. Morris, G., Arkadir, D., Nevet, A., Vaadia, E. & Bergman, H. Coincident but distinct messages of midbrain dopamine and striatal tonically active neurons. *Neuron* **43**, (2004).

124. Bromberg-Martin, Ethan S., Matsumoto, M. & Hikosaka, O. Dopamine in motivational: rewarding, aversive,and alerting. *Neuron* **68**, 815–834 (2011).

125. Schulz, J. M. & Reynolds, J. N. J. Pause and rebound: Sensory control of cholinergic signaling in the striatum. *Trends in Neurosciences* **36**, (2013).

126. Tepper, J. M., Koós, T. & Wilson, C. J. GABAergic microcircuits in the neostriatum. *Trends in Neurosciences* **27**, (2004).

127. Abudukeyoumu, N., Hernandez-Flores, T., Garcia-Munoz, M. & Arbuthnott, G. W. Cholinergic modulation of striatal microcircuits. *Eur. J. Neurosci.* **49**, 604–622 (2019).

128. Matamales, M., Götz, J. & Bertran-Gonzalez, J. Quantitative imaging of cholinergic interneurons reveals a distinctive spatial organization and a functional gradient across the mouse striatum. *PLoS One* **11**, e0157682 (2016).

129. Tepper, J. M., Wilson, C. J. & Koós, T. Feedforward and feedback inhibition in neostriatal GABAergic spiny neurons. *Brain Research Reviews* **58**, (2008).

130. Tepper, J. M., Tecuapetla, F., Koós, T. & Ibáñez-Sandoval, O. Heterogeneity and diversity of striatal GABAergic interneurons. *Front. Neuroanat.* **4**, 150 (2010).

131. Tepper, J. M. *et al.* Heterogeneity and diversity of striatal GABAergic interneurons: Update 2018. *Frontiers in Neuroanatomy* **12**, (2018).

132. Muñoz-Manchado, A. B. *et al.* Diversity of interneurons in the dorsal striatum revealed by single-cell RNA sequencing and PatchSeq. *Cell Rep.* **24**, 2179-2190. e7 (2018).

133. Rymar, V. V. & Sadikot, A. F. Laminar fate of cortical GABAergic interneurons is dependent on both birthdate and phenotype. *J. Comp. Neurol.* **501**, (2007).

134. Cowan, R. L., Wilson, C. J., Emson, P. C. & Heizmann, C. W. Parvalbumin-containing gabaergic interneurons in the rat neostriatum. *J. Comp. Neurol.* **302**, (1990).

135. Gerfen, C. R., Baimbridge, K. G. & Miller, J. J. The neostriatal mosaic: Compartmental distribution of calcium-binding protein and parvalbumin in the basal ganglia of the rat and monkey. *Proc. Natl. Acad. Sci. U. S. A.* **82**, (1985).

136. Kubota, Y. & Kawaguchi, Y. Spatial distributions of chemically identified intrinsic neurons in relation to patch and matrix compartments of rat neostriatum. *J. Comp. Neurol.* **332**, (1993).

137. Tritsch, N. X. & Sabatini, B. L. Dopaminergic Modulation of Synaptic Transmission in Cortex and Striatum. *Neuron* **76**, (2012).

138. Choi, K., Holly, E. N., Davatolhagh, M. F., Beier, K. T. & Fuccillo, M. V. Integrated anatomical and physiological mapping of striatal afferent projections. *Eur. J. Neurosci.* **49**, (2019).

139. Bennett, B. D. & Bolam, J. P. Localisation of parvalbumin-immunoreactive structures in primate caudate-putamen. *J. Comp. Neurol.* **347**, (1994).

140. Gittis, A. H., Nelson, A. B., Thwin, M. T., Palop, J. J. & Anatol, C. NIH Public Access. **30**, 2223–2234 (2010).

141. Kita, H., Kosaka, T. & Heizmann, C. W. Parvalbumin-immunoreactive neurons in the rat neostriatum: a light and electron microscopic study. *Brain Res.* **536**, (1990).

142. Gittis, A. H., Nelson, A. B., Thwin, M. T., Palop, J. J. & Kreitzer, A. C. Distinct roles of GABAergic interneurons in the regulation of striatal output pathways. *J. Neurosci.* **30**, 2223–34 (2010).

143. Luk, K. C. & Sadikot, A. F. GABA promotes survival but not proliferation of parvalbumin-immunoreactive interneurons in rodent neostriatum: An in vivo study with stereology. *Neuroscience* **104**, (2001).

144. Monteiro, P. *et al.* Dichotomous parvalbumin interneuron populations in

dorsolateral and dorsomedial striatum. *J. Physiol.* **596**, 3695–3707 (2018).

145. Chesselet, M. F. & Graybiel, A. M. Striatal neurons expressing somatostatin-like immunoreactivity: Evidence for a peptidergic interneuronal system in the cat. *Neuroscience* **17**, (1986).

146. Smith, Y. & Parent, A. Neuropeptide Y-immunoreactive neurons in the striatum of cat and monkey: Morphological characteristics, intrinsic organization and co-localization with somatostatin. *Brain Res.* **372**, (1986).

147. Ibáñez-Sandoval, O., Xenias, H. S., Tepper, J. M. & Koós, T. Dopaminergic and cholinergic modulation of striatal tyrosine hydroxylase interneurons. *Neuropharmacology* **95**, (2015).

148. Koós, T. & Tepper, J. M. Inhibitory control of neostriatal projection neurons by GABAergic interneurons. *Nat. Neurosci.* **2**, (1999).

149. Vincent, S. R. & Johansson, O. Striatal neurons containing both somatostatin- and avian pancreatic polypeptide (APP)-like immunoreactivities and NADPH-diaphorase activity: A light and electron microscopic study. *J. Comp. Neurol.* **217**, (1983).

150. Kubota, Y. *et al.* Neuropeptide Y-immunoreactive neurons receive synaptic inputs from dopaminergic axon terminals in the rat neostriatum. *Brain Res.* **458**, (1988).

151. DiFiglia, M. & Aronin, N. Ultrastructural features of immunoreactive somatostatin neurons in the rat caudate nucleus. *J. Neurosci.* **2**, (1982).

152. Vuillet, J., Kerkerian, L., Kachidian, P., Bosler, O. & Nieoullon, A. Ultrastructural correlates of functional relationships between nigral dopaminergic or cortical afferent fibers and neuropeptide Y-containing neurons in the rat striatum. *Neurosci. Lett.* **100**, (1989).

153. Vuillet, J., Kerkerian, L., Salin, P. & Nieoullon, A. Ultrastructural features of NPY-containing neurons in the rat striatum. *Brain Res.* **477**, (1989).

154. Kubota, Y. & Kawaguchi, Y. Dependence of GABAergic synaptic areas on the interneuron type and target size. *J. Neurosci.* **20**, (2000).

155. Vuillet, J., Dimova, R., Nieoullon, A. & Goff, L. K. Le. Ultrastructural relationships between choline acetyltransferase- and neuropeptide Y-containing neurons in the rat striatum. *Neuroscience* **46**, (1992).

156. Lopez-Huerta, V. G., Tecuapetla, F., Guzman, J. N., Bargas, J. & Galarraga, E. Presynaptic modulation by somatostatin in the neostriatum. *Neurochem. Res.* **33**, (2008).

157. Ibáñez-Sandoval, O. *et al.* A novel functionally distinct subtype of striatal neuropeptide Y interneuron. *J. Neurosci.* **31**, (2011).

158. English, D. F. *et al.* GABAergic circuits mediate the reinforcement-related signals of striatal cholinergic interneurons. *Nat. Neurosci.* **15**, (2012).

159. Koos, T., Tepper, J. M. & Wilson, C. J. Comparison of IPSCs evoked by spiny and fast-spiking neurons in the neostriatum. *J. Neurosci.* **24**, (2004).

160. Garas, F. N. *et al.* Structural and molecular heterogeneity of calretinin-expressing interneurons in the rodent and primate striatum. *J. Comp. Neurol.* **526**, (2018).

161. Petryszyn, S., Di Paolo, T., Parent, A. & Parent, M. The number of striatal cholinergic interneurons expressing calretinin is increased in parkinsonian monkeys. *Neurobiol. Dis.* **95**, (2016).

162. Dubach, M. *et al.* Primate neostriatal neurons containing tyrosine hydroxylase: Immunohistochemical evidence. *Neurosci. Lett.* **75**, (1987).

163. Meredith, G. E. Immunocytochemical characterization of catecholaminergic neurons in the rat striatum following dopamine-depleting lesions. *Eur. J. Neurosci.* **11**, (1999).

164. Cossette, M., Lecomte, F. & Parent, A. Morphology and distribution of dopaminergic neurons intrinsic to the human striatum. *J. Chem. Neuroanat.* **29**, (2005).

165. Mura, A., Jackson, D., Manley, M. S., Young, S. J. & Groves, P. M. Aromaticl-amino acid decarboxylase immunoreactive cells in the rat striatum: a possible site for the conversion of exogenousl-DOPA to dopamine. *Brain Res.* **704**, (1995).

166. Tashiro, Y. *et al.* Tyrosine hydroxylase-like immunoreactive neurons in the striatum of the rat. *Neurosci. Lett.* **97**, (1989).

167. Meredith, J. M., Auger, A. P. & Blaustein, J. D. D1 Dopamine Receptor Agonist (SKF-38393) Induction of FosImmunoreactivity in Progestin Receptor-Containing Areasof Female Rat Brain. *J. Neuroendocrinol.* **9**, (1997).

168. Mazloom, M. & Smith, Y. Synaptic microcircuitry of tyrosine hydroxylase-containing neurons and terminals in the striatum of 1-methyl-4-phenyl-1,2,3,6-tetrahydropyridine- treated monkeys. *J. Comp. Neurol.* **495**, (2006).

169. Gerfen, C. R., Paletzki, R. & Heintz, N. GENSAT BAC cre-recombinase driver lines to study the functional organization of cerebral cortical and basal ganglia circuits. *Neuron* **80**, (2013).

170. Faust, T. W., Assous, M., Shah, F., Tepper, J. M. & Koós, T. Novel fast adapting interneurons mediate cholinergic-induced fast GABAA inhibitory postsynaptic currents in striatal spiny neurons. *Eur. J. Neurosci.* **42**, (2015).

171. Assous, M. *et al.* Identification and characterization of a novel spontaneously active bursty gabaergic interneuron in the mouse striatum. *J. Neurosci.* **38**, (2018).

172. Khakh, B. S. & Sofroniew, M. V. Diversity of astrocyte functions and phenotypes in neural circuits. *Nat. Neurosci.* **18**, (2015).

173. Khakh, B. S. & Deneen, B. The Emerging Nature of Astrocyte Diversity. *Annu. Rev. Neurosci.* **42**, (2019).

174. Araque, A. *et al.* Gliotransmitters travel in time and space. *Neuron* **81**, (2014).

175. Perea, G. & Araque, A. Astrocytes potentiate transmitter release at single hippocampal synapses. *Science (80-.).* **317**, (2007).

176. Agulhon, C., Fiacco, T. A. & McCarthy, K. D. Hippocampal short- and long-term plasticity are not modulated by astrocyte Ca2+ signaling. *Science (80-.).* **327**, (2010).

177. Martín, R., Bajo-Grañeras, R., Moratalla, R., Perea, G. & Araque, A. Circuit-specific signaling in astrocyte-neuron networks in basal ganglia pathways. *Science (80-.).* **349**, (2015).

178. D'Ascenzo, M. *et al.* mGluR5 stimulates gliotransmission in the nucleus accumbens. *Proc. Natl. Acad. Sci. U. S. A.* **104**, (2007).

179. Scofield, M. D. *et al.* Gq-DREADD selectively initiates glial glutamate release and inhibits cue-induced cocaine seeking. *Biol. Psychiatry* **78**, (2015).

180. Corkrum, M. *et al.* Dopamine-Evoked Synaptic Regulation in the Nucleus Accumbens Requires Astrocyte Activity. *Neuron* **105**, (2020).

181. Shepherd, G. M. G. Corticostriatal connectivity and its role in disease. *Nature Reviews Neuroscience* **14**, (2013).

182. Cowan, R. L. & Wilson, C. J. Spontaneous firing patterns and axonal projections of single corticostriatal neurons in the rat medial agranular cortex. *J. Neurophysiol.* **71**, (1994).

183. Deschênes, M., Bourassa, J. & Parent, A. Two different types of thalamic fibers innervate the rat striatum. *Brain Res.* **701**, (1995).

184. Groh, A. *et al.* Cell-type specific properties of pyramidal neurons in neocortex underlying a layout that is modifiable depending on the cortical area. *Cereb. Cortex* **20**, (2010).

185. Larsen, D. L. D., Wickersham, I. R. & Callaway, E. M. Retrograde tracing with recombinant rabies virus reveals correlations between projection targets and dendritic architecture in layer 5 of mouse barrel cortex. *Front. Neural Circuits* **1**, (2008).

186. Lei, W., Jiao, Y., Del Mar, N. & Reiner, A. Evidence for differential cortical input to direct pathway versus indirect pathway striatal projection neurons in rats. *J. Neurosci.* **24**, 8289–8299 (2004).

187. Morita, K., Im, S. & Kawaguchi, Y. Differential Striatal Axonal Arborizations of the Intratelencephalic and Pyramidal-Tract Neurons: Analysis of the Data in the MouseLight Database. *Front. Neural Circuits* **13**, (2019).

188. Kim, E. J., Juavinett, A. L., Kyubwa, E. M., Jacobs, M. W. & Callaway, E. M. Three Types of Cortical Layer 5 Neurons That Differ in Brain-wide Connectivity and Function. *Neuron* **88**, (2015).

189. Kiritani, T., Wickersham, I. R., Seung, H. S. & Shepherd, G. M. G. Hierarchical

connectivity and connection-specific dynamics in the corticospinal-corticostriatal microcircuit in mouse motor cortex. *J. Neurosci.* **32**, (2012).

190. Turner, R. S. & DeLong, M. R. Corticostriatal activity in primary motor cortex of the macaque. *J. Neurosci.* **20**, (2000).

191. WEBSTER, K. E. Cortico-striate interrelations in the albino rat. *J. Anat.* **95**, (1961).

192. Rodriguez-Oroz, M. C. *et al.* Initial clinical manifestations of Parkinson's disease: features and pathophysiological mechanisms. *The Lancet Neurology* **8**, (2009).

193. Künzle, H. Bilateral projections from precentral motor cortex to the putamen and other parts of the basal ganglia. An autoradiographic study in Macaca fascicularis. *Brain Res.* **88**, (1975).

194. Haber, S. N. Corticostriatal circuitry. *Dialogues Clin. Neurosci.* **18**, 7–21 (2016).

195. Kimura, M. The role of primate putamen neurons in the association of sensory stimuli with movement. *Neurosci. Res.* **3**, (1986).

196. Wallis, J. D. & Miller, E. K. Neuronal activity in primate dorsolateral and orbital prefrontal cortex during performance of a reward preference task. *Eur. J. Neurosci.* **18**, (2003).

197. Selemon, L. D. & Goldman-Rakic, P. S. Topographic intermingling of striatonigral and striatopallidal neurons in the rhesus monkey. *J. Comp. Neurol.* **297**, (1990).

198. Corbit, L. H., Leung, B. K. & Balleine, B. W. The role of the amygdala-striatal pathway in the acquisition and performance of goal-directed instrumental actions. *J. Neurosci.* (2013). doi:10.1523/JNEUROSCI.3271-13.2013

199. Fudge, J. L. & Haber, S. N. Defining the caudal ventral striatum in primates: Cellular and histochemical features. *J. Neurosci.* **22**, (2002).

200. Russchen, F. T., Bakst, I., Amaral, D. G. & Price, J. L. The amygdalostriatal projections in the monkey. An anterograde tracing study. *Brain Res.* **329**, (1985).

201. Kandel, E. R., Schwartz, J. H. & Jessell, T. M. *Principles of Neural Science, fourth addition*. *McGraw-Hill Companies* (2000). doi:10.1036/0838577016

202. COGNITIVE NEUROSCIENCE; THE BIOLOGY OF THE MIND. *Cuad. Neuropsicol.* (2010).

203. Powell, T. P. S. & Cowan, W. M. A study of thalamo-striate relations in the monkey. *Brain* (1956). doi:10.1093/brain/79.2.364

204. Afifi, A. & A, B. Functional neuroanatomy : text and atlas / Adel K. Afifi. *SERBIULA (sistema Libr. 2.0)* (2005).

205. Granger, R. & Hearn, R. Models of thalamocortical system. *Scholarpedia* **2**, 1796 (2007).

206. Le Gros Clark, W. E. & Russell, W. R. Observations on the efferent connexions of the centre median nucleus. *J. Anat.* (1939).

207. Royce, G. J., Bromley, S. & Gracco, C. Subcortical projections to the centromedian and parafascicular thalamic nuclei in the cat. *J. Comp. Neurol.* (1991). doi:10.1002/cne.903060110

208. Mehler, W. R., Feferman, M. E. & Nauta, W. J. H. Ascending axon degeneration following anterolateral cordotomy. An experimental study in the monkey. *Brain* (1960). doi:10.1093/brain/83.4.718

209. Raeva, S. N. The role of the parafascicular complex (CM-Pf) of the human thalamus in the neuronal mechanisms of selective attention. *Neurosci. Behav. Physiol.* (2006). doi:10.1007/s11055-006-0015-y

210. Minamimoto, T., Hori, Y. & Kimura, M. Roles of the thalamic CM-PF complex-Basal ganglia circuit in externally driven rebias of action. *Brain Research Bulletin* (2009). doi:10.1016/j.brainresbull.2008.08.013

211. Weigel, R. & Krauss, J. K. Center median-parafascicular complex and pain control: Review from a neurosurgical perspective. *Stereotactic and Functional Neurosurgery* (2004). doi:10.1159/000079843

212. Groenewegen, H. J. & Berendse, H. W. The specificity of the 'nonspecific' midline and intralaminar thalamic nuclei. *Trends in Neurosciences* **17**, (1994).

213. Smith, Y., Raju, D. V., Pare, J. F. & Sidibe, M. The thalamostriatal system: A highly specific network of the basal ganglia circuitry. *Trends in Neurosciences* **27**, (2004).

214. Smith, Y. *et al.* The thalamostriatal systems: Anatomical and functional organization in normal and parkinsonian states. *Brain Research Bulletin* (2009). doi:10.1016/j.brainresbull.2008.08.015

215. Smith, J. B., Mowery, T. M. & Alloway, K. D. Thalamic POm projections to the dorsolateral striatum of rats: Potential pathway for mediating stimulus-response associations for sensorimotor habits. *J. Neurophysiol.* (2012). doi:10.1152/jn.00142.2012

216. Diamond, M. E., Armstrong-James, M., Budway, M. J. & Ebner, F. F. Somatic sensory responses in the rostral sector of the posterior group (POm) and in the ventral posterior medial nucleus (VPM) of the rat thalamus: Dependence on the barrel field cortex. *J. Comp. Neurol.* (1992). doi:10.1002/cne.903190108

217. Lavallée, P. *et al.* Feedforward inhibitory control of sensory information in higher-order thalamic nuclei. *J. Neurosci.* (2005). doi:10.1523/JNEUROSCI.2301-05.2005

218. Reig, R. & Silberberg, G. Distinct Corticostriatal and Intracortical Pathways Mediate Bilateral Sensory Responses in the Striatum. *Cereb Cortex* **26**, 4405–4415 (2016).

219. Castle, M. *et al.* Thalamic innervation of the direct and indirect basal ganglia pathways in the rat: Ipsi- and contralateral projections. *J. Comp. Neurol.* (2005).

doi:10.1002/cne.20421

220. Lanciego, J. L. *et al.* Thalamic innervation of striatal and subthalamic neurons projecting to the rat entopeduncular nucleus. *Eur. J. Neurosci.* (2004). doi:10.1111/j.1460-9568.2004.03244.x

221. Sidibé, M. & Smith, Y. Differential synaptic innervation of striatofugal neurones projecting to the internal or external segments of the globus pallidus by thalamic afferents in the squirrel monkey. *J. Comp. Neurol.* (1996). doi:10.1002/(SICI)1096-9861(19960212)365:3<445::AID-CNE8>3.0.CO;2-4

222. Dubé, L., Smith, A. D. & Bolam, J. P. Identification of synaptic terminals of thalamic or cortical origin in contact with distinct medium-size spiny neurons in the rat neostriatum. *J. Comp. Neurol.* (1988). doi:10.1002/cne.902670402

223. Záborszky, L. *et al.* Cholecystokinin innervation of the ventral striatum: A morphological and radioimmunological study. *Neuroscience* **14**, (1985).

224. Brog, J. S., Salyapongse, A., Deutch, A. Y. & Zahm, D. S. The patterns of afferent innervation of the core and shell in the "Accumbens" part of the rat ventral striatum: Immunohistochemical detection of retrogradely transported fluoro-gold. *J. Comp. Neurol.* **338**, (1993).

225. Heimer, L., Zahm, D. S., Churchill, L., Kalivas, P. W. & Wohltmann, C. Specificity in the projection patterns of accumbal core and shell in the rat. *Neuroscience* **41**, (1991).

226. Lüscher, C. & Malenka, R. C. Drug-Evoked Synaptic Plasticity in Addiction: From Molecular Changes to Circuit Remodeling. *Neuron* **69**, (2011).

227. Ferré, S. *et al.* Adenosine-cannabinoid receptor interactions. Implications for striatal function. *British Journal of Pharmacology* **160**, (2010).

228. Taylor, I. M., Ilitchev, A. I. & Michael, A. C. Restricted diffusion of dopamine in the rat dorsal striatum. *ACS Chem. Neurosci.* **4**, (2013).

229. Yager, L. M., Garcia, A. F., Wunsch, A. M. & Ferguson, S. M. The ins and outs of the striatum: Role in drug addiction. *Neuroscience* **301**, (2015).

230. Kim, B. S. & Im, H. I. The role of the dorsal striatum in choice impulsivity. *Annals of the New York Academy of Sciences* **1451**, (2019).

231. Graybiel, A. M. & Ragsdale, C. W. Histochemically distinct compartments in the striatum of human, monkey, and cat demonstrated by acetylthiocholinesterase staining (basal ganglia/caudate nucleus/cholinergic transmission/acetylcholine/acetylcholinesterase, EC 3.1.1.7). *Neurobiology* **75**, (1978).

232. Olson, L., Seiger, Å. & Fuxe, K. Heterogeneity of striatal and limbic dopamine innervation: Highly fluorescent islands in developing and adult rats. *Brain Res.* **44**, (1972).

233. Gerfen, C. R. The neostriatal mosaic: multiple levels of compartmental organization. *Trends in Neurosciences* **15**, (1992).

234. Herkenham, M. & Pert, C. B. Mosaic distribution of opiate receptors, parafascicular projections and acetylcholinesterase in rat striatum. *Nature* **291**, (1981).

235. Kincaid, A. E. & Wilson, C. J. Corticostriatal innervation of the patch and matrix in the rat neostriatum. *J. Comp. Neurol.* **374**, (1996).

236. Donoghue, J. P. & Herkenham, M. Neostriatal projections from individual cortical fields conform to histochemically distinct striatal compartments in the rat. *Brain Res.* **365**, (1986).

237. Fujiyama, F., Unzai, T., Nakamura, K., Nomura, S. & Kaneko, T. Difference in organization of corticostriatal and thalamostriatal synapses between patch and matrix compartments of rat neostriatum. *Eur. J. Neurosci.* **24**, (2006).

238. Gerfen, C. R. The neostriatal mosaic: Striatal patch-matrix organization is related to cortical lamination. *Science (80-.).* **246**, (1989).

239. Hauber, W. & Schmidt, W. J. Differential effects of lesions of the dorsomedial and dorsolateral caudate-putamen on reaction time performance in rats. *Behav. Brain Res.* **60**, (1994).

240. Graybiel, A. M. Habits, Rituals, and the Evaluative Brain. *Annu. Rev. Neurosci.* **31**, (2008).

241. Hilario, M. R. F. High on habits. *Front. Neurosci.* **2**, (2008).

242. Joel, D. & Weiner, I. The connections of the dopaminergic system with the striatum in rats and primates: An analysis with respect to the functional and compartmental organization of the striatum. *Neuroscience* **96**, (2000).

243. Chuhma, N., Mingote, S., Kalmbach, A., Yetnikoff, L. & Rayport, S. Heterogeneity in Dopamine Neuron Synaptic Actions Across the Striatum and Its Relevance for Schizophrenia. *Biological Psychiatry* **81**, (2017).

244. Nagy, A., Eördegh, G., Paróczy, Z., Márkus, Z. & Benedek, G. Multisensory integration in the basal ganglia. *Eur. J. Neurosci.* **24**, (2006).

245. Gerfen, C. R., Herkenham, M. & Thibault, J. The neostriatal mosaic: II. Patch- and matrix-directed mesostriatal dopaminergic and non-dopaminergic systems. *J. Neurosci.* **7**, (1987).

246. Ribak, C. E., Vaughn, J. E. & Roberts, E. The GABA Neurons and their axon terminals in rat corpus striatum as demonstrated by GAD immunocytochemistry. *J. Comp. Neurol.* **187**, (1979).

247. Oertel, W. H. & Mugnaini, E. Immunocytochemical studies of GABAergic neurons in rat basal ganglia and their relations to other neuronal systems. *Neurosci. Lett.* **47**, (1984).

248. Sonne, J. & Beato, M. R. *Neuroanatomy, Substantia Nigra*. *StatPearls* (2018).

249. Basso, M. A. & Sommer, M. A. Exploring the role of the substantia nigra pars reticulata in eye movements. *Neuroscience* **198**, (2011).

250. Koob, G. F. Drugs of abuse: anatomy, pharmacology and function of reward pathways. *Trends in Pharmacological Sciences* **13**, (1992).

251. Ikemoto, S. Dopamine reward circuitry: two projection systems from the ventral midbrain to the nucleus accumbens–olfactory tubercle complex. *Brain Res. Rev.* **56**, 27–78 (2007).

252. Wilson, C. J., Young, S. J. & Groves, P. M. Statistical properties of neuronal spike trains in the substantia nigra: Cell types and their interactions. *Brain Res.* **136**, (1977).

253. Baufreton, J., Atherton, J. F., Surmeier, D. J. & Bevan, M. D. Enhancement of excitatory synaptic integration by GABAergic inhibition in the subthalamic nucleus. *J. Neurosci.* **25**, (2005).

254. Zhou, F. W., Matta, S. G. & Zhou, F. M. Constitutively active TRPC3 channels regulate basal ganglia output neurons. *J. Neurosci.* **28**, (2008).

255. Lee, C. R. & Tepper, J. M. Basal ganglia control of substantia nigra dopaminergic neurons. *Journal of Neural Transmission, Supplementa* (2009). doi:10.1007/978-3-211-92660-4-6

256. Grace, A. A. & Bunney, B. S. The control of firing pattern in nigral dopamine neurons: Single spike firing. *J. Neurosci.* **4**, (1984).

257. Freeman, A. S., Meltzer, L. T. & Bunney, B. S. Firing properties of substantia nigra dopaminergic neurons in freely moving rats. *Life Sci.* **36**, (1985).

258. Hyland, B. I., Reynolds, J. N. J., Hay, J., Perk, C. G. & Miller, R. Firing modes of midbrain dopamine cells in the freely moving rat. *Neuroscience* **114**, (2002).

259. Tepper, J. M., Martin, L. P. & Anderson, D. R. GABA(A) receptor-mediated inhibition of rat substantia nigra dopaminergic neurons by pars reticulata projection neurons. *J. Neurosci.* **15**, (1995).

260. Tennyson, S. S., Brockett, A. T., Hricz, N. W., Bryden, D. W. & Roesch, M. R. Firing of putative dopamine neurons in ventral tegmental area is modulated by probability of success during performance of a stop-change task. *eNeuro* (2018). doi:10.1523/ENEURO.0007-18.2018

261. Clark, D. & Chiodo, L. A. Electrophysiological and pharmacological characterization of identified nigrostriatal and mesoaccumbens dopamine neurons in the rat. *Synapse* **2**, (1988).

262. Lee, C. R., Abercrombie, E. D. & Tepper, J. M. Pallidal control of substantia nigra dopaminergic neuron firing pattern and its relation to extracellular neostriatal dopamine levels. *Neuroscience* **129**, (2004).

263. Carlsson, A. Thirty years of dopamine research. *Advances in neurology* **60**, (1993).

264. Harley, C. W. Norepinephrine and dopamine as learning signals. *Neural Plasticity* **11**, (2004).

265. Nirenberg, M. J., Vaughan, R. A., Uhl, G. R., Kuhar, M. J. & Pickel, V. M. The dopamine transporter is localized to dendritic and axonal plasma membranes of nigrostriatal dopaminergic neurons. *J. Neurosci.* **16**, (1996).

266. Schultz, W. Reward functions of the basal ganglia. *J. Neural Transm.* (2016). doi:10.1007/s00702-016-1510-0

267. Valdés-Baizabal, C., Carbajal, G. V., Pérez-González, D. & Malmierca, M. S. Dopamine modulates subcortical responses to surprising sounds. *PLoS Biol.* (2020). doi:10.1371/journal.pbio.3000744

268. Sulzer, D., Cragg, S. J. & Rice, M. E. Striatal dopamine neurotransmission: Regulation of release and uptake. *Basal Ganglia* **6**, (2016).

269. Faure, A., Haberland, U., Condé, F. & El Massioui, N. Lesion to the nigrostriatal dopamine system disrupts stimulus-response habit formation. *J. Neurosci.* **25**, (2005).

270. Lerner, T. N. *et al.* Intact-Brain Analyses Reveal Distinct Information Carried by SNc Dopamine Subcircuits. *Cell* **162**, (2015).

271. Çakir, Y. Modeling influences of dopamine on synchronization behavior of striatum. *Netw. Comput. Neural Syst.* **28**, (2017).

272. Peroutka, S. J. & Snyder, S. H. Relationship of neuroleptic drug effects at brain dopamine, serotonin, α-adrenergic, and histamine receptors to clinical potency. *Am. J. Psychiatry* **137**, (1980).

273. Howes, O. D. & Kapur, S. The dopamine hypothesis of schizophrenia: Version III - The final common pathway. *Schizophrenia Bulletin* **35**, (2009).

274. Björklund, A. & Dunnett, S. B. Dopamine neuron systems in the brain: an update. *Trends in Neurosciences* **30**, (2007).

275. Iversen, S. D. & Iversen, L. L. Dopamine: 50 years in perspective. *Trends in Neurosciences* **30**, (2007).

276. Hartman, D. S. & Civelli, O. Dopamine receptor diversity: Molecular and pharmacological perspectives. *Progress in Drug Research* **48**, (1997).

277. Rivera, A. *et al.* Dopamine D4 receptors are heterogeneously distributed in the striosomes/matrix compartments of the striatum. *J. Neurochem.* **80**, (2002).

278. Augood, S. J., Hollingsworth, Z. R., Standaert, D. G., Emson, P. C. & Penney, J. B. Localization of dopaminergic markers in the human subthalamic nucleus. *J. Comp. Neurol.* **421**, (2000).

279. Baufreton, J. *et al.* D5 (not D1) dopamine receptors potentiate burst-firing in neurons of the subthalamic nucleus by modulating an L-type calcium conductance. *J. Neurosci.* **23**, (2003).

280. Velasco, M. *et al.* Dopaminergic receptors: A new antihypertensive mechanism. in *Journal of Hypertension* **20**, (2002).

281. Contreras, F. *et al.* Dopamine, hypertension and obesity. *J. Hum. Hypertens.* **16**,

(2002).

282. Beaulieu, J. M. & Gainetdinov, R. R. The physiology, signaling, and pharmacology of dopamine receptors. *Pharmacological Reviews* **63**, (2011).

283. Goldman-Rakic, P. S., Castner, S. A., Svensson, T. H., Siever, L. J. & Williams, G. V. Targeting the dopamine D1 receptor in schizophrenia: Insights for cognitive dysfunction. *Psychopharmacology* **174**, (2004).

284. Savasta, M., Dubois, A. & Scatton, B. Autoradiographic localization of D1 dopamine receptors in the rat brain with [3H]SCH 23390. *Brain Res.* **375**, (1986).

285. Wamsley, J. K., Gehlert, D. R., Filloux, F. M. & Dawson, T. M. Comparison of the distribution of D-1 and D-2 dopamine receptors in the rat brain. *J. Chem. Neuroanat.* **2**, (1989).

286. Savasta, M., Dubois, A., Benavides, J. & Scatton, B. Different neuronal location of [3H]SCH 23390 binding sites in pars reticulata and pars compacta of the substantia nigra in the rat. *Neurosci. Lett.* **72**, (1986).

287. Hersch, S. M. *et al.* Electron microscopic analysis of D1 and D2 dopamine receptor proteins in the dorsal striatum and their synaptic relationships with motor corticostriatal afferents. *J. Neurosci.* **15**, (1995).

288. Alvarez, V. A. & Sabatini, B. L. Anatomical and Physiological Plasticity of Dendritic Spines. *Annu. Rev. Neurosci.* **30**, (2007).

289. Wong, A. C., Shetreat, M. E., Clarke, J. O. & Rayport, S. D1- and D2-like dopamine receptors are co-localized on the presynaptic varicosities of striatal and nucleus accumbens neurons in vitro. *Neuroscience* (1999). doi:10.1016/S0306-4522(98)00284-X

290. Caillé, I., Dumartin, B. & Bloch, B. Ultrastructural localization of D1 dopamine receptor immunoreactivity in rat striatonigral neurons and its relation with dopaminergic innervation. *Brain Res.* (1996). doi:10.1016/0006-8993(96)00424-6

291. Svenningsson, P. *et al.* DARPP-32: An Integrator of Neurotransmission. *Annu. Rev. Pharmacol. Toxicol.* **44**, (2004).

292. Giros, B. *et al.* Alternative splicing directs the expression of two D2 dopamine receptor isoforms. *Nature* **342**, (1989).

293. Ben-Jonathan, N. Dopamine: A prolactin-inhibiting hormone. *Endocr. Rev.* **6**, (1985).

294. Nishi, A., Snyder, G. L., Nairn, A. C. & Greengard, P. Role of calcineurin and protein phosphatase-2A in the regulation of DARPP-32 dephosphorylation in neostriatal neurons. *J. Neurochem.* **72**, (1999).

295. Jackson, D. M. & Westlind-Danielsson, A. Dopamine receptors: Molecular biology, biochemistry and behavioural aspects. *Pharmacology and Therapeutics* **64**, (1994).

296. Missale, C., Russel Nash, S., Robinson, S. W., Jaber, M. & Caron, M. G. Dopamine receptors: From structure to function. *Physiological Reviews* (1998). doi:10.1152/physrev.1998.78.1.189

297. Mishra, A., Singh, S. & Shukla, S. Physiological and Functional Basis of Dopamine Receptors and Their Role in Neurogenesis: Possible Implication for Parkinson's disease. *Journal of Experimental Neuroscience* **12**, (2018).

298. De Mei, C., Ramos, M., Iitaka, C. & Borrelli, E. Getting specialized: presynaptic and postsynaptic dopamine D2 receptors. *Current Opinion in Pharmacology* **9**, (2009).

299. Schultz, W. Behavioral Theories and the Neurophysiology of Reward. *Annu. Rev. Psychol.* **57**, (2006).

300. Liu, C., Kershberg, L., Wang, J., Schneeberger, S. & Kaeser, P. S. Dopamine Secretion Is Mediated by Sparse Active Zone-like Release Sites. *Cell* (2018). doi:10.1016/j.cell.2018.01.008

301. Banerjee, A., Lee, J., Nemcova, P., Liu, C. & Kaeser, P. S. Synaptotagmin-1 is the Ca2+ sensor for fast striatal dopamine release. *Elife* (2020). doi:10.7554/eLife.58359

302. Howe, M. W. & Dombeck, D. A. Rapid signalling in distinct dopaminergic axons during locomotion and reward. *Nature* (2016). doi:10.1038/nature18942

303. Sho, Y. *et al.* A critical time window for dopamine actions on the structural plasticity of dendritic spines. *Science (80-.).* (2014).

304. Gerfen, C. R., Staines, W. A., Fibiger, H. C. & Arbuthnott, G. W. Crossed connections of the substantia nigra in the rat. *J. Comp. Neurol.* **207**, (1982).

305. Pérez-Fernández, J., Kardamakis, A. A., Suzuki, D. G., Robertson, B. & Grillner, S. Direct Dopaminergic Projections from the SNc Modulate Visuomotor Transformation in the Lamprey Tectum. *Neuron* **96**, (2017).

306. Young, W. S., Bonner, T. I. & Brann, M. R. Mesencephalic dopamine neurons regulate the expression of neuropeptide mRNAs in the rat forebrain. *Proc. Natl. Acad. Sci. U. S. A.* **83**, (1986).

307. Bergson, C. *et al.* Regional, cellular, and subcellular variations in the distribution of D1 and D5 dopamine receptors in primate brain. *J. Neurosci.* **15**, (1995).

308. Yan, Z., Song, W. J. & Surmeier, D. J. D2 dopamine receptors reduce N-type Ca2+ currents in rat neostriatal cholinergic interneurons through a membrane-delimited, protein-kinase-C- insensitive pathway. *J. Neurophysiol.* **77**, (1997).

309. Gerfen, C. R. Substance P (neurokinin-1) receptor mRNA is selectively expressed in cholinergic neurons in the striatum and basal forebrain. *Brain Res.* **556**, (1991).

310. Herve, D., Rogard, M. & Levi-Strauss, M. Molecular analysis of the multiple Golf alpha subunit mRNAs in the rat brain. *Brain Res Mol Brain Res* **32**, (1995).

311. Kitai, S. T. & Surmeier, D. J. Cholinergic and dopaminergic modulation of potassium conductances in neostriatal neurons. *Adv. Neurol.* **60**, (1993).

312. Surmeier, D. J., Bargas, J., Hemmings, H. C., Nairn, A. C. & Greengard, P. Modulation of calcium currents by a D1 dopaminergic protein kinase/phosphatase cascade in rat neostriatal neurons. *Neuron* **14**, (1995).

313. Hernández-López, S., Bargas, J., Surmeier, D. J., Reyes, A. & Galarraga, E. Receptor activation enhances evoked discharge in neostriatal medium spiny neurons by modulating an L-type Ca2+ conductance. *J. Neurosci.* **17**, (1997).

314. Snyder, G. L. *et al.* Regulation of phosphorylation of the GluR1 AMPA receptor in the neostriatum by dopamine and psychostimulants in vivo. *J. Neurosci.* **20**, (2000).

315. Nicola, S. M. & Malenka, R. C. Modulation of synaptic transmission by dopamine and norepinephrine in ventral but not dorsal striatum. *J. Neurophysiol.* **79**, (1998).

316. Surmeier, D. J. *et al.* Dopamine receptor subtypes colocalize in rat striatonigral neurons. *Proc. Natl. Acad. Sci. U. S. A.* **89**, (1992).

317. Gao, Z. G., Cui, W. Y. & Liu, C. G. Modulation of apomorphine-induced rotations in unilaterally 6- hydroxydopamine lesioned rats by cholinergic agonists and antagonists. *Life Sci.* **60**, (1997).

318. Levine, M. S., Zhiwei, L. I., Cepeda, C., Cromwell, H. C. & Altemus, K. L. Neuromodulatory actions of dopamine on synaptically-evoked neostriatal responses in slices. *Synapse* **24**, (1996).

319. Snyder, G., Fienberg, A. & Huganir, R. A dopamine/D1 receptor/protein kinase A/dopamine-and cAMP-regulated phosphoprotein (M r 32 kDa)/protein phosphatase-1 pathway regulates dephosphorylation. *J.* **18**, (1998).

320. Flores-Hernández, J. *et al.* Dopamine enhancement of NMDA currents in dissociated medium-sized striatal neurons: Role of D1 receptors and DARPP-32. *J. Neurophysiol.* **88**, (2002).

321. Schultz, W., Dayan, P. & Montague, P. R. A neural substrate of prediction and reward. *Science (80-.).* **275**, 1593–1599 (1997).

322. Wise, R. A. Neuroleptics and operant behavior: The anhedonia hypothesis. *Behav. Brain Sci.* **5**, (1982).

323. Stoof, J. C. & Kebabian, J. W. Two dopamine receptors: Biochemistry, physiology and pharmacology. *Life Sciences* **35**, (1984).

324. Nishi, A., Snyder, G. L. & Greengard, P. Bidirectional regulation of DARPP-32 phosphorylation by dopamine. *J. Neurosci.* **17**, (1997).

325. Hernádez-López, S. *et al.* D2 dopamine receptors in striatal medium spiny neurons reduce L-type Ca2+ currents and excitability via a novel PLCβ1-IP3-Calcineurin-signaling cascade. *J. Neurosci.* **20**, (2000).

326. Kotecha, S. A. *et al.* A D2 class dopamine receptor transactivates a receptor tyrosine kinase to inhibit NMDA receptor transmission. *Neuron* **35**, (2002).

327. Calabresi, P. *et al.* Abnormal synaptic plasticity in the striatum of mice lacking dopamine D2 receptors. *J. Neurosci.* **17**, (1997).

328. Kreitzer, A. C. & Malenka, R. C. Dopamine modulation of state-dependent endocannabinoid release and long-term depression in the striatum. *J. Neurosci.* **25**, (2005).

329. Giuffrida, A. *et al.* Dopamine activation of endogenous cannabinoid signaling in dorsal striatum. *Nat. Neurosci.* **2**, (1999).

330. Martín, A. B. *et al.* Expression and function of CB1 receptor in the rat striatum: Localization and effects on D1 and D2 dopamine receptor-mediated motor behaviors. *Neuropsychopharmacology* **33**, (2008).

331. Antonazzo, M., Gutierrez-Ceballos, A., Bustinza, I., Ugedo, L. & Morera-Herreras, T. Cannabinoids differentially modulate cortical information transmission through the sensorimotor or medial prefrontal basal ganglia circuits. *Br. J. Pharmacol.* **176**, (2019).

332. Haber, S. N. The primate basal ganglia: parallel and integrative networks. *J. Chem. Neuroanat.* **26**, 317–330 (2003).

333. French, E. D., Dillon, K. & Wu, X. Cannabinoids excite dopamine neurons in the ventral tegmentum and substantia nigra. *Neuroreport* **8**, (1997).

334. Covey, D. P., Mateo, Y., Sulzer, D., Cheer, J. F. & Lovinger, D. M. Endocannabinoid modulation of dopamine neurotransmission. *Neuropharmacology* **124**, (2017).

335. Hernández-Echeagaray, E., Starling, A. J., Cepeda, C. & Levine, M. S. Modulation of AMPA currents by D2 dopamine receptors in striatal medium-sized spiny neurons: Are dendrites necessary? *Eur. J. Neurosci.* **19**, (2004).

336. Håkansson, K. *et al.* Regulation of phosphorylation of the GluR1 AMPA receptor by dopamine D 2 receptors. *J. Neurochem.* **96**, (2006).

337. Bamford, N. S. *et al.* Dopamine modulates release from corticostriatal terminals. *J. Neurosci.* **24**, (2004).

338. Olson, P. A. *et al.* G-protein-coupled receptor modulation of striatal Cav1.3 L-type Ca2+ channels is dependent on a shank-binding domain. *J. Neurosci.* **25**, (2005).

339. Greif, G. J., Lin, Y. J., Liu, J. C. & Freedman, J. E. Dopamine-modulated potassium channels on rat striatal neurons: Specific activation and cellular expression. *J. Neurosci.* **15**, (1995).

340. Chuhma, N., Mingote, S., Moore, H. & Rayport, S. Dopamine neurons control striatal cholinergic neurons via regionally heterogeneous dopamine and glutamate signaling. *Neuron* **81**, (2014).

341. Aosaki, T., Kiuchi, K. & Kawaguchi, Y. Dopamine D1-like receptor activation excites rat striatal large aspiny neurons in vitro. *J. Neurosci.* **18**, (1998).

342. Maurice, N. *et al.* D2 dopamine receptor-mediated modulation of voltage-dependent Na+ channels reduces autonomous activity in striatal cholinergic interneurons. *J. Neurosci.* **24**, (2004).

343. Calabresi, P., Centonze, D., Gubellini, P., Pisani, A. & Bernardi, G. Endogenous ACh enhances striatal NMDA-responses via M1-like muscarinic receptors and PKC activation. *Eur. J. Neurosci.* **10**, (1998).

344. Levey, A. I. *et al.* Localization of D1 and D2 dopamine receptors in brain with subtype-specific antibodies. *Proc. Natl. Acad. Sci. U. S. A.* **90**, (1993).

345. Lindroos, R. *et al.* Basal ganglia neuromodulation over multiple temporal and structural scales—simulations of direct pathway MSNs investigate the fast onset of dopaminergic effects and predict the role of Kv4.2. *Front. Neural Circuits* **12**, (2018).

346. Staley, J. K. *et al.* Human tobacco smokers in early abstinence have higher levels of β2* nicotinic acetylcholine receptors than nonsmokers. *J. Neurosci.* (2006). doi:10.1523/JNEUROSCI.0546-06.2006

347. Aosaki, T. *et al.* Responses of tonically active neurons in the primate's striatum undergo systematic changes during behavioral sensorimotor conditioning. *J. Neurosci.* **14**, (1994).

348. Aosaki, T., Kimura, M. & Graybiel, A. M. Temporal and spatial characteristics of tonically active neurons of the primate's striatum. *J. Neurophysiol.* **73**, (1995).

349. Aosaki, T., Miura, M., Suzuki, T., Nishimura, K. & Masuda, M. Acetylcholine-dopamine balance hypothesis in the striatum: An update. *Geriatrics and Gerontology International* **10**, (2010).

350. Chuhma, N. *et al.* Dopamine neuron glutamate cotransmission evokes a delayed excitation in lateral dorsal striatal cholinergic interneurons. *Elife* **7**, 1–29 (2018).

351. Parent, A. & Hazrati, L. N. Functional anatomy of the basal ganglia. I. The cortico-basal ganglia-thalamo-cortical loop. *Brain Research Reviews* **20**, (1995).

352. Middleton, F. A. & Strick, P. L. Basal ganglia output and cognition: Evidence from anatomical, behavioral, and clinical studies. *Brain Cogn.* **42**, (2000).

353. Haber, S. N., Kunishio, K., Mizobuchi, M. & Lynd-Balta, E. The orbital and medial prefrontal circuit through the primate basal ganglia. *J. Neurosci.* **15**, (1995).

354. Mink, J. W. The basal ganglia and involuntary movements: Impaired inhibition of competing motor patterns. *Archives of Neurology* **60**, (2003).

355. Gómez-Benito, M. *et al.* Modeling Parkinson's Disease With the Alpha-Synuclein Protein. *Frontiers in Pharmacology* **11**, (2020).

356. Schneider, S. A. & Obeso, J. A. Clinical and pathological features of Parkinson's

disease. *Curr. Top. Behav. Neurosci.* **22**, (2014).

357. Kojima, H. *et al.* Adenovirus-mediated transduction with human glial cell line-derived neurotrophic factor gene prevents 1-methyl-4-phenyl-l,2,3,6-tetrahydropyridine-induced dopamine depletion in striatum of mouse brain. *Biochem. Biophys. Res. Commun.* **238**, (1997).

358. Munro-Davies, L. E., Winter, J., Aziz, T. Z. & Stein, J. F. The role of the pedunculopontine region in basal-ganglia mechanisms of akinesia. *Exp. Brain Res.* **129**, (1999).

359. Büttner, T. *et al.* Visual hallucinosis: The major clinical determinant of distorted chromatic contour perception in Parkinson's disease. *J. Neural Transm.* **103**, (1996).

360. Ravina, B. *et al.* Diagnostic criteria for psychosis in Parkinson's disease: Report of an NINDS, NIMH Work Group. *Movement Disorders* **22**, (2007).

361. Howe, T. E., Lövgreen, B., Cody, F. W. J., Ashton, V. J. & Oldham, J. A. Auditory cues can modify the gait of persons with early-stage Parkinson's disease: A method for enhancing parkinsonian walking performance? *Clin. Rehabil.* **17**, (2003).

362. Azulay, J. P. *et al.* Visual control of locomotion in Parkinson's disease41. *Brain* **122**, (1999).

363. Arias, P. & Cudeiro, J. Effects of rhythmic sensory stimulation (auditory, visual) on gait in Parkinson's disease patients. *Exp. Brain Res.* **186**, (2008).

364. Alonso-Frech, F. *et al.* Slow oscillatory activity and levodopa-induced dyskinesias in Parkinson's disease. *Brain* **129**, (2006).

365. Brown, P. Oscillatory nature of human basal ganglia activity: Relationship to the pathophysiology of parkinson's disease. *Movement Disorders* **18**, (2003).

366. Kühn, A. A. *et al.* The relationship between local field potential and neuronal discharge in the subthalamic nucleus of patients with Parkinson's disease. *Exp. Neurol.* **194**, (2005).

367. Priori, A. *et al.* Rhythm-specific pharmacological modulation of subthalamic activity in Parkinson's disease. *Exp. Neurol.* **189**, (2004).

368. West, T. O. *et al.* Propagation of beta/gamma rhythms in the cortico-basal ganglia circuits of the parkinsonian rat. *J. Neurophysiol.* **119**, (2018).

369. Kühn, A. A. *et al.* Modulation of beta oscillations in the subthalamic area during motor imagery in Parkinson's disease. *Brain* **129**, (2006).

370. Weinberger, M. *et al.* Beta oscillatory activity in the subthalamic nucleus and its relation to dopaminergic response in Parkinson's disease. *J. Neurophysiol.* **96**, (2006).

371. Aristieta, A., Ruiz-Ortega, J. A., Miguelez, C., Morera-Herreras, T. & Ugedo, L. Chronic L-DOPA administration increases the firing rate but does not reverse

enhanced slow frequency oscillatory activity and synchronization in substantia nigra pars reticulata neurons from 6-hydroxydopamine-lesioned rats. *Neurobiol. Dis.* **89**, 88–100 (2016).

372. Bergman, H., Wichmann, T., Karmon, B. & DeLong, M. R. The primate subthalamic nucleus. II. Neuronal activity in the MPTP model of parkinsonism. *J. Neurophysiol.* **72**, (1994).

373. Brazhnik, E. *et al.* State-dependent spike and local field synchronization between motor cortex and substantia nigra in hemiparkinsonian rats. *J. Neurosci.* **32**, (2012).

374. Delaville, C. *et al.* Oscillatory activity in basal ganglia and motor cortex in an awake behaving rodent model of Parkinson's disease. *Basal Ganglia* **3**, (2014).

375. Mallet, N. *et al.* Parkinsonian beta oscillations in the external globus pallidus and their relationship with subthalamic nucleus activity. *J. Neurosci.* **28**, (2008).

376. Murer, M. G., Tseng, K. Y., Kasanetz, F., Belluscio, M. & Riquelme, L. A. Brain oscillations, medium spiny neurons, and dopamine. *Cellular and Molecular Neurobiology* **22**, (2002).

377. Sharott, A. *et al.* Dopamine depletion increases the power and coherence of β-oscillations in the cerebral cortex and subthalamic nucleus of the awake rat. *Eur. J. Neurosci.* **21**, (2005).

378. Tseng, K. Y. *et al.* Subthalamic nucleus lesions reduce low frequency oscillatory firing of substantia nigra pars reticulata neurons in a rat model of Parkinson's disease. *Brain Res.* **904**, (2001).

379. Faraone, S. V., Po, M. D., Komolova, M. & Cortese, S. Sleep-associated adverse events during methylphenidate treatment of attention-deficit/hyperactivity disorder: A meta-analysis. *J. Clin. Psychiatry* **80**, (2019).

380. Tenenbaum, R. B. *et al.* Response Inhibition, Response Execution, and Emotion Regulation among Children with Attention-Deficit/Hyperactivity Disorder. *J. Abnorm. Child Psychol.* **47**, (2019).

381. Lenzi, F., Cortese, S., Harris, J. & Masi, G. Pharmacotherapy of emotional dysregulation in adults with ADHD: A systematic review and meta-analysis. *Neuroscience and Biobehavioral Reviews* **84**, (2018).

382. Castellanos, F. X. *et al.* Quantitative brain magnetic resonance imaging in girls with attention-deficit/hyperactivity disorder. *Arch. Gen. Psychiatry* **58**, (2001).

383. Filipek, P. A. *et al.* Volumetric MRI analysis comparing subjects having attention-deficit hyperactivity disorder with normal controls. *Neurology* **48**, (1997).

384. Ehrsson, H. H., Holmes, N. P. & Passingham, R. E. Touching a rubber hand: Feeling of body ownership is associated with activity in multisensory brain areas. *J. Neurosci.* **25**, (2005).

385. Farnè, A., Iriki, A. & Làdavas, E. Shaping multisensory action-space with tools:

Evidence from patients with cross-modal extinction. in *Neuropsychologia* **43**, (2005).

386. Green, A. M. & Angelaki, D. E. Multisensory integration: Resolving sensory ambiguities to build novel representations. *Current Opinion in Neurobiology* **20**, (2010).

387. King, A. J. Multisensory integration: Strategies for synchronization. *Current Biology* **15**, (2005).

388. Ghazanfar, A. A. & Schroeder, C. E. Is neocortex essentially multisensory? *Trends in Cognitive Sciences* **10**, (2006).

389. Pavani, F. & Galfano, G. The multisensory body revealed through its cast shadows. *Frontiers in Psychology* **6**, (2015).

390. Kuraoka, K. & Nakamura, K. Responses of single neurons in monkey amygdala to facial and vocal emotions. *J. Neurophysiol.* **97**, (2007).

391. DEVRIES, S. Gordon L. Fain, Sensory Transduction, Sinauer Associates, Sunderland Massachusetts (2003) 288 pp., 159 illus. Price: US$ 64.95. *Surv. Ophthalmol.* **49**, (2004).

392. Meredith, M. A., Nemitz, J. W. & Stein, B. E. Determinants of multisensory integration in superior colliculus neurons. I. Temporal factors. *J. Neurosci.* **7**, (1987).

393. Stein, B. E. & Stanford, T. R. Multisensory integration: Current issues from the perspective of the single neuron. *Nature Reviews Neuroscience* **9**, (2008).

394. Alvarado, J. C., Vaughan, J. W., Stanford, T. R. & Stein, B. E. Multisensory versus unisensory integration: Contrasting modes in the superior colliculus. *J. Neurophysiol.* **97**, (2007).

395. Elliott, M. T., Wing, A. M. & Welchman, A. E. Multisensory cues improve sensorimotor synchronisation. *Eur. J. Neurosci.* **31**, (2010).

396. Vroomen, J. & de Gelder, B. Perceptual effects of cross-modal stimulation: Ventriloquism and the freezing phenomenon. in *The handbook of multisensory processes* (2004).

397. Slutsky, D. A. & Recanzone, G. H. Temporal and spatial dependency, of the ventriloquism effect. *Neuroreport* **12**, (2001).

398. Miu, A. C., Piţur, S. & Szentágotai-Tatar, A. Aesthetic emotions across arts: A comparison between painting and music. *Front. Psychol.* **6**, (2016).

399. Piwek, L., Pollick, F. & Petrini, K. Audiovisual integration of emotional signals from others' social interactions. *Front. Psychol.* **6**, (2015).

400. Gallese, V. Mirror neurons and the social nature of language: The neural exploitation hypothesis. *Soc. Neurosci.* **3**, (2008).

401. Myachykov, A., Garrod, S. & Scheepers, C. Determinants of structural choice in visually situated sentence production. *Acta Psychol. (Amst).* **141**, (2012).

402. Cox, D. & Hong, S. W. Semantic-based crossmodal processing during visual suppression. *Front. Psychol.* **6**, (2015).

403. Homma, C. T. & Ashida, H. What makes space-time interactions in human vision asymmetrical? *Front. Psychol.* **6**, (2015).

404. Pasqualotto, A., Dumitru, M. L. & Myachykov, A. Editorial: Multisensory integration: Brain, body, and world. *Frontiers in Psychology* **6**, (2016).

405. Marks, W. N., Parker, M. E. & Howland, J. G. Variants of the Spontaneous Recognition Procedure Assessing Multisensory Integration Reveal Behavioral Alterations in Rodent Models of Psychiatric and Neurological Disorders. in *Handbook of Behavioral Neuroscience* **27**, (2018).

406. Wood, R. A., Hopkins, S. A., Moodley, K. K. & Chan, D. Fifty percent prevalence of extracampine hallucinations in Parkinson's disease patients. *Front. Neurol.* **6**, (2015).

407. Ding, C. *et al.* Parkinson's disease alters multisensory perception: Insights from the Rubber Hand Illusion. *Neuropsychologia* **97**, (2017).

408. Pastor, M. A., Artieda, J., Jahanshahi, M. & Obeso, J. A. Time estimation and reproduction is abnormal in parkinson's disease. *Brain* **115**, (1992).

409. Artieda, J., Pastor, M. A., Lacruz, F. & Obeso, J. A. Temporal discrimination is abnormal in parkinson's disease. *Brain* **115**, (1992).

410. Bulens, C., Meerwaldt, J. D., Van der Wildt, G. J. & Van Deursen, J. B. P. Effect of levodopa treatment on contrast sensitivity in Parkinson's disease. *Ann. Neurol.* **22**, (1987).

411. Conte, A., Khan, N., Defazio, G., Rothwell, J. C. & Berardelli, A. Pathophysiology of somatosensory abnormalities in Parkinson disease. *Nature Reviews Neurology* **9**, (2013).

412. Shin, J. H., Kim, D. & Jung, M. W. Differential coding of reward and movement information in the dorsomedial striatal direct and indirect pathways. *Nat. Commun.* (2018). doi:10.1038/s41467-017-02817-1

413. Yin, H. H., Ostlund, S. B., Knowlton, B. J. & Balleine, B. W. The role of the dorsomedial striatum in instrumental conditioning. *Eur. J. Neurosci.* (2005). doi:10.1111/j.1460-9568.2005.04218.x

414. Balleine, B. W., Delgado, M. R. & Hikosaka, O. The role of the dorsal striatum in reward and decision-making. *Journal of Neuroscience* (2007). doi:10.1523/JNEUROSCI.1554-07.2007

415. Klapoetke, N. C. *et al.* Independent optical excitation of distinct neural populations. *Nat. Methods* **11**, 338–346 (2014).

416. Katz, Y., Yizhar, O., Staiger, J. & Lampl, I. Optopatcher—an electrode holder for simultaneous intracellular patch-clamp recording and optical manipulation. *J. Neurosci. Methods* **214**, 113–117 (2013).

417. Paxinos, G. & Franklin, K. B. J. The Mouse Brain in Stereotaxic Coordinates, 2nd edition. *Academic Press* 360 p. (2001).

418. Mahon, S., Deniau, J. M. & Charpier, S. Corticostriatal plasticity: Life after the depression. *Trends Neurosci.* **27**, 460–467 (2004).

419. Nisenbaum, E. S. & Wilson, C. J. Potassium currents responsible for inward and outward rectification in rat neostriatal spiny projection neurons. *J. Neurosci.* **15**, 4449–4463 (1995).

420. Holtmaat, A. *et al. Through a Chronic Cranial Window*. *Nature protocols* **4**, (2009).

421. Katz, Y., Yizhar, O., Staiger, J. & Lampl, I. Optopatcher-An electrode holder for simultaneous intracellular patch-clamp recording and optical manipulation. *J. Neurosci. Methods* **214**, 113–117 (2013).

422. Katz, Y., Sokoletsky, M. & Lampl, I. In-vivo optogenetics and pharmacology in deep intracellular recordings. *J. Neurosci. Methods* **325**, 108324 (2019).

423. Patriarchi, T. *et al.* Ultrafast neuronal imaging of dopamine dynamics with designed genetically encoded sensors. *Science (80-.).* **360**, (2018).

424. Alegre-Cortés, J. *et al.* Time-frequency analysis of neuronal populations with instantaneous resolution based on noise-assisted multivariate empirical mode decomposition. *J. Neurosci. Methods* **267**, 35–44 (2016).

425. Averbeck, B. B., Latham, P. E. & Pouget, A. Neural correlations, population coding and computation. *Nature Reviews Neuroscience* **7**, (2006).

426. Cole, S. R. & Voytek, B. Brain Oscillations and the Importance of Waveform Shape. *Trends in Cognitive Sciences* **21**, (2017).

427. Cooley, J. W. & Tukey, J. W. An Algorithm for the Machine Calculation of Complex Fourier Series. *Math. Comput.* **19**, (1965).

428. Winograd, S. On computing the Discrete Fourier Transform. *Proc. Natl. Acad. Sci. U. S. A.* **73**, (1976).

429. Zhan, Y., Halliday, D., Jiang, P., Liu, X. & Feng, J. Detecting time-dependent coherence between non-stationary electrophysiological signals-A combined statistical and time-frequency approach. *J. Neurosci. Methods* **156**, (2006).

430. Samar, V. J., Bopardikar, A., Rao, R. & Swartz, K. Wavelet analysis of neuroelectric waveforms: A conceptual tutorial. *Brain Lang.* **66**, (1999).

431. Ur Rehman, N. & Mandic, D. P. Filter bank property of multivariate empirical mode decomposition. *IEEE Trans. Signal Process.* **59**, 2421–2426 (2011).

432. Huang, N. E. *et al.* The empirical mode decomposition and the Hilbert spectrum for nonlinear and non-stationary time series analysis. *Proc. R. Soc. A* **454**, 903–995 (1996).

433. Wu, Z. & Huang, N. E. Ensemble empirical mode decomposition: A noise-assisted data analysis method. *Adv. Adapt. Data Anal.* **1**, (2009).

434. Flandrin, P., Rilling, G. & Gonçalvés, P. Empirical mode decomposition as a filter bank. *IEEE Signal Processing Letters* **11**, (2004).

435. Rilling, G., Flandrin, P. & Goncalves, P. On empirical mode decomposition and its algorithms. in *IEEE-EURASIP workshop on nonlinear signal and image processing* **3**, (2003).

436. Reig, R. & Sanchez-Vives, M. V. Synaptic transmission and plasticity in an active cortical network. *PLoS One* **2**, (2007).

437. Petersen, C. C. H., Hahn, T. T. G., Mehta, M., Grinvald, A. & Sakmann, B. Interaction of sensory responses with spontaneous depolarization in layer 2/3 barrel cortex. *Proc. Natl. Acad. Sci. U. S. A.* **100**, (2003).

438. Pasik, P., Pasik, T., Holstein, G. R. & Hámori, J. GABAergic elements in the neuronal circuits of the monkey neostriatum: A light and electron microscopic immunocytochemical study. *J. Comp. Neurol.* **270**, (1988).

439. Corre, J. *et al.* Dopamine neurons projecting to medial shell of the nucleus accumbens drive heroin reinforcement. *Elife* **7**, 1–22 (2018).

440. Robinson, J. E. *et al.* Optical dopamine monitoring with dLight1 reveals mesolimbic phenotypes in a mouse model of neurofibromatosis type 1. *Elife* **8**, (2019).

441. Mingote, S. *et al.* Dopamine neuron dependent behaviours mediated by glutamate cotransmission. *Elife* (2017). doi:10.7554/eLife.27566

442. Trudeau, L. E. *et al.* The multilingual nature of dopamine neurons. in *Progress in Brain Research* **211**, (2014).

443. Kim, J. I. *et al.* Aldehyde dehydrogenase 1a1 mediates a GABA synthesis pathway in midbrain dopaminergic neurons. *Science (80-.).* (2015). doi:10.1126/science.aac4690

444. Lahiri, A. K. & Bevan, M. D. Dopaminergic Transmission Rapidly and Persistently Enhances Excitability of D1 Receptor-Expressing Striatal Projection Neurons. *Neuron* **106**, (2020).

445. Feingold, J., Gibson, D. J., Depasquale, B. & Graybiel, A. M. Bursts of beta oscillation differentiate postperformance activity in the striatum and motor cortex of monkeys performing movement tasks. *Proc. Natl. Acad. Sci. U. S. A.* **112**, (2015).

446. Womelsdorf, T., Fries, P., Mitra, P. P. & Desimone, R. Gamma-band synchronization in visual cortex predicts speed of change detection. *Nature* **439**, (2006).

447. Saalmann, Y. B., Pigarev, I. N. & Vidyasagar, T. R. Neural mechanisms of visual attention: How top-down feedback highlights relevant locations. *Science (80-.).* **316**, (2007).

448. Tallon-Baudry, C., Mandon, S., Freiwald, W. A. & Kreiter, A. K. Oscillatory synchrony in the monkey temporal lobe correlates with performance in a visual

short-term memory task. *Cereb. Cortex* **14**, (2004).

449. Pesaran, B., Pezaris, J. S., Sahani, M., Mitra, P. P. & Andersen, R. A. Temporal structure in neuronal activity during working memory in macaque parietal cortex. *Nat. Neurosci.* **5**, (2002).

450. Steriade, M., Amzica, F. & Contreras, D. Synchronization of fast (30-40 Hz) spontaneous cortical rhythms during brain activation. *J. Neurosci.* **16**, (1996).

451. Levy, R. *et al.* Dependence of subthalamic nucleus oscillations on movement and dopamine in Parkinson's disease. *Brain* **125**, (2002).

452. Brown, P. *et al.* Dopamine dependency of oscillations between subthalamic nucleus and pallidum in Parkinson's disease. *J. Neurosci.* **21**, (2001).

453. Ur Rehman, N. & Mandic, D. P. Filter bank property of multivariate empirical mode decomposition. *IEEE Trans. Signal Process.* **59**, 2421–2426 (2011).

454. Hunnicutt, B. J. *et al.* A comprehensive excitatory input map of the striatum reveals novel functional organization. *Elife* **5**, 1–32 (2016).

455. Morgenstern, N. Pyramidal tract corticostriatal inputs convey biphasic signals to medium spiny neurons through cholinergic interneurons. in (International Basal Ganglia Society (IBAGS) Meeting, 2019).

456. Surmeier, D. J., Ding, J., Day, M., Wang, Z. & Shen, W. D1 and D2 dopamine-receptor modulation of striatal glutamatergic signaling in striatal medium spiny neurons. *Trends Neurosci.* **30**, 228–235 (2007).

457. Gibson, I. M. & McIlwain, H. Continuous recording of changes in membrane potential in mammalian cerebral tissues in vitro; recovery after depolarization by added substances. *J. Physiol.* **176**, (1965).

458. Neumann, E., Schaefer-Ridder, M., Wang, Y. & Hofschneider, P. H. Gene transfer into mouse lyoma cells by electroporation in high electric fields. *EMBO J.* **1**, (1982).

459. Matsuzaki, M. *et al.* Dendritic spine geometry is critical for AMPA receptor expression in hippocampal CA1 pyramidal neurons. *Nat. Neurosci.* **4**, (2001).

460. Sanchez-Vives, M. V. *et al.* Inhibitory modulation of cortical up states. *J. Neurophysiol.* **104**, (2010).

461. Paspalas, C. D. & Goldman-Rakic, P. S. Presynaptic D1 dopamine receptors in primate prefrontal cortex: Target-specific expression in the glutamatergic synapse. *J. Neurosci.* **25**, 1260–1267 (2005).

462. Timofeev, I., Contreras, D. & Steriade, M. Synaptic responsiveness of cortical and thalamic neurones during various phases of slow sleep oscillation in cat. *J. Physiol.* (1996). doi:10.1113/jphysiol.1996.sp021489

463. Crochet, S., Fuentealba, P., Cissé, Y., Timofeev, I. & Steriade, M. Synaptic plasticity in local cortical network in vivo and its modulation by the level of neuronal activity. *Cereb. Cortex* (2006). doi:10.1093/cercor/bhj008

464. Sachdev, R. N. S., Ebner, F. F. & Wilson, C. J. Effect of subthreshold up and down states on the whisker-evoked response in somatosensory cortex. *J. Neurophysiol.* (2004). doi:10.1152/jn.00347.2004

465. Pidoux, M., Mahon, S., Deniau, J. M. & Charpier, S. Integration and propagation of somatosensory responses in the corticostriatal pathway: An intracellular study in vivo. *J. Physiol.* (2011). doi:10.1113/jphysiol.2010.199646

466. Tunstall, M. J., Oorschot, D. E., Kean, A. & Wickens, J. R. Inhibitory interactions between spiny projection neurons in the rat striatum. *J. Neurophysiol.* (2002). doi:10.1152/jn.2002.88.3.1263

467. Reig, R., Zerlaut, Y., Vergara, R., Destexhe, A. & Sanchez-Vives, M. V. Gain modulation of synaptic inputs by network state in auditory cortex in vivo. *J. Neurosci.* (2015). doi:10.1523/JNEUROSCI.2004-14.2015

468. Nicolas, H. Ô. & Destexhe, A. Synaptic background activity enhances the responsiveness of neocortical pyramidal neurons. *J. Neurophysiol.* (2000). doi:10.1152/jn.2000.84.3.1488

469. Rice, M. E., Cragg, S. J. & Greenfield, S. A. Characteristics of electrically evoked somatodendritic dopamine release in substantia nigra and ventral tegmental area in vitro. *J. Neurophysiol.* **77**, (1997).

470. Bouchet, C. A. *et al.* Activation of Nigrostriatal Dopamine Neurons during Fear Extinction Prevents the Renewal of Fear. *Neuropsychopharmacology* (2018). doi:10.1038/npp.2017.235

471. Tritsch, N. X., Ding, J. B. & Sabatini, B. L. Dopaminergic neurons inhibit striatal output through non-canonical release of GABA. *Nature* **490**, 262–6 (2012).

472. Tritsch, N. X., Granger, A. J. & Sabatini, B. L. Mechanisms and functions of GABA co-release. *Nat. Rev. Neurosci.* (2016). doi:10.1038/nrn.2015.21

473. Hnasko, T. S. & Edwards, R. H. Neurotransmitter corelease: Mechanism and physiological role. *Annu. Rev. Physiol.* (2012). doi:10.1146/annurev-physiol-020911-153315

474. Mingote, S. *et al.* Functional connectome analysis of dopamine neuron glutamatergic connections in forebrain regions. *J. Neurosci.* **35**, (2015).

475. Tritsch, N. X., Oh, W. J., Gu, C. & Sabatini, B. L. Midbrain dopamine neurons sustain inhibitory transmission using plasma membrane uptake of GABA, not synthesis. *Elife* (2014). doi:10.7554/eLife.01936

476. Straub, C., Tritsch, N. X., Hagan, N. A., Gu, C. & Sabatini, B. L. Multiphasic modulation of cholinergic interneurons by nigrostriatal afferents. *J. Neurosci.* (2014). doi:10.1523/JNEUROSCI.0589-14.2014

477. Jun, N. Y. & Cardin, J. A. Activation of distinct channelrhodopsin variants engages different patterns of network activity. *eNeuro* **7**, (2020).

478. Wall, N. R., DeLaParra, M., Callaway, E. M. & Kreitzer, A. C. Differential innervation of direct- and indirect-pathway striatal projection neurons. *Neuron*

79, (2013).

479. Kress, G. J. *et al.* Convergent cortical innervation of striatal projection neurons. *Nat. Neurosci.* **16**, (2013).

480. Sharot, T., Shiner, T., Brown, A. C., Fan, J. & Dolan, R. J. Dopamine Enhances Expectation of Pleasure in Humans. *Curr. Biol.* (2009). doi:10.1016/j.cub.2009.10.025

481. Sarno, S. *et al.* Midbrain dopamine firing activity codes reward expectation and motivation in a parametric working memory task. *bioRxiv* 2020.05.01.071977 (2020). doi:10.1101/2020.05.01.071977

482. Schultz, W. Dopamine reward prediction error coding. *Dialogues Clin. Neurosci.* (2016).

483. Kawagoe, R., Takikawa, Y. & Hikosaka, O. Expectation of reward modulates cognitive signals in the basal ganglia. *Nat. Neurosci.* (1998). doi:10.1038/1625

484. Hassani, O. K., Cromwell, H. C. & Schultz, W. Influence of expectation of different rewards on behavior-related neuronal activity in the striatum. *J. Neurophysiol.* (2001). doi:10.1152/jn.2001.85.6.2477

485. Siddall, E. C. & Marples, N. M. Better to be bimodal: The interaction of color and odor on learning and memory. *Behav. Ecol.* (2008). doi:10.1093/beheco/arm155

486. Rowe, C. & Halpin, C. Why are warning displays multimodal? *Behavioral Ecology and Sociobiology* (2013). doi:10.1007/s00265-013-1515-8

487. Rubi, T. L. & Stephens, D. W. Does multimodality per se improve receiver performance? An explicit comparison of multimodal versus unimodal complex signals in a learned signal following task. *Behav. Ecol. Sociobiol.* (2016). doi:10.1007/s00265-016-2061-y

488. Rowe, C. Receiver psychology and the evolution of multicomponent signals. *Animal Behaviour* (1999). doi:10.1006/anbe.1999.1242

489. Stein, B. E., Scott Huneycutt, W. & Alex Meredith, M. Neurons and behavior: the same rules of multisensory integration apply. *Brain Res.* (1988). doi:10.1016/0006-8993(88)91276-0

490. Stein, B. E., Meredith, M. A., Huneycutt, W. S. & McDade, L. Behavioral indices of multisensory integration: Orientation to visual cues is affected by auditory stimuli. *J. Cogn. Neurosci.* (1989). doi:10.1162/jocn.1989.1.1.12

491. Wilkinson, L. K., Meredith, M. A. & Stein, B. E. The role of anterior ectosylvian cortex in cross-modality orientation and approach behavior. *Exp. Brain Res.* (1996). doi:10.1007/BF00227172

492. Bolognini, N., Frassinetti, F., Serino, A. & Làdavas, E. 'Acoustical vision' of below threshold stimuli: Interaction among spatially converging audiovisual inputs. *Exp. Brain Res.* (2005). doi:10.1007/s00221-004-2005-z

493. Harrington, L. K. & Peck, C. K. Spatial disparity affects visual-auditory interactions in human sensorimotor processing. *Exp. Brain Res.* (1998). doi:10.1007/s002210050512

494. Laurienti, P. J., Kraft, R. A., Maldjian, J. A., Burdette, J. H. & Wallace, M. T. Semantic congruence is a critical factor in multisensory behavioral performance. *Exp. Brain Res.* (2004). doi:10.1007/s00221-004-1913-2

495. Calabresi, P., Picconi, B., Tozzi, A., Ghiglieri, V. & Di Filippo, M. Direct and indirect pathways of basal ganglia: A critical reappraisal. *Nature Neuroscience* (2014). doi:10.1038/nn.3743

496. Mohr, P., Decker, M., Enzensperger, C. & Lehmann, J. Dopamine/Serotonin Receptor Ligands. 12: SAR Studies on Hexahydro-dibenz[d,g]azecines Lead to 4-Chloro-7-methyl-5,6,7,8,9,14-hexahydrodibenz[d,g]azecin-3-ol, the First Picomolar D5-Selective Dopamine-Receptor Antagonist. *J. Med. Chem.* **49**, 2110–2116 (2006).

Annex

A new micro-holder device for local drug delivery during *in vivo* whole-cell recordings.

María Saez,[a] Maya Ketzef,[b] Javier Alegre-Cortés,[a] Ramón Reig[a*] and Gilad Silberberg [b*]

[a] Instituto de Neurociencias CSIC-UMH, San Juan de Alicante, Spain

[b] Department of Neuroscience, Karolinska Institutet, Stockholm, Sweden

**Correspondence: Ramón Reig (ramon.reig@umh.es), Gilad Silberberg (gilad.silberberg@ki.se).*

ABSTRACT

Focal administration of pharmacological agents during *in vivo* recordings is a useful technique to study the functional properties of neural microcircuits. However, the lack of visual control makes this task difficult and inaccurate, especially when targeting small and deep regions where spillover to neighboring regions is likely to occur. An additional problem with recording stability arises when combining focal drug administration with *in vivo* intracellular recordings, which are highly sensitive to mechanical vibrations. To address these technical issues, we designed a micro-holder that enables accurate local application of pharmacological agents during *in vivo* whole-cell recordings. The holder couples the recording and drug delivery pipettes with adjustable distance between the respective tips adapted to the experimental needs. To test the efficacy of the micro-holder we first performed *whole-cell* recordings in mouse primary somatosensory cortex (S1) with simultaneous extracellular recordings in S1 and motor cortex (M1), before and after local application of bicuculline (BMI 200 µM). The blockade of synaptic inhibition resulted in increased amplitudes and rising slopes of "Up states", and shortening of their duration. We then checked the usability of the micro-holder in a deeper brain structure, the striatum. We applied tetrodotoxin (TTX 10 µM) during whole-cell recordings in the striatum, while simultaneously obtaining extracellular recordings in S1 and M1. The focal application of TTX in the striatum blocked Up states in the recorded striatal neurons, without affecting the cortical activity. We also describe two different approaches for precisely releasing the drugs without unwanted leakage along the pipette approach trajectory.

Key words: neuropharmacology, cortex, striatum, slow oscillations, *in vivo* patch-clamp, bicuculline.

INTRODUCTION

Electrophysiological recordings from neurons are often combined with administration of drugs such as agonists, blockers, and inhibitors. Pharmacological studies are essential for studying synaptic transmission and neuromodulation of neural circuits in health and disease. Experiments in brain slices (*ex vivo*) traditionally combine electrophysiological recordings with controlled drug application, either globally via bath application, or locally by visually aided puffing, electroporation, or uncaging of pharmacological agents (Li and Mc, 1957, Gibson and McIlwain, 1965, Yamamoto and McIlwain, 1966, Neumann et al., 1982, Matsuzaki et al., 2001). In contrast, the combination of *in vivo* electrophysiological recordings and pharmacology is more difficult and poses specific challenges, in particular when drugs are to be applied locally at the recording site. Systemic application of pharmacological agents is influenced by the kinetics of their absorption, distribution and elimination from the body and the local concentration of the agent at the recording site may vary. The effect of a drug on other regions than the region of interest, its ability to cross the blood brain barrier, and its toxic properties should also be considered. Focal application, particularly during recordings from deep brain regions, poses additional problems. If the drug is delivered through a separate cannula, the distance between the recording site and the drug delivery point might be quite large, thus affecting the timing and concentration of drug application at the recording site. Moreover, there is an increased probability of leakage into neighboring areas, especially when the targeted recording area is a deep and small nucleus. Hence, an optimal focal application method would prevent the contamination of neighboring or on-route structures.

Different methods are available for focal *in vivo* pharmacological applications. Iontophoresis can be used for drug delivery during extracellular recordings (Thiele et al., 2006), however it is not useful for drug application during simultaneous intracellular recordings. Another approach is targeting the deep structure using two parallel glued pipettes. However, the pressure used to release the drug induces mechanical vibration, generating small tip movements in the recording pipette, and compromising the intracellular recording. Moreover, the distance between the two tips is constrained by the outer pipette diameter which in most cases is between 1200-1500 µm for patch clamp recordings. Last, while optogenetic solutions are available (Boyden et al., 2005, Katz et al., 2013, Ketzef et al., 2017), they cannot yet replace the large variety of available drugs used in electrophysiological experiments.

To address this challenge we constructed a holding apparatus, the “micro-holder”, which is mounted on to the recording pipette and enables a stable local perfusion of pharmacological agents at the designated recording site during *in vivo* whole-cell recordings.

The micro-holder allows for precise perfusion with a versatile distance ranging from 100 to 500 µm between the respective tips, while avoiding the need for a second entry point. Here, using two different procedures we successfully used the micro-holder to deliver the $GABA_A$ blocker bicuculline (BMI 200 µM) to primary sensory cortex (S1), and the sodium channel blocker tetrodotoxin (TTX 10 µM) to dorsal striatum. We performed *in vivo* whole-cell recordings combined with simultaneous extracellular field recordings to show the local pharmacological effect of the respective drugs, without affecting ongoing activity in adjacent areas.

EXPERIMENTAL PROCEDURES

Micro-holder manufacturing and properties

The micro-holder is a 12.85 x 6 x 5 mm box-shaped construct made of polypropylene with 2 screws to secure the pipettes at the desired position (Fig. 1A-C). The body is perforated in two sites; the patch-clamp recording pipette hole that is drilled perpendicular to the holder body and the drug delivery pipette hole, drilled with 12 degrees angle (Fig. 1C-D). Both holes have 1.7 mm of diameter and the distance between them at the top is 4.62 mm and 3.35 mm at the bottom (Fig. 1 B). The pipettes are manually inserted to allow close proximity between the recorded cell and the delivery pipette tip (Fig. 1D-E). For our recordings, the distance between tips was 100-400 µm, but they can be as close as needed for the specific experiment. To facilitate the alignment of the tips we used a lens lighted lamp (magnification of x1.75 or x4). The distance between tips is measured by means of a reticle (5 / 0.05 mm) placed in the microscope eyepiece (Leica M60). The pipettes are fixed in the desired position by two 2 mm screws aligned perpendicularly to the respective pipettes. A video file showing the method is available in the supplementary information. The micro-holder can be manufactured using a 3D printer (See supplementary information).

Animals and surgery

C57BL6 mice of both sexes between 2-6 months old were used to perform the experiments (N = 13). Anesthesia was induced by intraperitoneal injection of ketamine (75 mg/kg) and medetomidine (1 mg/kg) diluted in 0.9 % NaCl. A maintaining dose of ketamine (30 mg/kg I.M.) was administrated every 2 hours or after changes in the EEG or reflex responses to paw pinching. Tracheotomy was performed to increase the mechanical stability during recordings by decreasing breathing related movements. Mice were placed in a stereotaxic device and air enriched with oxygen was delivered through a thin tube placed 1 cm from the tracheal cannula. Temperature was maintained between 36-37.5º C using a feedback-controlled

heating pad (FHC Inc.). The skull was exposed and three craniotomies were drilled for Striatal-TTX experiments, or two craniotomies for S1-BMI experiments (in millimeters; S1: AP: -1.5, ML: 3.25. M1: AP: 2, ML: 2. ST: AP: 0, ML: 3.5-4). The craniotomy through which the access to the cortex and striatum was done with slightly larger diameter (1 mm) to allow the insertion of both the recording and delivery pipettes. Animals were sacrificed after recordings by receiving an overdose of sodium pentobarbital (200 mg/kg I.P.).

Recordings

Whole-cell recordings were performed as described previously (Reig and Silberberg, 2016), with the addition of the holding device and the delivery pipette attached to it. The pipettes used for both recordings and drug delivery had the following properties: resistance of 6-9 MΩ, borosilicate, filamented, with 1.5 and 0.84 mm outer and inner diameters, respectively (Hilgenberg and WPI). We used a magnifying lamp (4x magnification) to position both pipettes in the micro-holder. When the pipettes were mounted onto the micromanipulator (Luigs & Neumann) a reticle installed in the microscope eyepiece was used to measure the tip distance. Pipettes were then advanced through the cortex while applying positive pressure (~1000 mbar) in the recording pipette until reaching the cortical infragranular layers (791-1303 µm in depth, n=4) or the dorsal striatum (between 2143-2610 µm in depth, n=7). At that point, the search for neurons began and the pipette pressure was reduced to 30-35 mbar and pipettes were advanced with 1 µm steps. Once a suitable cell was encountered, the pressure was removed, forming a Gigaseal in the recording pipette. A ramp of negative pressure was delivered to the recording pipette to break the seal and obtain a stable whole-cell recording. The neuronal electrophysiological properties were extracted by a set of positive and negative current injections. The intracellular solution contained (in mM): 130 K-gluconate, 5 KCl, 10 HEPES, 4 Mg-ATP, 0.3 GTP, and 10 phosphocreatine (measured pH: 7.25, and osmolarity: ~275 mOsm). Signals were amplified using MultiClamp 700B amplifier (Molecular Devices) and digitized at 20 KHz with a CED acquisition board and Spike 2 software (Cambridge Electronic Design). Extracellular local field potential (LFP) recordings from S1 and M1 were done simultaneously with the intracellular recordings using unipolar tungsten electrodes (FHC, Bowdoinham, ME, Fig. 1F) with impedances between 1-2 MΩ that were inserted 1 mm deep from the surface. Signals were amplified using a Differential AC Amplifier model 1700 (A-M Systems) and digitized at 20 KHz with CED and Spike 2 parallel to whole-cell recording.

Drug delivery

The delivery pipette was made as described above for the recording pipette (Fig. 1D), using the same borosilicate glass capillaries. In order to prevent the perfusion of the drug during crossing of the cortex and while searching for the cell to record, the delivery pipette was back-filled (Horn and Marty, 1988) with artificial cerebrospinal fluid (ACSF, 2 µl), followed by ACSF containing the BMI (200 µM) or the TTX (10 µM) and BDA 10% (10,000 MW lysine-fixable biotin dextran amine, Molecular Probes). The ACSF composition was (in mM): 125 NaCl, 25 glucose, 25 NaHCO3, 2.5 KCl, 2 CaCl2, 1.25 NaH2PO4, 1 MgCl2.

Two different procedures were used to release BMI and TTX in S1 and striatum, respectively. For cortical recordings, bicuculline was released in infragranular layers of S1. Using a piece of tissue paper, the tip of the delivery pipette was delicately broken, thus increasing its diameter, and consequently decreasing its resistance from 6-9 MΩ to 0.8-2 MΩ. Before penetrating the neocortex, the positive-pressure value in which the delivery pipette released a single micro-drop was measured using a digital manometer (Extech 407910, Differential Pressure Manometer), ranging from 30 to 60 mbar (n=6). We observed that pressure exceeding these values induced mechanical instability in the vicinity of the recorded cell, and as a consequence, loss of the whole-cell recording. While crossing the cortical supragranular layers we injected ~1000 mbar of positive pressure in the recording pipette, and 0 mbar in the delivery pipette. When both pipettes reached layer 5, the pressure was reduced to ~30 mbar in the recording pipette allowing searching for the cell to be recorded. Neurons were recorded in control condition, after which a slow ramp of positive pressure was applied in the delivery pipette using a syringe, until reaching the release value (~ 30-60 mbar). The average time in which the positive pressure was applied to release BMI was 186 ± 85.32 seconds, and the distance between the tips of the intracellular recording and the delivery pipette was 251 ± 64 µm (N=4).

A second procedure was performed to release TTX in the striatum. In this case, the delivery pipette was not modified, having the same tip diameter and resistance as the recording pipette. As for the recording pipette, the pressure in the delivery pipette was ~1000 mbar while crossing the cortex, and 30-35 mbar while searching for the neuron in the striatum, and reduced to 0 when forming a Gigaseal. With this pressure profile (~1000 mbar), the drug would be able to be released within ~5 minutes (see 2.6, *drug delivery pipette calibration)*, allowing us to insert the pipettes to the appropriate depth. After reaching the required depth for recordings, the pressure applied to the delivery pipette was reduced to 0, while the recording pipette was used to search for and record from neurons. After the initial characterization of the recorded neuron, a slow ramp of positive pressure was applied to the

delivery pipette and maintained at ~300 mbar for 196.2± 132 seconds (N= 7). The pressure was then removed to allow drug wash-out. In both experimental procedures, positive pressure was applied to both the recording and delivery pipettes by using two syringes independently connected to digital manometers (Extech 407910, Differential Pressure Manometer), thus enabling continuous monitoring of the pressure in both pipettes.

Drug delivery pipette pressure profile and time calibration

To avoid drug spillage during the delivery pipette propagation through the neocortex and white matter, we measured the time until drug release from the delivery pipette by repeating the pressure profile in a pipette back filled with 2 µl of ACSF, followed by fast green FCF (Sigma-Aldrich) dissolved in ACSF. The pipette was inserted into a tube with distilled water, and positive pressure of ~1000 mbar was applied. Using a stereomicroscope (Leica M60) we measured the time when the fast green reached the pipette tip and started spreading in the distilled water. For pipettes with access resistances between 6-9 MΩ, the time until release of fast green was 305± 42 seconds (N= 4), while the travel of the pipette to the dorsal striatum was typically between 60 to 120 seconds. We recommend that a similar calibration procedure is done for different types of pipettes.

Histology

At the end of the recording session, mice were given an overdose of pentobarbital (200 mg/kg I.P.) and transcardially perfused with 4% PFA. The brain was removed, post-fixed for 2 hours and kept in PBS 0.01M. Coronal cryo-sections (14-20 micrometers) were produced, mounted on gelatin-coated slides and stained with 1:500 cy2-streptavidin in staining solution (1% BSA, 0.1% Na Deoxycholic acid and 0.3% triton in 0.01 PBS) overnight at 4^{o}C. Slides were washed in PBS and viewed on fluorescent microscope (Olympus AB, and Leica DM 6000B). Photomicrographs of the slices were taken with Leica DFC 350 FX or an Olympus XM10 (Olympus AB) digital camera.

Data analysis

Slow oscillations, with transitions between “Up” and “Down” states were detected in the intracellular recording trace. The transition points were defined by computing the local mean and standard deviation (S.D.) on a sliding window of 30 seconds. A dynamic threshold consisting of the mean + 1.5 S.D. was used to separate Up from Down states in each window. We then used the times of the detected intracellular Up states to search for the Up states in the LFP recordings. To prevent loss of information due to temporal delays between the striatal

and cortical Up states, we extended the detected Up state regions by 200 milliseconds in both directions. Once Up states were roughly localized in both traces, transition slope magnitudes were extracted by computing the first derivative at the Down to Up state transition. To do this, we thresholded the obtained derivative using its mean +1 S.D. in the case of the membrane voltage, or -1 S.D. for the LFP traces. The detected slope was then adjusted with a first order linear fitting in order to compute its magnitude. In order to analyze the changes in Down to Up states transitions slopes induced by BMI, we extracted the mean transition slope magnitude by averaging transitions during 40 seconds before and after BMI application in the intra- and extracellular recordings (Fig. 2D). The time in which the BMI diffused from the delivery pipette to the recorded neuron differed among recordings, due to the different distances between recording and delivery pipettes. For this reason, the 40 seconds window used to average the slopes during BMI application was centered with respect to the maximum slope value detected after application.

For statistical analysis Mann-Whitney U test was used. Data are presented as means with standard error of the mean (SEM).

RESULTS

Bicuculline application to infragranular cortical layers

To demonstrate the viability of the micro-holder to locally deliver a drug to the recording site, we loaded the delivery pipettes with extracellular solution containing the $GABA_A$ receptor antagonist bicuculline methiodide (BMI). We performed whole-cell recordings in layer 5 of the barrel field in S1 before, during, and after BMI application, and simultaneous extracellular recordings in S1 and M1. The average whole-cell recording duration was 35 minutes (n=6), with a maximum of 44 minutes and a minimum of 14 minutes. The distance between the patch-clamp electrode and the respective local field recording electrode was: Vm-S1= 0.99±0.02, Vm-M1=2.43±0.092 mm (n=4). Cortical slow oscillations, organized in Up and Down states, were recorded extracellularly in both cortical areas and intracellularly in pyramidal neurons. In the example showed in Fig. 2, under control conditions, the neuron displays subthreshold Up and Down states transitions. Following BMI application (Fig. 2A), the slope of the Down to Up transitions is increased (Fig. 2B-C), as was previously described *in vitro* in slices (Sanchez-Vives et al., 2010). The upward state transition slopes were also measured in the extracellular recordings (Fig. 2C-D). The LFP recordings from S1 and M1 only showed a slight change after BMI application, more evident for the LFP located in S1 (Fig. 2D), and in all cases

were delayed with respect to the observed alteration in the intracellular activity (Fig. 2C). The average transition slopes normalized to control conditions, measured at the peak of maximum change, were; Vm=5.028± 2.375; S1=1.675± 0.289; M1=1.256± 0.166 (n=4, Fig. 2D, p≤0.05). Simultaneously, the amplitude of the Up states (Ctrl=15.89± 0.646; BMI=39.59± 0.386 in mV, p≤0.001, Fig. 2F) and the duration of the Down states (Ctrl=0.87± 0.64; BMI=1.37± 0.97 in seconds, p≤0.001, Fig. 2G) increased significantly in the recorded neurons, while the duration of the Up states decreased (Ctrl= 0.54± 0.34; BMI= 0.15± 0.06 in seconds, p≤0.001, Fig. 2G). Recorded neurons also increased their action potential discharge following BMI application (Fig. 2E, Ctrl= 0.16± 0.19; BMI= 5.15± 3.09 in Hz, p= 0.028), generating bursts of action potentials during Up states (Fig. 2A). Importantly, BMI application did not induce changes in duration of Up states recorded extracellularly in S1 and M1 (Fig. 2G), while only a slight difference was observed in the LFP slopes (Fig. 2C-F). To verify that the changes observed in the whole-cell recordings indeed reflect a network phenomenon, and not a result of the different recording techniques (patch-clamp vs. LFPs), we performed a subset of experiments in which we recorded the LFP signal instead of the whole-cell recording. As in the case of whole-cell recordings from a single neuron, BMI release in the vicinity of the recording site resulted in a marked increase of the Down to Up state transition slope (normalized: 7.79± 2.65, p= 0.002; absolute values in mV/s; Ctrl= 5.65± 1.58; BMI= 28.59± 6.42). As shown above, BMI application induced only slight changes in the transition slopes recorded by distal LFPs placed in S1 (normalized: 1.65± 0.38, p=0.047 ; absolute values in mV/s; Ctrl= 3.6± 0.52; BMI= 5.22± 0.48) and M1 (normalized: 1.18± 0.09, p= 0.047; absolute values in mV/s; Ctrl= 2.71±0.64; BMI= 3.06± 0.64). These results demonstrate that locally applied BMI induced large changes in both intracellular and LFP recordings, followed by smaller and delayed changes in LFPs recorded at distal cortical sites.

Tetrodotoxin application in the striatum.

In order to test drug delivery using the micro-holder in a deep brain area, we locally perfused tetrodotoxin (TTX, 10 μM) during simultaneous whole-cell recordings in striatum and LFP recordings in S1 and M1. We loaded the delivery pipettes with ACSF containing TTX (10 μM), which locally blocks neuronal action potential discharge. An example of such a recording is shown in Fig. 3. The average recording duration was 53 minutes (n=7), with a maximum of 85 minutes and a minimum of 34 minutes. Slow oscillatory activity can be observed in both cortical areas and the recorded striatal medium spiny neurons (MSNs, Fig. 3Aa), as shown previously (Wilson and Kawaguchi, 1996, Mahon et al., 2001, Kasanetz et al., 2002, Reig and

Silberberg, 2014, 2016) under control conditions. After 1.5± 1.84 minutes of TTX perfusion, the MSN stopped firing action potentials and the transitions to Up states were nearly abolished, while no change in cortical activity was observed in the LFP recordings (Fig. 3Ab, 3Bb, 3C-E). After drug delivery was stopped, TTX was cleared from the tissue, as evident by the recovery of MSNs action potential discharge and state transitions (3Ac, 3Bc and 3E). We observed a full recovery in 3 of 7 MSNs (recording duration = 60.38± 8.45 minutes, N=3). To visualize the spread of the injected solution within the tissue, we added dextran-biotin to the delivery pipette (10% dissolved in ACSF, Fig. 3F). The stained area was confined to the striatum and no staining could be seen throughout the cortex, including the pipette trajectory, verifying the efficiency of the back-filling procedure. Our results show that the micro-holder enables local drug application during whole-cell recordings. The delivery was efficient and spatially confined in both examples shown from cortical and striatal recordings.

DISCUSSION

In this paper, we describe the micro-holder, an apparatus for local drug application which does not compromise the stability of in vivo intracellular recordings. We have demonstrated the feasibility of such application during *in vivo* whole cell recordings in the mouse cortex and striatum. The small device is of low cost and easy to produce by means of 3D printing (see 3D printer files in the supplementary information). With the aid of a magnifying lamp (4x magnification), the pipettes tips can be easily positioned, and through a reticle installed in the microscope eyepiece the pipette tips distance can be measured. In our experiments, the average distance between the delivery and recording pipettes was 251.4 µm. Pipettes tips can be easily aligned up to 100 µm, however, the closer the pipettes are the more likely it is to generate mechanical instability in recorded neurons. The minimal distance for stable application was found to be 156 µm in our hands. This distance allows applying, with high accuracy, the desired drug during intra- or extracellular recordings in subcortical nuclei of mice, reducing the possibility of contamination in neighboring areas. Example of the spreading can be found in Fig. 2H and 3F, where BDA 10% was mixed with BMI and TTX, respectively.

Local BMI application in S1

Local application of BMI in infragranular layers of S1 caused a decrease in the duration and increase in amplitude of Up states, coincident with an increase in the slope of Down-to-Up state transitions, resulting in increased discharge frequency (Fig. 2A). These results match

previously described data from ferret slices (Sanchez-Vives et al., 2010), in which BMI application modulated spontaneous activity in the cortex, showing an increase in firing rate as well as acceleration of the upward state transition slope. In contrast to the bath application in slice experiments (Sanchez-Vives et al., 2010), we did not see changes in the oscillation frequency, and the changes in state durations were mainly limited to the whole-cell recordings, in close proximity to the drug application point. The fact that no global changes in the frequency were observed, and the small impact on the state durations recorded in LFP signals (Fig. 2C-D) both suggest that the BMI effect was indeed spatially restricted (Fig. 2H).

Local TTX application in striatum

In our recordings from striatal MSNs we showed baseline activity followed by TTX application and, finally, after drug washout. Application of TTX was limited to the recording area and did not propagate to neighboring structures such as cortex and probably also thalamus, as shown by the lack of effect on cortical oscillatory activity (Fig. 3A) and staining (Fig. 3F). To prevent the spread of TTX in the cortex while avoiding a possible pipette blockage, we back-filled the delivery pipette tip with ACSF, and traversed the cortex with high pressure, as used for the recording pipette (see Methods). In this study we applied TTX in the striatum to test the micro-holder due to the obvious effect on neuronal activity, however, the micro-holder is not limited only to TTX application. The striatum receives massive dopaminergic input, mediated via receptor subtypes with very different effects (Pennartz et al., 1992, Harvey and Lacey, 1997, Nicola and Malenka, 1997, Pisani et al., 2000, Bamford et al., 2004, Salgado et al., 2005, Planert et al., 2013). It would, therefore, be of special interest to use the micro-holder for focal application of dopamine agonists and antagonists in order to study their impact on striatal circuits *in vivo.* A recent *ex vivo* study has shown the pathogenic expression of NMDA receptor subunit GluN3A in striatal medium spiny neurons underlying Huntington's disease (Marco et al., 2013). The micro-holder can be used to study the role of NMDA receptors on striatal neurons during *in vivo* recordings.

Employing the precision and stability of the micro-holder, we used it for *in vivo* whole-cell recordings, however, the device is versatile enough to be used with other types of electrodes such as extracellular tungsten electrodes, or together with a fiber optic during optogenetics experiments. Small modifications such as the diameter and length of the support screws can be easily done according to the specific experimental needs. Moreover, in the case of very deep recordings, possible tissue damage can be reduced by pulling a capillary in a not centered filament. The "lateralization" of the filament with respect to the center of the pipette will create a shank that is not along its central axis. This modification in the delivery pipette

could help to further reduce the angle between the delivery and the recording pipettes. To conclude, the micro-holder is a new tool for studying neuronal circuits *in vivo*, enabling an optimal combination of whole-cell recordings and local application of pharmacological agents.

APPENDIX A. SUPPLEMENTARY DATA

Supplementary data associated with this article can be found, in the online version, at https://doi.org/10.1016/j. neuroscience.2018.04.011.

ACKNOWLEDGMENTS

We thank Anders Lindquist (Karolinska Institutet) and Victor Rodríguez Milán (Instituto de Neurociencias) for their contribution in the micro holder construction and Stuart Ingham for the video (Instituto de Neurociencias).

The study was supported by the following grants; to **R.R.**: MINECO Fellowship [BES-2015-072187], starting grant I+D Jovenes investigadores [BFU2014-60809-JIN], and CSIC-Severo Ochoa Grant Instituto de Neurociencias [SEV-2013-0317-05], to **G.S.**: ERC starting grant [SENSTRIATUM - 282012], Knut and Alice Wallenberg Foundation Fellowship [KAW 2012.0131] and grant [KAW 2014.0051], Swedish medical research council [VR 2015-02403], and support from the Swedish Brain Foundation (Hjärnfonden), and Karolinska Institutet research grants.

FIGURE LEGENDS

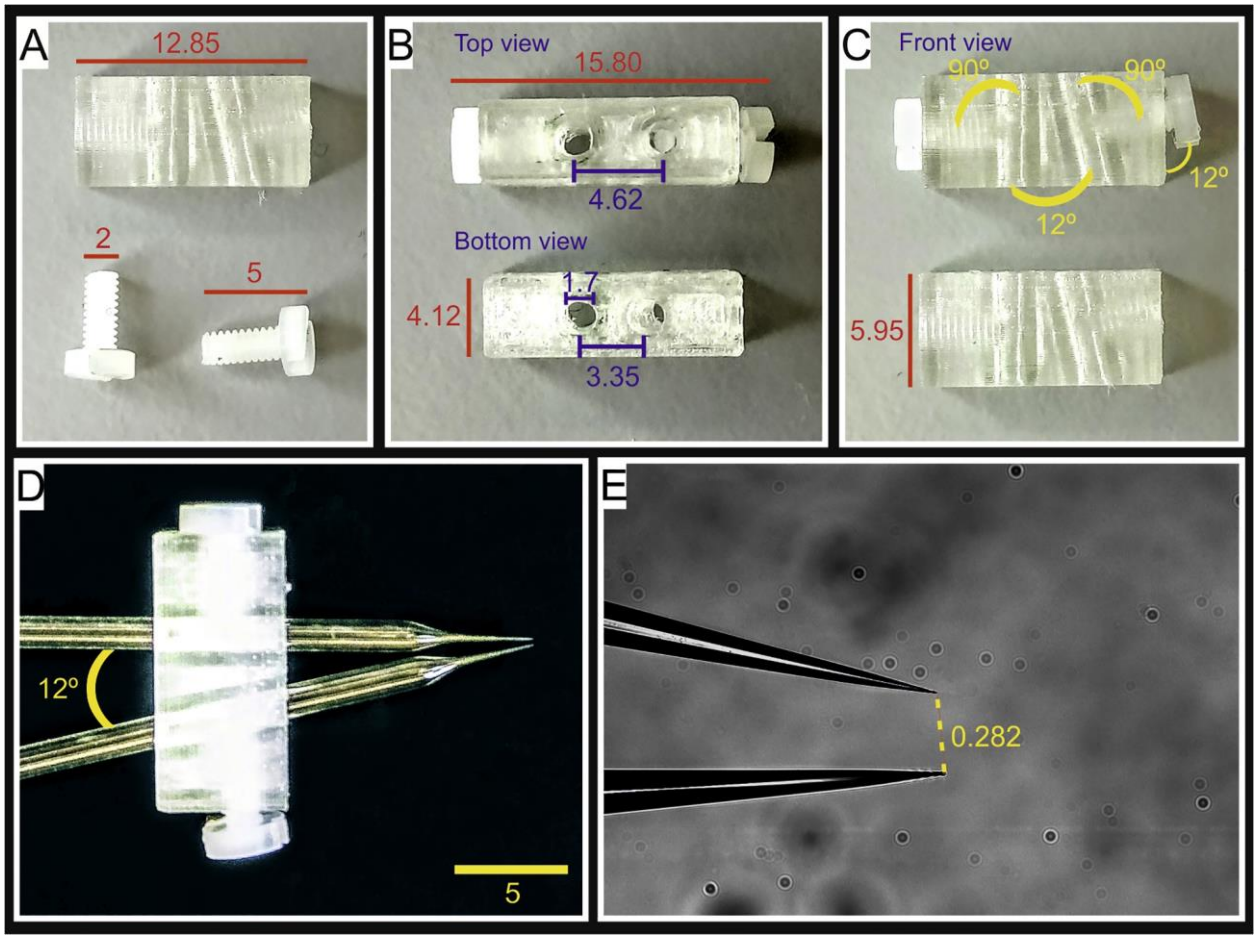

Fig. 1. Properties of the micro-holder. The micro-holder body and two screws used for securing the recording and drug delivery pipettes. **A.** Length of the main construct and screws dimensions **B.** Total length with the screws and pipette holes distance (top view), width without screws and pipette holes distance and diameter (bottom view). **C.** the angles between pipette holes and the screws, and both insertion pipette holes (top). Height of the main construct (bottom). **D.** The construct with the 2 pipettes inserted, demonstrating a 12° angle between them. **E.** The distance between the 2 pipettes in higher magnification. All measurements are in millimeters.

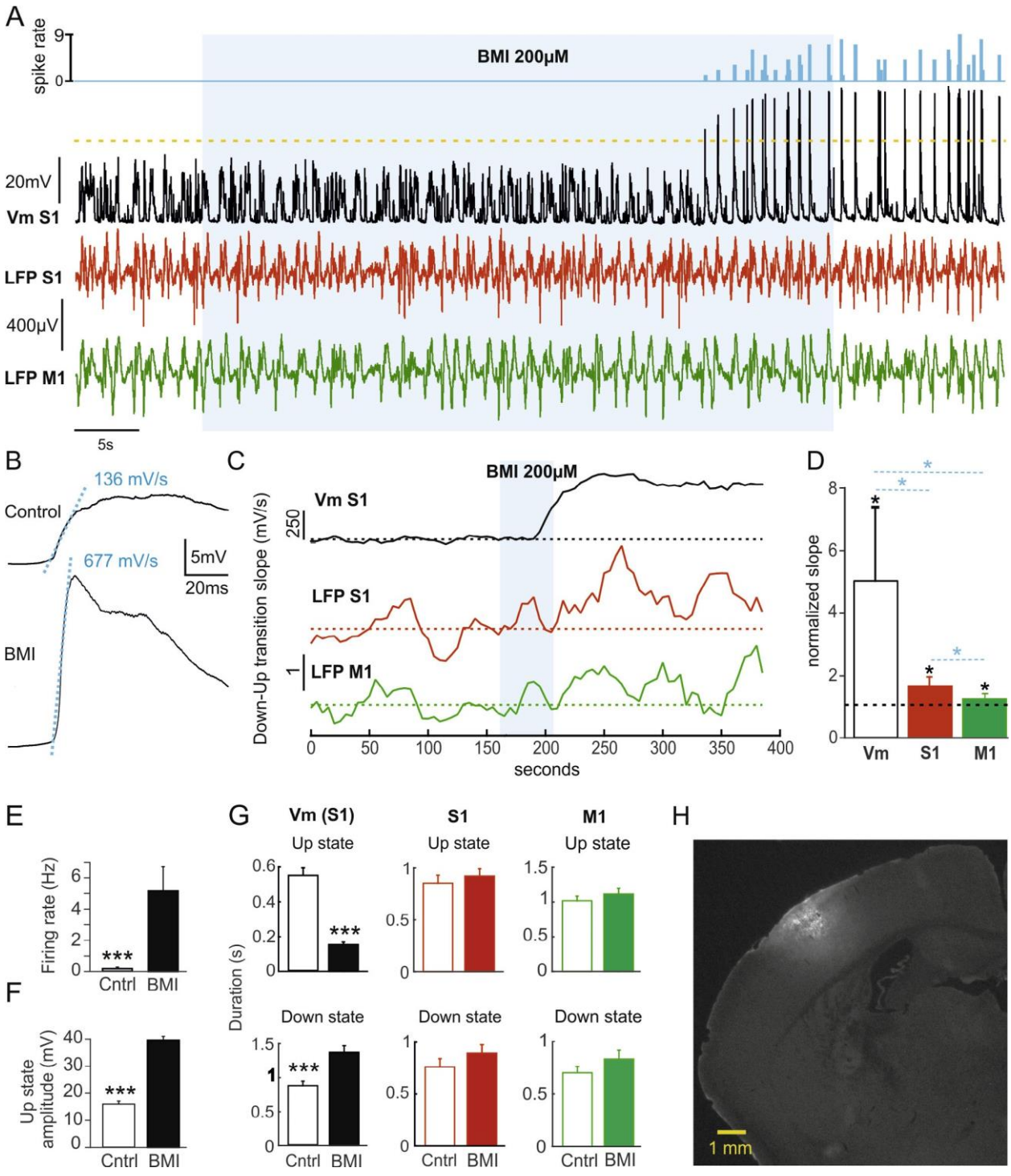

Fig. 2. Focal BMI delivery in S1. Spatially restricted modulation of spontaneous activity in S1 by focal application of BMI 200 µm. **A.** Histogram of action potentials (top, blue) counted from the intracellular recoding of spontaneous activity in a layer 5 pyramidal neuron (middle, black), LFPs in S1 (middle, red) and M1 (bottom, green). Note the modulation in the whole-cell recorded spontaneous activity, and the lack of effect in simultaneously recorded LFPs. The light grey shade indicates the time where BMI was released. **B.** Waveform average of the membrane potential whole-cell recorded neuron in A, before (top) and after (bottom) BMI

application. The upward transition slopes (dashed blue line) were calculated by fitting a linear regression (See Methods section). **C.** Transition slope values are plotted over 400 seconds for the same recordings as in A. The light grey bar designates the duration of BMI application. **D.** Average of the upward transition slopes normalized to control values (n=4). **E-F.** Firing rate and Up state amplitude of whole-cell recordings under control conditions and following BMI application (n=4). **G.** Average of the Up state duration for the intra- and extracellular recordings. **H.** A coronal section showing the local spread of biotin-dextran amine in S1. Histogram bin size = 100 ms. * p<0.05, *** p<0.001, Mann-Whitney U test.

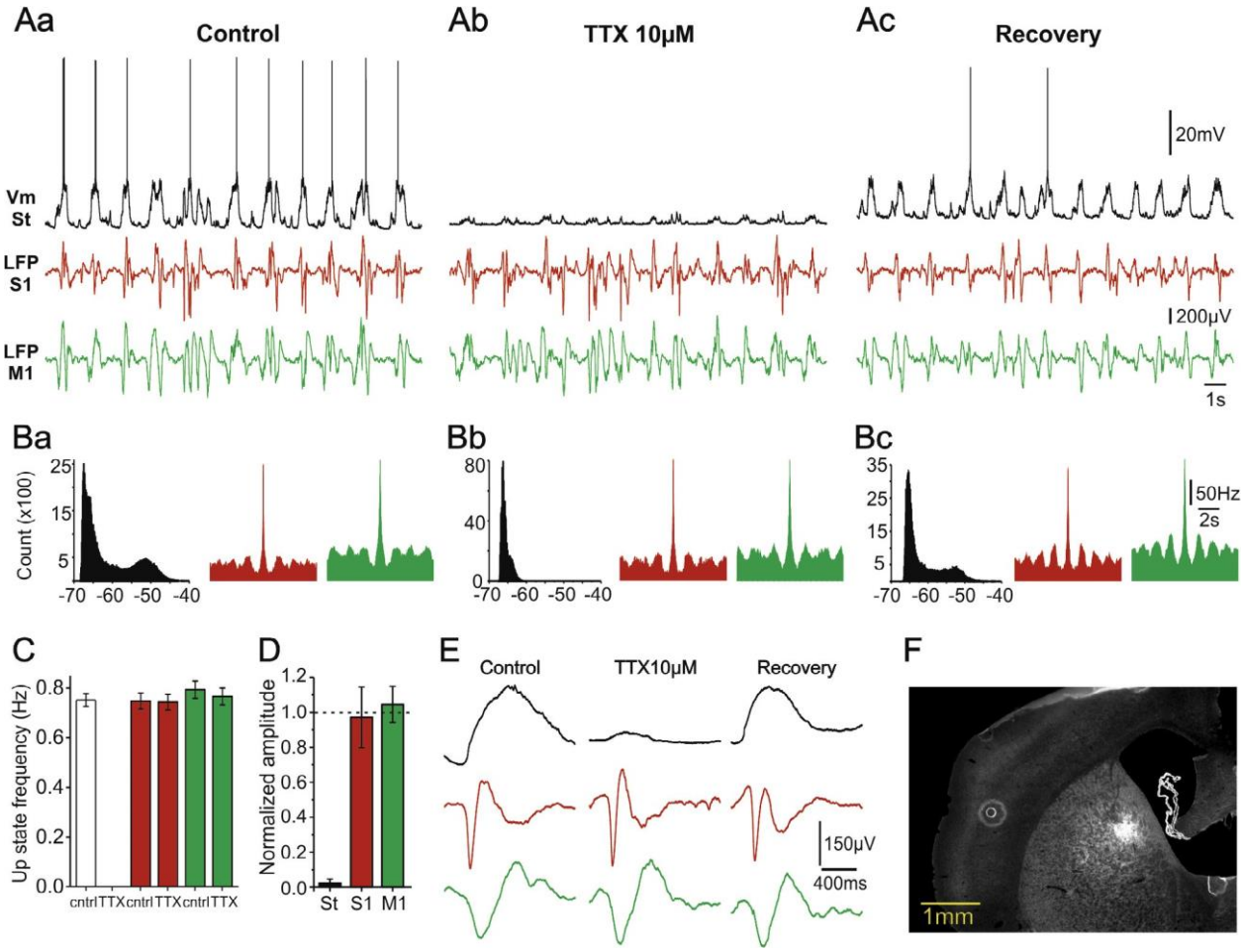

Fig. 3. Focal TTX delivery in the striatum. Focal application of TTX in the striatum does not affect cortical activity. **A.** Whole-cell recordings from a striatal MSN (top, black) and simultaneous LFP recordings from cortical S1 (middle, red) and M1 (bottom, green) during

slow oscillatory activity, under control conditions (left panel, a), following application of 10 µM TTX (middle panel, b) and after washout (right panel, c). **B.** All-point-histogram of the MSN membrane potential (black) and cortical auto-correlograms (S1 in red and M1 in green), for the same conditions as in A. **C.** Frequency of the Down to Up state transitions under control conditions (ctrl) and in the presence of 10 µM TTX in a whole-cell recorded MSN (black), and cortical LFP recordings in S1 (red) and M1 (green). **D.** Amplitude of the Down to Up state transition in TTX conditions normalized to control conditions for MSN (black), S1 (red) and M1 (green). **E.** Averaged waveform of the Up state recorded in an MSN (top, black), S1 (middle, red) and M1 (bottom, green) under control conditions (left panel), in the presence of 10 µM TTX (middle panel) and after washout (right panel). **F.** A coronal section showing the local spread of biotin-dextran amine in the striatum without staining the cortex.

REFERENCES

Bamford NS, Zhang H, Schmitz Y, Wu NP, Cepeda C, Levine MS, Schmauss C, Zakharenko SS, Zablow L, Sulzer D (2004) Heterosynaptic dopamine neurotransmission selects sets of corticostriatal terminals. Neuron 42:653-663.

Boyden ES, Zhang F, Bamberg E, Nagel G, Deisseroth K (2005) Millisecond-timescale, genetically targeted optical control of neural activity. Nat Neurosci 8:1263-1268.

Gibson IM, McIlwain H (1965) Continuous Recordings of Changes in Membrane Potential in Mammalian Cerebral Tissues in Vitro; Recovery after Depolarization by Added Substances. J Physiol 176:261-283.

Harvey J, Lacey MG (1997) A postsynaptic interaction between dopamine D1 and NMDA receptors promotes presynaptic inhibition in the rat nucleus accumbens via adenosine release. J Neurosci 17:5271-5280.

Horn R, Marty A (1988) Muscarinic activation of ionic currents measured by a new whole-cell recording method. J Gen Physiol 92:145-159.

Kasanetz F, Riquelme LA, Murer MG (2002) Disruption of the two-state membrane potential of striatal neurones during cortical desynchronisation in anaesthetised rats. J Physiol 543:577-589.

Katz Y, Yizhar O, Staiger J, Lampl I (2013) Optopatcher--an electrode holder for simultaneous intracellular patch-clamp recording and optical manipulation. J Neurosci Methods 214:113-117.

Ketzef M, Spigolon G, Johansson Y, Bonito-Oliva A, Fisone G, Silberberg G (2017) Dopamine Depletion Impairs Bilateral Sensory Processing in the Striatum in a Pathway-Dependent Manner. Neuron 94:855-865 e855.

Li CL, Mc IH (1957) Maintenance of resting membrane potentials in slices of mammalian cerebral cortex and other tissues in vitro. J Physiol 139:178-190.

Mahon S, Deniau JM, Charpier S (2001) Relationship between EEG potentials and intracellular activity of striatal and cortico-striatal neurons: an in vivo study under different anesthetics. Cereb Cortex 11:360-373.

Marco S, Giralt A, Petrovic MM, Pouladi MA, Martinez-Turrillas R, Martinez-Hernandez J, Kaltenbach LS, Torres-Peraza J, Graham RK, Watanabe M, Lujan R, Nakanishi N, Lipton SA, Lo DC, Hayden MR, Alberch J, Wesseling JF, Perez-Otano I (2013) Suppressing aberrant GluN3A expression rescues synaptic and behavioral impairments in Huntington's disease models. Nat Med 19:1030-1038.

Matsuzaki M, Ellis-Davies GC, Nemoto T, Miyashita Y, Iino M, Kasai H (2001) Dendritic spine geometry is critical for AMPA receptor expression in hippocampal CA1 pyramidal neurons. Nat Neurosci 4:1086-1092.

Neumann E, Schaefer-Ridder M, Wang Y, Hofschneider PH (1982) Gene transfer into mouse lyoma cells by electroporation in high electric fields. EMBO J 1:841-845.

Nicola SM, Malenka RC (1997) Dopamine depresses excitatory and inhibitory synaptic transmission by distinct mechanisms in the nucleus accumbens. J Neurosci 17:5697-5710.

Pennartz CM, Dolleman-Van der Weel MJ, Kitai ST, Lopes da Silva FH (1992) Presynaptic dopamine D1 receptors attenuate excitatory and inhibitory limbic inputs to the shell region of the rat nucleus accumbens studied in vitro. J Neurophysiol 67:1325-1334.

Pisani A, Bonsi P, Centonze D, Calabresi P, Bernardi G (2000) Activation of D2-like dopamine receptors reduces synaptic inputs to striatal cholinergic interneurons. J Neurosci 20:RC69.

Planert H, Berger TK, Silberberg G (2013) Membrane properties of striatal direct and indirect pathway neurons in mouse and rat slices and their modulation by dopamine. PLoS One 8:e57054.

Reig R, Silberberg G (2014) Multisensory integration in the mouse striatum. Neuron 83:1200-1212.

Reig R, Silberberg G (2016) Distinct Corticostriatal and Intracortical Pathways Mediate Bilateral Sensory Responses in the Striatum. Cereb Cortex 26:4405-4415.

Salgado H, Tecuapetla F, Perez-Rosello T, Perez-Burgos A, Perez-Garci E, Galarraga E, Bargas J (2005) A reconfiguration of CaV2 Ca2+ channel current and its dopaminergic D2 modulation in developing neostriatal neurons. J Neurophysiol 94:3771-3787.

Sanchez-Vives MV, Mattia M, Compte A, Perez-Zabalza M, Winograd M, Descalzo VF, Reig R (2010) Inhibitory modulation of cortical up states. J Neurophysiol 104:1314-1324.

Thiele A, Delicato LS, Roberts MJ, Gieselmann MA (2006) A novel electrode-pipette design for simultaneous recording of extracellular spikes and iontophoretic drug application in awake behaving monkeys. J Neurosci Methods 158:207-211.

Wilson CJ, Kawaguchi Y (1996) The origins of two-state spontaneous membrane potential fluctuations of neostriatal spiny neurons. J Neurosci 16:2397-2410.

Yamamoto C, McIlwain H (1966) Electrical activities in thin sections from the mammalian brain maintained in chemically-defined media in vitro. J Neurochem 13:1333-1343.